POLITECNICO DI MILANO

School of Civil, Environmental and Land Management Engineering

Master of Science Degree in Civil Engineering – Structures

Academic Year 2016/2017

A MECHANICAL MODEL FOR WIRE ROPES

Master Dissertation of

Alessandro Marengo

Supervisor

Luca Martinelli

Co-Supervisor

Francesco Foti

April 2018

AKNOWLEDGMENTS

The present thesis is the result of several months of hard work. I have been guided and helped by prof. Luca Martinelli and Francesco Foti to whom I send my truest gratitude for their support.
This is the final step of long university career and I would like to dedicate this work to my family and to all my friends.

TABLE OF CONTENTS

LIST OF FIGURES

LIST OF TABLES

INTRODUCTION

I. APPLICATIONS

The main purpose of structural engineering is the pursuit of the best system able to carry out the external loads of the problem under investigation. The choice is based on many variables which aim to optimize the result from an economical vantage point.
Wire ropes are complex systems that can be seen like composite structures. Their main peculiarity is the relatively high strength in tension compared to the very light weight. This means that they are very efficient in terms of material saving. Moreover, they are often considered and designed as perfectly flexible structures, as a matter of fact wire ropes show very little stiffness in bending if related with the axial stiffness. This property is fundamental when the element needs to be coiled like in lifting systems where the rope is forced to follow the radius of a sheave or a winch.
The reason of paying big concern on the modelling of this structural typology lies in the very wide range of applications that it covers. While a perfectly flexible analysis of this system may provide reliable results for a large-scale design in statics, a more refined approach is needed when the wire rope is experiencing complex stress states. This occurs in static analyses mainly in critical regions, for instance close to clamping devices or when the rope is forced to bend over a pulley and undergoes cyclic flexure. Moreover, hysteretic bending may cause further phenomena as inter wire slipping and friction. Finally, this latter behaviour may affect significantly the dynamic response in term of damping of the structure.
The main applications span from civil to mechanical engineering. For instance, they are used in lifting systems like cranes, elevators or in mining. Furthermore, metallic cables are used for overhead electrical lines, because of their good conductivity properties and light weight. Other famous examples are the tenso-structures like roofing systems, cable stayed and suspension bridges. Finally, they are very spread in offshore engineering like Oil & Gas plants, where they are employed for either lifting or as anchoring systems.

II. MANIFACTURING

The complexity of the mechanical behaviour of the wire ropes stem from the internal geometry and thus in the manufacturing process. The main concept to understand the framing of that structural typology is the hierarchy. In fact, the wire rope may be decomposed into several sub-components that represent the different hierarchical levels of the whole system.
The basic component is the wire. It is a structural element that may be considered as one-dimensional, i.e. a dimension is prevailing on the other two, where the principal or longitudinal dimension coincides with the centreline of the wire, while the other dimensions define a plane in space orthogonal to the centreline in every point and define the wire cross section. As a matter of fact, it can be seen like a solid obtained by extrusion of a cross section along a path, i.e. the centreline. Moreover, this element is endowed with a peculiar feature: it is very slender, i.e. the cross section maximum dimension is significantly lower with respect to the longitudinal dimension, such that it can be considered a line. This feature is the responsible for the high deformability in bending that usually allows the assumption of perfectly flexible system. Beside the structural behaviour, it is very important for the manufacturing process as well.
As a matter of fact, the wire is used to produce strands that represent the subsequent level within the structural system. The strand is a sub component composed by a core and several layers concentric to the core itself. In the straight configuration, the core is a straight wire, while the layer is the set of wires helicoidally wounded about the straight one forming a three-dimensional helix shape that share the same distance from the central axis of the strand. The coiling follows a precise rule, i.e. all wires share the same shape in terms of rotation about the core. This trend of the production is the reason of coupling between tensile force and other actions like torque. The strand is the new basic component then, and it is used to produce ropes in many shapes. The simplest idea is to exploit the same hierarchical structure between the wire and the strand, between the strand and the wire rope as well. Hence, a straight core strand is surrounded by several layers of strands helicoidally wounded. The Fig. I.1 shows this kind of structures: the core strand is straight, and it is composed by a layer of wires coiled about the straight core wire, while the outer strand that has the same internal structure is not straight, yet it has a helix shape. It is important to notice that the outer wire of the core strand and the core wire of the outer strand form a single helix curve in space, conversely the outer wire of the outer strand is a double, or nested helix. The last curve is basically a single helix which axis is not straight, still it is a single helix itself.

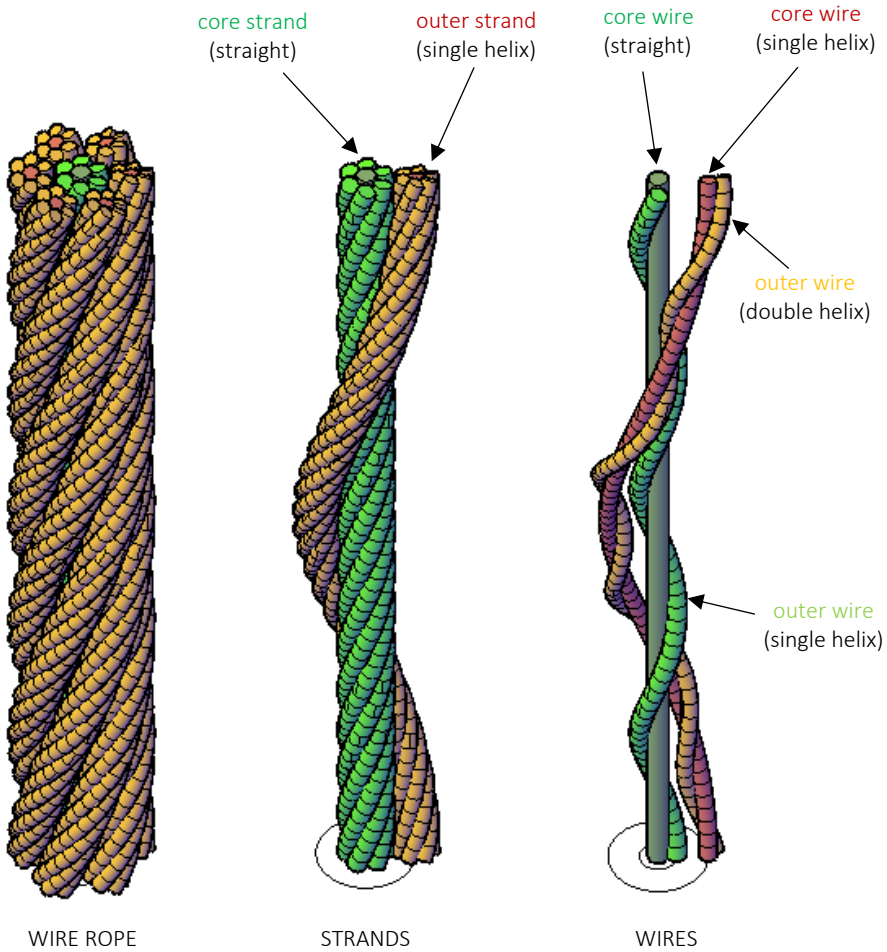

Fig I.1 Wire Rope Hierarchy - Overview

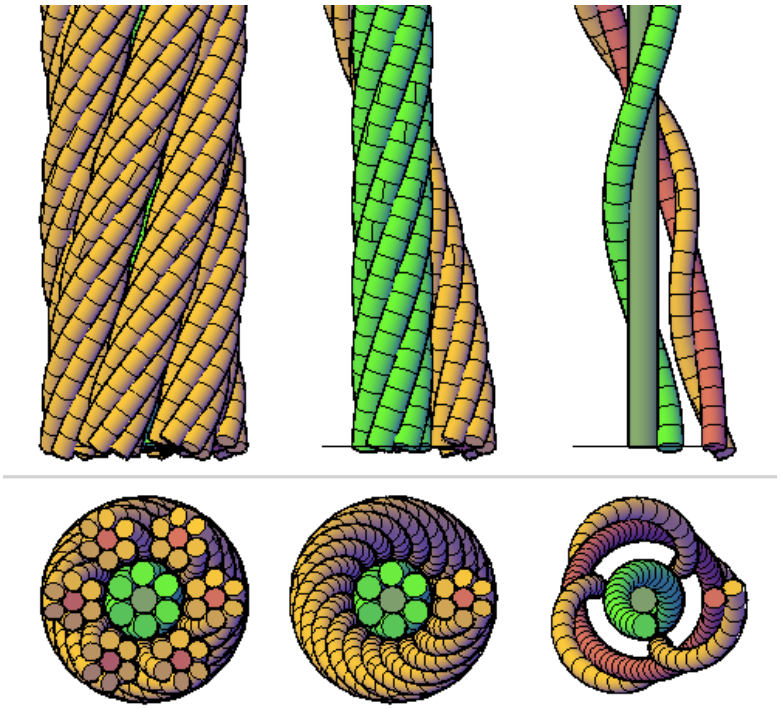

Fig I.2 Wire Ropes Hierarchy – Front and Top Views

1. LAY ANGLE

A very important geometrical feature of a wire rope is the lay angle. If the single helix is seen in a front view, its projection on the correspondent plane has a rectilinear shape, like it will be further explained in the chapter about geometry, and it forms an angle with the longitudinal axis of the helix as it is shown in Fig I.3. This angle is called "lay angle" and is usually denoted with the Greek letter α. This quantity is endowed of sign. Specifically, the positive angle is obtained when the helix is coiled according to the right-hand screw, in this case the lay direction is said to be right (symbol z), it is left otherwise (symbol s).

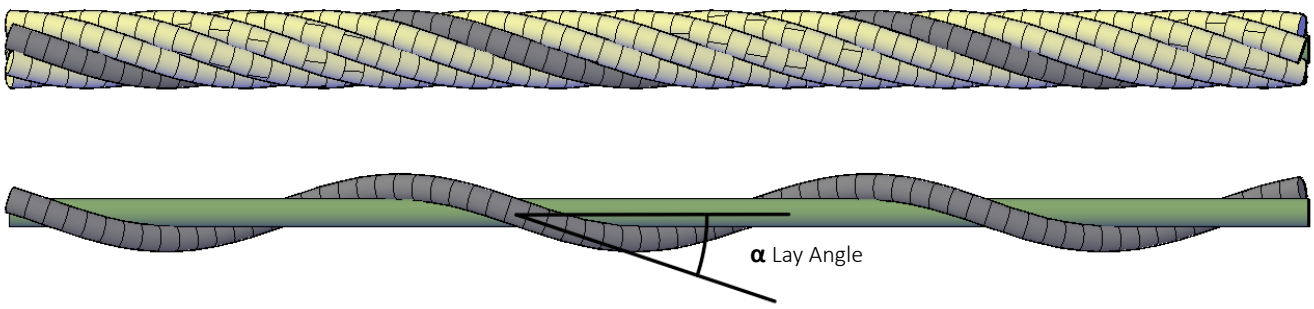

Fig I.3 Helix Lay Angle

2. LANG AND REGULAR LAY STRANDS

The outer wire of a straight strand is a single helix, and, on the other hand, the outer strand of a rope is a single helix as well. This means that the outer wire has a lay direction independent upon the outer strand it belongs to. The lay direction of the outer wire is indicated with the lower case “s” for the left lay and “z” for the right lay, while the lay direction of the strand is called with the upper case “S” for the left lay and “Z” for the right lay. The strand is said to be Lang lay if the two lay directions coincide, conversely it is called Regular lay. For both cases two combinations are possible. The lang lay may be sS or zZ, while the regular lay may be sZ or zS.
In the present work we will use the always zZ lang lay ropes, still the lay direction is controlled by the sole sign of the lay angle.

3. CLASSIFICATION

There are many possible geometries for wire ropes, still in the following let us introduce the two typologies that will be studied in the present work because of their great interest. The nomenclature is provided by the standard ISO 17893:2004 *Steel wire ropes – Vocabulary, designation and classification.* A rope with a steel core is made of steel wires and it is indicated as WC. The core is made by either a strand, thus the rope will be called “wire strand core” (WSC), or an independent wire rope, hence it is called “independent wire rope core” (IWRC). In both cases the core is surrounded by strands helicoidally wounded about its straight axis.
The WSC is showed in Fig. I.4. This typology has small diameters usually, and it is used in applications like mining. The example shows a single layer rope, still it may be endowed with more layers.

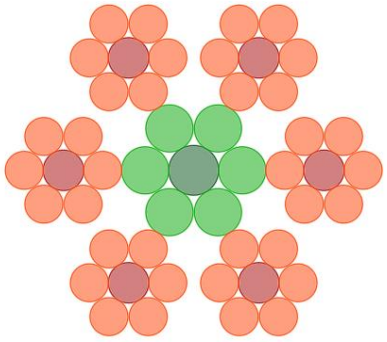

Fig I.4 Strand Core Wire Rope (WSC)

Conversely, the IWRC has higher diameters. The core in Fig I.5 is a WSC rope and the outer strands are multi-layered. The usual application is in the offshore.

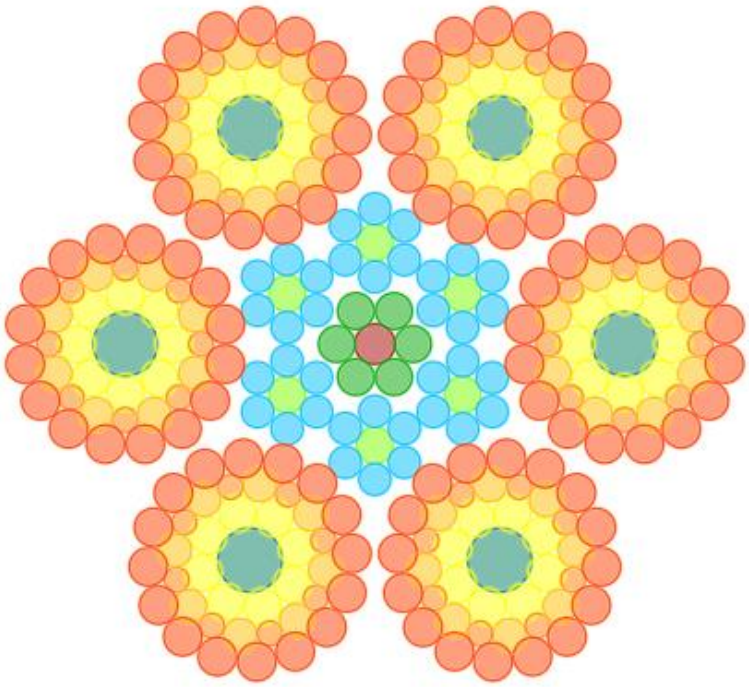

Fig I.5 Independent Wire Rope Core (IWRC)

4. NOMENCLATURE

Now let us introduce the principal nomenclature involved for naming of wire ropes. The aim is to provide the minimum amount of information to describe the geometry of the wire rope.
The first value that is provided is the global diameter of the rope in mm, i.e. the maximum dimension of the cross section, then it is followed by a couple of numbers that are multiplied one with the other and represent respectively the number of strands in the rope and the number of wires inside the strand.
A 20 - 18x7 - WSC is a 20 mm global diameter multi stranded rope made by eighteen strands with seven wires each and with a strand core. Conversely, a 22 - 6x36 WS – IWRC is a 22 mm diameter independent wire rope core with a stranded rope core made by 6 outer strands with 36 wires each.

5. LUBRICATION

A very important treatment done on wire ropes is lubrication. Greases or oils are used to decrease friction among the wires. Specifically, this procedure is used during manufacturing and the lubricant persists inside the rope for some time after it is kept in service. The importance of lubrification is related to bending of the wire rope. As a matter of fact, this kinematic perturbation produces sliding among the wires to the arising gradient of displacement on the rope cross section. This gradient induces a gradient on the axial force experienced by the adjacent wires that can be equilibrated only by inter wire friction forces. These forces are caused by internal slipping between wires. The phenomenon is important in many applications like the passage of ropes over sheaves or winches.
This peculiar technological treatment will be fundamental in the following work to establish the kinematic hypothesis the model is based on.

III. PRESENT WORK

The present work aims to provide a simple tool to predict the structural response of wire ropes in terms of either global (internal actions) and local (stresses) quantities.
This objective is pursued with a relatively simple kinematic assumption on the behaviour of the system introduced in the second chapter. As a matter of fact, the single wire is modelled according to the Love thin curved rod theory (Huang, 1973) accounting biaxial bending and torsion, further then axial stiffness only. Then the rope response is studied with a sectional approach and it is modelled like a Euler Bernoulli beam, i.e. the cross section is considered rigid. This approach is the natural extension of the modelling used in (Foti & Martinelli, 2016) for the analysis of single strands.
Furthermore, the thesis offers to different approaches for the derivation of the mechanical quantities of the rope. The first is called direct model, or wire by wire model, and it exploits the actual geometry of the single wire to define the rope response, i.e. either single helix geometry of double helix geometry. Conversely, the recursive model, or hierarchical model, introduces an approximation: the relations holding true between the strand and the rope are derived in exact form, while the relations between the wire and the rope are computed recursively passing through the strand. Specifically, the mechanics between wire and strand in evaluated in the strand straight configuration, thus not accounting for the actual double helix geometry of the wire.
The global response of the wire rope is evaluated in the linear elastic field. Hence, the response of the whole structural system may be seen like the sum of the contributions provided by the single wire. For that reason, a chapter will be dedicated to that topic.
Finally, either global and local response are investigated in the last chapter.

REFERENCES

(Love, 1944) Love A.E.H., 1944. *A treatise on the Mathematical Theory of Elasticity*. Dover Publications, New York.

(Huang, 1973) Huang N.C., 1973. *Theories of Elastic Slender Curved Rods.* Journal of Applied Mathematics and Physics Vol.24 (1973).

(ISO 17893, 2004) ISO 17893:2004 *Steel wire ropes – Vocabulary, designation and classification*

(Feyrer, 2007) Feyrer K., 2007. *Wire Ropes. Tension, Endurance, Reliability*. Springer.

(Foti & Martinelli, 2016) Foti F., Martinelli L., 2016. *Mechanical modelling of metallic strands subjected to tension, torsion and bending*. International Journal of Solids and Structures 91 (2016) 1-17.

CHAPTER 1

GEOMETRY OF WIRES

I. INTRODUCTION

Wire ropes are structural elements which present a complex geometrical framing. The construction process follows a strict hierarchy that can be described going through the sub components of the whole system. The base element is the wire, a mono-dimensional component that is wrapped within a strand. This latter is made up by a straight central wire, called core wire, and by other wires coiled about the core with the shape of a single helix curve, called outer wires. The outer wires are grouped in layers, i.e. set of wires having the same distance between centerline and strand axis.
The strand is the new base element for the construction of ropes and depending upon how it is inserted within the whole system, different kind of ropes can be obtained. A stranded rope is a rope presenting the same hierarchical relation holding between strand and rope for wire and strand. Hence, it has a central straight strand and about that one, several strands are wrapped in layers always with a single helix shape. This has an important geometrical consequence: the single wire within an outer strand shows a single helix geometry, while it is a double helix inside the rope.

The previous description gives a clue of the reason why so much interest is paid for the inspection of the single and double helix geometry. As a matter of fact, they are the starting point for the mechanical response of the whole system as it will be shown in the subsequent chapters. In literature of wire ropes, there is always an introduction declaring the geometry involved in the models. Some references for the double helix may be found in (Wang, 1998); (Usabiaga and Pagalday, 2008); (Xiang et al., 2015).

In the present chapter a complete description of the equations governing the geometry is introduced. The first step is the general theory for describing three-dimensional curves in space, afterwards the single and double helixes are presented as peculiar cases. The final part of the chapter shows how these models may be implemented with real ropes and comparison is performed with some examples available in literature. In the last example is also showed a 3D geometrical model for a simple 7x7 stranded rope. This is a very interesting result, since the use of excel and Autocad only allows to generate the exact shape of a wire with either single and double helix geometry.

II. DIFFERENTIAL GEOMETRY OF CURVES IN SPACE

1. PARAMETRIC DEFINITION OF THE CURVE

The geometry of a curve embedded in the three-dimensional Euclidean space can be conveniently described within a Cartesian reference system, which will be denoted in the following as the *global* reference system. The axes of the global reference system will be (x_1, x_2, x_3), while the corresponding unit vectors are $\underline{e}_1$, $\underline{e}_2$, $\underline{e}_3$. Let us introduce a parametric representation of an arch $\in \Gamma$ of a curve as follows

$$\Gamma: t \in [a,b] \rightarrow \underline{x}(t) \in \mathbb{R}^3$$

Where t is scalar parameter and $\underline{x}(t)$ is the position vector of a generic point of Γ in the global reference frame.
The total length of the arch can be computed by integration of infinitesimal segments directed as the local tangent vector.

$$S = \int_a^b \left|\underline{x}'(t)\right| dt$$

Where the apex indicates the total derivative with respect the parameter t and the symbol $|.|$ is the Euclidean norm in R^3.
The intrinsic parametrization consists of using as free coordinate to describe the curve the curvilinear abscissa defined as follows.

$$(1.II.1.1) \quad s(t) = \int_{t_0}^{t} \left|\underline{x}'(t)\right| d\tau$$

This peculiar geometrical quantity may be called the natural parameter for the representation of the curve and from its definition the fundamental differential relation between the intrinsic and the generic parametrization is introduced like in (Kreyszig, 1992).

$$(1.II.1.2) \quad \frac{ds}{dt} = s'(t) = \left|\underline{x}'(t)\right|$$

The operation of derivation with respect the natural coordinate will be indicated with an upper dot to be distinguished from the generic parametrization.

2. THE SERRET-FRENET FRAME OF THE CURVE

In literature, an intrinsic, or *local*, reference frame is usually defined, such that one of its axes is always tangent to the curve. The natural parametrization is the principal framework to set the description of the local reference system, also named as the Serret-Frenet frame like in Kryeszig's book. Still it is not the only possible representation, as a matter of fact all allowable parametrizations can be used introducing suitable modifications to the formulas.
In the following the main formulas for a complete description of the local reference system will be developed.

2.1. TANGENT VECTOR AND DIRECTION

The tangent vector detects the direction of the curve in every point. By definitions, it is locally tangent to the curve. Moreover, the norm is always one.

NATURAL PARAMETRIZATION

$$(1.II.2.1) \quad \underline{t}(s) \stackrel{\text{def}}{=} \dot{\underline{x}}(s)$$

GENERIC PARAMETRIZATION

The first derivative of the vector does not coincide with the tangent vector. For that reason, a normalization must be performed.

$\dot{\underline{x}}(t) = s'(t)\,\underline{x}'(t) \quad \Rightarrow \quad |\dot{\underline{x}}(t)| = s'(t)\,|\underline{x}'(t)| = 1$

$\underline{t}(t) = s'(t)\,\underline{x}'(t)$

2.2. NORMAL VECTOR AND CURVATURE

The first consequence following from the definition of the tangent vector is the so-called orthogonality condition. This relation states the normality between the first and second derivative vectors of the curve.

$\underline{t} * \underline{t} = 1 \;\rightarrow\; \dot{\underline{x}} * \dot{\underline{x}} = 1 \;\rightarrow\; \frac{\partial}{\partial s}(\dot{\underline{x}} * \dot{\underline{x}}) = 0$

Hence the following result holds

$(1.II.2.2) \quad \dot{\underline{x}}(s) * \ddot{\underline{x}}(s) = 0$

2.2.1. CURVATURE

The relation (II.1) allows to introduce the concept of curvature. This geometrical quantity measures the local relative variation of the tangent vector through a rotation about a specific direction. The direction under investigation is detected by the second derivative vector, hence normal to the tangent one, according to the orthogonality condition.

NATURAL PARAMETRIZATION

$\kappa \overset{\text{def}}{=} \frac{d\theta}{ds}$

Where dθ is the angle variation about the previously described direction, between two points of the curve at distance ds.

$d\theta \to 0 \;\Rightarrow d\theta \cong \sin d\theta = \frac{|\underline{t}(s) \wedge \underline{t}(s+ds)|}{|\underline{t}(s)|\,|\underline{t}(s+ds)|}$

Since $|\underline{t}|$ is equal to one along the whole curve and the first order Taylor expansion of the tangent vector is

$\underline{t}(s+ds) = \dot{\underline{x}}(s) + \ddot{\underline{x}}(s)\,ds + \underline{o}(s) \;\Rightarrow\; \underline{t}(s) \wedge \underline{t}(s+ds) = \dot{\underline{x}}(s) \wedge \cancel{\dot{\underline{x}}(s)} + \dot{\underline{x}}(s) \wedge \ddot{\underline{x}}(s)\,ds + \underline{o}(s) = \dot{\underline{x}}(s) \wedge \ddot{\underline{x}}(s)\,ds + \underline{o}(s)$

The last equality holds true because the velocity vector is parallel to itself. Moreover, because of the orthogonality condition, also the following relation can be introduced:

$d\theta = |\dot{\underline{x}}(s) \wedge \ddot{\underline{x}}(s)|\,ds = |\dot{\underline{x}}(s)|\,|\ddot{\underline{x}}(s)|\,ds = |\ddot{\underline{x}}(s)|\,ds$

Hence the curvature within the natural parametrization has the following shape

$(1.II.2.3a) \quad \kappa(s) = |\ddot{\underline{x}}(s)|$

Conversely, the inverse of the curvature is named the radius of curvature and its geometrical interpretation will be clarified afterwards.

$(1.II.2.3b) \quad \rho(s) = \kappa^{-1}(s)$

GENERIC PARAMETRIZATION

By recalling eq. (II.1.2) and (II.2.3a) the curvature can be evaluated as follows:

$(1.II.2.4) \quad \kappa(t) = s'^{2}(t)\,|\underline{x}''(t)|$

The definition of the radius of curvature follows.

2.2.2. NORMAL VECTOR

The normal vector is parallel to the second derivative vector and has unit norm. Hence, the relative rotation measuring the curvature is about this unit vector. Tangent and normal direction define a plane inside which the curvature can be measured. Specifically, the radius of curvature represents the radius of the circumference tangent to the curve and belonging to the mentioned plane.

NATURAL PARAMETRIZATION

$$(1.II.2.5) \quad \underline{n}(s) = \rho(s)\ \ddot{\underline{x}}(s)$$

GENERIC PARAMETRIZATION

$$(1.II.2.6) \quad \underline{n}(t) = \rho(t)\, s'^{2}(t)\, \underline{x}''(t) = \frac{\underline{x}''(t)}{\left|\underline{x}''(t)\right|}$$

2.3. BINORMAL VECTOR AND TORSION

2.3.1. BINORMAL VECTOR

The binormal vector ~~it~~ is defined according to the right-hand screw rule, starting from the knowledge of the tangent and normal vectors

$$\underline{b} = \underline{t} \wedge \underline{n}$$

NATURAL PARAMETRIZATION

$$(1.II.2.7) \quad \underline{b}(s) = \rho(s)\, \dot{\underline{x}}(s) \wedge \ddot{\underline{x}}(s)$$

GENERIC PARAMETRIZATION

$$(1.II.2.8) \quad \underline{b}(t) = \rho(t)\, s'^{3}(t)\, \underline{x}'(t) \wedge \underline{x}''(t) = s'(t)\, \frac{\underline{x}'(t)\ \wedge\ \underline{x}''(t)}{\left|\underline{x}''(t)\right|}$$

2.3.2. OSCULATING PLANE

The plane orthogonal to the binormal vector is called osculating plane. By definitions, the tangent and normal vectors belong to that plane. The plane equation is provided by the following relations.

$$\left[\underline{x}^{OP} - \underline{x}(s)\right] * \underline{b}(s) = 0 \quad \Rightarrow \quad \left[\underline{x}^{OP} - \underline{x}(s)\right] * \dot{\underline{x}}(s) \wedge \ddot{\underline{x}}(s) = 0$$

2.3.3. TORSION

NATURAL PARAMETRIZATION

The torsion is defined as the angular variation of the osculating plane about the curve path.

$$\tau \overset{\text{def}}{\equiv} \frac{d\varphi}{ds}$$

Where dϕ is the angular variation of the binormal vector along the curve.

$$d\varphi \to 0 \ \Rightarrow d\varphi \cong \sin d\varphi = \frac{\left|\underline{b}(s) \wedge \underline{b}(s+ds)\right|}{\left|\underline{b}(s)\right| \left|\underline{b}(s+ds)\right|}$$

With an approach like the one adopted to evaluate the curvature, and exploiting the first order Taylor expansions, the following equations can be easily derived:

$\underline{\dot{x}}(s+ds) \wedge \underline{\ddot{x}}(s+ds) = \left[\underline{\dot{x}}(s) + \underline{\ddot{x}}(s)\, ds + \underline{o}(s)\right] \wedge \left[\underline{\ddot{x}}(s) + \underline{\dddot{x}}(s)\, ds + \underline{o}(s)\right] = \underline{\dot{x}}(s) \wedge \underline{\ddot{x}}(s) + \underline{\dot{x}}(s) \wedge \underline{\dddot{x}}(s)\, ds + \underline{o}(s)$

$\left[\underline{\dot{x}}(s) \wedge \underline{\ddot{x}}(s)\right] \wedge \left[\underline{\dot{x}}(s) \wedge \underline{\ddot{x}}(s) + \underline{\dot{x}}(s) \wedge \underline{\dddot{x}}(s)\, ds + \underline{o}(s)\right] = \left[\underline{\dot{x}}(s) \wedge \underline{\ddot{x}}(s)\right] \wedge \left[\underline{\dot{x}}(s) \wedge \underline{\dddot{x}}(s)\, ds\right] + \underline{o}(s) = \left[\left(\underline{\dot{x}} * \left(\underline{\dot{x}} \wedge \underline{\ddot{x}}\right)\right) * \underline{\ddot{x}} - \left(\underline{\ddot{x}} * \left(\underline{\dot{x}} \wedge \underline{\ddot{x}}\right)\right) * \underline{\dot{x}}\right] ds$

$= \left[\underline{\dot{x}} * \underline{\ddot{x}} \wedge \underline{\ddot{x}}\right] * \underline{\dot{x}}\, ds$

$\left|\left[\underline{\dot{x}} * \underline{\ddot{x}} \wedge \underline{\ddot{x}}\right] * \underline{\dot{x}}\right| = \left|\underline{\dot{x}} * \underline{\ddot{x}} \wedge \underline{\ddot{x}}\right| * \left|\underline{\dot{x}}\right| = \left|\underline{\dot{x}} * \underline{\ddot{x}} \wedge \underline{\ddot{x}}\right|$

Hence the final shape of the torsion is the following

$$(1.II.2.8) \quad \tau(s) = \rho^2(s) \left|\underline{\dot{x}}(s) * \underline{\ddot{x}}(s) \wedge \underline{\dddot{x}}(s)\right|$$

GENERIC PARAMETRIZATION

$$(1.II.2.9) \quad \tau(t) = \rho^2(t)\, s'^6(t) \left|\underline{x}'(t) * \underline{x}''(t) \wedge \underline{x}'''(t)\right| = s'^2(t) \frac{\left|\underline{x}'(t) * \underline{x}''(t) \wedge \underline{x}'''(t)\right|}{\left|\underline{x}''(t)\right|^2}$$

3. SERRET-FRENET FORMULAE

In the literature the Serret-Frenet formulae describe the relations holding between tangent, normal and binormal unit vectors derivatives and the vectors themselves. Firstly, the relations will be derived through simple geometrical considerations, then they will be collected in compact matrix form.

3.1. DERIVATION OF THE FORMULAE

Since the purpose is to obtain a relation between the derivative of a generic unit vector and all the unit vectors of the Serret-Frenet frame, the procedure is based on evaluating the components of the derivative vector within the local system.

3.1.1. TANGENT VECTOR DERIVATIVE

The tangent vector derivative is a direct consequence of the definition of the normal unit vector (II.2.5).

$\underline{n} = \rho\, \underline{\ddot{x}} \quad \Rightarrow \quad \underline{\dot{t}} = \kappa\, \underline{n}$

3.1.2. BINORMAL VECTOR DERIVATIVE

The derivative vector component of the binormal unit vector are derived through projection on the axis of the Serret-Frenet frame.

$\underline{b} * \underline{b} = 1 \quad \Rightarrow \quad \underline{\dot{b}} * \underline{b} = 0$

$\underline{b} * \underline{t} = 0 \quad \Rightarrow \quad \underline{\dot{b}} * \underline{t} + \underline{b} * \underline{\dot{t}} = 0 \quad \Rightarrow \quad \underline{\dot{b}} * \underline{t} + \cancel{\kappa * \underline{b} * \underline{n}} = 0 \quad \Rightarrow \quad \underline{\dot{b}} * \underline{t} = 0$

Being the derivative vector orthogonal to tangent and binormal vector, it must be parallel to the normal unit vector.

$\underline{\dot{b}} = \dot{\rho}\, \underline{\dot{x}} \wedge \underline{\ddot{x}} + \cancel{\rho\, \underline{\ddot{x}} \wedge \underline{\ddot{x}}} + \rho\, \underline{\dot{x}} \wedge \underline{\dddot{x}}$

$\underline{\dot{b}} * \underline{n} = \dot{\rho}\, \cancel{\rho\, \underline{\dot{x}} \wedge \underline{\ddot{x}} * \underline{\ddot{x}}} + \rho^2\, \underline{\dot{x}} \wedge \underline{\dddot{x}} * \underline{\ddot{x}} = -\tau$

3.1.3. NORMAL VECTOR DERIVATIVE

The derivative vector component of the normal unit vector is derived through projection on the axis of the Serret-Frenet frame.

$\underline{n} * \underline{n} = 1 \quad \Rightarrow \quad \underline{\dot{n}} * \underline{n} = 0$

$\underline{n} * \underline{t} = 0 \quad \Rightarrow \quad \underline{\dot{n}} * \underline{t} + \underline{n} * \underline{\dot{t}} = 0 \quad \Rightarrow \quad \underline{\dot{n}} * \underline{t} + \kappa = 0 \quad \Rightarrow \quad \underline{\dot{n}} * \underline{t} = -\kappa$

$\underline{n} * \underline{b} = 0 \quad \Rightarrow \quad \dot{\underline{n}} * \underline{b} + \underline{n} * \dot{\underline{b}} = 0 \quad \Rightarrow \quad \dot{\underline{n}} * \underline{b} + \tau = 0 \quad \Rightarrow \quad \dot{\underline{n}} * \underline{t} = -\tau$

3.2. FRAME DERIVATION MATRIX

The derivative operation of the Serret-Frenet reference frame's unit vectors is completely defined by a skew symmetric matrix dependent only upon curvature and torsion.

$$\underline{\underline{\Omega}}(s) = \begin{bmatrix} 0 & \kappa(s) & 0 \\ -\kappa(s) & 0 & \tau(s) \\ 0 & -\tau(s) & 0 \end{bmatrix} \quad \Rightarrow \quad \begin{vmatrix} \dot{\underline{t}}(s) \\ \dot{\underline{n}}(s) \\ \dot{\underline{b}}(s) \end{vmatrix} = \begin{bmatrix} 0 & \kappa(s) & 0 \\ -\kappa(s) & 0 & \tau(s) \\ 0 & -\tau(s) & 0 \end{bmatrix} * \begin{vmatrix} \underline{t}(s) \\ \underline{n}(s) \\ \underline{b}(s) \end{vmatrix}$$

Alternatively, the formulae may be explicitly written as follows.

$\dot{\underline{t}}(s) = \kappa(s)\, \underline{n}(s)$

$\dot{\underline{n}}(s) = -\kappa(s)\, \underline{t}(s) + \tau(s)\, \underline{b}(s)$

$\dot{\underline{b}}(s) = -\tau(s)\, \underline{n}(s)$

III. SINGLE HELIX GEOMTRY

1. CONSTRUCTION OF THE HELIX

A single helix is a tridimensional curve in space. The geometry may be generated as shown in the picture below. Firstly, a straight line shall be drawn inside a vertical plane. Then the plane would be bent about an axis with the following features: it is parallel to the plane, at a constant distance and forming an angle with the original line. The horizontal projection of the curve is a circumference once the plane is bent. The original line is the single helix itself, the second one is the helix axis, the distance is called the radius and the angle between the two is named lay angle of the helix. All geometrical features referred to the single helix are endowed with the subscript upper-case I.
Moreover, if the distance between the plane and the helix axis is chosen such that the vertical projection of the original line is equal to 2π the distance as shown in figure 1.1, the side projection of the line will be the pitch of the helix. The pitch is the length along the curve axis identifying the period.

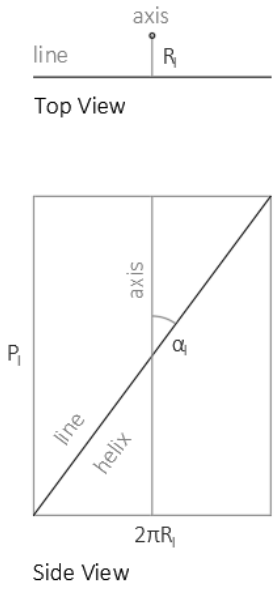

Fig 1.6 Developed Geometry of the Single Helix

From these definitions it's possible to compute the relation holding among helix radius R_I, pitch or lay length P_I and lay angle α_I.

$$(1.III.1) \quad \tan \alpha_I = \frac{2\pi R_I}{P_I}$$

2. DEVELOPED VIEW OF THE HELIX

The former description shows how a single helix, which is a three-dimensional curve, can be developed within a plane. Moreover, it is possible to find an important relation which links at infinitesimal level the curvilinear abscissa with the swept angle. This last geometrical quantity is named with the Greek letter θ. In the following picture it is demonstrated where the geometrical relations are coming from.

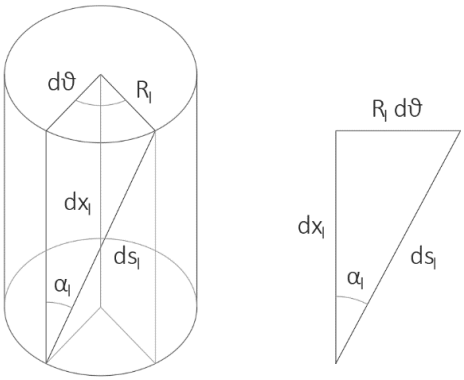

Fig 1.7 Differential Developed Geometry of the Single Helix

$dx_1 \tan \alpha_I = R_I d\vartheta$

$ds_I \sin \alpha_I = R_I d\vartheta$

These are the fundamental expressions of the developed geometry, where x_1 is the global coordinate parallel to the helix axis. The first differential equation leads to the following relation:

$$(1.III.2) \quad \theta'(x_1) = \frac{d\vartheta}{dx_1} = \frac{\tan \alpha_I}{R_I}$$

Hence, the swept angle may be related to the coordinate x_1 with a linear relation.

$$\vartheta(x_1) = \vartheta_0 + \frac{\tan \alpha_I}{R_I} x_1$$

3. LOCAL AND GLOBAL REFERENCE FRAMES

The global reference frame is (x_1, x_2, x_3) and it's obtained with the right-handed screw. Here the x_1 axis coincide with the single helix axis, while x_2 and x_3 belong to the orthogonal plane where the single helix projection coincides with a circumference. The attached Serret-Frenet frames are denoted as (t_I, n_I, b_I). The curvilinear coordinate is s_I. The swept angle is $\theta(s_I)$, while θ_0 is the initial swept angle representing the phase shift of the helix along its axis. The helix radius is R_I.

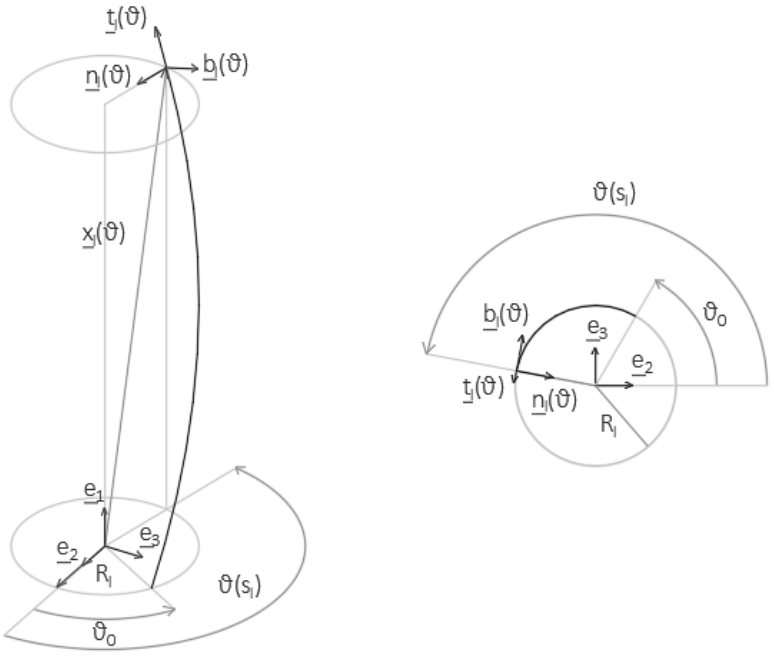

Fig 1.8 Single Helix Geometry

4. POSITION VECTOR OF THE HELIX

Since the global coordinate x_1 is linked with the swept angle and the local abscissa with the differential relation aforesaid (III.2), the position of the single helix curve within the global reference frame can be expressed as follows.

$$x_{I1}(x_1) = x_1$$

$$(1.III.4) \quad x_{I2}(x_1) = R_I \cos\theta(x_1)$$

$$x_{I3}(x_1) = R_I \sin\theta(x_1)$$

Where $x_{Ii}(x_1)$ is the i-th component of the position vector in the global reference frame (x_1, x_2, x_3), R_I is the helix radius and $\theta(x_1)$ the swept angle.

5. SERRET-FRENET FRAME OF THE SINGLE HELIX

5.1. TANGENT VECTOR AND ARCH LENGHT

The developed geometry leads to the following differential relation

$$\frac{dx_1}{ds_I} = \cos\alpha_I$$

$$\frac{d\vartheta}{ds_I} = \frac{\sin\alpha_I}{R_I}$$

The first derivative of the position vector has the following components:

$$\dot{x}_{I1}(x_1) = \frac{\partial}{\partial x_1}(x_1)\ \frac{dx_1}{ds_I} = \cos\alpha_I$$

$$\dot{x}_{I2}(x_1) = \frac{\partial}{\partial \theta}(R_I \cos\theta(x_1))\frac{d\vartheta}{ds_I} = -\sin\alpha_I\ \sin\theta(x_1)$$

$$\dot{x}_{I3}(x_1) = \frac{\partial}{\partial \theta}(R_I \sin\theta(x_1))\frac{d\vartheta}{ds_I} = \sin\alpha_I \cos\theta(x_1)$$

5.1.1. TANGENT VECTOR

Since the derivatives are with the dot, they are computed with respect the curvilinear abscissa. Hence, they correspond with the components of the tangent vector.

$$t_{I1}(x_1) = \cos\alpha_I$$

$$(1.III.5.1) \quad t_{I2}(x_1) = -\sin\alpha_I\ \sin\theta(x_1)$$

$$t_{I3}(x_1) = \sin\alpha_I \cos\theta(x_1)$$

Where $t_{Ii}(x_1)$ is the i-th component of the tangent unit vector in the global reference frame (x_1, x_2, x_3), α_I is the helix lay angle and $\theta(x_1)$ the swept angle.

5.1.2. ARCH LENGHT

The length of a portion of the double helix may be computed through the following relation

$$S_I(x_1) = \int_0^{x_1} \left\| \underline{x}'_I(x_1) \right\| dx_1$$

Differentiating both members of the previous equation we obtain the constraint holding between the global coordinate x_1 and the curvilinear coordinate of the single helix s_I.

$$\frac{ds_I}{dx_1}(x_1) = \left\| \underline{x}'_I(x_1) \right\|$$

It is important to underline that the apex is the derivative with respect the global coordinate x_1. From the developed geometry (1.III.2) we get the following relation which allows to compute the afore mentioned derivative vector.

$$\frac{d\vartheta}{dx_1} = \frac{\tan\alpha_I}{R_I}$$

The explicit expressions of the components of the first derivative vector with respect the global coordinate x_1 is introduced in the following.

$$x'_{I1}(x_1) = \frac{\partial}{\partial x_1}(x_1) = 1$$

$$x'_{I2}(x_1) = \frac{\partial}{\partial \theta}(R_I \cos\theta(x_1))\frac{d\vartheta}{dx_1} = -\tan\alpha_I \sin\theta(x_1)$$

$$x'_{I3}(x_1) = \frac{\partial}{\partial \theta}(R_I \sin\theta(x_1))\frac{d\vartheta}{dx_1} = \tan\alpha_I \cos\theta(x_1)$$

Hence, the modulus of the first derivative vector can be computed.

$$\left\| \underline{x}'_I(x_1) \right\| = \sqrt{1 + \tan^2\alpha_I} = \frac{1}{\cos\alpha_I}$$

This result would have been obtained by the developed geometry as well. Hence, this prove that the single helix may be perfectly developed within a plane.

$$(1.III.5.2) \quad \frac{ds_I}{dx_1}(x_1) = \frac{1}{\cos\alpha_I}$$

5.2. NORMAL VECTOR AND CURVATURE

The second derivative of the position vector has the following components:

$$\ddot{x}_{I1}(x_1) = \frac{\partial}{\partial x_1}(\cos\alpha_I)\ \frac{dx_1}{ds_I} = 0$$

$$\ddot{x}_{I2}(x_1) = \frac{\partial}{\partial\theta}(-\sin\alpha_I\ \sin\theta(x_1))\frac{d\vartheta}{ds_I} = -\frac{\sin^2\alpha_I}{R_I}\cos\theta(x_1)$$

$$\ddot{x}_{I3}(x_1) = \frac{\partial}{\partial\theta}(\sin\alpha_I\cos\theta(x_1))\frac{d\vartheta}{ds_I} = -\frac{\sin^2\alpha_I}{R_I}\sin\theta(x_1)$$

5.2.1. CURVATURE

If we recall the formulas providing the curvature we get the following result.

$$(1.III.5.3) \quad \kappa_I(x_1) = \left|\underline{\ddot{x}}_I(x_1)\right| = \frac{\sin^2\alpha_I}{R_I}$$

Where κ_I is the curvature, α_I is the lay angle and R_I is the radius of the single helix.
The curvature is constant along the single helix.

5.2.2. NORMAL VECTOR

The final shape of the normal vector is as follows.

$$n_{I1}(x_1) = 0$$

$$(1.III.5.4) \quad n_{I2}(x_1) = -\cos\theta(x_1)$$

$$n_{I3}(x_1) = -\sin\theta(x_1)$$

Where $n_{Ii}(x_1)$ is the i-th component of the normal unit vector in the global reference frame (x_1, x_2, x_3) and $\theta(x_1)$ the swept angle.
It is interesting to notice that the first component is always identically null. This means that the normal vector lays within the plane orthogonal to the helix axis and thus it doesn't depend upon the lay angle of the helix. Moreover, it points towards the global axis x_1.

5.3. BINORMAL VECTOR AND TORSION

The third derivative of the position vector has the following components:

$$\dddot{x}_{I1}(x_1) = 0$$

$$\dddot{x}_{I2}(x_1) = \frac{\partial}{\partial\theta}\left(-\frac{\sin^2\alpha_I}{R_I}\cos\theta(x_1)\right)\frac{d\vartheta}{ds_I} = \frac{\sin^3\alpha_I}{R_I^2}\sin\theta(x_1)$$

$$\dddot{x}_{I3}(x_1) = \frac{\partial}{\partial\theta}\left(-\frac{\sin^2\alpha_I}{R_I}\sin\theta(x_1)\right)\frac{d\vartheta}{ds_I} = -\frac{\sin^3\alpha_I}{R_I^2}\cos\theta(x_1)$$

5.3.1. BINORMAL VECTOR

It is obtained by the tangent and normal vector with the right-handed screw.

$$\underline{b}_I(x_1) = \underline{t}_I(x_1) \wedge \underline{n}_I(x_1) = \begin{vmatrix} \underline{e}_x & \underline{e}_y & \underline{e}_z \\ \cos\alpha_I & -\sin\alpha_I \sin\theta(x_1) & \sin\alpha_I \cos\theta(x_1) \\ 0 & -\cos\theta(x_1) & -\sin\theta(x_1) \end{vmatrix}$$

The result is as follows.

$$b_{I1}(x_1) = \sin\alpha_I$$

$$(1.III.5.5) \quad b_{I2}(x_1) = \cos\alpha_I \ \sin\theta(x_1)$$

$$b_{I3}(x_1) = -\cos\alpha_I \ \cos\theta(x_1)$$

Where $b_{Ii}(x_1)$ is the i-th component of the binormal unit vector in the global reference frame (x_1, x_2, x_3), α_I is the helix lay angle and $\theta(x_1)$ the swept angle.

5.3.2. TORSION

$$\tau_I(x_1) = \rho_I^2(x_1) \left| \dot{\underline{x}}_I(x_1) * \ddot{\underline{x}}_I(x_1) \wedge \dddot{\underline{x}}_I(x_1) \right|$$

The result is the following.

$$(1.III.5.6) \quad \tau_I(x_1) = \frac{\sin\alpha_I \ \cos\alpha_I}{R_I}$$

Where τ_I is the torsion, α_I is the lay angle and R_I is the radius of the single helix.
The torsion is a geometrical property of the single helix which maintain the same value along the curve like the curvature.

IV. DOUBLE HELIX GEOMETRY

1. CONSTRUCTION OF THE HELIX

A double, or nested, helix is a 3D curve in space. It is obtained by coiling a single helix about an axis which isn't straight, but it is a single helix itself. The quantities referred to the single and double helices are denoted respectively with the I and II subscripts.

2. LOCAL AND GLOBAL REFERENCE FRAME

The global reference frame is (x_1, x_2, x_3) and it's obtained with the right-handed screw. Here the x_1 axis coincide with the single helix axis, while x_2 and x_3 belong to the orthogonal plane where the single helix projection coincides with a circumference. The attached Serret-Frenet frames are denoted as (t_i, n_i, b_i) being i either I or II. The curvilinear coordinates are s_i being i either I or II. Furthermore, two angles are introduced. The swept angle of the single helix θ is spanning from the axis x_2 to the vector of length R_I obtained from the origin of the global frame to the generic point of the single helix projection in the x_2x_3 plane. Hence, this angle detects a point on the circumference of radius R_I. Conversely, the swept angle of the double helix ϕ is defined into the single helix attached frame. Specifically, it spans from the position vector of the double helix $\underline{\mathbf{r}}(x_1)$ in the local frame of the single helix to the normal vector $\underline{\mathbf{n}}_I(x_1)$.

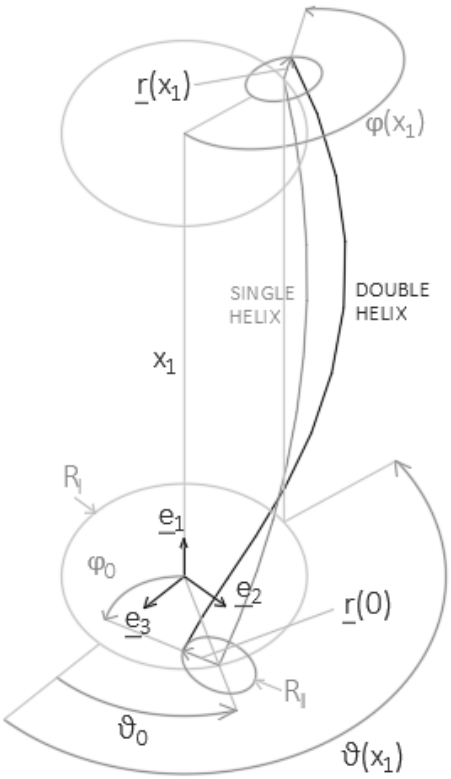

Fig 1.9 Double or Nested Helix Geometry

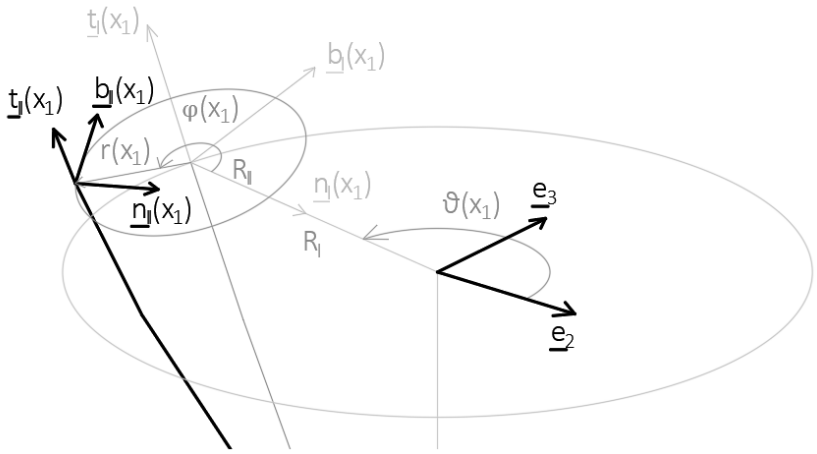

Fig 1.10 Serret-Frenet Frame of Single and Double Helix

3. DEVELOPED VIEW OF THE HELIX

In literature it is assumed that at the local level the nested helix geometry may be developed into a plane such that the following trigonometric relations hold. The idea is the same shown for the single helix, the difference is that it is applied twice with a proper order like is shown in the papers of Usabiaga and Pagalday, 2008 and Xiang et al.,2015.

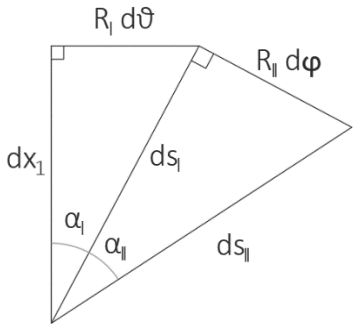

Fig 1.11 Differential Developed Geometry of the Double Helix

$dx_1 \tan \alpha_I = R_I d\vartheta$

$ds_I \sin \alpha_I = R_I d\vartheta$

$ds_I \tan \alpha_{II} = R_{II} d\varphi$

$ds_{II} \cos \alpha_{II} = ds_I$

Where x_1 is the global coordinate coincident with the single helix axis, s_i is the curvilinear coordinate of the i-th helix, α_i is the lay angle of the i-th helix and R_i is the i-th helix radius. The index i may be either I for the single helix or II for the double helix. The coordinate θ and ϕ are the swept angle of the single and nested helix respectively like it shown in Fig 1.4 and Fig. 1.5.

From these relations it is possible to link the different coordinates of the geometrical problem. The fundamental constraint is introduced through the parameter m.

$$d\varphi = \frac{R_I}{R_{II}} \frac{\tan \alpha_{II}}{\sin \alpha_I} \, d\vartheta = m \, d\vartheta$$

This relation lead to the following differential relations

$$(1.IV.3.1) \quad \theta'(x_1) = \frac{d\vartheta}{dx_1} = \frac{\tan \alpha_I}{R_I}$$

$$(1.IV.3.2) \quad \varphi'(x_1) = \frac{d\varphi}{dx_1} = \frac{\tan \alpha_{II}}{R_{II} \cos \alpha_I}$$

Hence, the two swept angles may be related to the coordinate x_1 as follows.

$$\vartheta(x_1) = \vartheta_0 + \frac{\tan \alpha_I}{R_I} \, x_1$$

$$\varphi(x_1) = \varphi_0 + \frac{\tan \alpha_{II}}{R_{II} \cos \alpha_I} \, x_1$$

4. POSITION VECTOR OF THE HELIX

The position vector of the double helix may be computed through simple geometrical considerations from Fig. 1.4.

$$\underline{x}_{II}(\vartheta, \varphi) = \underline{x}_I(\vartheta) + \underline{r}(\varphi)$$

The vector $\underline{r}$ is described into the attached frame of the single helix. Specifically, it belongs to the plane $\underline{n}_I \, \underline{b}_I$ and identifies the position of the point of the double helix intersecting such plane with respect the origin of the Serret-Frenet coordinate system.

$$\underline{r}(\varphi) = R_{II} \cos \varphi \, \underline{n}_I + R_{II} \sin \varphi \, \underline{b}_I$$

Introducing the definitions of the normal and binormal unit vectors of the single helix into the global reference system, it is possible to compute the component of the target position vector.

$$\underline{x}_{II} = \underline{x}_I + R_{II} \cos \varphi \left(-\cos \theta \, \underline{e}_2 - \sin \theta \, \underline{e}_3 \right) + R_{II} \sin \varphi \left(\sin \alpha_I \, \underline{e}_1 + \cos \alpha_I \sin \theta \, \underline{e}_2 - \cos \alpha_I \cos \theta \, \underline{e}_3 \right)$$

The components are explicitly written as follows.

$$(1.IV.4) \quad \begin{aligned} x_{II1}(x_1) &= x_1 + R_{II} \sin \alpha_I \sin \varphi(x_1) \\ x_{II2}(x_1) &= R_I \cos \theta(x_1) - R_{II} \cos \varphi(x_1) \cos \vartheta(x_1) + R_{II} \cos \alpha_I \sin \varphi(x_1) \sin \vartheta(x_1) \\ x_{II3}(x_1) &= R_I \sin \theta(x_1) - R_{II} \cos \varphi(x_1) \sin \vartheta(x_1) - R_{II} \cos \alpha_I \sin \varphi(x_1) \cos \vartheta(x_1) \end{aligned}$$

Where $x_{IIi}(x_1)$ is the i-th component of the position vector of the nested helix in the global reference frame (x_1, x_2, x_3), R_I is the radius, α_I is the lay angle and $\theta(x_1)$ the swept angle of the single helix, while R_{II} is the radius, α_{II} is the lay angle and $\phi(x_1)$ the swept angle of the double helix.

5. SERRET-FRENET FRAME OF THE DOUBLE HELIX

The derivation of the Serret-Frenet frame is not simple as for the single helix. For the computation let us introduce some auxiliary trigonometric functions. They come from the additional terms to the single helix in the components of the position vector of the double helix (IV.4). The derivatives of these functions will be exploited in the following.

5.1. AUXILIARY TRIGONOMETRIC FUNCTIONS

The derivations are developed introducing the following auxiliary trigonometric functions

$$F_{cc}(x_1) = -\cos\varphi(x_1)\cos\vartheta(x_1)$$

$$F_{ss}(x_1) = +\sin\varphi(x_1)\sin\vartheta(x_1)$$

$$F_{cs}(x_1) = -\cos\varphi(x_1)\sin\vartheta(x_1)$$

$$F_{sc}(x_1) = -\sin\varphi(x_1)\cos\vartheta(x_1)$$

The derivative of these functions with respect the global coordinate x_1 may be computed through the rule for composite functions.

$$F'_{ij}(x_1) = \frac{dF_{ij}}{d\vartheta}\theta' + \frac{dF_{ij}}{d\varphi}\,\varphi'$$

First derivatives

$$F'_{cc} = -F_{cs}\theta' - F_{sc}\varphi'$$

$$F'_{ss} = -F_{sc}\theta' - F_{cs}\varphi'$$

$$F'_{cs} = +F_{cc}\theta' + F_{ss}\varphi'$$

$$F'_{sc} = +F_{ss}\theta' + F_{cc}\varphi'$$

Second derivatives

$$F''_{cc} = -\left(\theta'^2 + \varphi'^2\right)F_{cc} - 2\theta'\varphi' F_{ss}$$

$$F''_{ss} = -\left(\theta'^2 + \varphi'^2\right)F_{ss} - 2\theta'\varphi' F_{cc}$$

$$F''_{cs} = -\left(\theta'^2 + \varphi'^2\right)F_{cs} - 2\theta'\varphi' F_{sc}$$

$$F''_{sc} = -\left(\theta'^2 + \varphi'^2\right)F_{sc} - 2\theta'\varphi' F_{cs}$$

Third derivatives

$$F'''_{cc} = +\left(\theta'^3 + 3\theta'\varphi'^2\right)F_{cs} + \left(\varphi'^3 + 3\varphi'\theta'^2\right)F_{sc}$$

$$F'''_{ss} = +\left(\theta'^3 + 3\theta'\varphi'^2\right)F_{sc} + \left(\varphi'^3 + 3\varphi'\theta'^2\right)F_{cs}$$

$$F'''_{cs} = -\left(\theta'^3 + 3\theta'\varphi'^2\right)F_{cc} - \left(\varphi'^3 + 3\varphi'\theta'^2\right)F_{ss}$$

$$F'''_{sc} = -\left(\theta'^3 + 3\theta'\varphi'^2\right)F_{ss} - \left(\varphi'^3 + 3\varphi'\theta'^2\right)F_{cc}$$

5.2. TANGENT VECTOR AND ARCH LENGTH

First derivative of the position vector of the double helix

$$x'_{II1} = 1 + R_{II}\sin\alpha_I\cos\varphi\,\varphi'$$

$$x'_{II2} = -R_I\sin\theta\,\theta' + R_{II}[F'_{cc} + \cos\alpha_I\,F'_{ss}] = -R_I\sin\theta\,\theta' + R_{II}[(-F_{cs}\theta' - F_{sc}\varphi') + \cos\alpha_I\,(-F_{sc}\theta' - F_{cs}\varphi')]$$

$$x'_{II3} = +R_I\cos\theta\,\theta' + R_{II}[F'_{cs} + \cos\alpha_I\,F'_{sc}] = +R_I\cos\theta\,\theta' + R_{II}[(+F_{cc}\theta' + F_{ss}\varphi') + \cos\alpha_I\,(+F_{ss}\theta' + F_{cc}\varphi')]$$

Hence, collecting the common terms we get the following expressions

$$x'_{II1}(x_1) = 1 + R_{II}\sin\alpha_I\cos\varphi(x_1)\,\varphi'$$

$$x'_{II2}(x_1) = -R_I\theta'\sin\theta(x_1) + R_{II}(\theta' + \cos\alpha_I\,\varphi')\cos\varphi(x_1)\sin\vartheta(x_1) + R_{II}(\varphi' + \cos\alpha_I\,\theta')\sin\varphi(x_1)\cos\vartheta(x_1)$$

$$x'_{II3}(x_1) = +R_I\theta'\cos\theta(x_1) - R_{II}(\theta' + \cos\alpha_I\,\varphi')\cos\varphi(x_1)\cos\vartheta(x_1) + R_{II}(\varphi' + \cos\alpha_I\,\theta')\sin\varphi(x_1)\sin\vartheta(x_1)$$

5.2.1. TANGENT VECTOR

Defining the norm of the first derivative of the position vector as follows

$$\left\|\underline{x}'_{II}(x_1)\right\| = \sqrt{\sum_{i=1}^{3} x'^2_{IIi}(x_1)}$$

This quantity is not constant since the curve has been parametrized through a variable which is not the curvilinear coordinate of the double helix, yet it can be appreciated that the norm shows a periodical trend. An example of this function may be found in V. Case Study.

$$(1.IV.5.1)\quad \underline{t}_{II}(x_1) = \left(t_{II1}(x_1), t_{II2}(x_1), t_{II3}(x_1)\right)^T = \left\|\underline{x}'_{II}(x_1)\right\|^{-1}\left(x'_{II1}(x_1), x'_{II2}(x_1), x'_{II3}(x_1)\right)^T$$

5.2.2. ARCH LENGTH

The length of a portion of the double helix may be computed through the following relation

$$S_{II}(x_1) = \int_0^{x_1}\left\|\underline{x}'_{II}(x_1)\right\| dx_1$$

Differentiating both members of the previous equation we obtain the constraint holding between the global coordinate x_1 and the curvilinear coordinate s_{II}.

$$(1.IV.5.2a)\quad \frac{ds_{II}}{dx_1}(x_1) = \left\|\underline{x}'_{II}(x_1)\right\|$$

An important remark must be done so far. The last relation would have been derived also from the geometrical constraints coming from the developed geometry of the double helix (par 3). The result has the following shape:

$$(1.IV.5.2b)\quad \frac{ds_{II}}{dx_1} = \frac{1}{\cos\alpha_I\cos\alpha_{II}}$$

This representation provides a constant derivative with respect the global coordinate x_1, which do not correspond to the actual trend of the double helix second derivative modulus. That result shows that the developed geometry is an approximation for the double helix, hence it can't be developed exactly into a plane, differently from the single helix. The importance of this result will be evident in the following chapter regarding the wire mechanics. As a matter of fact, the response will be significantly affected by this function, since the local stresses in the single wire are directly proportional to the square power of this quantity.
The plot of this function may be seen in V. Case Study.

5.3. NORMAL VECTOR AND CURVATURE

Second derivative of the position vector of the double helix

$$x''_{II1} = -R_{II}\sin\alpha_I\sin\varphi\,\varphi'^2$$

$$x''_{II2} = -R_I\cos\theta\,\theta'^2 + R_{II}[F''_{cc} + \cos\alpha_I\,F''_{ss}] = -R_I\cos\theta\,\theta'^2 + R_{II}\left[\left(-\left(\theta'^2 + \varphi'^2\right)F_{cc} - 2\theta'\varphi'F_{ss}\right) + \cos\alpha_I\left(-\left(\theta'^2 + \varphi'^2\right)F_{ss} - 2\theta'\varphi'F_{cc}\right)\right]$$

$$x''_{II3} = -R_I\sin\theta\,\theta'^2 + R_{II}[F''_{cs} + \cos\alpha_I\,F''_{sc}] = -R_I\sin\theta\,\theta'^2 + R_{II}\left[\left(-\left(\theta'^2 + \varphi'^2\right)F_{cs} - 2\theta'\varphi'F_{sc}\right) + \cos\alpha_I\left(-\left(\theta'^2 + \varphi'^2\right)F_{sc} - 2\theta'\varphi'F_{cs}\right)\right]$$

Hence, collecting the common terms we get the following expressions

$$x''_{II1}(x_1) = -R_{II}\sin\alpha_I\,\varphi'^2\sin\varphi(x_1)$$

$$x''_{II2}(x_1) = -R_I\theta'^2\cos\theta(x_1) + R_{II}[(\theta'^2+\varphi'^2) + 2\cos\alpha_I\,\theta'\varphi']\cos\varphi(x_1)\cos\vartheta(x_1) - R_{II}[\cos\alpha_I\,(\theta'^2+\varphi'^2) + 2\theta'\varphi']\sin\varphi(x_1)\sin\vartheta(x_1)$$

$$x''_{II3}(x_1) = -R_I\theta'^2\sin\theta(x_1) + R_{II}[(\theta'^2+\varphi'^2) + 2\cos\alpha_I\,\theta'\varphi']\cos\varphi(x_1)\sin\vartheta(x_1) - R_{II}[\cos\alpha_I\,(\theta'^2+\varphi'^2) + 2\theta'\varphi']\sin\varphi(x_1)\sin\vartheta(x_1)$$

5.3.1. NORMAL VECTOR

Defining the norm of the second derivative of the position vector as follows

$$\left\|\underline{x}''_{II}(x_1)\right\| = \sqrt{\sum_{i=1}^{3} x''^2_{IIi}(x_1)}$$

This quantity is not constant since the curve has been parametrized through a variable which is not the curvilinear coordinate of the double helix, yet it can be appreciated that the norm shows a periodical trend.

$$(1.IV.5.3)\quad \underline{n}_{II}(x_1) = \left(n_{II1}(x_1), n_{II2}(x_1), n_{II3}(x_1)\right)^T = \left\|\underline{x}''_{II}(x_1)\right\|^{-1}\left(x''_{II1}(x_1), x''_{II2}(x_1), x''_{II3}(x_1)\right)^T$$

5.3.2. CURVATURE

The definition of curvature must be slightly modified because of the choice of parametrization which differs from the curvilinear coordinate of the curve.

$$(1.IV.5.5)\quad \kappa_{II}(x_1) = \left[\frac{ds_{II}}{dx_1}(x_1)\right]^2 \left\|\underline{x}''_{II}(x_1)\right\|$$

The expression of the radius follows this definition

$$(1.IV.5.6)\quad \rho_{II}(x_1) = \kappa_{II}^{-1}(x_1)$$

It is worth it to notice the periodical trend of the curvature and the curvature radius, differently from the constant values of the single helix along the curve path.

5.4. BINORMAL VECTOR AND TORSION

Third derivative of the position vector of the double helix

$$x'''_{II1} = -R_{II}\sin\alpha_I\cos\varphi\,\varphi'^3$$

$$x'''_{II2} = +R_I\sin\theta\,\theta'^3 + R_{II}[F'''_{cc} + \cos\alpha_I\,F'''_{ss}] = +R_I\sin\theta\,\theta'^3 + R_{II}\left[\left(+\left(\theta'^3+3\theta'\varphi'^2\right)F_{cs} + \left(\varphi'^3+3\varphi'\theta'^2\right)F_{sc}\right) + \cos\alpha_I\left(+\left(\theta'^3+3\theta'\varphi'^2\right)F_{sc} + \left(\varphi'^3+3\varphi'\theta'^2\right)F_{cs}\right)\right]$$

$$x'''_{II3} = -R_I\cos\theta\,\theta'^3 + R_{II}[F'''_{cs} + \cos\alpha_I\,F'''_{sc}] = -R_I\cos\theta\,\theta'^3 + R_{II}\left[\left(-\left(\theta'^3+3\theta'\varphi'^2\right)F_{cc} - \left(\varphi'^3+3\varphi'\theta'^2\right)F_{ss}\right) + \cos\alpha_I\left(-\left(\theta'^3+3\theta'\varphi'^2\right)F_{ss} - \left(\varphi'^3+3\varphi'\theta'^2\right)F_{cc}\right)\right]$$

Hence, collecting the common terms we get the following expressions

$$x'''_{II1}(x_1) = -R_{II}\sin\alpha_I\,\varphi'^3\cos\varphi(x_1)$$

$$x'''_{II2}(x_1) = +R_I\theta'^3\sin\theta(x_1) - R_{II}[(\theta'^3+3\theta'\varphi'^2) + \cos\alpha_I\,(\varphi'^3+3\varphi'\theta'^2)]\cos\varphi(x_1)\sin\vartheta(x_1) - R_{II}[\cos\alpha_I\,(\theta'^3+3\theta'\varphi'^2) + (\varphi'^3+3\varphi'\theta'^2)]\sin\varphi(x_1)\cos\vartheta(x_1)$$

$$x'''_{II3}(x_1) = -R_I\theta'^3\cos\theta(x_1) + R_{II}[(\theta'^3+3\theta'\varphi'^2) + \cos\alpha_I\,(\varphi'^3+3\varphi'\theta'^2)]\cos\varphi(x_1)\cos\vartheta(x_1) - R_{II}[\cos\alpha_I\,(\theta'^3+3\theta'\varphi'^2) + (\varphi'^3+3\varphi'\theta'^2]\sin\varphi(x_1)\sin\vartheta(x_1)$$

5.4.1. BINORMAL VECTOR

The binormal vector is derived directly by the tangent and normal ones in order to obtain a right-handed screw.

$$\underline{b}_{II}(x_1) = \underline{t}_{II}(x_1) \wedge \underline{n}_{II}(x_1)$$

Hence the components are obtained through the vector product.

$$(1.IV.5.6)\quad \begin{aligned} b_{II1}(x_1) &= t_{II2}(x_1)n_{II3}(x_1) - t_{II3}(x_1)n_{II2}(x_1) \\ b_{II2}(x_1) &= t_{II3}(x_1)n_{II1}(x_1) - t_{II1}(x_1)n_{II3}(x_1) \\ b_{II3}(x_1) &= t_{II1}(x_1)n_{II2}(x_1) - t_{II2}(x_1)n_{II1}(x_1) \end{aligned}$$

5.4.2. TORSION

The definition of torsion must be slightly modified because of the choice of parametrization which differs from the curvilinear coordinate of the curve.

$$\tau_{II}(x_1) = \left[\frac{ds_{II}}{dx_1}(x_1)\right]^6 \rho_{II}(x_1) \left|\underline{x}'_{II}(x_1) * \underline{x}''_{II}(x_1) \wedge \underline{x}'''_{II}(x_1)\right|$$

The explicit expression is as follows

$$(1.IV.5.7)\quad \tau_{II} = \left(\frac{ds_{II}}{dx_1}\right)^6 \rho_{II} \left|x'_{II1}(x''_{II2}x'''_{II3} - x'''_{II2}x''_{II3}) - x'_{II2}(x''_{II1}x'''_{II3} - x'''_{II1}x''_{II3}) + x'_{II3}(x''_{II1}x'''_{II2} - x'''_{II1}x''_{II2})\right|$$

V. CASE STUDY: NESTED HELIX IN STRANDED WIRE ROPES

The purpose of the following case studies is to provide an example of application of the mathematical model developed in this work to describe the internal geometry of metallic strands and wire ropes. When talking about wire ropes the subscripts “w” and “s” represent respectively wire and strand quantities. In the following the first will be used to denote the nested helix, while the second will be involved for the strand.

1. WIRE ROPE 33 mm 6x19 SEALE IWRC

The comparison between the results of the proposed formulation and the ones coming from (Wang et al., 1998) will be reported in the following. The single and double helix that are investigated are the core and the outer wires centerlines of a single layer strand. Hence the strand we are analysing is coiled within the rope to form a single helix itself. The length of the rope considered is about 103 mm, which corresponds to two periods of the the double helix.

1.1. INPUT GEOMETRY

The analysis is performed over two wires. The first is called W20 and it has a single helix centreline, while W21 has a double helix one that depends upon the W20 single helix.
The main geometrical feature used for the computations are reported in Table 1. In Fig. 1.7 it is possible to see in plan view the position of the wires under inspection and the correspondent helix radius. In Fig. 1.8 a three-dimensional view of the two wires is showed.

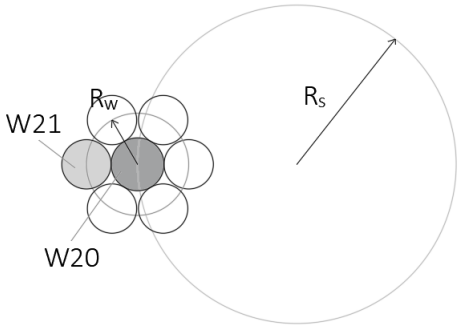

Fig 1.12 Single and Double Helix Wires Scheme

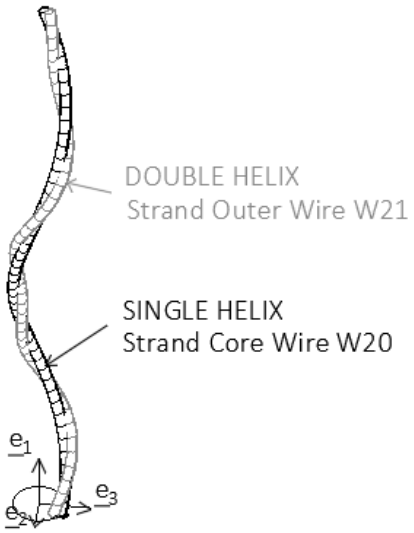

Fig 1.13 Single and Double Helix Wires Three-Dimensional View

Table 1.1 Wire Geometry Data

	R [mm]	P [mm]	α [°]	θ_0 [°]	ϕ_0 [°]
Single W20	4.287	77.48	19.17	180	180
Double W21	1.36	54.37	8.93		

Where R is the radius of the helix, P is the pitch and α is the lay angle. While θ_0 and ϕ_0 are the initial swept angles respectively of the strand and the wire. The wire W21 double helix centreline depends upon the single helix centreline of W20.

1.2. POSITION VECTOR OF THE WIRE

The position vector of the core wire W20 is computed with the single helix geometry (III.4) and the centreline corresponds to the strand itself, while the outer wire W21 is evaluated with the relations of the double helix (IV.4).
First, a comparison is performed between core and outer wire projections on the planes defined by $\underline{e}_2$ and $\underline{e}_3$ respectively. Afterwards, the wire centerlines are plotted within the (x_2, x_3) plane.

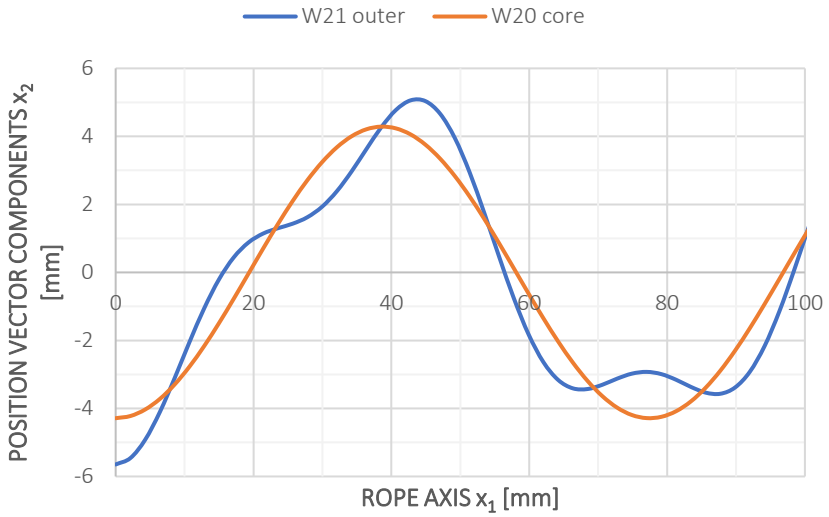

Fig 1.14 Wire Centerline Geometry in Plane (x_1, x_2)

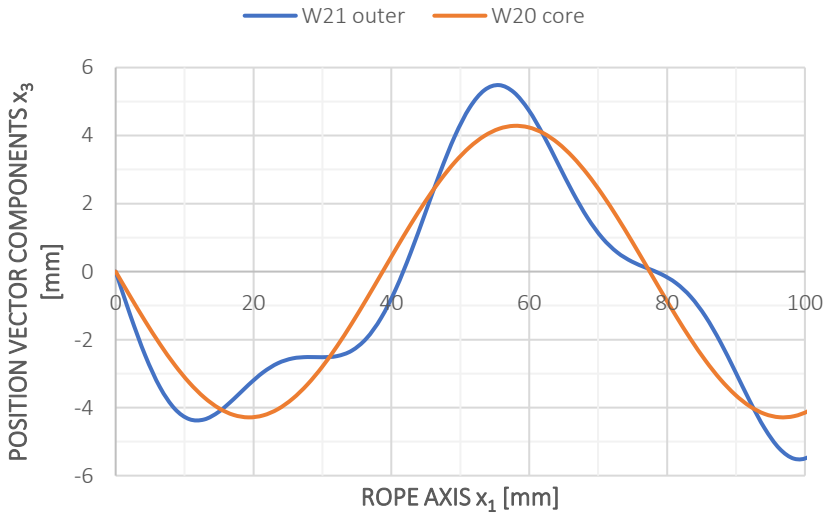

Fig 1.15 Wire Centerline Geometry in Plane (x_1, x_3)

The sinusoidal trend of the single helix is evident. On the other hand, from the previous plots it can be appreciated the oscillatory behaviour of the double helix about the single one.
Finally, the plot of these functions is presented into a plane orthogonal to the rope axis.

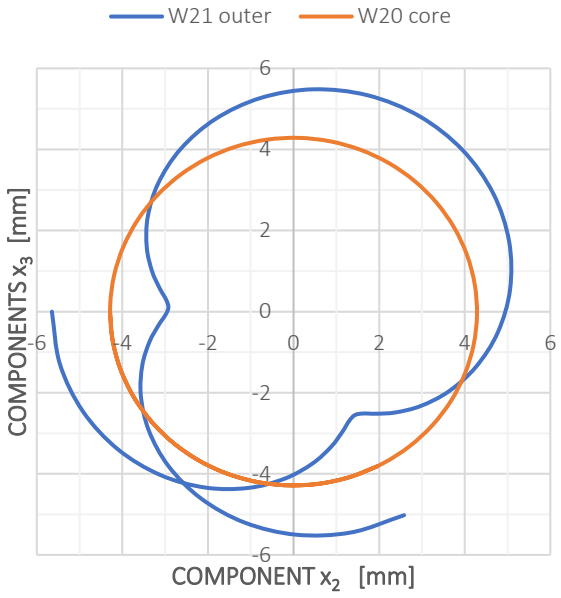

Fig 1.16 Wire Centerline Geometry in Plane (x_2, x_3)

From the last two expressions of the single helix in (III.4) it can be clearly appreciated that they describe in the plane (x_2, x_3) the equations of a circumference of radius equal to R_I, which in the specific case is 4.287 mm. Conversely, the corresponding double helix components oscillate about this circumference with a maximum distance equal to R_{II}, which in this example is 1.36 mm.

1.3. TANGENT VECTOR

A geometrical parameter very important for the determination of the mechanical response of the wire and the rope is the first component of the tangent vector. As a matter of fact, it represents the projection of the wire local direction along the rope axis. According to equation (III.5.1) the single helix shows a constant trend. It is a consequence of the geometrical definition of this peculiar curve described in III.1. On the other hand, the double helix has a periodical trend as it can be clearly recognized in (IV.5.1).

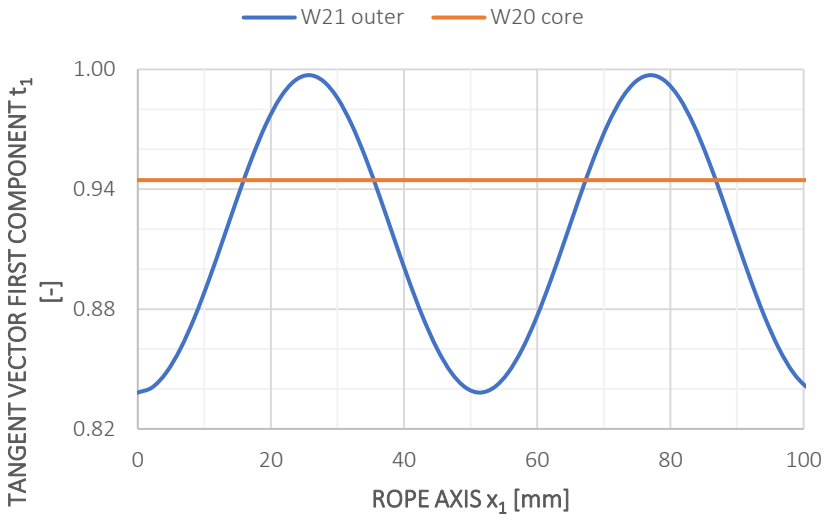

Fig 1.17 Wire Tangent Vector First Component

1.4. ARCH LENGH OF THE WIRE

The comparison between the two different approaches for the computation of the arch length of the double helix, already introduced with the relations (IV.5.2), is shown below.

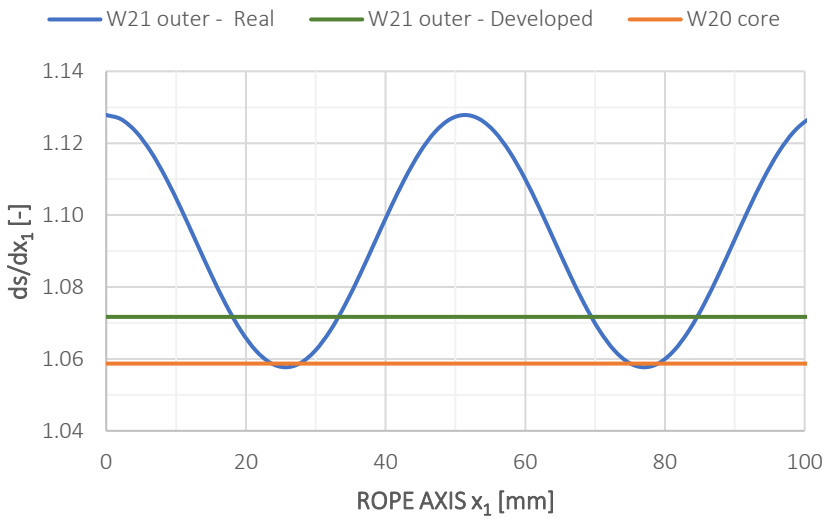

Fig 1.18 Wire Arch Length

The following table show the errors in percentage for the maximum, minimum and mean values of the real geometry compared with the developed view.

Table 1.2 Arch Length

	W20	W21 dev	W21 real	error
max			1.13	5.24%
min			1.06	-1.31%
mean	1.06	1.07	1.09	1.97%

The result is very important for two aspects. Firstly, the mean value of the real arch length is the geometrical parameter directly related to the global response of the rope in terms of strain, since the integration of the oscillations about the wire will filter out only the mean. Conversely, the maximum and minimum influence the local response of the single wire in terms of stresses. Hence, the choice of one of the two geometrical representations influences the system response.

1.5. CURVATURE AND TORSION

The results are reported as functions of the swept angle of the double helix. In this manner, the dependence on the initial swept angle is lost. Moreover, it is worth to remember that due to the differential relation of the developed view (IV.3.2), the aforesaid angle is linearly related to the rope longitudinal axis, hence it is the same to talk in terms of one or the other because the difference is only a scale factor between them.

$$\Delta\varphi(x_1) = \varphi(x_1) - \varphi_0 = \frac{\tan\alpha_{II}}{R_{II}\cos\alpha_I}\, x_1$$

In the following it is possible to see the comparison between the results.

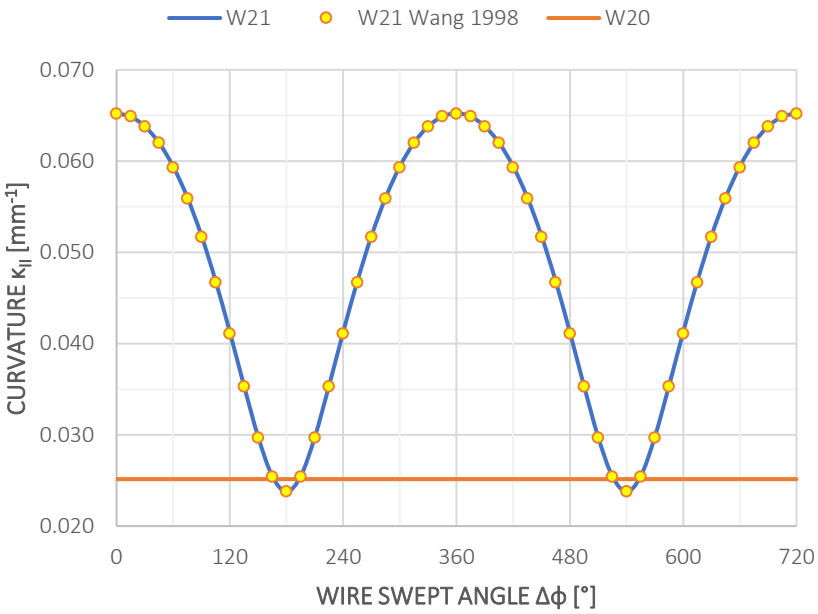

Fig 1.19 Wire Geometrical Curvature

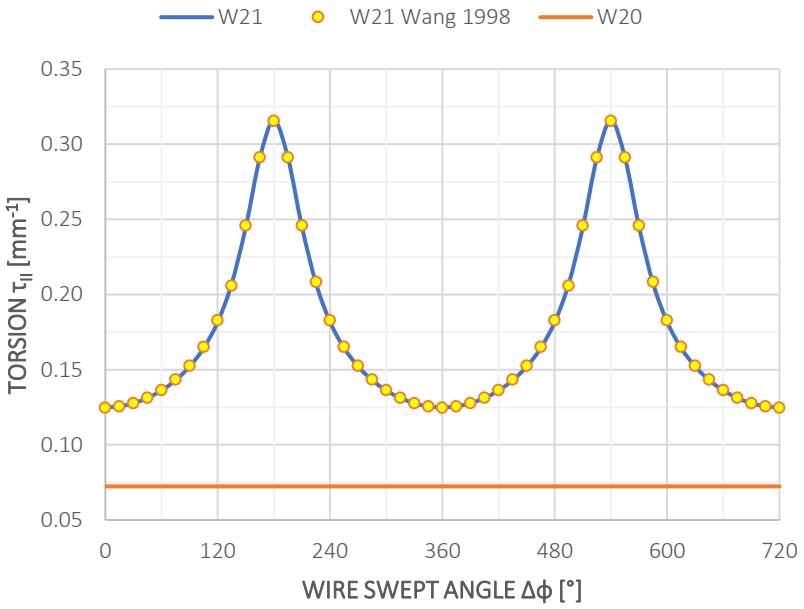

Fig 1.20 Wire Geometrical Torsion

The two geometrical features do not show a constant trend, instead they are periodical. The period of this function is the pitch of the double helix.

2. STRANDED ROPE 30 mm 7x7 WSC

The comparison between the results of the proposed formulation and the ones coming from (Xiang et al., 2015) will be reported in the following. The single and double helix that are investigated are the core and the outer wires centerlines of a single layer stranded rope. The length of the rope considered is about 141 mm, which corresponds to few more of two periods of the the double helix.

2.1. INPUT GEOMETRY

The main geometrical feature used for the computations are reported in the following table.

Table 1.3 Stranded Rope 30 mm 7x7 WSC Geometry

Rope layer	wire layer	wire radius r_w [mm]	wire lay angle α_w [°]	number of wires per strand layer	wire helix radius R_w [mm]	wire lay length p_w [mm]	strand lay angle α_s [°]	number of strands per rope layer	strand helix radius R_s [mm]	strand lay length p_s [mm]
	0	1.970	-	1	-	-				
0	1	1.865	18.99	6	3.835	70	-	1	-	-
	0	1.600	-	1	-	-				
1	1	1.500	15.55	6	3.100	70	18.54	6	10.3	193

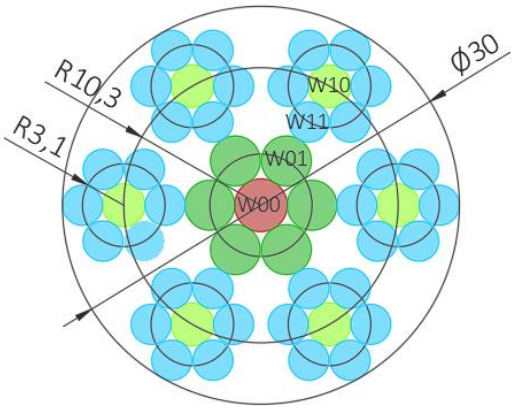

Fig 1.21 Stranded Rope 30 mm 7x7 WSC Geometry

The wire involved in the analysis are indicated in Fig. 1.10. Specifically, W10 and W11 are denoted as W3 and W4 respectively.

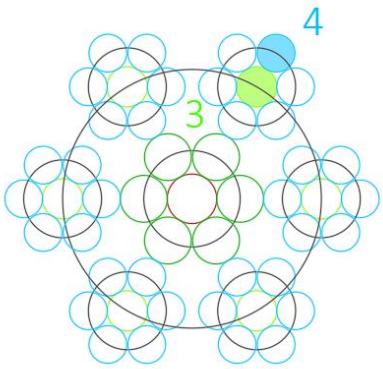

Fig 1.22 Stranded Rope 30 mm 7x7 WSC Wires

2.2. POSITION VECTOR OF THE WIRE

The position vector of the core wire W3 is computed with the single helix geometry (III.4) and the centreline corresponds to the strand itself, while the outer wire W4 is evaluated with the relations of the double helix (IV.4).
First, a comparison is performed between core and outer wire projections on the planes defined by $\underline{e}_2$ and $\underline{e}_3$ respectively. Afterwards, the wire centerlines are plotted within the (x_2, x_3) plane.

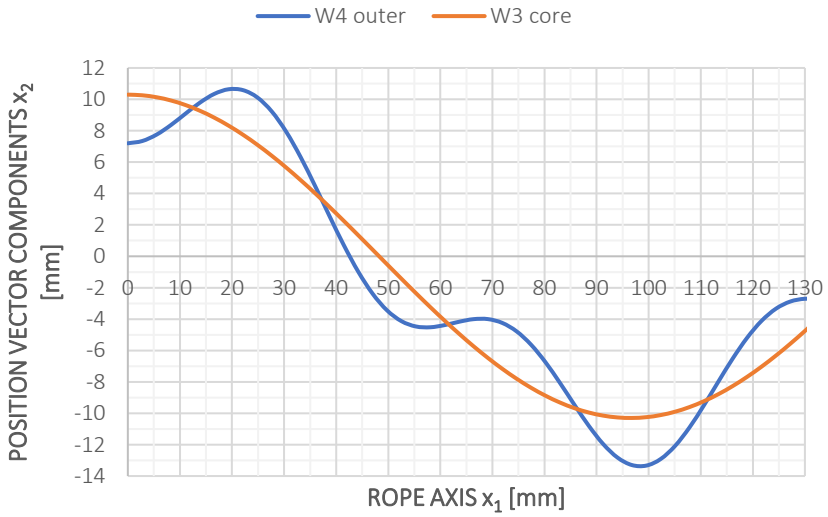

Fig 1.23 Wire Centerline Geometry in Plane (x_1, x_2)

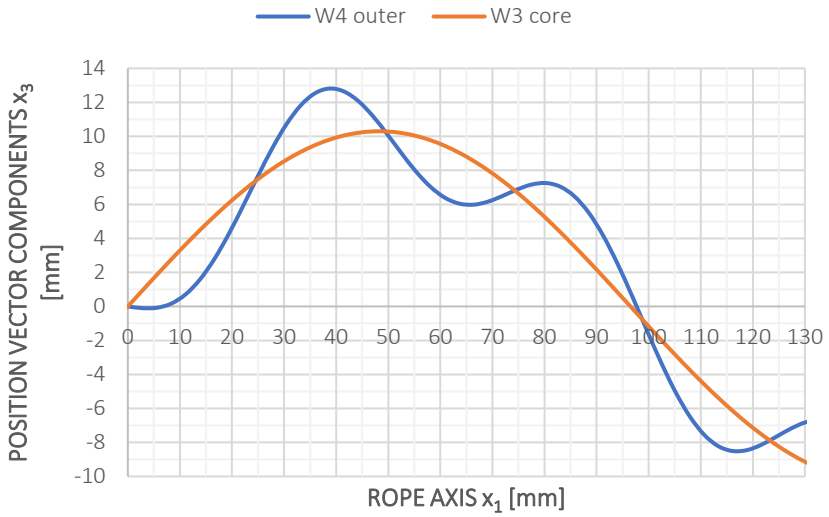

Fig 1.24 Wire Centerline Geometry in Plane (x_1, x_3)

The sinusoidal trend of the single helix is evident. On the other hand, from the previous plots it can be appreciated the oscillatory behaviour of the double helix about the single one. For this function further comments need to be done. If the plot of the in-plane components of the double helix is performed for a length of the rope axis long enough, a curve with the following shape is obtained.

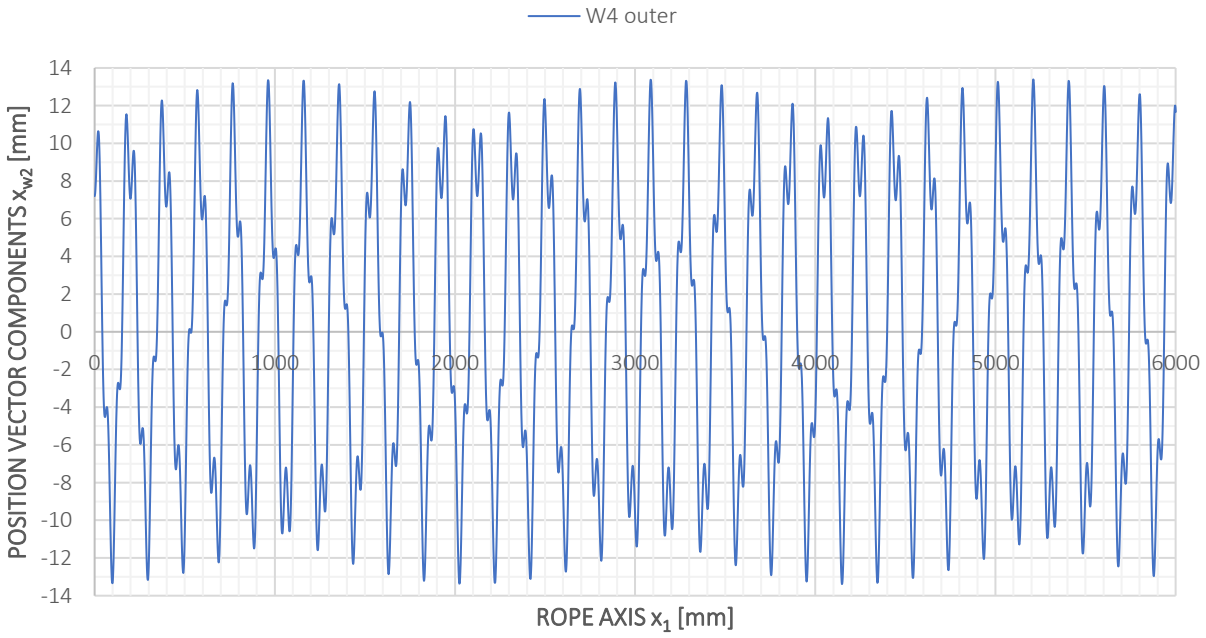

Fig 1.25 Wire Centerline Geometry in Plane (x_1, x_2)

The function is not sinusoidal, still it has periodical features. This will be a key point for the kinematic model that will be developed in the following chapter.

Finally, the plot of these functions is presented into a plane orthogonal to the rope axis. Two cases are illustrated, the first correspond to a rope length of 130mm and it allows to have a zoom in on the oscillation of the double helix about the single one, while the second is performed for a length of 6000mm in order to have a global overview of the helices trend.

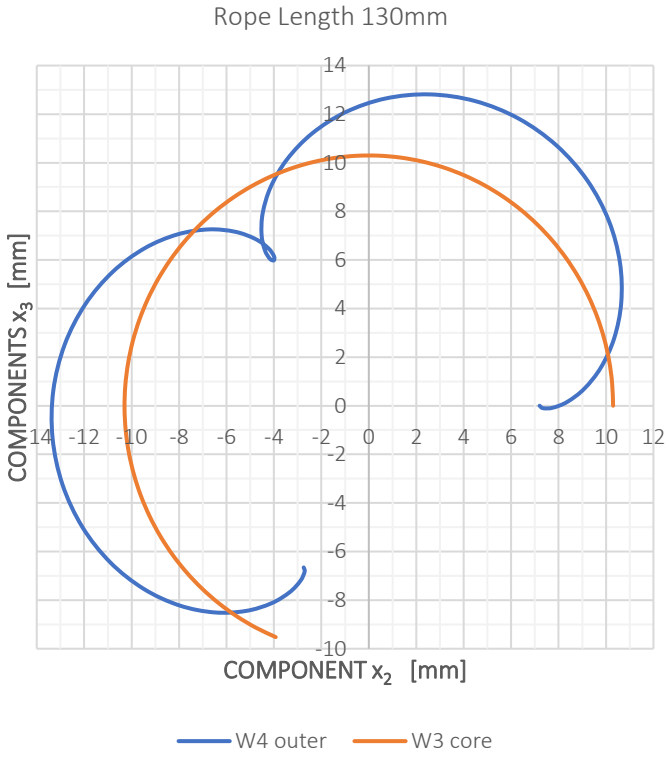

Fig 1.26 Wire Centerline Geometry in Plane (x_2, x_3)

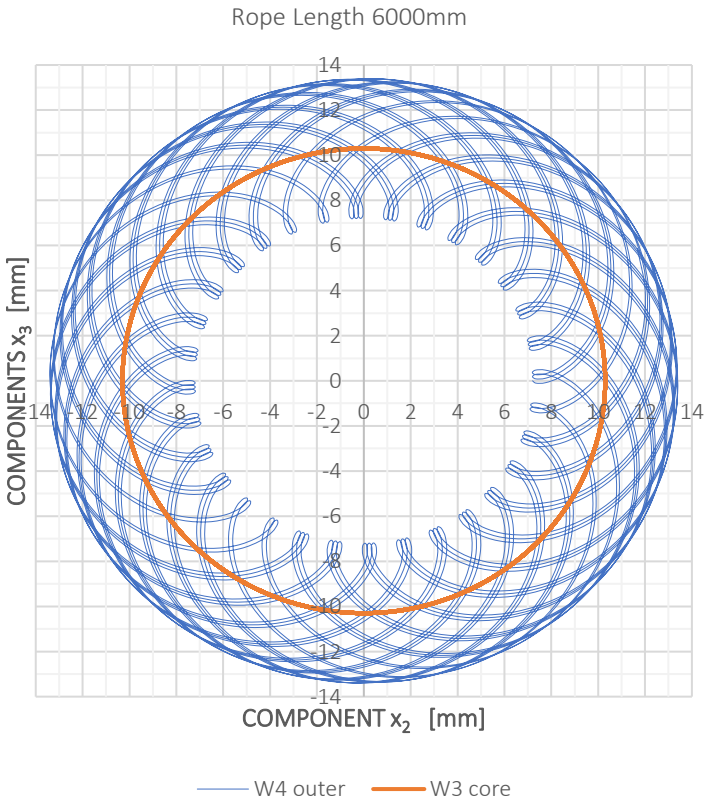

Fig 1.27 Wire Centerline Geometry in Plane (x_2, x_3)

From the last two expressions of the single helix in (III.4) it can be clearly appreciated that they describe in the plane (x_2, x_3) the equations of a circumference of radius equal to R_I, which in the specific case is 10.3 mm. Conversely, the corresponding double helix components oscillate about this circumference with a maximum distance equal to R_{II}, which in this example is 3.1 mm.

2.3. TANGENT VECTOR

A geometrical parameter very important for the determination of the mechanical response of the wire and the rope is the first component of the tangent vector. As a matter of fact, it represents the projection of the wire local direction along the rope axis. According to equation (III.5.1) the single helix shows a constant trend. It is a consequence of the geometrical definition of this peculiar curve described in III.1. On the other hand, the double helix has a periodical trend as it can be clearly recognized in (IV.5.1).

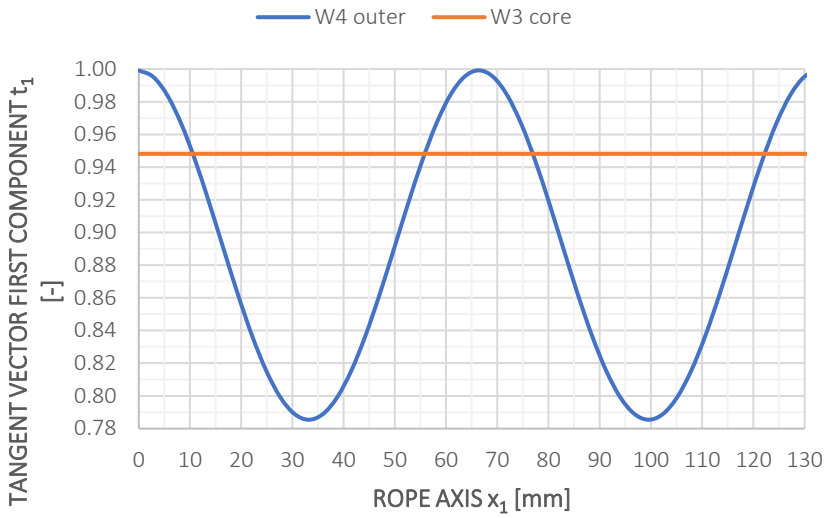

Fig 1.28 Wire Tangent Vector First Component

2.4. ARCH LENGH OF THE WIRE

The comparison between the two different approaches for the computation of the arch length of the double helix, already introduced with the relations (IV.5.2), is shown below.

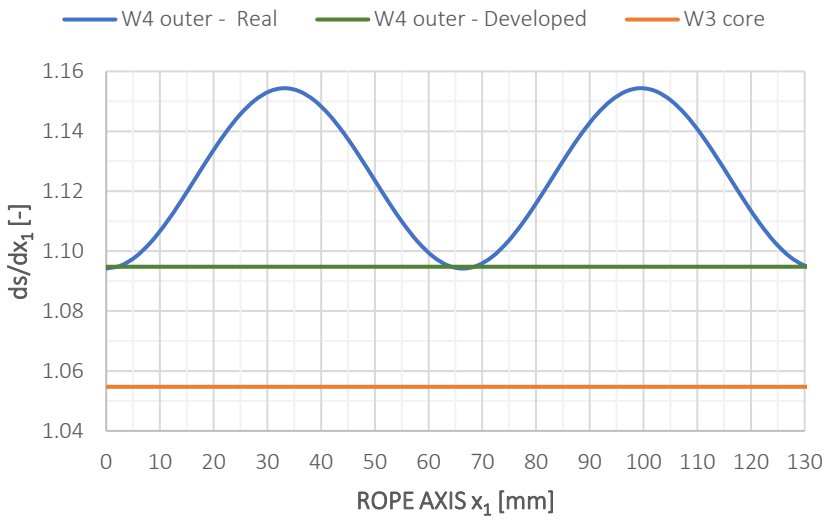

Fig 1.29 Wire Arch Length

The following table show the errors in percentage for the maximum, minimum and mean values of the real geometry compared with the developed view.

Table 1.4 Arch Length

	W3	W4 dev	W4 real	error
max			1.15	5.44%
min			1.09	-0.06%
mean	1.05	1.09	1.12	2.69%

The result is very important for two aspects. Firstly, the mean value of the real arch length is the geometrical parameter directly related to the global response of the rope in terms of strain, since the integration of the oscillations about the wire will filter out only the mean. Conversely, the maximum and minimum influence the local response of the single wire in terms of stresses. Hence, the choice of one of the two geometrical representations influences the system response.

2.5. CURVATURE AND TORSION

The results are reported as functions of the swept angle of the double helix. In this manner, the dependence on the initial swept angle is lost. Moreover, it is worth to remember that due to the differential relation of the developed view (IV.3.2), the aforesaid angle is linearly related to the rope longitudinal axis, hence it is the same to talk in terms of one or the other because the difference is only a scale factor between them.

$$\Delta\varphi(x_1) = \varphi(x_1) - \varphi_0 = \frac{\tan\alpha_{II}}{R_{II}\,\cos\alpha_I}\,x_1$$

In the following it is possible to see the comparison between the results.

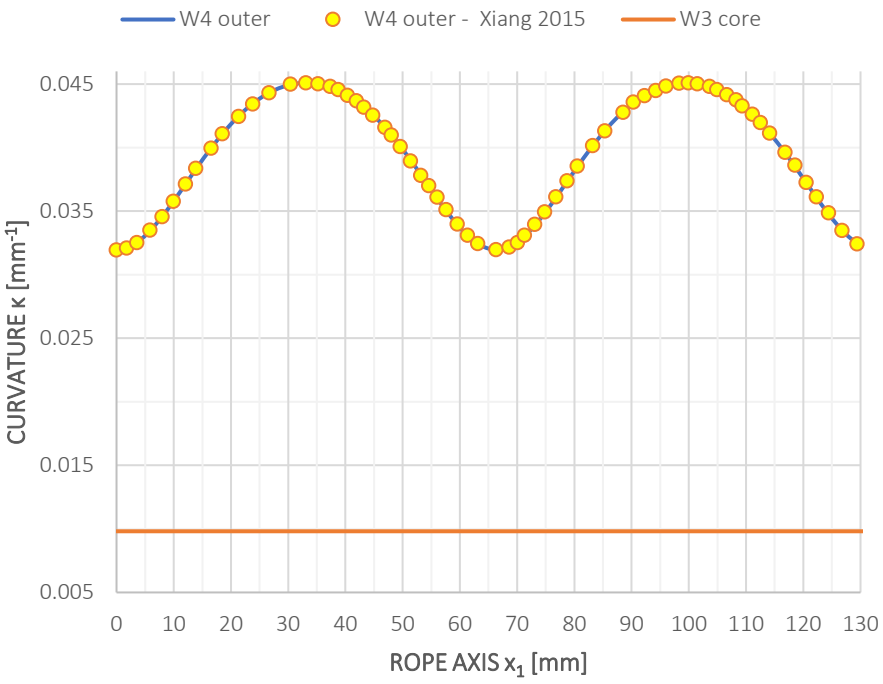

Fig 1.30 Wire Geometrical Curvature

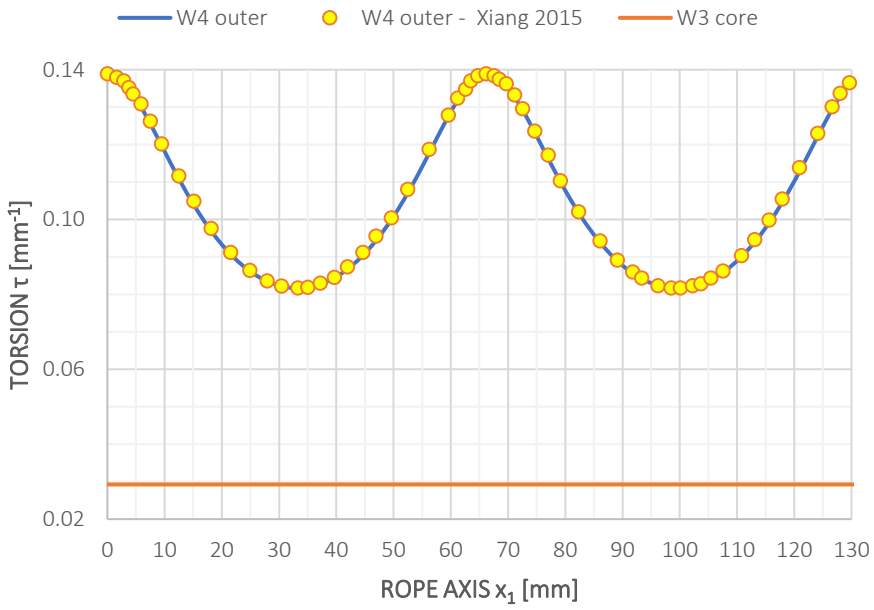

Fig 1.31 Wire Geometrical Torsion

The two geometrical features do not show a constant trend, instead they are periodical. The period of this function is the pitch of the double helix.

2.6. 3D MODELLING

The first output of the analytical description of the helixes geometry is the possibility to easily build a 3D model of the single wire and of the rope itself. As a matter of fact, all the aforesaid relations describing the single and double helix position may be inputted within an excel spread sheet and for a discrete number of point it is possible to compute the exact position of the wire centreline. Moreover, the local Serret-Frenet frame enable the user to detect the exact orientation of the wire cross section with respect to the centreline. These features can be easily exploited to generate a 3D model in a CAD software. The importance of having such a simple tool to handle the geometry appears to be evident. In fact, the 3D model can be imported in FEA software.
In the pictures below this result is clearly shown for the 30m 7x7 WSC Stranded Rope for a length of the central straight wire of about 130 mm. All the numerical results exposed before refers exactly to this geometry.

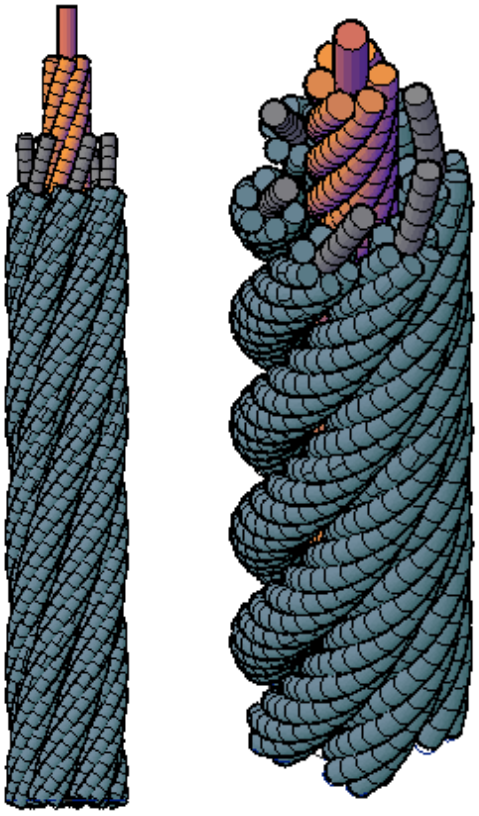

Fig 1.32 Three-Dimensional Wire Rope Geometry

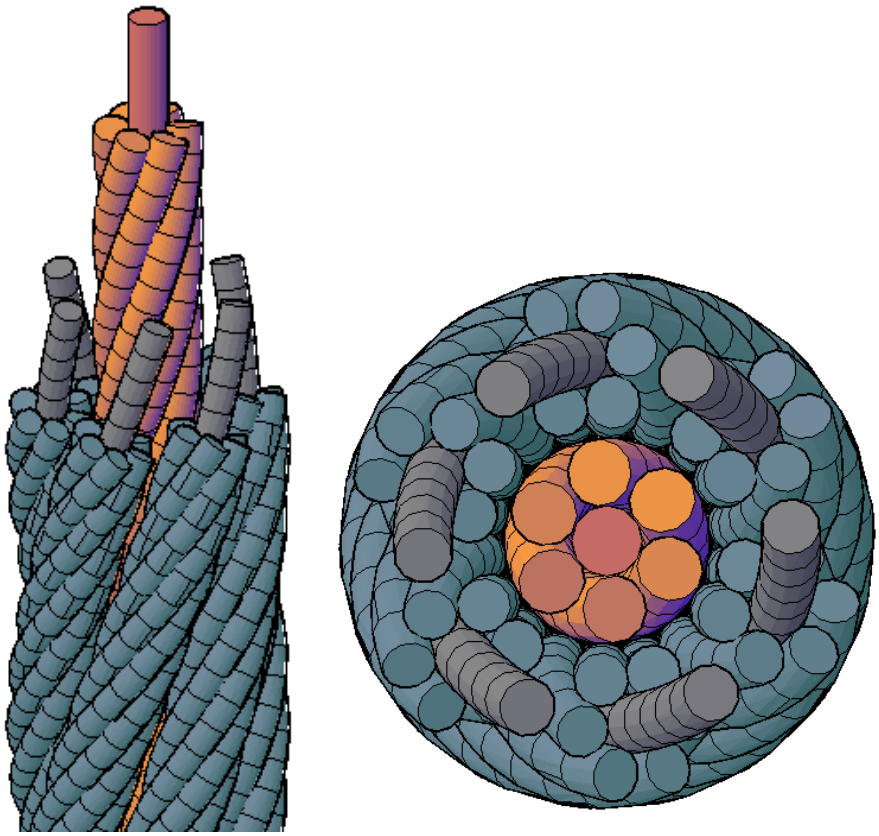

Fig 1.33 Three-Dimensional Wire Rope Geometry

REFERENCES

(Kreyszig, 1991) Kreyszig E., 1991. *Differential Geometry*. Dover Publications, New York USA.

(Citrini, 1992) Citrini C., 1992. *Analisi Matematica 2*. Bollati Boringhieri.

(Wang et al., 1998) Wang R.C., Miscoe A.J., McKewan W.M., 1998. *Model for the Structure of Round-Strand Wire Ropes*. Report of investigations 9644.

(Usabiaga & Pagalday, 2008) Usabiaga H., Pagalday J.M., 2008. *Analytical procedure for modelling recursively and wire by wire stranded ropes subjected to traction and torsion loads.* International Journal of Solids and Structures 45 (2008) 5503-5520.

(Xiang et al., 2015) Xiang L., Wang H.Y., Chen Y., Guan Y.J., Wang Y.L., Dai L.H., 2015. *Modelling of multi-stranded wire ropes subjected to axial tension and torsion loads*. International Journal of Solids and Structures 58 (2015) 233-246.

CHAPTER 2

KINEMATICS

I. INTRODUCTION

Wire ropes are complex systems with a hierarchical structure where the basic element is the wire. In many applications it is treated as a component providing a reaction to tensile excitations only. Truly, the behaviour of this object includes torsional and bending stiffness as well, even if numerically low compared to the axial one.
When more wires are helicoidally wounded about a straight wire, called either king or core wire, within a layer, they form a strand. Wires belonging to the same layer have the feature to be equally distant from the core. Strands may be composed by several layers.
The wire rope finally is the sum of more strands. The hierarchy between rope and strand is the same of strand and wires. Hence, the rope is made by a straight core strand and it is surrounded by strands helicoidally coiled about its axis.
The internal framing of this peculiar structural system is the starting point for the kinematic hypothesis of the model.

1. LITERATURE OVERVIEW

The issue of the mathematical modelling of wire rope kinematics has been treated in different ways by various authors during the years. The reason is the intrinsic complexity of this mechanical system and of the phenomena experienced when subject to a perturbation.

The first aspect regarding the modelling of wire ropes concerns the geometry. As a matter of fact, the early models developed for these systems were based on the single helix only. The reason is in the higher simplicity of this curve with respect to the double helix. The operation involved was the homogenization. The wire within the rope is a nested helix, yet it is a single helix inside the strand. Hence, the mechanical properties of the strand were studied in its straight configuration, afterwards the strand were treated as a homogenized wire with a single helix centerline. In this way the direct relation between mechanics of rope and wire is not easy to recover.
The second step for the definition of the kinematics is the lubrication condition. This technological treatment has the main purpose of reducing considerably friction among the wires. Hence, the terms friction and lubrication are closely correlated.
Usually, in literature there is reference to two extreme conditions: frictionless or perfectly lubricated, when all the wires are not bonded together, but behave independently as a bundle; infinite friction or unlubricated, when all wires are working within the rope like a whole. These two extreme scenarios are translated into two opposite kinematic conditions: full slip and full stick state. References about this nomenclature may be found in (Raoof & Kraincanic 1995) and (Foti & Martinelli, 2016).

In the following a set of relevant papers will be illustrated as they are considered significant for the development of the present work.
The first model that we mention is due to (Velinsky et al., 1984). In this paper the rope is studied in full slip conditions, hence the response of the rope is the sum of the responses of the single wires seen as a bundle. Specifically, the article describes the response of a wire rope subject to axial torsional loads. When the rope experiences a twisting rotation, the material points of the rope cross section do not behave like a rigid plane, as it happens in beams for instance. Moreover, the wires are homogenized within the strand, so that the strand inside the rope is seen as a wire inside the strand. This approach leads to the loss of local information on the single wire.
A second model has been developed by (Raoof & Kraincanic, 1995). They established the so called Orthotropic Sheet Theory. That approach sees each layer of wires like an orthotropic thin layer in plane-stress state. This element has high in plane stiffness, while has much lower out of plane stiffness. This model is able to predict the two limit bounds of full stick and full slip condition in axial torsion regime. Furthermore, it can catch a specific behavior that was encountered during experimental tests: when undergoing axial cyclic loading superimposed on a mean value, a rope being pre-loaded with a tensile force experiences a reduction in axial stiffness. The reason is mainly due to slipping within the rope.
An improvement in the geometrical description was introduced by (Elata et al., 2004). The nested helix was fully considered to predict the response of wire rope with IWRC in the axial regime. The model involved the two kinematic bounds: full stick, called locked rope-level sieves and full slip, called unlocked rope-level sieves.
A different approach for kinematics was used in the paper of (Usabiaga & Pagalday, 2008). Specifically, the model is based on the work of Ashkenazi et al. 2003 and the general thin rod theory of (Love, 1944). The material points of the wire centerlines belonging to the rope cross section are not considered rigidly attached to the wire rope axis. Conversely, these points are considered linked with the strand axis. Consequently, this theory mixes the hypothesis of full stick and full slip. In fact, infinite friction is considered between wires inside the strand, while the strands are considered perfectly lubricated within the rope.

The work of (Xiang et al., 2015) fully considers the double helix geometry and it is based on the Love thin rode theory as well. Still, the kinematic assumption is of frictionless internal contact surfaces.
Finally, we consider the model developed by (Foti & Martinelli, 2016). They developed a mechanical model for the strand only. The wire kinematics is based on the Kirchoff-Clebsch-Love theory of curved thin rod. Conversely, the straight strand is modelled as a Euler Bernoulli beam, whose sectional response is provided by the contributions of the single wires. Based on the recursive procedure firstly outlined in (Foti, 2013), the model was later extended in (Meleddu et al., 2017) to characterize the response of metallic wire ropes subjected to a generic combination of axial, torsional and bending loads.

2. HYPOTESIS

The present model is the natural extension of the kinematics proposed by Foti & Martinelli, 2016. The aforesaid model was based on the single helix geometry and the curved thin rod theory for the wire, while an Euler Bernoulli kinematics was assumed for the straight strand. Now we want to extend this concept to the whole rope. Specifically, the geometry of the wire will be that of the nested helix and the mechanics will be always that of the curved thin rod theory, then the Euler Bernoulli model will be adopted for the rope.
Firstly, it is worth to remark what is meant with the expression "rope cross section". As a matter of fact, the wire rope does not have a continuous cross section as a beam does. The reason is that the kinematics of the rope is dictated by the kinematics of the wires centerline and not by the wires cross sections. Let us refer to Fig 2.1 where the wire rope cross section is represented only with two strands. Moreover, the outer strand and outer wires are representative of all the strands and wires of the corresponding layer. The core straight strand is colored in green where the representative wires are the core wire 1 and the outer wire 2 (this latter has a single helix geometry). On the other hand, the outer strand with single helix shape is colored in orange where 3 is the core single helix wire, while 4 and 5 are the outer double helix wires. The material point is defined as the wire centerline point that contributes to the definition of the wire cross section and it is represented by a solid black dot in figure. The material point has the numbering equal to the correspondent wire. Let us introduce one by one the different types of material point. The point 1 represents the wire rope axis material point at coordinate x_1 and it is the center of gravity of the rope cross section. The point 2 and 3 represents the material points of the of the correspondent wires and are obtained with the intersection between wire centerline and circumferences 1 and 2 respectively (the circumferences lay in the plane orthogonal to the rope axis – the cutting plane). Conversely, the points 4 and 5 come from the intersection of the correspondent centerlines and the circumference 3. This latter circumference is not in plane with the other two, but it lays on a plane that have normal unit vector parallel to the tangent direction of wire 3 in point 3. Hence, the material point 4 belongs to the plane of the circumferences 1 and 2, while point 5 doesn't. The reason is in the definition of the double helix position vector first component (1.IV.4) that is along the global coordinate x_1.
This consideration states four important facts: first, the wire rope cross section is lumped in a discrete set of points, i.e. the material points; second, the material points of the same wire rope section x_1 do not all belong to the section cutting plane; third, the material points own an orientation that is provided by the correspondent wire centerline Serret-Frenet frame. Fourth, the wire cross sections are oriented as the local attached frame and they aren't parallel to the cutting plane.

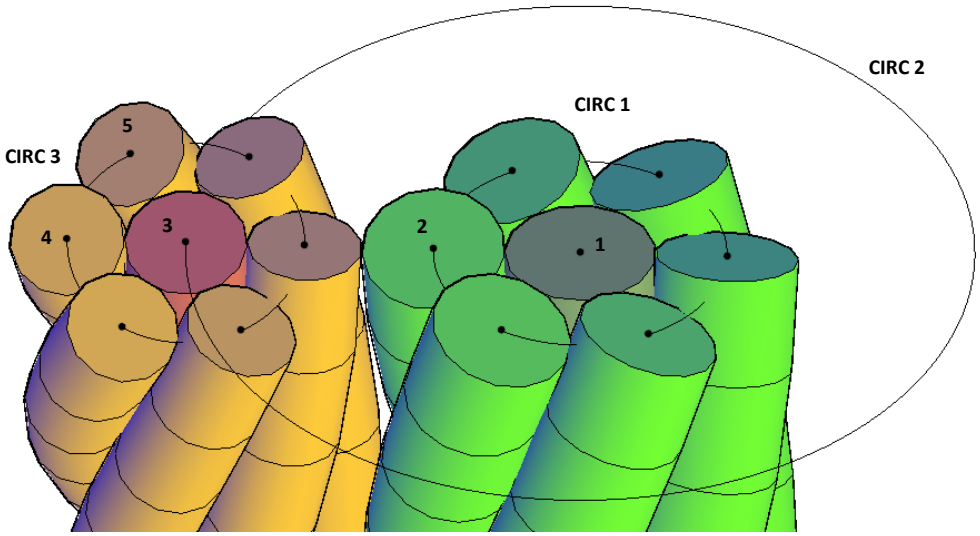

Fig 2.34 Wire Rope Cross Section – Material Points

The Euler Bernoulli hypothesis implies that every material point of the rope cross section is rigidly attached to the rope axis. Indeed, after a perturbation occurs, the rope cross section will translate and rotate, still the same relative position between material point and rope centerline will be preserved in the deformed configuration. Hence, the material points, belonging to the wire centerline, may be seen like the discrete counterpart of a beam section.
For certain, this hypothesis applies when infinite friction is assumed among the wires. Thus, we are trying to model this system in the stiffer mechanical condition.

A further hypothesis is that of small strains. In this framework the kinematics results to be linear and thus the superposition principle holds true.

3. DIRECT AND RECURSIVE MODEL

In the present thesis work two different models are proposed for the mechanical modeling of the wire rope. The first model is called direct or wire by wire. Here a general approach for the definition of the kinematic and mechanical quantities is involved. As a matter of fact, according to the previous kinematic hypothesis the rope cross section is assumed to behave like an Euler-Bernoulli beam cross section, while the single wire is treated according to the Love curved thin rod theory. Specifically, the last theory is developed for a generic curved thin rod geometry, i.e. the expressions regarding the position vector, the Serret-Frenet frame components, the curvature and torsion are not provided for a peculiar shape of the curve. The same philosophy will apply to the direct model. Hence, in the following the word “wire” will stand for a generic three-dimensional curve in space. Since the purpose of the present thesis is to model the behavior of actual wires, the reader must keep in mind that the geometry is always implied for either the single or double helix although the theory works for a generic one. Furthermore, because of the simplicity in handling its equations, the explicit expressions of the single helix will be provided only.
The latter fact is also the starting point for the recursive model. As a matter of fact, this formulation aims to describe the kinematics and mechanical response of the rope avoiding the explicit definition of the double helix. Conversely, it will involve recursively, or hierarchically, the single helix mechanical response. In this model an approximation is introduced. The relations holding true between wire rope and strand are exact indeed, since the strand has a single helix geometry within the rope. On the other hand, the single wire is a double helix within the rope, still it is a single helix inside the strand. The latter statement will be exploited as follows: the kinematic and mechanical quantities regarding the wire will be evaluated within the strand in the strand straight configuration and not in the single helix shape. Here the approximation is evident, since the model does not account the actual single helix shape of the strand centerline. Afterwards, the hierarchical structure of the system is exploited, thus having the relations between rope and strand, and the relations between strand and wire, it will be possible to find a link between wire and rope.

II. DIRECT MODEL

1. DISPLACEMENTS

In the present paragraph the main purpose is to provide the kinematic links holding true between the rope generalized displacements and the generic wire generalized displacements. This aim will be pursuit introducing the displacement field of the rope cross section according to the Euler Bernoulli hypothesis firstly. Here it will be possible to detect the generalized displacements of the rope. Afterwards, the same operation is performed for the wire cross section, still it will be needed to establish the relations between the wire and the rope generalized displacements. Finally, the case of the general wire will be specialized to the core wire of the strand, which shows a single helix shape. The subscripts "w" and "R" will refer to the generic wire and rope respectively. The subscript "s" will hold for the core wire of the strand, hence it will stand at the same time for single helix and strand.

1.1. ROPE GENERALIZED DISPLACEMENTS

The rigid and plane cross section hypothesis leads to the usual displacement field which correspond to the equations of a plane in the principal reference frame of the cross section. The displacements of the material points of the wire rope cross section are described within the global reference frame (x_1, x_2, x_3).

$$
\begin{aligned}
& s_{R1}(\underline{x}) = u_{R1}(x_1) + \varphi_{R2}(x_1)\, x_3 - \varphi_{R3}(x_1)\, x_2 \\
(2.II.1)\quad & s_{R2}(\underline{x}) = v_{R2}(x_1) - \varphi_{RT}(x_1)\, x_3 \\
& s_{R3}(\underline{x}) = v_{R3}(x_1) + \varphi_{RT}(x_1)\, x_2
\end{aligned}
$$

Where $s_{Ri}(\underline{x})$ is the displacement component of the rope cross section point along the global direction x_i. The generalized displacements u_{R1}, v_{R2} and v_{R3} are the displacements of the rope axis along the global directions x_1, x_2 and x_3 respectively. The generalized rotations ϕ_{RT}, ϕ_{R2} and ϕ_{R3} are the rigid rotations of the rope cross section about the global directions x_1, x_2 and x_3 respectively. Finally, the position vector (x_2, x_3) is within the rope cross section and it is referred only to the discrete set of point composed by the wire cross sections center of gravity. These points are obtained by the intersection of the rope section cutting plane and the wire centerlines. Hence, the displacement field (2.II.1) holds true for a discrete number of points, i.e. the material points of the wire cross sections, like it is showed in Fig 2.2 and not for all the points of the wires cross section.
Furthermore, the orthogonality assumption constraints the transverse displacement's components with the relevant rotations

$$
\begin{aligned}
& \varphi_{R2}(x_1) = -v'_{R3}(x_1) \\
& \varphi_{R3}(x_1) = +v'_{R2}(x_1)
\end{aligned}
$$

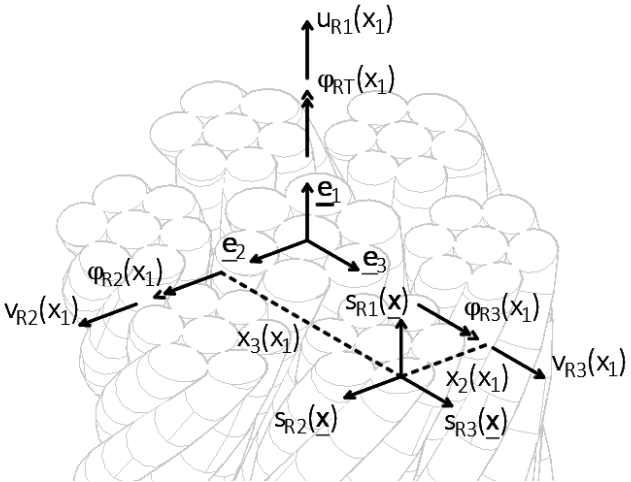

Fig 2.35 Wire Rope Displacement Field

1.2. WIRE GENERALIZED DISPLACEMENTS

The displacements are written within the local reference frame of the wire (y_1, y_2, y_3), corresponding to tangent, normal and binormal directions of the centerline Serret-Frenet frame. Specifically, the plane (y_2, y_3) coincide with the wire cross section.

$$
\begin{aligned}
& s_{w1}(\underline{x}, y_2, y_3) = u_{w1}(\underline{x}) + \varphi_{w2}(x_1)\, y_3 - \varphi_{w3}(x_1)\, y_2 \\
(2.II.2) \quad & s_{w2}(\underline{x}, y_2, y_3) = v_{w2}(\underline{x}) - \varphi_{wT}(x_1)\, y_3 \\
& s_{w3}(\underline{x}, y_2, y_3) = v_{w3}(\underline{x}) + \varphi_{wT}(x_1)\, y_2
\end{aligned}
$$

Where $s_{wi}(\underline{x})$ is the displacement of the point of the wire cross section $\underline{x}$ in direction of the local axis y_i. The coordinates y_2 and y_3 detect the position of one point of the cross section in the cross-section plane itself. The generalized displacement u_{w1}, v_{w2} and v_{w3} are the displacements of the wire centerline in the directions y_1, y_2 and y_3 respectively. The rotations ϕ_{wT}, ϕ_{w2} and ϕ_{w3} are the rigid rotations of the wire cross section about the directions y_1, y_2 and y_3 respectively. The subrscript "R" is substituted with "w" standing for wire.
The generalized displacement components of the wire cross section may be derived projecting the rope displacements into the principal reference frame of the wire, hence along the Serret-Frenet frame.

$$
\begin{aligned}
& u_{w1}(\underline{x}) = \sum_{i=1}^{3} s_{Ri}(\underline{x})\, \underline{e}_i\, \underline{t}_w = \sum_{i=1}^{3} s_{Ri}(\underline{x})\, t_{wi} \\
(2.II.3a) \quad & v_{w2}(\underline{x}) = \sum_{i=1}^{3} s_{Ri}(\underline{x})\, \underline{e}_i\, \underline{n}_w = \sum_{i=1}^{3} s_{Ri}(\underline{x})\, n_{wi} \\
& v_{w3}(\underline{x}) = \sum_{i=1}^{3} s_{Ri}(\underline{x})\, \underline{e}_i\, \underline{b}_w = \sum_{i=1}^{3} s_{Ri}(\underline{x})\, b_{wi}
\end{aligned}
$$

The same operation may be performed for the rotations.

$$
\begin{aligned}
& \varphi_{wT}(x_1) = \sum_{i=1}^{3} \varphi_{Ri}(x_1)\, \underline{e}_i\, \underline{t}_w = \sum_{i=1}^{3} \varphi_{Ri}(x_1)\, t_{wi} \\
(2.II.3b) \quad & \varphi_{w2}(x_1) = \sum_{i=1}^{3} \varphi_{Ri}(x_1)\, \underline{e}_i\, \underline{n}_w = \sum_{i=1}^{3} \varphi_{Ri}(x_1)\, n_{wi} \\
& \varphi_{w3}(x_1) = \sum_{i=1}^{3} \varphi_{Ri}(x_1)\, \underline{e}_i\, \underline{b}_w = \sum_{i=1}^{3} \varphi_{Ri}(x_1)\, b_{wi}
\end{aligned}
$$

In Fig.2.3 it is possible to appreciate the geometrical relations (2.II.3).

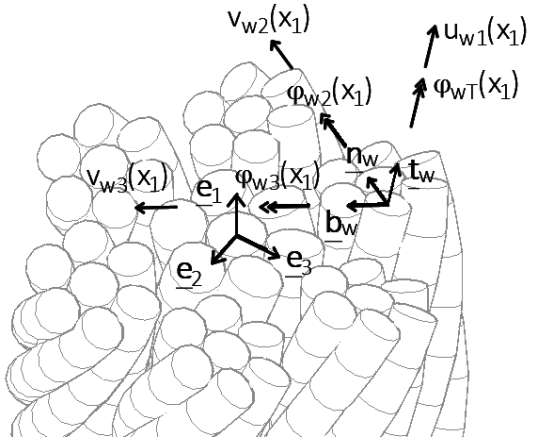

Fig 2.36 Wire Generalized Displacements

1.3. STRAND GENERALIZED DISPLACEMENTS

The displacement field is the consequence of the first kinematic hypothesis of the model and it can be written within the local reference frame of the strand (z_1, z_2, z_3), corresponding to tangent, normal and binormal directions of the strand centerline Serret-Frenet frame.

$$
\begin{aligned}
& s_{s1}(\underline{x}, z_2, z_3) = u_{s1}(\underline{x}) + \varphi_{s2}(x_1)\, z_3 - \varphi_{s3}(x_1)\, z_2 \\
& s_{s2}(\underline{x}, z_2, z_3) = v_{s2}(\underline{x}) - \varphi_{sT}(x_1)\, z_3 \\
& s_{s3}(\underline{x}, z_2, z_3) = v_{s3}(\underline{x}) + \varphi_{sT}(x_1)\, z_2
\end{aligned}
\qquad (2.II.4)
$$

Where $s_{si}(\underline{x})$ is the displacement of the point of the strand cross section in direction of the local axis z_i. The coordinates z_2 and z_3 detect the position of one point of the cross section in the cross-section plane itself. The generalized displacement u_{s1}, v_{s2} and v_{s3} are the displacements of the strand centerline in the directions z_1, z_2 and z_3 respectively. The rotations ϕ_{sT}, ϕ_{s2} and ϕ_{s3} are the rigid rotations of the strand cross section about the directions z_1, z_2 and z_3 respectively. The subrscript "R" is substituted with "s" standing for strand, remembering that the generalized displacements of the strand hold true for either the strand and its core wire.
The generalized displacement components of the strand cross section are derived from (2.II.3) introducing (2.II.1) and the components of the single helix Serret-Frenet frame.

$$
\begin{aligned}
u_{s1}(\underline{x}) &= \sum_{i=1}^{3} s_{Ri}(\underline{x})\, t_{si} = s_{R1}(\underline{x})\, \cos\alpha_s - s_{R2}(\underline{x}) \sin\alpha_s \sin\vartheta(x_1) + s_{R3}(\underline{x}) \sin\alpha_s \cos\vartheta(x_1) \\
v_{s2}(\underline{x}) &= \sum_{i=1}^{3} s_{Ri}(\underline{x})\, n_{si} = -s_{R2}(\underline{x}) \cos\vartheta(x_1) - s_{R3}(\underline{x}) \sin\vartheta(x_1) \\
v_{s3}(\underline{x}) &= \sum_{i=1}^{3} s_{Ri}(\underline{x})\, b_{si} = s_{R1}(\underline{x}) \sin\alpha_s + s_{R2}(\underline{x}) \cos\alpha_s \sin\vartheta(x_1) - s_{R3}(\underline{x}) \cos\alpha_s \cos\vartheta(x_1)
\end{aligned}
$$

Let us collect the common terms once the equations (2.II.1) are introduced with the position vector of the single helix.

$$
\begin{aligned}
u_{s1}(\underline{x}) &= \cos\alpha_s\; u_{R1}(x_1) + R_s \sin\alpha_s\; \varphi_{RT}(x_1) + R_s \cos\alpha_s \left[\sin\vartheta(x_1)\, \varphi_{R2}(x_1) - \cos\vartheta(x_1)\, \varphi_{R3}(x_1)\right] \\
&\quad - \sin\alpha_s \left[\sin\vartheta(x_1)\, v_{R2}(x_1) - \cos\vartheta(x_1)\, v_{R3}(x_1)\right] \\
v_{s2}(\underline{x}) &= -\cos\vartheta(x_1)\, v_{R2}(x_1) - \sin\vartheta(x_1)\, v_{R3}(x_1) \\
v_{s3}(\underline{x}) &= \sin\alpha_s\, u_{R1}(x_1) - R_s \cos\alpha_s\, \varphi_{RT}(x_1) + + R_s \sin\alpha_s \left[\sin\vartheta(x_1)\, \varphi_{R2}(x_1) - \cos\vartheta(x_1)\, \varphi_{R3}(x_1)\right] \\
&\quad + \cos\alpha_s \left[\sin\vartheta(x_1)\, v_{R2}(x_1) - \cos\vartheta(x_1)\, v_{R3}(x_1)\right]
\end{aligned}
\qquad (2.II.5a)
$$

The generalized rotations are defined as follows.

$$
\begin{aligned}
\varphi_{sT}(x_1) &= \sum_{i=1}^{3} \varphi_{Ri}(x_1)\, t_{si} = \cos\alpha_s\, \varphi_{R1}(x_1) - \sin\alpha_s \sin\vartheta(x_1)\, \varphi_{R2}(x_1) + \sin\alpha_s \cos\vartheta(x_1)\, \varphi_{R3}(x_1) \\
\varphi_{s2}(x_1) &= \sum_{i=1}^{3} \varphi_{Ri}(x_1)\, n_{si} = -\cos\vartheta(x_1)\, \varphi_{R2}(x_1) - \sin\vartheta(x_1)\; \varphi_{R3}(x_1) \\
\varphi_{s3}(x_1) &= \sum_{i=1}^{3} \varphi_{Ri}(x_1)\, b_{si} = \sin\alpha_s\, \varphi_{R1}(x_1) + \cos\alpha_s \sin\vartheta(x_1)\, \varphi_{R2}(x_1) - \cos\alpha_s \cos\vartheta(x_1)\, \varphi_{R3}(x_1)
\end{aligned}
\qquad (2.II.5b)
$$

It is worth to notice the peculiar behavior of this structural element. Specifically, from the third of (2.II.5b) an axial torsional deformation in the rope produces an axial torsional deformation in the strand as well, still in addition the strand experiences also bending about the binormal direction.

2. STRAIN FIELD

In the present paragraph let us introduce the kinematic quantities describing the strain field of wire, strand and wire rope. For the latter, since a Euler-Bernoulli kinematics has been assumed, the generalized strains are the same of a beam described with the same structural theory, i.e. the axial elongation η_R, the torsional curvature χ_{RT} and the flexural curvatures χ_{R2} χ_{R3}. Conversely, for the wire and the strand the choice of the strain variables is done according to the structural theory of the Love curved thin rod like in the paper of Huang, 1973.

2.1. ROPE GENERALIZED STRAINS

The definition of the kinematic variables comes directly from the Euler Bernoulli beam theory. The comma represents the partial derivatives with respect the variable that follows. Specifically, the coordinate 1 indicates the global coordinate x_1 that coincide with the rope axis, while 2 and 3 are x_2 and x_3. The non- zero strains are:

$$\varepsilon_{R1} = s_{R1,1} = u_{R1,1} + \varphi_{R2,1}\, x_3 - \varphi_{R3,1}\, x_2$$
$$\gamma_{R12} = s_{R1,2} + s_{R2,1} = -\varphi_{R3} + v_{R2,1} - \varphi_{RT,1}\, x_3$$
$$\gamma_{R13} = s_{R1,3} + s_{R3,1} = +\varphi_{R2} + v_{R3,1} + \varphi_{RT,1}\, x_2$$

In terms of generalized quantities, the strains may be written as follows

$$\varepsilon_{R1}(\underline{x}) = \eta_R(x_1) + \chi_{R2}(x_1)\, x_3 - \chi_{R3}(x_1)\, x_2 + \varphi_{R2}(x_1)\, x'_3 - \varphi_{R3}(x_1)\, x'_2$$
$$\gamma_{R12}(\underline{x}) = -\chi_{RT}(x_1)\, x_3 - \varphi_{RT}(x_1)\, x'_3$$
$$\gamma_{R13}(\underline{x}) = +\chi_{RT}(x_1)\, x_2 + \varphi_{RT}(x_1)\, x'_2$$

Hence, the generalized axial strain of the rope is measured as follows.

$$(2.II.6a) \qquad \boldsymbol{\eta_R(x_1) = \frac{du_{R1}}{dx_1}(x_1)}$$

While the torsional and bending curvatures are defined in the following manner.

$$\boldsymbol{\chi_{RT}(x_1) = \frac{d\varphi_{RT}}{dx_1}(x_1)}$$
$$(2.II.6b) \qquad \boldsymbol{\chi_{R2}(x_1) = \frac{d\varphi_{R2}}{dx_1}(x_1)}$$
$$\boldsymbol{\chi_{R3}(x_1) = \frac{d\varphi_{R3}}{dx_1}(x_1)}$$

Where u_{R1}, ϕ_{RT}, ϕ_{R2} and ϕ_{R3} are respectively the axial displacement of the rope, the torsional rotation and the bending rotations about the principal axis.

2.2. WIRE GENERALIZED STRAINS

The structural theory of the curved thin rod allows to define the generalized strains as a function of the initial geometrical curvature and torsion within the small deformation hypothesis. This result is achieved enforcing local equilibrium of the curved element and through the principle of virtual work. The partial derivatives are computed with respect the Serret-Frenet frame coordinates in the passages that follows and are denoted with the comma. These coordinates are (y_1, y_2, y_3) respectively directed as ($\underline{t}_w$, $\underline{n}_w$, $\underline{b}_w$). Specifically, the variable y_1 corresponds to the curvilinear coordinate of the wire centerline s_w.

$$(2.II.7a) \qquad \eta_w = u_{w,1} - \kappa_w\, v_{w2}$$
$$\chi_{wT} = \varphi_{wT,1} - \kappa_w\, \varphi_{w2}$$
$$(2.II.7b) \qquad \chi_{w2} = \varphi_{w2,1} + \kappa_w\, \varphi_{wT} - \tau_w\, \varphi_{w3}$$
$$\chi_{w3} = \varphi_{w3,1} + \tau_w\, \varphi_{w2}$$

Where η_w is the axial strain, χ_{wT} is the torsional curvature, χ_{w2} is the bending curvature about the normal direction and χ_{w3} is the bending curvature about the binormal direction of the wire. The generalized displacements are defined in paragraph II.1.2. Finally, κ_w and τ_w are the wire curvature and torsion respectively.

2.2.1. WIRE AXIAL STRAIN

The first contribution to investigate is the axial strain of the curved element. This quantity represents the stretching experienced by the wire centerline during the deformation process. In the next passages we will exploit the Serret-Frenet formulas.

$$\eta_w = \frac{\partial}{\partial y_1}(u_w) - \kappa_w\, v_{w2} = \sum_{i=1}^{3} \frac{\partial}{\partial y_1}(s_{Ri})\, t_{wi} + \sum_{i=1}^{3} s_{Ri}\, \frac{\partial}{\partial y_1}(t_{wi}) - \kappa_w \sum_{i=1}^{3} s_{Ri}\, n_{wi} = \frac{dx_1}{dy_1} \sum_{i=1}^{3} \frac{\partial}{\partial x_1}(s_{Ri})\, t_{wi}$$

The term of (2.II.7a) containing the geometrical curvature drops, thus the measure of the generalized axial strain of the wire is the derivative of the longitudinal displacement with respect the local abscissa of the wire. The computation of the derivatives is as follows.

$$\eta_w = \frac{dx_1}{dy_1}\left[(\eta_R + \chi_{R2}\, x_{w3} - \chi_{R3}\, x_{w2} + \varphi_{R2}\, x'_{w3} - \varphi_{R3}\, x'_{w2})\, t_{w1} + (v_{R2,1} - \chi_{RT}\, x_{w3} - \varphi_{RT}\, x'_{w3})\, t_{w2} + (v_{R3,1} + \chi_{RT}\, x_{w2} + \varphi_{RT}\, x'_{w2})\, t_{w3}\right]$$

$$\eta_w = \frac{dx_1}{dy_1}\left[t_{w1}(\eta_R + x_{w3}\, \chi_{R2} - x_{w2}\, \chi_{R3}) + (x_{w2}\, t_{w3} - x_{w3}\, t_{w2})\, \chi_{RT} + (x'_{w1} - 1)\,(t_{w3}\, \varphi_{R2} - t_{w2}\, \varphi_{R3})\right]$$

Let us split the contribution due to the rope axial torsional (η_R, χ_{RT}) and biaxial bending (χ_{R2}, χ_{R3}, ϕ_{R2}, ϕ_{R3}).

2.2.1.1. ROPE'S AXIAL TORSIONAL CONTRIBUTIONS

$$(2.II.8)\quad \boldsymbol{\eta_w^{AT} = \frac{dx_1}{dy_1}\left[t_{w1}\,\eta_R + (x_{w2}\,t_{w3} - x_{w3}\,t_{w2})\,\chi_{RT}\right]}$$

The superscripts "A" and "T" stand for axial and torsional strain within the rope respectively. In the graphs below, we can see the two terms plotted for unit kinematic strains of the wire rope for the 7x7 WRC stranded rope analyzed in the geometry chapter. Two different wires are considered: W4 is the outer wire of the strand, hence it has a double helix shape of the centerline; while W3 is the core wire of the strand, thus it has a single helix geometry. The outer wire is plotted for the two different arch lengths "real" and "developed".
Firstly, the coefficient providing the contribution of the wire rope axial strain to the axial stretching of the wire.

$$(2.II.8a)\quad \eta_w^A = \left(\frac{dx_1}{dy_1}\, t_{w1}\right)\eta_R$$

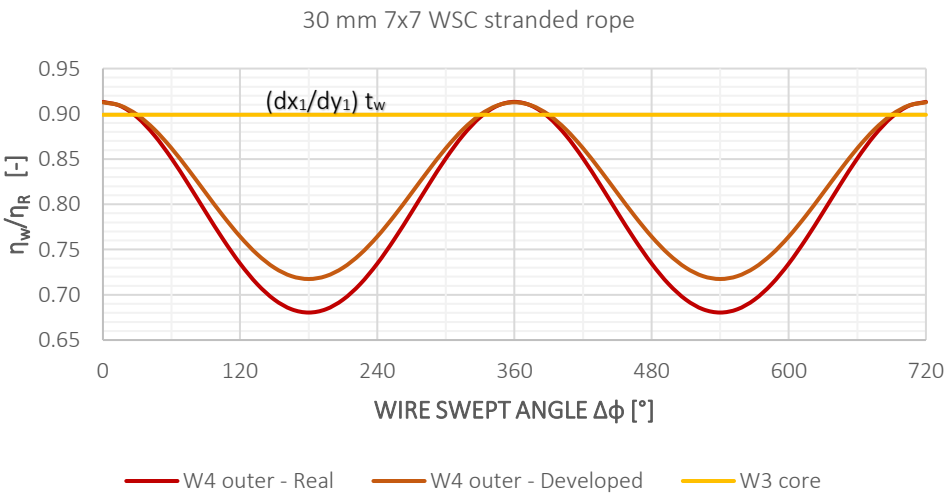

Fig 2.37 Wire Axial Strain due to Rope Axial Strain

The coefficient provides the axial strain of the wire when the rope experiences an axial stretching only. For the core wire W3, i.e. the single helix geometry, the trend is constant along the rope axis; while the outer wire W4 shows a sinusoidal trend with the same period of the double helix. The result is very important since the axial stretching of the wire affects the response at two levels. The global response of the rope is determined by the mean value of that function, while the local response, for instance the average stress of the wire, depends upon the maximum value of the axial strain in absolute value.
The latter statement has a crucial role since the present model assumes a perfect bonding condition between the wires. This hypothesis holds true when slipping is prevented among the wires. If the all the wires of the cross section experience the same mean stress, like it occurs for the case of the single helix W3, no tangential stresses arise to restore equilibrium among adjacent wires. Conversely, in the double helix a sinusoidal trend of the mean stress of the wire involves that, even in the simplest scenario where the rope experiences axial deformation only, tangential stresses do arise to ensure that the wires are in equilibrium.
In the following table a comparison between the results obtained through the real and developed arch length is showed for the outer wire W4.

Table 2.5 Wire Axial Strain due to Rope Axial Strain

η_w/η_R	max	min	mean
W4 real	0.9132	0.6804	0.7968
W4 developed	0.9127	0.7174	0.8151
error	0.06%	-5.16%	-2.24%

The second coefficient provide the rope torsional contribution to the wire axial strain.

$$(2.II.8b) \quad \eta_w^T = \left[\frac{dx_1}{dy_1}\left(x_{w2}\, t_{w3} - x_{w3}\, t_{w2}\right)\right]\chi_{RT}$$

The geometrical quantity ($x_2\, t_{w3} - x_3\, t_{w2}$) represents the distance between the rope middle line and the wire centerline and it arises because of the hypothesis of rigid rotation of the wire rope cross section. In fact, it is like the two centerlines are constrained by a rigid link directed as the distance vector orthogonal to the rope axis.

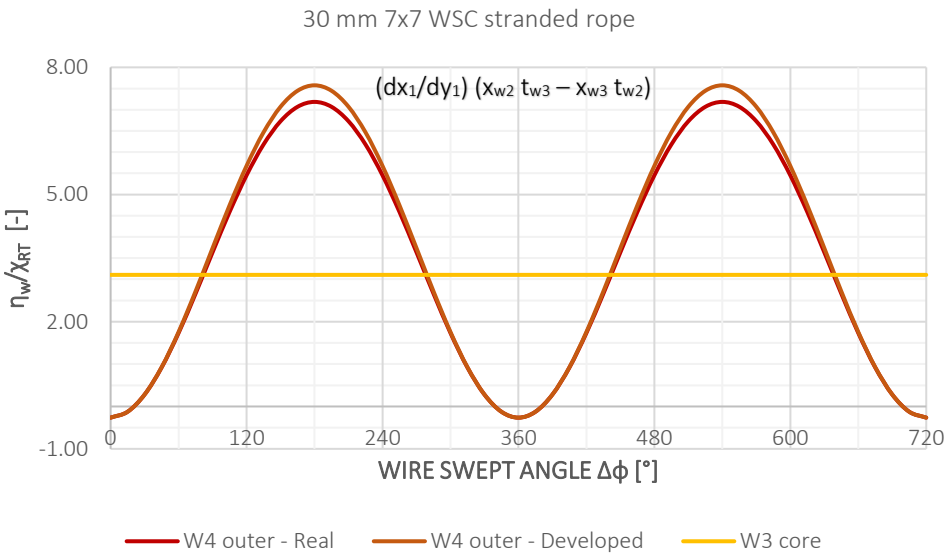

Fig 2.38 Wire Axial Strain due to Rope Torsion

In the following table a comparison between the results obtained through the real and developed arch length is showed for the outer wire W4.

Table 2.6 Wire Axial Strain due to Rope Torsion

η_w/χ_{RT}	max	min	mean
W4 real	7.1846	-0.2637	3.4604
W4 devel	7.5757	-0.2636	3.6561
error	-5.16%	0.06%	-5.35%

The higher error in absolute value occurs in the maximum of the two functions. It can be appreciated a greater difference in the mean value with respect of the previous coefficient (2.II.3a).

2.2.1.2. ROPE'S BENDING CONTRIBUTIONS

$$\eta_w = \frac{dx_1}{dy_1}\left[(\chi_{R2}\, x_{w3} - \chi_{R3}\, x_{w2} + \varphi_{R2}\, x'_{w3} - \varphi_{R3}\, x'_{w2})\, t_{w1} + v_{R2,1}\, t_{w2} + v_{R3,1}\, t_{w3}\right]$$

It can be noticed that in the definition of the wire axial strain there is a dependence on the rope bending curvatures, like it usually occurs in beam theories, and on the transverse displacement and bending rotations of the rope. The kinematic interpretation of this terms is provided in the following.

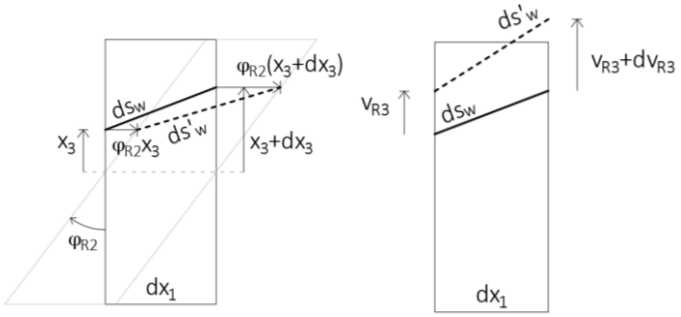

Figura 2.39 Constant Bending Rotation and Variation of Transverse Displacement Effects on Wire Stretching

The first image shows the contribution to the wire axial strain due to a constant rotation axis along the rope axis about the x_2.

$$\eta_w = \frac{ds'_w - ds_w}{ds_w} = \frac{\varphi_{R2}\, dx_3\, \underline{e}_1 * \underline{t}_w}{ds_w} = \frac{\varphi_{R2}\, dx_3\, t_{w1}}{dx_1}\frac{dx_1}{ds_w} = \frac{dx_1}{ds_w} t_{w1}\, x'_{w3}\, \varphi_{R2}$$

This term arises because of the orientation of the wire with respect to the rope axis. The second image shows the contribution due to transverse displacement.

$$\eta_w = \frac{ds'_w - ds_w}{ds_w} = \frac{dv_{R3}\, \underline{e}_3 * \underline{t}_w}{ds_w} = \frac{dv_{R3}\, t_{w3}}{dx_1}\frac{dx_1}{ds_w} = \frac{dx_1}{ds_w} t_{w3}\, v'_{R3}$$

The two contributions are not uncorrelated, since the kinematic constraint introduced by the Euler Bernoulli hypothesis of the rope cross section holds. As a matter of fact, the following relations hold:

$$\varphi_{R2}(x_1) = -v'_{R3}(x_1)$$
$$\varphi_{R3}(x_1) = +v'_{R2}(x_1)$$

Hence, let us sum the two previous contributions to the wire axial strain

$$\frac{dx_1}{ds_w} t_{w1}\, x'_{w3}\, \varphi_{R2} + \frac{dx_1}{ds_w} t_{w3}\, v'_{R3} = \frac{dx_1}{ds_w} t_{w3}\, x'_{w1}\, \varphi_{R2} - \frac{dx_1}{ds_w} t_{w3}\, \varphi_{R2} = \frac{dx_1}{ds_w}\,(x'_{w1} - 1)\, t_{w3}\ \varphi_{R2}$$

Analouge passages may be done for the other rotation and transverse displacement. The final shape of the wire axial strain is as follows.

$$(2.II.9)\quad \eta_w^B = \frac{dx_1}{dy_1}\left[t_{w1}\left(x_{w3}\,\chi_{R2} - x_{w2}\,\chi_{R3}\right) + \left(x'_{w1} - 1\right)\left(t_{w3}\,\varphi_{R2} - t_{w2}\,\varphi_{R3}\right)\right]$$

It can be appreciated that the axial strain of the wire depends not only on the curvatures about the transverse direction of the rope, but also from the rotations. This result depends on the geometry feature of the double helix (1.IV.4). As a matter of fact, the term x'_1-1 can be explicitly written from the nested helix geometry.

$$(2.II.10)\quad x'_{w1}(x_1) - 1 = \tan\alpha_s \tan\alpha_w \cos\varphi(x_1)$$

This term is oscillatory with zero mean value according to a cosine function, hence when it is integrated along the wire arch length corresponding to the pitch, it provides zero. The last statement implies that globally the wire doesn't experience any elongation, while locally it does. It's worth to notice that in the single helix, i.e. the centreline of the strand, this term is identically zero because of the peculiar geometry of this type of curve.

Let us analyse the trend of the bending coefficients that multiply either curvatures and rotations. First, a close-up view will be provided within the same span of swept angles used for axial torsion. From this choice of the interval, it will be clear the need of enlarging the length of the rope axis under investigation, in order to catch the actual trend of the plotted functions. In either case, the quantity regarding the global axis 2 will be investigated only, since the other one is simply obtained by shifting along the rope axis of the previous ones.
Firstly, let us introduce the coefficients that multiply the bending curvature about the axis 2.

$$(2.II.9a)\quad \eta_w^{B2} = \left(\frac{dx_1}{dy_1}\,t_{w1}\,x_{w3}\right)\chi_{R2}$$

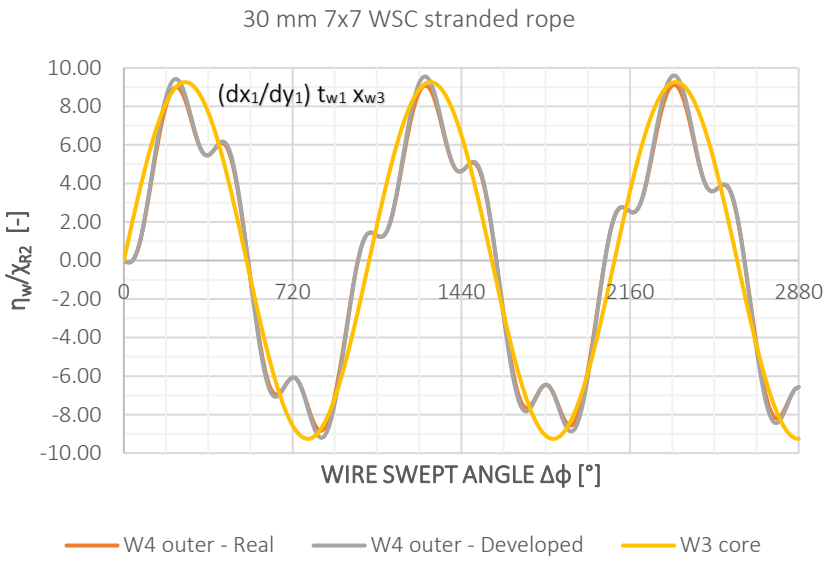

Fig 2.40 Wire Axial Strain due to Rope Bending Curvature - Detail

The function seems to be non-periodic, but this result is a consequence of the choice of the interval of rope length where we analyse the quantity. As a matter of fact, the axial torsion kinematic quantities (2.II.8) have the same period of the double helix. Hence, if the plot is extended for enough length of the rope axis, it can be appreciated that a periodical behaviour may be detected like it is shown in the graph below. This feature has extreme importance from the energetic vantage point. As a matter of fact, the present paragraph is leading the influence of the rope bending on wire stretching, hence a non-periodic behaviour means that if this kind of term is integrated along the rope axis it produces a net elongation of the wire. Thus, bending of the rope induces stretching of the rope as well, which do not correspond to the actual physical behaviour. A wrong choice of the kinematic variables would lead to an energetically inconsistent model like it happens in Ramsey, 1988, where secular terms arise in the expression of the generalized strain of the wire.

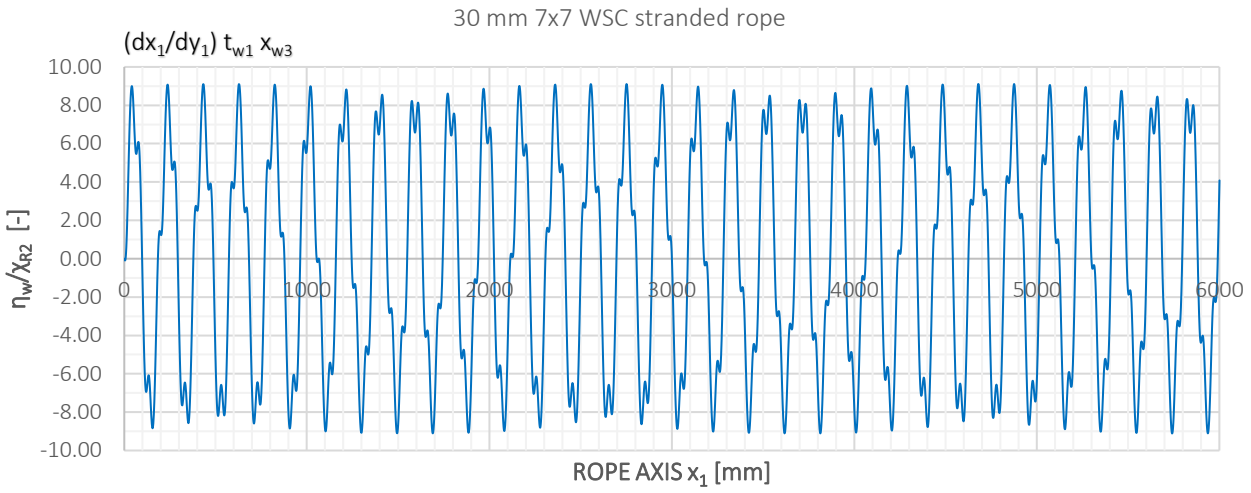

Fig 2.41 Wire Axial Strain due to Rope Bending Curvature - Overview

The last coefficient that it is plotted is the one providing the axial strain of the wire due to the rope bending rotation. It must be remembered that this kind of term arise only for the double helix geometry, since for the single helix it is identically equal to zero. The superscript "R2" stands for contribution due to the rope bending rotation about the global axis 2.

$$(2.II.9b) \quad \eta_w^{R2} = \left[\frac{dx_1}{dy_1}(x'_{w1} - 1)\, t_{w3}\right] \varphi_{R2}$$

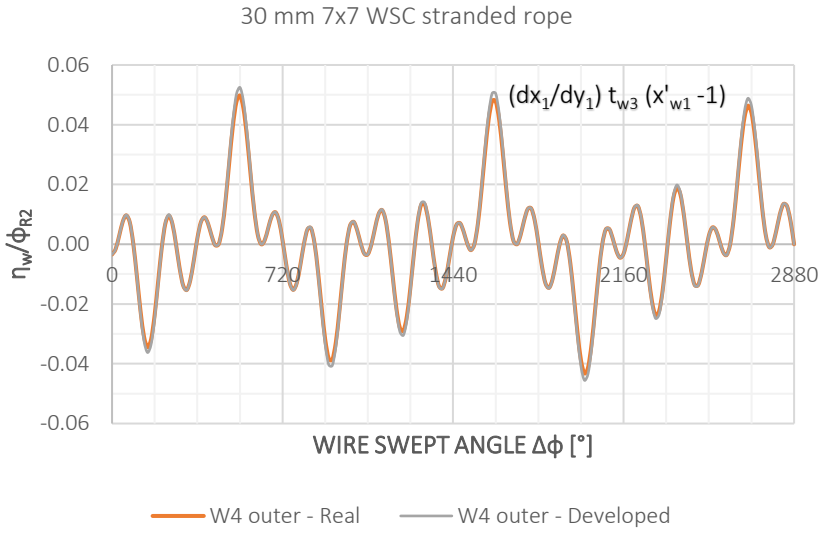

Fig 2.42 Wire Axial Strain due to Rope Bending Rotation - Detail

The same reasoning aforesaid for the function (2.II.9a) holds true. Hence, in order to appreciate the periodicity of the quantity (2.II.9b) the rope length under investigation must be enlarged as follows.

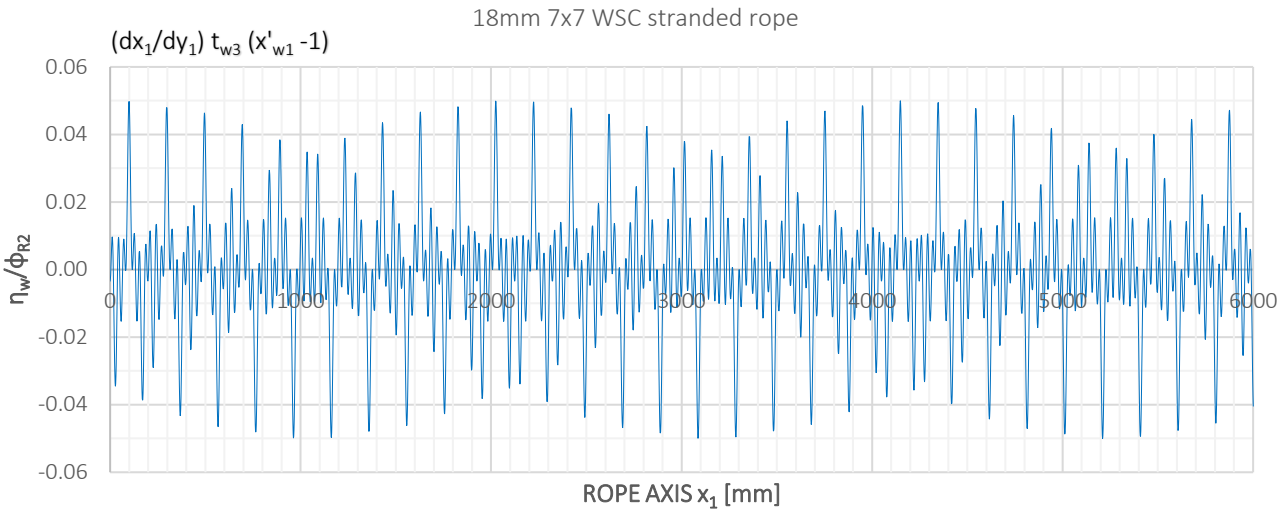

Fig 2.43 Wire Axial Strain due to Rope Bending Rotation - Overview

An alternative way to analyse the problem of energy consistency of the model and the correct choice of the kinematic variables is focusing on the rope cross section. The function causing the non-sinusoidal trend is the in plane component of the double helix position of the double helix inside the rope cross section x_{w3}. This is ensured by the sinusoidal trend of dx_1/ds_w and t_{w1} with period equal to cos(ϕ) and sin(ϕ), like it has been shown before.

$$x_{w3}(x_1) = R_s \sin\theta(x_1) - R_w \cos\varphi(x_1) \sin\vartheta(x_1) - R_w \cos\alpha_s \sin\varphi(x_1) \cos\vartheta(x_1)$$

If the cross section is symmetric, the last two addends vanishes within strand cross section, while the first term does inside the rope cross section. Hence, two wires with the same ϕ into the strand but θ and θ+180° inside the rope show opposite values of the previous functions. Again, the result is consistent because within the cross section may happen that locally a wire undergoes stretching, while globally the rope does not experience any elongation

2.2.2. WIRE CURVATURES

The derivation of the curvatures follows the same path of reasoning of the axial strain. Specifically, the terms depending on the geometrical curvature and torsion vanish because of the choice of the reference frame, when we exploit the Serret-Frenet formulas. Only the passages for the torsional curvature are shown explicitly.

$$\chi_{wT} = \frac{\partial}{\partial y_1}(\varphi_{wT}) - \kappa_w\, \varphi_{w2} = \sum_{i=1}^{3} \frac{\partial}{\partial y_1}(\varphi_{Ri}) t_{wi} + \sum_{i=1}^{3} \varphi_{Ri}\, \frac{\partial}{\partial y_1}(\, t_{wi}) - \kappa_w \sum_{i=1}^{3} \varphi_{Ri}\, n_{wi} = \frac{dx_1}{dy_1} \sum_{i=1}^{3} \frac{\partial}{\partial x_1}(\varphi_{Ri}) t_{wi}$$

The curvatures do not depend upon the geometrical curvature and torsion. The result is that they are defined like in the beam theories, i.e. relative rotation over the distance between the considered sections, but with reference to the curvilinear abscissa.

$$(2.II.11) \quad \begin{aligned} \boldsymbol{\chi_{wT}} &= \frac{\boldsymbol{dx_1}}{\boldsymbol{dy_1}} \sum_{i=1}^{3} \boldsymbol{\chi_{Ri}}\, \boldsymbol{t_{wi}} \\ \boldsymbol{\chi_{w2}} &= \frac{\boldsymbol{dx_1}}{\boldsymbol{dy_1}} \sum_{i=1}^{3} \boldsymbol{\chi_{Ri}}\, \boldsymbol{n_{wi}} \\ \boldsymbol{\chi_{w3}} &= \frac{\boldsymbol{dx_1}}{\boldsymbol{dy_1}} \sum_{i=1}^{3} \boldsymbol{\chi_{Ri}}\, \boldsymbol{b_{wi}} \end{aligned}$$

2.3. STRAND GENERALIZED STRAINS

The strain field has the same formal shape of the wire. The difference is in the Serret-Frenet frame components as well as for the displacements. Hence, the results coming from the wire strains are exploited substituting the suitable values for the local reference frame. The contribution coming from axial torsion and bending of the rope will be split in order to highlight them. Obviously, the total strain experienced by the strand will be the sum of the two contributions.

2.3.1. STRAND AXIAL STRAIN

2.3.1.1. ROPE'S AXIAL TORSIONAL CONTRIBUTIONS

$$\eta_s^{AT} = \frac{dx_1}{dy_1}\left[t_{s1}\,\eta_R + (x_{s2}\,t_{s3} - x_{s3}\,t_{s2})\,\chi_{RT}\right]$$

The factor accounting the coordinate transformation from the global reference frame to the local one is obtained through the developed geometry of the single helix.

$$\frac{dx_1}{dy_1} = \cos\alpha_s$$

Moreover, it is possible to explicit the term multiplying the torsional curvature.

$$x_{s2}\,t_{s3} - x_{s3}\,t_{s2} = R_s\,\cos\vartheta\sin\alpha_s\cos\vartheta - (-R_s\,\sin\vartheta\sin\alpha_s\sin\vartheta) = R_s\,\sin\alpha_s$$

Thus, the expression of the rope's axial torsional contribution to the axial strain of the strand can be written as follows.

$$(2.II.12)\quad \boldsymbol{\eta_s^{AT}(x_1) = \cos^2\alpha_s\;\eta_R(x_1) + R_s\;\cos\alpha_s\sin\alpha_s\;\chi_{RT}(x_1)}$$

2.3.1.2. ROPE'S BENDING CONTRIBUTIONS

$$\eta_s^B = \frac{dx_1}{dy_1}\left[t_{s1}(\,x_{s3}\,\chi_{R2} - x_{s2}\,\chi_{R3}) + (x'_{s1} - 1)\,(t_{s3}\,\varphi_{R2} - t_{s2}\,\varphi_{R3})\right]$$

Differently from the double helix geometry the term x_{s1} is identical to the global coordinate x_1, hence the derivative with respect this coordinate $x'_{s1} = 1$. Consequently, the term containing the rotations vanishes.

$$(2.II.13)\quad \boldsymbol{\eta_s^B(x_1) = \cos^2\alpha_s R_s\sin\vartheta(x_1)\;\chi_{R2}(x_1) - \cos^2\alpha_s R_s\cos\vartheta(x_1)\;\chi_{R3}(x_1)}$$

2.3.2. STRAND CURVATURES

They are obtained directly from the double helix formulas substituting the suitable expressions for the components of the Serret-Frenet frame vectors and the arch length of the single helix.

$$\frac{dx_1}{ds_s} = \cos\alpha_s$$

2.3.2.1. ROPE'S AXIAL TORSIONAL CONTRIBUTIONS

$$\begin{aligned}
&\boldsymbol{\chi_{sT}^{AT}(x_1) = \cos^2\alpha_s\,\chi_{RT}(x_1)}\\
(2.II.14)\quad &\boldsymbol{\chi_{s2}^{AT}(x_1) = 0}\\
&\boldsymbol{\chi_{s3}^{AT}(x_1) = \cos\alpha_s\sin\alpha_s\,\chi_{RT}(x_1)}
\end{aligned}$$

It's interesting to observe that a torsional strain field in the rope induces a torsional deformation in the strand as well, furthermore it produces bending about the binormal direction of the strand. This result is a direct consequence of the single helix geometry, as a matter of fact the component of the normal vector along the rope axis is null.

2.3.2.2. ROPE'S BENDING CONTRIBUTIONS

$$\chi_{sT}^{B}(x_1) = -\cos\alpha_s \sin\alpha_s \sin\vartheta(x_1)\,\chi_{R2}(x_1) + \cos\alpha_s \sin\alpha_s \cos\vartheta(x_1)\,\chi_{R3}(x_1)$$

(2.*II*.15) $$\chi_{s2}^{B}(x_1) = -\cos\alpha_s \cos\vartheta(x_1)\,\chi_{R2}(x_1) - \cos\alpha_s \sin\vartheta(x_1)\,\chi_{R3}(x_1)$$

$$\chi_{s3}^{B}(x_1) = \cos^2\alpha_s \sin\vartheta(x_1)\,\chi_{R2}(x_1) - \cos^2\alpha_s \cos\vartheta(x_1)\,\chi_{R3}(x_1)$$

III. RECURSIVE MODEL

In this section a simplified model for kinematics is developed, based on a hierarchical description of the geometry of the rope and the recursive approach firstly outlined in (Foti, 2013); (Meleddu et al., 2017). So far, only the kinematic constraints between rope and strand have been explicitly provided (2.II.12-15). This type of relation will be enforced with the same expressions between strand and wire.
The reason of this choice is due to the technological procedure for the manufacturing of wire ropes. As a matter of fact, a clear hierarchy may be detected within this peculiar assembly. Let us imagine that the rope system is the last level and the wire is the first level. The wire is the basic component and it is used to construct a strand: the core wire is left straight, and the outer wires are wounded about the core with a single helix shape. Moreover, the layer is the set of outer wires having the same distance (R_l) from the strand axis. A strand can be endowed with several layers. This element is the second level of the hierarchy and the previous description holds for the manufacturing of a straight strand. The subsequent step is the assembly of more strands to form the next level. It may be performed in different ways, the simplest one is the stranded rope, i.e. when the same relation holding between wire and strand is introduced for the strand and the rope. Hence, the strand is seen as the new basic component and more strands will be coiled with a single helix geometry about a straight core.
It is trivial that the original wire will have a nested helix shape. If the rigorous geometry of the wire is exploited, the mechanical model has the kinematic features showed in the previous paragraph II. Conversely, here let us use a different approach. The kinematic of the wire will be described with respect to the strand kinematics using the same relations (2.II.12-15) developed for the single helix or strand geometry in the previous chapter: this is the point where the approximation is introduced, and the hierarchy is exploited. Afterwards, the kinematic quantities of the strand will be substituted according to the relations (2.II.12-15) to have the explicit link between wire and rope. The term "recursive" hints to the hierarchical use of the kinematic relations of the single helix.

1. STRAND STRAINS

Here the relations (2.II.12-15) are directly reported without changes. Since the kinematics is linear, let us exploit the superposition principle and separate the contribution of axial torsion and biaxial bending of the rope for the kinematic quantities of the strand. The subscript "s" stands for "strand", while in the strand generalized strains the superscripts "AT" and "B" correspond to "rope axial torsion" and "rope biaxial bending" respectively.

1.1. ROPE AXIAL TORSION CONTRIBUTION

From equations (2.II.12) and (2.II.14), the following relations are obtained for the strand generalized strains when the rope experiences axial torsion perturbation.

$$
\begin{aligned}
&\eta_s^{AT}(x_1) = \cos^2\alpha_s\ \eta_R(x_1) + R_s\ \cos\alpha_s \sin\alpha_s\ \chi_{RT}(x_1) \\
&\chi_{sT}^{AT}(x_1) = \cos^2\alpha_s\, \chi_{RT}(x_1) \\
&\chi_{s2}^{AT}(x_1) = 0 \\
&\chi_{s3}^{AT}(x_1) = \cos\alpha_s \sin\alpha_s\, \chi_{RT}(x_1)
\end{aligned}
\qquad (2.III.1)
$$

The rope axial torsion strain field induces in the strand axial torsion as well, still bending about the binormal direction arises as well.

1.2. ROPE BENDING CONTRIBUTION

From equations (2.II.13) and (2.II.15), the following relations are obtained for the strand generalized strains when the rope experiences biaxial bending perturbation.

$$
\begin{aligned}
&\eta_s^{B}(x_1) = \cos^2\alpha_s\, R_s \sin\vartheta(x_1)\ \chi_{R2}(x_1) - \cos^2\alpha_s\, R_s \cos\vartheta(x_1)\ \chi_{R3}(x_1) \\
&\chi_{sT}^{B}(x_1) = -\cos\alpha_s \sin\alpha_s \sin\vartheta(x_1)\, \chi_{R2}(x_1) + \cos\alpha_s \sin\alpha_s \cos\vartheta(x_1)\, \chi_{R3}(x_1) \\
&\chi_{s2}^{B}(x_1) = -\cos\alpha_s \cos\vartheta(x_1)\, \chi_{R2}(x_1) - \cos\alpha_s \sin\vartheta(x_1)\, \chi_{R3}(x_1)
\end{aligned}
\qquad (2.III.2)
$$

$$\chi_{s3}^{B}(x_1) = \cos^2\alpha_s \sin\vartheta(x_1)\,\chi_{R2}(x_1) - \cos^2\alpha_s \cos\vartheta(x_1)\,\chi_{R3}(x_1)$$

The rope biaxial bending induces axial torsion and biaxial bending in the strand.

2. WIRE STRAINS

This is the point where the approximation is introduced. As a matter of fact, the equation (2.III.1) and (2.III.2) holding between the rope and the strand are enforced also for the strand and the wire. Thus, the subscript "s" will be changed with "w" standing for "wire, while, in order to exploit superposition within the strand as well, the contributions of strand axial torsion and biaxial bending will be separated, and they are denoted with the superscripts "sAT" and "sB" respectively. The reader shall pay attention to distinguish the strain field experienced by the rope and the strain field experienced by either strand and wire, since they never coincide in practice.

$$\begin{aligned}
&\eta_w^{sAT}(x_1) = \cos^2\alpha_w\ \eta_s(x_1) + R_w\ \cos\alpha_w \sin\alpha_w\ \chi_{sT}(x_1)\\
&\chi_{wT}^{sAT}(x_1) = \cos^2\alpha_w\,\chi_{sT}(x_1)\\
&\chi_{w2}^{sAT}(x_1) = 0\\
&\chi_{w3}^{sAT}(x_1) = \cos\alpha_w \sin\alpha_w\,\chi_{sT}(x_1)
\end{aligned} \qquad (2.III.3)$$

$$\begin{aligned}
&\eta_w^{sB}(x_1) = \cos^2\alpha_w R_w \sin\varphi(x_1)\ \chi_{s2}(x_1) - \cos^2\alpha_w R_w \cos\varphi(x_1)\ \chi_{s3}(x_1)\\
&\chi_{wT}^{sB}(x_1) = -\cos\alpha_w \sin\alpha_w \sin\varphi(x_1)\,\chi_{s2}(x_1) + \cos\alpha_w \sin\alpha_w \cos\varphi(x_1)\,\chi_{s3}(x_1)\\
&\chi_{w2}^{sB}(x_1) = -\cos\alpha_w \cos\varphi(x_1)\,\chi_{s2}(x_1) - \cos\alpha_w \sin\varphi(x_1)\,\chi_{s3}(x_1)\\
&\chi_{w3}^{sB}(x_1) = \cos^2\alpha_w \sin\varphi(x_1)\,\chi_{s2}(x_1) - \cos^2\alpha_w \cos\varphi(x_1)\,\chi_{s3}(x_1)
\end{aligned} \qquad (2.III.4)$$

Furthermore, the superposition principle is exploited for the rope kinematics as well. In fact, the strains in the strand are split according to the axial torsion and biaxial bending of the rope.

$$\begin{aligned}
&\eta_s(x_1) = \eta_s^{AT}(x_1) + \eta_s^{B}(x_1)\\
&\chi_{sT}(x_1) = \chi_{sT}^{AT}(x_1) + \chi_{sT}^{B}(x_1)\\
&\chi_{s2}(x_1) = \chi_{s2}^{AT}(x_1) + \chi_{s2}^{B}(x_1)\\
&\chi_{s3}(x_1) = \chi_{s3}^{AT}(x_1) + \chi_{s3}^{B}(x_1)
\end{aligned} \qquad (2.III.5)$$

2.1. ROPE AXIAL TORSION CONTRIBUTION

The first set of relation is coming from the rope subject to axial torsional perturbation only. This means that the kinematic quantities exciting the strand are: axial strain η_s, torsional curvature χ_{sT} and bending curvature about the binormal direction χ_{s3}. For that reason, axial torsion of the strand will be separated from bending.

2.1.1. STRAND AXIAL TORSION DUE TO ROPE AXIAL TORSION

The relations between wire and strand (2.III.3) are used for the first contribution of (2.III.5). The superscript "sAT" means "strand axial torsion".

$$\begin{aligned}
&\eta_w^{sAT}(x_1) = \cos^2\alpha_w\ \eta_s^{AT}(x_1) + R_w\ \cos\alpha_w \sin\alpha_w\ \chi_{sT}^{AT}(x_1)\\
&\chi_{wT}^{sAT}(x_1) = \cos^2\alpha_w\ \chi_{sT}^{AT}(x_1)\\
&\chi_{w2}^{sAT}(x_1) = 0\\
&\chi_{w3}^{sAT}(x_1) = \cos\alpha_w \sin\alpha_w\ \chi_{sT}^{AT}(x_1)
\end{aligned}$$

Introducing into the latter expressions the η_s and χ_{sT} from (2.III.1):

$$\begin{aligned}
&\eta_s^{AT}(x_1) = \cos^2\alpha_s\ \eta_R(x_1) + R_s\ \cos\alpha_s \sin\alpha_s\ \chi_{RT}(x_1)\\
&\chi_{sT}^{AT}(x_1) = \cos^2\alpha_s\,\chi_{RT}(x_1)
\end{aligned}$$

The following kinematic constraints is obtained between rope and wire.

$$\eta_w^{sAT}(x_1) = \cos^2\alpha_w\ [\cos^2\alpha_s\ \eta_R(x_1) + R_s\ \cos\alpha_s \sin\alpha_s\ \chi_{RT}(x_1)] + R_w\ \cos\alpha_w \sin\alpha_w\ [\cos^2\alpha_s\ \chi_{RT}(x_1)]$$
$$\chi_{wT}^{sAT}(x_1) = \cos^2\alpha_w\ [\cos^2\alpha_s\ \chi_{RT}(x_1)]$$
$$\chi_{w2}^{sAT}(x_1) = 0$$
$$\chi_{w3}^{sAT}(x_1) = \cos\alpha_w \sin\alpha_w\ [\cos^2\alpha_s\ \chi_{RT}(x_1)]$$

Collecting all the common terms, it's possible to find the final expression of the axial strain in the wire due to axial torsion in the strand.

$$\boldsymbol{\eta_w^{sAT}(x_1) = \cos^2\alpha_w \cos^2\alpha_s\ \eta_R(x_1) + [R_s\ \cos\alpha_s \sin\alpha_s \cos^2\alpha_w + R_w\ \cos\alpha_w \sin\alpha_w \cos^2\alpha_s\ ]\ \chi_{RT}(x_1)}$$
$$(2.III.6a)\quad \boldsymbol{\chi_{wT}^{sAT}(x_1) = \cos^2\alpha_w \cos^2\alpha_s\ \chi_{RT}(x_1)}$$
$$\boldsymbol{\chi_{w2}^{sAT}(x_1) = 0}$$
$$\boldsymbol{\chi_{w3}^{sAT}(x_1) = \cos\alpha_w \sin\alpha_w \cos^2\alpha_s\ \chi_{RT}(x_1)}$$

2.1.1.1. AXIAL STRAIN OF THE WIRE DUE TO AXIAL STRAIN OF THE ROPE

Let us compare the two coefficients of the first equation of (2.III.6a) for the recursive model and the direct formulation with the real arch length. The first coefficient is the responsible of the axial strain of the wire when the rope experiences stretching only.

$$(2.III.6aa)\quad \eta_w^{sA}(x_1) = [\cos^2\alpha_w \cos^2\alpha_s]\ \eta_R(x_1)$$

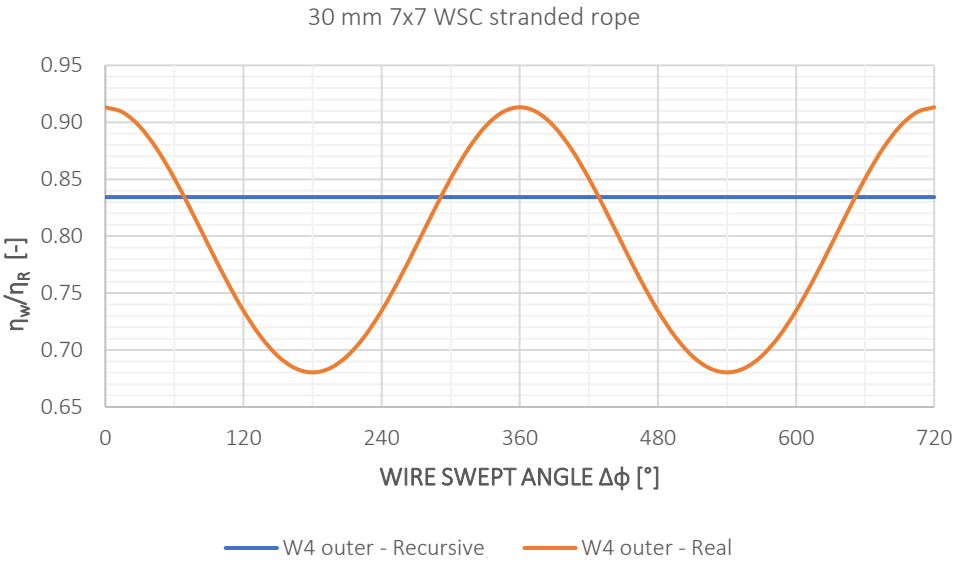

Fig 2.44 Wire Axial Strain due to Rope Axial Strain

The following table shows the difference occurring between the two formulations.

Table 2.7 Wire Axial Strain due to Rope Axial Strain– Total Strand Contribution

η_w/η_R	max	min	mean
direct	0.9132	0.6804	0.7968
recursive	0.8343	0.8343	0.8343
error	9.45%	-18.45%	-4.50%

The difference in the local response of the wire is provided by the gap between the two formulations in correspondence of the maximum and minimum value. It can be appreciated that the difference is not negligible, since it ranges from 9% to 18%. This is the consequence of the approximation made in the recursive model. In this coefficient it can be noticed the constant trend against the sinusoidal one of the direct model. Conversely, the global response of the robe, being affected by the mean value of the coefficient, is less significantly different in the two formulations and specifically it is almost 5% higher for the recursive model.

2.1.1.2. AXIAL STRAIN OF THE WIRE DUE TO TORSIONAL CURVATURE OF THE ROPE

The second coefficient that is investigated is the cause of axial strain in the wire due to the rope torsional curvature. In the first equation of (2.III.6a) it is the last coefficient.

$$(2.III.6ab)\quad \eta_w^{sT}(x_1) = [R_s\ \cos\alpha_s \sin\alpha_s \cos^2\alpha_w + R_w\ \cos\alpha_w \sin\alpha_w \cos^2\alpha_s\ ]\ \chi_{RT}(x_1)$$

A remark needs to be done: the previous quantity is not directly comparable to the correspondent quantity in the direct model (2.II.8b), since for the present formulation the contribution of axial torsion and bending of the strand are split according to (2.III.5). The missing part can be found in the following paragraph. The contribution due to axial torsion of the strand to the coefficient η_w/η_R in (2.III.6a) represents the mean value to the coefficient itself.
In the following plot, it possible to appreciate the difference between (2.III.6ab), that since correspond to the mean value of the searched quantity it is called "Rec.Mean" where Rec stands for recursive, and the correspondent quantity in the direct model (2.II.8b) for the real arch length.

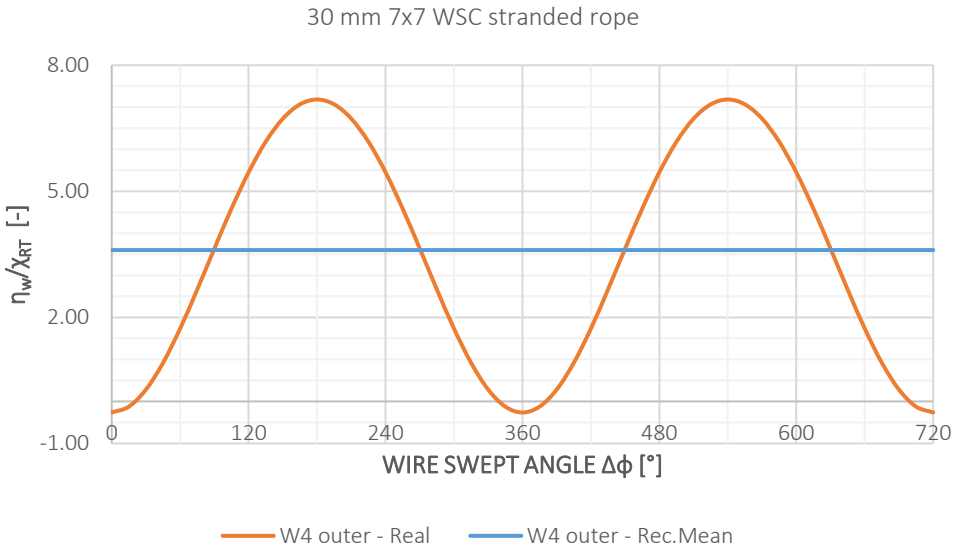

Fig 2.45 Wire Axial Strain due to Rope Torsion – Recursive Axial Torsional Contribution of the Strand

In the following table let us provide the maximum, minimum and mean values for the two functions.

Table 2.8 Wire Axial Strain due to Rope Torsion – Axial Torsional Contribution of the Strand

η_w/χ_{RT}	max	min	mean
direct	7.1846	-0.2637	3.4604
rec.mean	3.6013	3.6013	3.6013
error	99.50%	-107.32%	-3.91%

The mean value of the recursive model is pretty like the mean value of the direct model. For that reason, the difference in correspondence of maximum and minimum value is the higher possible in both case.

2.1.2. STRAND BENDING DUE TO ROPE AXIAL TORSION

The relations between wire and strand (2.III.4) are used for the first contribution of (2.III.5) remembering that χ_{s2} due to torsion is identically zero. The superscript "sB" means "strand bending".

$$\eta_w^{sB}(x_1) = -\cos^2\alpha_w\, R_w \cos\varphi(x_1)\ \chi_{s3}^{AT}(x_1)$$

$$\chi_{wT}^{sB}(x_1) = \cos\alpha_w \sin\alpha_w \cos\varphi(x_1)\,\chi_{s3}^{AT}(x_1)$$
$$\chi_{w2}^{sB}(x_1) = -\cos\alpha_w \sin\varphi(x_1)\,\chi_{s3}^{AT}(x_1)$$
$$\chi_{w3}^{sB}(x_1) = -\cos^2\alpha_w \cos\varphi(x_1)\,\chi_{s3}^{AT}(x_1)$$

Introducing the value bending curvature of the strand about the binormal direction χ_{s3}:

$$\chi_{s2}^{AT}(x_1) = 0$$
$$\chi_{s3}^{AT}(x_1) = \cos\alpha_s \sin\alpha_s\,\chi_{RT}(x_1)$$

The following kinematic constraints is obtained between rope and wire.

$$\begin{aligned}
&\boldsymbol{\eta_w^{sB}(x_1) = -\cos^2\alpha_w\ \cos\alpha_s \sin\alpha_s\, R_w \cos\varphi(x_1)\,\chi_{RT}(x_1)}\\
(2.III.6b)\quad &\boldsymbol{\chi_{wT}^{sB}(x_1) = \cos\alpha_w \sin\alpha_w \cos\alpha_s \sin\alpha_s \cos\varphi(x_1)\,\chi_{RT}(x_1)}\\
&\boldsymbol{\chi_{w2}^{sB}(x_1) = -\cos\alpha_w \cos\alpha_s \sin\alpha_s \sin\varphi(x_1)\,\chi_{RT}(x_1)}\\
&\boldsymbol{\chi_{w3}^{sB}(x_1) = -\cos^2\alpha_w \cos\alpha_s \sin\alpha_s \cos\varphi(x_1)\,\chi_{RT}(x_1)}
\end{aligned}$$

The last relations show how complex the kinematics may be within the wire, when the rope is subject to axial torsion only. As a matter of fact, torsion in the rope induces torsion and bending about the binormal axis inside the strand, while torsion of the strand induces either torsion and bending about the binormal direction within the wire and in addition a three-dimensional kinematic field is induced in the wire by the strand bending about the binormal direction.

2.1.2.1. AXIAL STRAIN OF THE WIRE DUE TO TORSIONAL CURVATURE OF THE ROPE

Now let us complete the coefficient with the missing oscillatory part aforesaid in the previous paragraph 2.1.1.2.

$$(2.III.6ba)\quad \eta_w^{sB}(x_1) = -\cos^2\alpha_w\ \cos\alpha_s \sin\alpha_s\, R_w \cos\varphi(x_1)\,\chi_{RT}(x_1)$$

The coefficient may be completed summing to (2.III.6ba) the mean value (2.III.6ab).

$$(2.III.6bb)\quad \eta_w(x_1) = \eta_w^{sT} + \eta_w^{sB} = [R_s\ \cos\alpha_s \sin\alpha_s \cos^2\alpha_w + R_w\ \cos\alpha_w \sin\alpha_w \cos^2\alpha_s - \cos^2\alpha_w\ \cos\alpha_s \sin\alpha_s\, R_w \cos\varphi(x_1)]\,\chi_{RT}(x_1)$$

Hence, a more consistent comparison may be done with the corresponding coefficient in the direct model (2.II.8b) in the case of real arch length. In the following plot, "Real", "Rec.Tot" and "Rec.Mean" stand respectively for direct model with real arch length (2.II.8b), recursive model with the total value (2.III.6bb) and recursive model with the mean value (2.III.6ab).

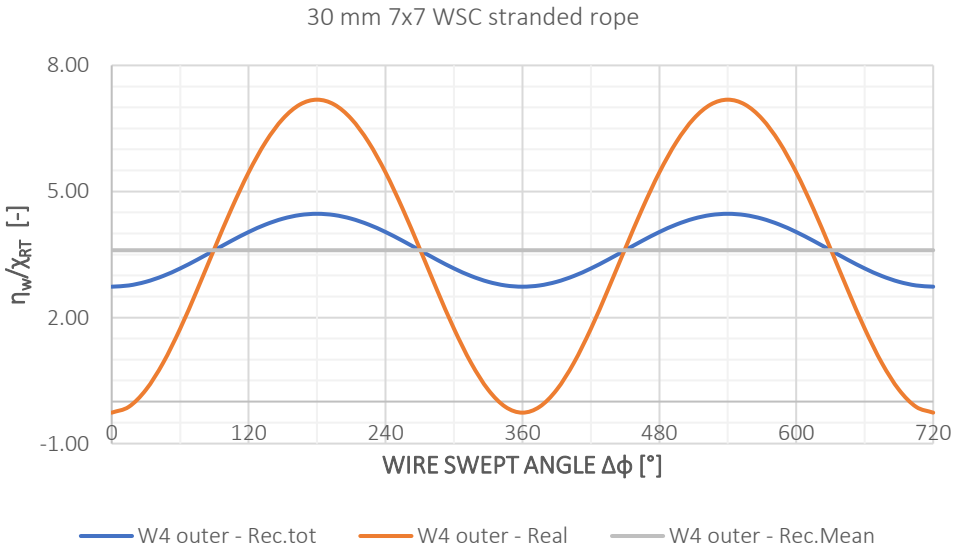

Fig 2.46 Wire Axial Strain due to Rope Torsion – Recursive Total Value

Let us compare the maximum, minimum and mean value for the two formulations.

Table 2.9 Wire Axial Strain due to Rope Torsion– Total Strand Contribution

η_w/χ_{RT}	max	min	mean
direct	7.1846	-0.2637	3.4604
rec.tot	4.4686	2.7340	3.6013
error	60.78%	-109.65%	-3.91%

The difference occurring in correspondence of maximum and minimum value is very high. Hence, very big differences will be introduced in the local stresses of wires, even though at global level the two responses won't be so far.

2.2. ROPE BENDING CONTRIBUTION

The second set of relation is coming from the rope subject to biaxial bending perturbation only. This means that the kinematic quantities exciting the rope are: normal bending curvature χ_{R2} and binormal bending curvature χ_{R3}. These excitations will cause a three-dimensional kinematic field in the strand and the wire.

2.2.1. STRAND AXIAL TORSION DUE TO ROPE BIAXIAL BENDING

The relations between wire and strand (2.III.3) are used for the second contribution of (2.III.5). The superscript "sAT" means "strand axial torsion".

$$\eta_w^{sAT}(x_1) = \cos^2\alpha_w\ \eta_s^B(x_1) + R_w\ \cos\alpha_w \sin\alpha_w\ \chi_{sT}^B(x_1)$$
$$\chi_{wT}^{sAT}(x_1) = \cos^2\alpha_w\, \chi_{sT}^B(x_1)$$
$$\chi_{w2}^{sAT}(x_1) = 0$$
$$\chi_{w3}^{sAT}(x_1) = \cos\alpha_w \sin\alpha_w\, \chi_{sT}^B(x_1)$$

Introducing into the latter expressions the η_s and χ_{sT} from (2.III.2):

$$\eta_s^B(x_1) = \cos^2\alpha_s\, R_s \sin\vartheta(x_1)\ \chi_{R2}(x_1) - \cos^2\alpha_s\, R_s \cos\vartheta(x_1)\ \chi_{R3}(x_1)$$
$$\chi_{sT}^B(x_1) = -\cos\alpha_s \sin\alpha_s \sin\vartheta(x_1)\,\chi_{R2}(x_1) + \cos\alpha_s \sin\alpha_s \cos\vartheta(x_1)\,\chi_{R3}(x_1)$$

The following kinematic constraints is obtained between rope and wire.

$$\eta_w^{sAT}(x_1) = \cos^2\alpha_w\ [\cos^2\alpha_s\, R_s \sin\vartheta(x_1)\ \chi_{R2}(x_1) - \cos^2\alpha_s\, R_s \cos\vartheta(x_1)\ \chi_{R3}(x_1)] + R_w\ \cos\alpha_w \sin\alpha_w\ [-\cos\alpha_s \sin\alpha_s \sin\vartheta(x_1)\,\chi_{R2}(x_1) + \cos\alpha_s \sin\alpha_s \cos\vartheta(x_1)\,\chi_{R3}(x_1)]$$
$$\chi_{wT}^{sAT}(x_1) = \cos^2\alpha_w\,[-\cos\alpha_s \sin\alpha_s \sin\vartheta(x_1)\,\chi_{R2}(x_1) + \cos\alpha_s \sin\alpha_s \cos\vartheta(x_1)\,\chi_{R3}(x_1)]$$
$$\chi_{w2}^{sAT}(x_1) = 0$$
$$\chi_{w3}^{sAT}(x_1) = \cos\alpha_w \sin\alpha_w\,[-\cos\alpha_s \sin\alpha_s \sin\vartheta(x_1)\,\chi_{R2}(x_1) + \cos\alpha_s \sin\alpha_s \cos\vartheta(x_1)\,\chi_{R3}(x_1)]$$

Collecting all the common terms, it's possible to find the final expression of the axial strain and curvatures in the wire due to axial torsion in the strand.

$$\boldsymbol{\eta_w^{sAT}(x_1) = [\cos^2\alpha_w \cos^2\alpha_s R_s\ - \cos\alpha_w \sin\alpha_w \cos\alpha_s \sin\alpha_s R_w]\ [\sin\vartheta(x_1)\ \chi_{R2}(x_1) - \cos\vartheta(x_1)\ \chi_{R3}(x_1)]}$$
$$(2.III.7a)\quad \boldsymbol{\chi_{wT}^{sAT}(x_1) = \cos^2\alpha_w \cos\alpha_s \sin\alpha_s\,[-\sin\vartheta(x_1)\,\chi_{R2}(x_1) + \cos\vartheta(x_1)\,\chi_{R3}(x_1)]}$$
$$\boldsymbol{\chi_{w2}^{sAT}(x_1) = 0}$$
$$\boldsymbol{\chi_{w3}^{sAT}(x_1) = \cos\alpha_w \sin\alpha_w \cos\alpha_s \sin\alpha_s\,[-\sin\vartheta(x_1)\,\chi_{R2}(x_1) + \cos\vartheta(x_1)\,\chi_{R3}(x_1)]}$$

2.2.1.1. AXIAL STRAIN OF THE WIRE DUE TO BENDING CURVATURE OF THE ROPE ABOUT GLOBAL AXIS 2

Let us compare the first coefficient η_w/χ_{R2} of the first equation of (2.III.7a) with the correspondent coefficient in the direct formulation (2.II.9a). Like it happens for the term η_w/χ_{RT} in paragraph 2.1.1.2, this quantity is not directly comparable with (2.II.9a), since the kinematic contributions due to the strand axial torsion and bending have been split according to (2.III.5).

$$(2.III.7aa)\quad \eta_w^{sAT}(x_1) = [(\cos^2\alpha_w \cos^2\alpha_s R_s - \cos\alpha_w \sin\alpha_w \cos\alpha_s \sin\alpha_s R_w)\sin\vartheta(x_1)]\,\chi_{R2}(x_1)$$

In the following plot the quantities (2.III.7aa) and (2.II.9a) are represented. As usual, for the direct model only the result corresponding to the real arch length are involved. The functions are indicated respectively "Rec.sAT" and "Real" standing for recursive model contribution due to axial torsion in the strand and direct model for the real arch length.

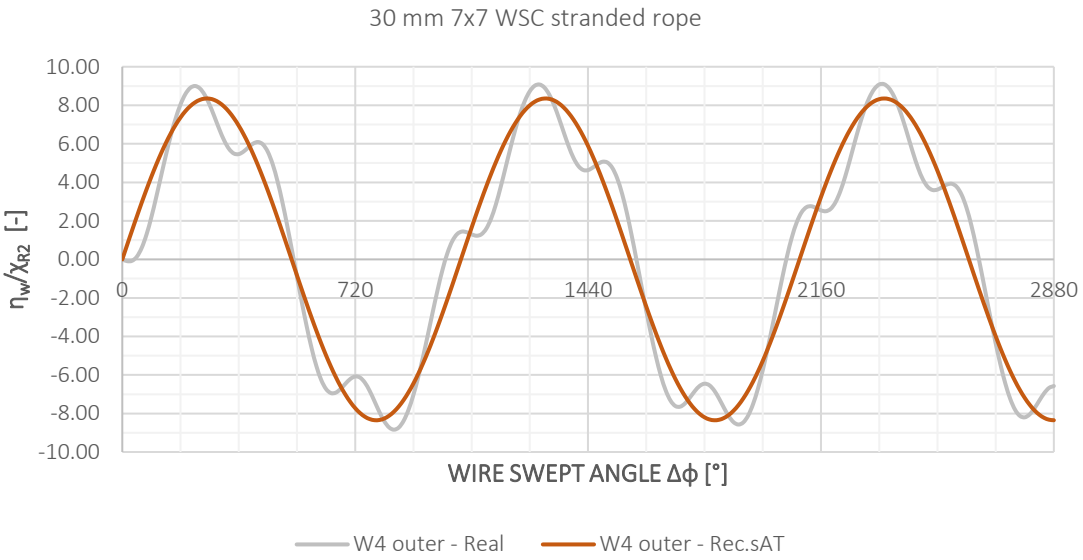

Fig 2.47 Wire Axial Strain due to Rope Torsion – Recursive Axial Torsional Contribution of the Strand

It can be clearly appreciated that both functions have zero-mean value. Hence, neither of them will influence the global response of the wire rope. In the following table a comparison in introduced between maximum, minimum and mean value for the two quantities.

Table 2.10 Wire Axial Strain due to Rope Bending Curvature– Axial Torsional Contribution of the Strand

η_w/χ_{R2}	max	min	mean
direct	9.1092	-9.1133	-0.0021
rec.sAT	8.3522	-8.3522	0.0000
error	9.06%	9.11%	-

2.2.2. STRAND BENDING DUE TO ROPE BIAXIAL BENDING

The relations between wire and strand (2.III.4) are used for the second contribution of (2.III.5). The superscript "sB" means "strand bending".

$$\eta_w^{sB}(x_1) = \cos^2\alpha_w R_w \sin\varphi(x_1)\ \chi_{s2}^B(x_1) - \cos^2\alpha_w R_w \cos\varphi(x_1)\ \chi_{s3}^B(x_1)$$
$$\chi_{w1}^{sB}(x_1) = -\cos\alpha_w \sin\alpha_w \sin\varphi(x_1)\,\chi_{s2}^B(x_1) + \cos\alpha_w \sin\alpha_w \cos\varphi(x_1)\,\chi_{s3}^B(x_1)$$
$$\chi_{w2}^{sB}(x_1) = -\cos\alpha_w \cos\varphi(x_1)\,\chi_{s2}^B(x_1) - \cos\alpha_w \sin\varphi(x_1)\,\chi_{s3}^B(x_1)$$
$$\chi_{w3}^{sB}(x_1) = \cos^2\alpha_w \sin\varphi(x_1)\,\chi_{s2}^B(x_1) - \cos^2\alpha_w \cos\varphi(x_1)\,\chi_{s3}^B(x_1)$$

Introducing into the latter expressions the curvatures χ_{s2} and χ_{s3} from (2.III.2):

$$\chi_{s2}^{B}(x_1) = -\cos\alpha_s \cos\vartheta(x_1)\,\chi_{R2}(x_1) - \cos\alpha_s \sin\vartheta(x_1)\,\chi_{R3}(x_1)$$
$$\chi_{s3}^{B}(x_1) = \cos^2\alpha_s \sin\vartheta(x_1)\,\chi_{R2}(x_1) - \cos^2\alpha_s \cos\vartheta(x_1)\,\chi_{R3}(x_1)$$

The following kinematic constraints is obtained between rope and wire.

$$\eta_w^{sB}(x_1) = \cos^2\alpha_w\, R_w \sin\varphi(x_1)\ [-\cos\alpha_s \cos\vartheta(x_1)\,\chi_{R2}(x_1) - \cos\alpha_s \sin\vartheta(x_1)\,\chi_{R3}(x_1)] - \cos^2\alpha_w\, R_w \cos\varphi(x_1)\ [\cos^2\alpha_s \sin\vartheta(x_1)\,\chi_{R2}(x_1) - \cos^2\alpha_s \cos\vartheta(x_1)\,\chi_{R3}(x_1)]$$
$$\chi_{wT}^{sB}(x_1) = -\cos\alpha_w \sin\alpha_w \sin\varphi(x_1)\,[-\cos\alpha_s \cos\vartheta(x_1)\,\chi_{R2}(x_1) - \cos\alpha_s \sin\vartheta(x_1)\,\chi_{R3}(x_1)] + \cos\alpha_w \sin\alpha_w \cos\varphi(x_1)\,[\cos^2\alpha_s \sin\vartheta(x_1)\,\chi_{R2}(x_1) - \cos^2\alpha_s \cos\vartheta(x_1)\,\chi_{R3}(x_1)]$$
$$\chi_{w2}^{sB}(x_1) = -\cos\alpha_w \cos\varphi(x_1)\,[-\cos\alpha_s \cos\vartheta(x_1)\,\chi_{R2}(x_1) - \cos\alpha_s \sin\vartheta(x_1)\,\chi_{R3}(x_1)] - \cos\alpha_w \sin\varphi(x_1)\,[\cos^2\alpha_s \sin\vartheta(x_1)\,\chi_{R2}(x_1) - \cos^2\alpha_s \cos\vartheta(x_1)\,\chi_{R3}(x_1)]$$
$$\chi_{w3}^{sB}(x_1) = \cos^2\alpha_w \sin\varphi(x_1)\,[-\cos\alpha_s \cos\vartheta(x_1)\,\chi_{R2}(x_1) - \cos\alpha_s \sin\vartheta(x_1)\,\chi_{R3}(x_1)] - \cos^2\alpha_w \cos\varphi(x_1)\,[\cos^2\alpha_s \sin\vartheta(x_1)\,\chi_{R2}(x_1) - \cos^2\alpha_s \cos\vartheta(x_1)\,\chi_{R3}(x_1)]$$

Collecting all the common terms, it's possible to find the final expression of the curvatures in the wire due to biaxial bending in the strand.

$$\boldsymbol{\eta_w^{sB}(x_1) = \cos^2\alpha_w \cos\alpha_s\, R_w\, \{-[\sin\varphi(x_1)\cos\vartheta(x_1) + \cos\alpha_s \cos\varphi(x_1)\sin\vartheta(x_1)]\,\chi_{R2}(x_1) + [-\sin\varphi(x_1)\sin\vartheta(x_1) + \cos\alpha_s \cos\varphi(x_1)\cos\vartheta(x_1)]\,\chi_{R3}(x_1)\}}$$

$$(2.III.7b)\quad \boldsymbol{\chi_{wT}^{sB}(x_1) = \cos\alpha_w \sin\alpha_w \cos\alpha_s\, \{[\sin\varphi(x_1)\cos\vartheta(x_1) + \cos\alpha_s \cos\varphi(x_1)\sin\vartheta(x_1)]\,\chi_{R2}(x_1) + [\sin\varphi(x_1)\sin\vartheta(x_1) - \cos\alpha_s \cos\varphi(x_1)\cos\vartheta(x_1)]\chi_{R3}(x_1)\}}$$

$$\boldsymbol{\chi_{w2}^{sB}(x_1) = \cos\alpha_w \cos\alpha_s\, \{[\cos\varphi(x_1)\cos\vartheta(x_1) - \cos\alpha_s \sin\varphi(x_1)\sin\vartheta(x_1)]\,\chi_{R2}(x_1) + [\cos\varphi(x_1)\sin\vartheta(x_1) + \cos\alpha_s \sin\varphi(x_1)\cos\vartheta(x_1)]\,\chi_{R3}(x_1)]\}}$$

$$\boldsymbol{\chi_{w3}^{sB}(x_1) = \cos^2\alpha_w \cos\alpha_s\, \{[-\sin\varphi(x_1)\cos\vartheta(x_1) - \cos\alpha_s \cos\varphi(x_1)\sin\vartheta(x_1)]\chi_{R2}(x_1) + [-\sin\varphi(x_1)\sin\vartheta(x_1) + \cos\alpha_s \cos\varphi(x_1)\cos\vartheta(x_1)]\,\chi_{R3}(x_1)\}}$$

2.2.2.1. AXIAL STRAIN OF THE WIRE DUE TO BENDING CURVATURE OF THE ROPE ABOUT GLOBAL AXIS 2

Let us introduce the missing term of paragraph 2.2.1.1 to be able to compare the coefficient η_w/χ_{R2}.

$$(2.III.7ba)\quad \eta_w^{sB}(x_1) = \{-\cos^2\alpha_w \cos\alpha_s\, R_w\, [\sin\varphi(x_1)\cos\vartheta(x_1) + \cos\alpha_s \cos\varphi(x_1)\sin\vartheta(x_1)]\}\,\chi_{R2}(x_1)$$

It must be added to the contribution (2.III.7aa) to be able to compare it with (2.II.9a).

$$(2.III.7bb)\quad \eta_w(x_1) = \eta_w^{sAT}(x_1) + \eta_w^{sB}(x_1) = \{(\cos^2\alpha_w \cos^2\alpha_s\, R_s - \cos\alpha_w \sin\alpha_w \cos\alpha_s \sin\alpha_s\, R_w)\sin\vartheta(x_1) - \cos^2\alpha_w \cos\alpha_s\, R_w\, [\sin\varphi(x_1)\cos\vartheta(x_1) + \cos\alpha_s \cos\varphi(x_1)\sin\vartheta(x_1)]\}\,\chi_{R2}(x_1)$$

In the following graph we will indicate respectively the direct model with the real arch length, the recursive model contribution due to axial torsion of the strand and the recursive model contribution due to bending of the strand with "Real", "Rec.sAT" and "Rec.sB". The functions introduced in the first plot are respectively (2.II.9a), (2.III.7aa) and (2.III.7ba). The contributions are represented separately to better understand the structure of (2.III.7bb).

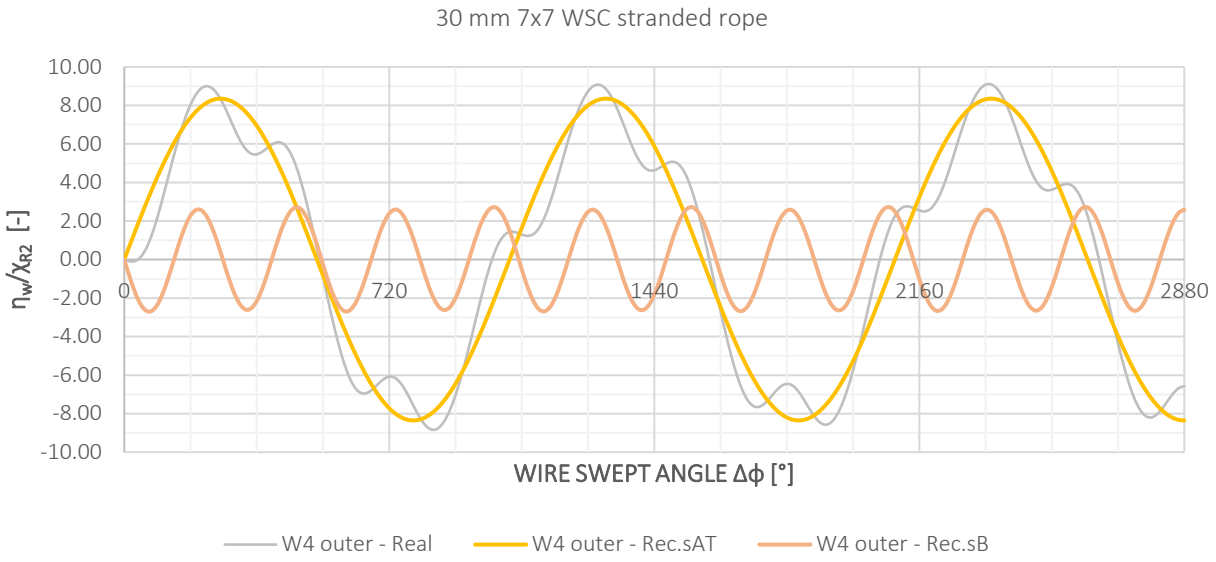

Fig 2.48 Wire Axial Strain due to Rope Bending Curvature – Recursive Axial Torsional and Bending Contributions of the Strand

It can be appreciated that either functions involved in the sum (2.III.7bb) have zero-mean value. Hence, this consideration ensures the zero-mean value of the sum itself. In the last graph the direct comparison between (2.II.9a) and (2.III.7bb).

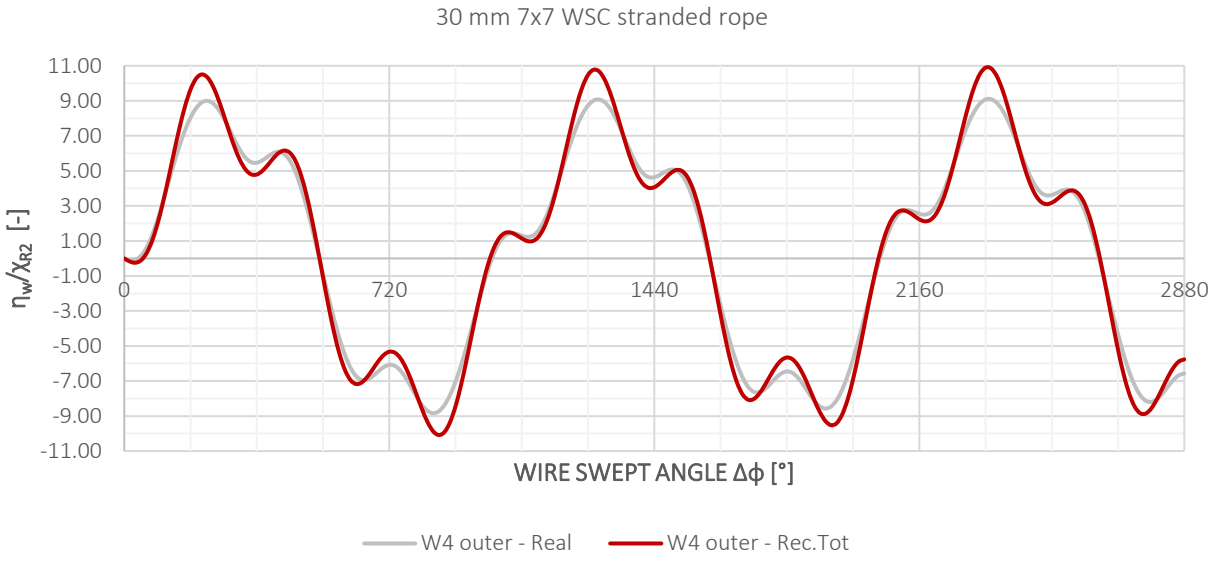

Fig 2.49 Wire Axial Strain due to Rope Bending Curvature – Recursive Total Value

The trend of the two formulations is very alike, still a non-negligible error occurs in correspondence of the peaks as it can be appreciated in the following table. Hence, a difference will arise in the computation of the local stresses of the wire.

Table 2.11 Wire Axial Strain due to Rope Bending Curvature – Total Strand Contribution

η_w/χ_{R2}	max	min	mean
direct	9.1092	-9.1133	-0.0021
rec.Tot	10.9289	-10.9339	-0.0025
error	-16.65%	-16.65%	-

IV. CONCLUSIONS

In the present chapter the main kinematic relations holding true between the wire rope and its sub components, i.e. the single wire and the single strand, have been established. The Euler Bernoulli hypothesis was introduced for the rope cross section, while the single wire was modelled according to the Love thin curved rod theory. These assumptions hold for either the direct model, where the single wire is directly related to the rope, and the recursive model, where the single wire is related to the rope through the strand. The two formulations lead to different results in terms of generalized strains. The main mechanical quantity affecting the response of the rope is the axial strain of the wire that provides the average normal stress on the wire cross section (the greater contribution in term of magnitude). Firstly, the axial strain of the wire is directly proportional to the rope axial strain in the recursive model (2.III.6aa), while in the direct model the proportionality coefficient has a sinusoidal trend (2.II.8a). This difference has great importance, since the maximum and minimum value of that function determine the average normal stress on the wire cross section, thus the local response of the rope. In table 2.3 it is shown that for a 30mm 7x7 WSC this error may be up to 18%. Conversely, the mean value of the two formulations affects the global response of the wire rope, mainly in term of axial stiffness. Here the error is much lower, i.e. of the order of 4.5%. The second quantity under investigation is the coefficient that provides the axial strain of the wire as a function of the rope torsional curvature that will be responsible for either coupling between axial and torsion and for the torsional stiffness of the rope. It is provided by (2.II.8b) in the direct model and by (2.III.6bb) in the recursive model. In table 2.5 a comparison is performed between the two formulations. The mean value is not very different with 4%, while the oscillations differ considerably with 60%. Hence, the local response strongly depends upon the chosen formulation. Finally, the last coefficient is the one relating the wire axial strain with the rope bending curvature. The two formulations (2.II.9a) and (2.III.7bb) are identical in term of mean value (which is always zero) and slightly differ in term of oscillation with an error up to 16% as it is shown in table 2.7. It is interesting to notice the perfect matching between the trend of these two functions in Fig. 2.16 despite the different approaches.

REFERENCES

(Love, 1944) Love A.E.H., 1944. *A treatise on the Mathematical Theory of Elasticity*. Dover Publications, New York.

(Huang, 1973) Huang N.C., 1973. *Theories of Elastic Slender Curved Rods.* Journal of Applied Mathematics and Physics Vol.24 (1973).

(Velinsky et al., 1984) Velinsky S.A., Anderson G.L., Costello G.A., 1984. *Wire rope with complex cross sections.* Eng. Mech. Div., ASCE 110 (3), 380-391.

(Ramsey, 1988) Ramsey, H., 1988. *A theory of thin rods with application to helical constituent wires in cables*. Int. J. Mech. Sci., 30(8), 559–570.

(Raoof & Kraincanic, 1995) Raoof M., Kraincanic I., 1995. *Analysis of large diameter steel ropes.* Journal of Engineering Mechanics / June 1995 / 667-675.

(Elata et a., 2004) Elata D., Eshkenazy R., Weiss M.P., 2004. *The mechanical behaviour of a wire rope with an independent wire rope core.* International Journal of Solids and Structures 41 (2004) 1157-1172.

(Feyrer, 2007) Feyrer K., 2007. *Wire Ropes. Tension, Endurance, Reliability*. Springer.

(Usabiaga & Pagalday, 2008) Usabiaga H., Pagalday J.M., 2008. *Analytical procedure for modelling recursively and wire by wire stranded ropes subjected to traction and torsion loads.* International Journal of Solids and Structures 45 (2008) 5503-5520.

(Foti, 2013) Foti. F., 2013. *A corotational beam element and a refined mechanical model for the nonlinear dynamic analysis of cables*. Doctoral dissertation. Doctoral Programme in Structural, Seismic and Geotechnical Engineering XXV Cycle. Politecnico di Milano.

(Xiang et al., 2015) Xiang L., Wang H.Y., Chen Y., Guan Y.J., Wang Y.L., Dai L.H., 2015. *Modelling of multi-stranded wire ropes subjected to axial tension and torsion loads*. International Journal of Solids and Structures 58 (2015) 233-246.

(Foti & Martinelli, 2016) Foti F., Martinelli L., 2016. *Mechanical modelling of metallic strands subjected to tension, torsion and bending*. International Journal of Solids and Structures 91 (2016) 1-17.

(Meleddu et al., 2017) Meleddu M., Foti F., Martinelli L., 2017. *Temperature in active heave compensation ropes*. OIPEEC Conference – Le Rochelle – April 2017.

CHAPTER 3

MECHANICAL RESPONSE OF THE SINGLE WIRE TO THE ROPE FUNDAMENTAL MODES

I. INTRODUCTION

The response of the wire rope is studied under the assumption of small displacements and strains and within the linear-elastic field; hence the superposition principle holds true for the behavior of this structural system. Specifically, the global response of the rope to a certain excitation may be interpreted as the sum of the responses of the single wires to the same excitation.
In that light, it is interesting to investigate the behavior of the single wire subject to the fundamental actions and strains that are experienced by the rope. This means that in the present chapter, the response of the wire rope is analyzed in term of the single wire contribution to the global response.

In the first paragraph the generalized constitutive model, or sectional response, of the single wire will be provided. It is a simple extension of the Euler Bernoulli constitutive model to the curved thin rod theory.
Then the single wire contribution to the rope global response will be investigated with reference to the two kinematic models introduced in the previous chapter: the direct and the recursive formulation.
The objective in both cases will be to provide the stiffness matrix of the rope, where the single entries are to be interpreted as the contribution of the single wire only. The actual global response will be computed performing an integration over the rope cross section of the single wire contributions.

II. WIRE CONSTITUTIVE MODEL

The generalized constitutive model of the wire comes from the definition of the internal actions within the wire cross section and the generalized strain field. The usual assumption in structural theories for the elastic constitutive model is the fiber behavior. Hence all fibers are considered independent one from the other. Assuming the subscripts 1,2,3 respectively for tangent, normal and binormal direction of the Serret-Frenet frame of the wire centerline, the model may be written as follows.

$$\sigma_{w1} = E\,\varepsilon_{w1}$$
$$\tau_{w12} = G\,\gamma_{w12}$$
$$\tau_{w13} = G\,\gamma_{w13}$$

The internal actions within the cross section are computed by integration of the contribution coming from each fiber. The coordinates in the wire reference frame are (y_1, y_2, y_3) for tangent, normal and binormal directions.

$$N_w = \int_{A_w} \sigma_{w1}\, dA_w = \int_{A_w} E\,\varepsilon_{w1}\, dA_w = E \int_{A_w} (\eta_w + y_3\,\chi_{w2} - y_2\,\chi_{w3})\, dA_w$$

$$M_{wT} = \int_{A_w} (\tau_{w13}\, y_2 - \tau_{w12}\, y_3)\, dA_w = \int_{A_w} G\,(\gamma_{w13}\, y_2 - \gamma_{w12}\, y_3)\, dA_w = G \int_{A_w} (y_2^2 + y_3^2)\,\chi_{wT}\, dA_w$$

$$M_{w2} = \int_{A_w} \sigma_{w1}\, y_3\, dA_w = \int_{A_w} E\,\varepsilon_{w1}\, y_3\, dA_w = E \int_{A_w} (y_3\,\eta_w + y_3^2\,\chi_{w2} - y_2\, y_3\,\chi_{w3})\, dA_w$$

$$M_{w3} = -\int_{A_w} \sigma_{w1}\, y_2\, dA_w = -\int_{A_w} E\,\varepsilon_{w1}\, y_2\, dA_w = E \int_{A_w} (-y_2\,\eta_w + -y_2\, y_3\,\chi_{w2} + y_2^2\,\chi_{w3})\, dA_w$$

The previous expressions can be considerably simplified when the reference frame coincide with the principal axis of inertia for the cross section, since the first order moment and the product moment of inertia are identically null. Moreover, if we specialize the expressions for a double symmetric section like the circular one, the two second order moments are the same and the equations can be written as follows:

$$\begin{aligned} N_w &= EA_w\,\eta_w \\ M_{wT} &= \frac{1}{1+\nu} EI_w \chi_{wT} \\ M_{w2} &= EI_w \chi_{w2} \\ M_{w3} &= EI_w \chi_{w3} \end{aligned} \qquad (3.II.1)$$

Where N_w, M_{wT}, M_{w2} and M_{w3} are respectively the axial force, the torque, the bending moment about normal and binormal direction of the wire. While A_w and I_w are respectively the area and moment of inertia of the wire cross section. E and **ν** are the Young modulus and the Poisson coefficient of the wire.

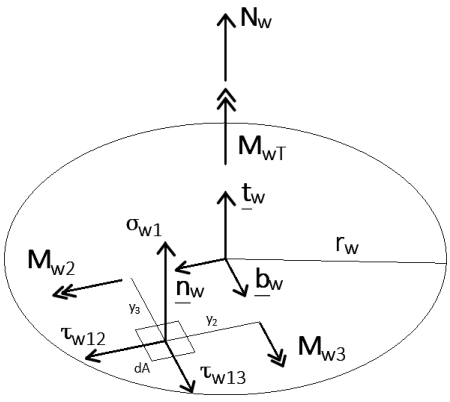

Fig 3.50 Wire Cross Section Internal Actions and Stresses

III. DIRECT MODEL

The model developed so far is a linearly elastic one. Hence, it is possible to exploit the superposition principle. As a matter of fact, the global response of the rope is the sum of the responses of the single wires. For that reason, the present paragraph wants to investigate the response of single wire subject to the fundamental excitations experienced by the rope, i.e. axial strain, torsion and biaxial bending. The reasoning is divided into two steps: the first is to seek for the internal actions induced within the rope by a generic stress state inside the wire, then, making use of the constitutive model of the wire afore mentioned (3.II.1), a direct link between the rope internal actions generated by the wire and the wire strain field is introduced. The last step exploits the kinematic relations between wire and rope developed in the previous chapter. The final result will be the constitutive model of the rope. It must be underlined again that the relations that will be found inside this paragraph represent the contribution of the single wire only, and not the global response of the rope yet. The global response will be obtained summing over all the wires.

1. SINGLE WIRE CONTRIBUTION TO THE ROPE INTERNAL ACTIONS

The contribution of a single wire on the rope internal actions may be computed through two steps: the first is projecting the wire cross-section resultants on the global reference frame, subsequently the projections of the axial force of the wire in the global frame produce some transport terms which contribute to torsion and bending. For that reason, from now on the subscripts 1,2,3 will indicate respectively the rope axis and the two orthogonal directions according to the right screw, hence the global reference frame components. The vector $\underline{e}_i$ is the unit vector correspondent to direction x_i, the quantities t_{wi}, n_{wi} and b_{wi} are the i-th component of tangent, normal and binormal unit vectors of the wire centerline. Finally, x_{w2} and x_{w3} are the component of the position vector directed as x_2 and x_3 respectively.

$$
\begin{aligned}
N_R &= N_w\, \underline{t}_w\, \underline{e}_1 \\
M_{RT} &= \left(M_{wT}\, \underline{t}_w + M_{w2}\, \underline{n}_w + M_{w3}\, \underline{b}_w\right)\underline{e}_1 + N_w\, \underline{t}_w [\, \underline{e}_1 \wedge \left(x_{w2}\, \underline{e}_2 + x_{w3}\, \underline{e}_3\right)] \\
M_{R2} &= \left(M_{wT}\, \underline{t}_w + M_{w2}\, \underline{n}_w + M_{w3}\, \underline{b}_w\right)\underline{e}_2 + N_w\, \underline{t}_w\, \underline{e}_1\, x_{w3} \\
M_{R3} &= \left(M_{wT}\, \underline{t}_w + M_{w2}\, \underline{n}_w + M_{w3}\, \underline{b}_w\right)\underline{e}_3 - N_w\, \underline{t}_w\, \underline{e}_1\, x_{w2}
\end{aligned}
$$

The previous expressions lead to the following equations, where N_R, M_{RT}, M_{R2} and M_{R3} are respectively the axial force, the torque and the bending moments about the principal directions x_2 and x_3.

$$
\begin{aligned}
N_R &= t_{w1}\, N_w \\
M_{RT} &= t_{w1}\, M_{wT} + n_{w1}\, M_{w2} + b_{w1}\, M_{w3} + (x_{w2}\, t_{w3} - x_{w3}\, t_{w2})\, N_w \\
M_{R2} &= t_{w2}\, M_{wT} + n_{w2}\, M_{w2} + b_{w2}\, M_{w3} + t_{w1}\, x_{w3}\, N_w \\
M_{R3} &= t_{w3}\, M_{wT} + n_{w3}\, M_{w2} + b_{w3}\, M_{w3} - t_{w1}\, x_{w2}\, N_w
\end{aligned}
\qquad (3.III.1)
$$

An important remark must be done on notation. The subscript "w" indicates that the quantity is referred to the wire, while "R" is referred to the rope. Attention is to be paid to (3.III.1), as a matter of fact it refers to the contribution of the specific wire to the rope and not to the whole response. The choice is due to simplicity in notation.
In Figure 3.2 it is possible to appreciate the geometrical relations holding true between the wire axial force only and the four internal actions of the wire rope. Specifically, the components of the wire axial force are highlighted in the global reference frame.

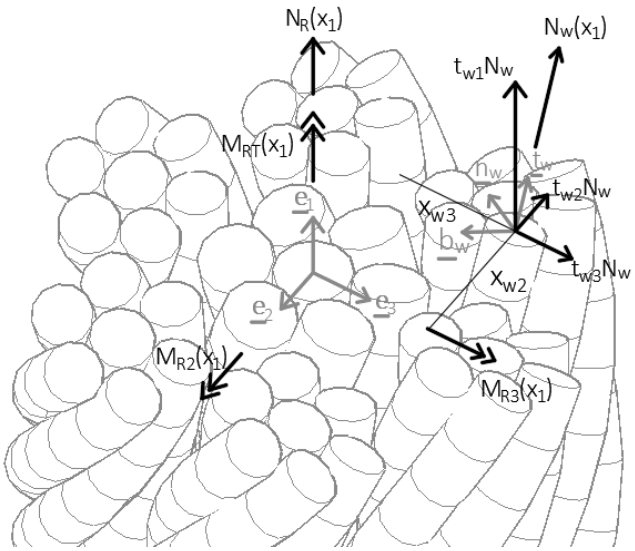

Fig 3.51 Wire Rope Internal Actions due to Wire Axial Force

2. SINGLE WIRE CONTRIBUTION TO THE ROPE GLOBAL RESPONSE

In the present paragraph the objective is the definition of the mechanical quantities that identify the response of the single wire in terms of wire rope internal actions, when the wire undergoes the fundamental modes of the rope. For that reason, the constitutive model provided with the following work concerns the rope, still it is the contribution of a single wire of the rope itself.
Let us define the vectors of the single wire contributions to the generalized stresses $\underline{\sigma}$, generalized strains $\underline{\varepsilon}$ and rotations of the wire rope as follows.

$$\underline{\sigma} = (N_R, M_{RT}, M_{R2}, M_{R3})^T$$
$$\underline{\varepsilon} = (\eta_R, \chi_{RT}, \chi_{R2}, \chi_{R3})^T$$
$$\underline{\omega} = (\varphi_{R2}, \varphi_{R3})^T$$

The stiffness matrix of the structural system is conventionally defined through the generalized stresses and strains of the model.

$$\underline{\underline{K}}_R = \frac{\partial \underline{\sigma}}{\partial \underline{\varepsilon}} = \begin{bmatrix} EA_R & C_{AT} & C_{AB2} & C_{AB3} \\ C_{TA} & GJ_R & C_{TB2} & C_{TB3} \\ C_{B2A} & C_{B2T} & EI_{R2} & C_{B23} \\ C_{B3A} & C_{B3T} & C_{B32} & EI_{R3} \end{bmatrix}$$

It is interesting to notice that the contribution to the rope generalized stresses of the single wire do not depend upon the corresponding work conjugated strains only, yet on the bending rotations as well. This result is a consequence of the kinematic model of the wire rope. Specifically, these contributions arise from the variation of position of the single wire between two subsequent cross sections of the rope.

$$\begin{pmatrix} N_R \\ M_{RT} \\ M_{R2} \\ M_{R3} \end{pmatrix} = \begin{bmatrix} EA_R & C_{AT} & C_{AB2} & C_{AB3} \\ C_{TA} & GJ_R & C_{TB2} & C_{TB3} \\ C_{B2A} & C_{B2T} & EI_{R2} & C_{B23} \\ C_{B3A} & C_{B3T} & C_{B32} & EI_{R3} \end{bmatrix} \begin{pmatrix} \eta_R \\ \chi_{RT} \\ \chi_{R2} \\ \chi_{R3} \end{pmatrix} + \begin{bmatrix} C_{AR2} & C_{AR3} \\ C_{TR2} & C_{TR3} \\ C_{B2R2} & C_{B2R3} \\ C_{B3R2} & C_{B3R3} \end{bmatrix} \begin{pmatrix} \varphi_{R2} \\ \varphi_{R3} \end{pmatrix}$$

The kinematic field may be divided into two contributions, corresponding to rope axial torsion and biaxial bending kinematic perturbations.

$$(3.III.2a) \quad \underline{\varepsilon} = \underline{\varepsilon}^{AT} + \underline{\varepsilon}^{B}$$
$$(3.III.2b) \quad \underline{\varepsilon}^{AT} = (\eta_R, \chi_{RT}, 0, 0)^T = (\eta_R, \chi_{RT})^T$$
$$(3.III.2c) \quad \underline{\varepsilon}^{B} = (0, 0, \chi_{R2}, \chi_{R3})^T = (\chi_{R2}, \chi_{R3})^T$$

The generalized stresses and the stiffness matrix may be split accordingly.

$$\begin{pmatrix} N_R \\ M_{RT} \\ M_{R2} \\ M_{R3} \end{pmatrix} = \begin{bmatrix} EA_R & C_{AT} \\ C_{TA} & GJ_R \\ C_{B2A} & C_{B2T} \\ C_{B3A} & C_{B3T} \end{bmatrix} \begin{pmatrix} \eta_R \\ \chi_{RT} \end{pmatrix} + \begin{bmatrix} C_{AB2} & C_{AB3} \\ C_{TB2} & C_{TB3} \\ EI_{R2} & C_{B23} \\ C_{B32} & EI_{R3} \end{bmatrix} \begin{pmatrix} \chi_{R2} \\ \chi_{R3} \end{pmatrix} + \begin{bmatrix} C_{AR2} & C_{AR3} \\ C_{TR2} & C_{TR3} \\ C_{B2R2} & C_{B2R3} \\ C_{B3R2} & C_{B3R3} \end{bmatrix} \begin{pmatrix} \varphi_{R2} \\ \varphi_{R3} \end{pmatrix}$$

The previous equality allows to define two new sub matrices for axial torsion and biaxial bending

$$(3.III.3a) \quad \underline{\underline{K}}_R^{AT} = \begin{bmatrix} EA_R & C_{AT} \\ C_{TA} & GJ_R \\ C_{B2A} & C_{B2T} \\ C_{B3A} & C_{B3T} \end{bmatrix}$$

$$(3.III.3b) \quad \underline{\underline{K}}_R^{B} = \begin{bmatrix} C_{AB2} & C_{AB3} \\ C_{TB2} & C_{TB3} \\ EI_{R2} & C_{B23} \\ C_{B32} & EI_{R3} \end{bmatrix}$$

While the third matrix is conventionally defined as follows.

$$(3.III.3c) \quad \underline{\underline{A}}_R = \begin{bmatrix} C_{AR2} & C_{AR3} \\ C_{TR2} & C_{TR3} \\ C_{B2R2} & C_{B2R3} \\ C_{B3R2} & C_{B3R3} \end{bmatrix}$$

Hence the constitutive model can be written as follows.

$$(3.III.4) \quad \underline{\sigma} = \underline{\sigma}^{AT} + \underline{\sigma}^{B} + \underline{\sigma}^{R} = \underline{\underline{K}}_R^{AT} \ \underline{\varepsilon}^{AT} + \underline{\underline{K}}_R^{B} \ \underline{\varepsilon}^{B} + \underline{\underline{A}}_R \ \underline{\omega}$$

The objective that will be pursuit in the following is the definition of the coefficients of the stiffness matrix. Specifically, the contribution of each wire to the global stiffness of the rope is obtained through different manipulations of the relations among wire and rope internal actions (3.III.1). The first step is to substitute the wire internal actions with the wire generalized constitutive model, thus the rope internal actions are related to the single wire kinematics. Afterwards, the relations holding between wire and rope kinematics are exploited to explicit the relation between internal actions of the rope and its own generalized strains.

$$(3.III.5) \quad \begin{aligned} N_R &= t_{w1} \, EA_w \, \eta_w \\ M_{RT} &= EI_w \left(\frac{1}{1+\nu} t_{w1} \, \chi_{wT} + n_{w1} \, \chi_{w2} + b_{w1} \, \chi_{w3} \right) + (x_{w2} \, t_{w3} - x_{w3} \, t_{w2}) \, EA_w \, \eta_w \\ M_{R2} &= EI_w \left(\frac{1}{1+\nu} t_{w2} \, \chi_{wT} + n_{w2} \, \chi_{w2} + b_{w2} \, \chi_{w3} \right) + t_{w1} \, x_{w3} \, EA_w \, \eta_w \\ M_{R3} &= EI_w \left(\frac{1}{1+\nu} t_{w3} \, \chi_{wT} + n_{w3} \, \chi_{w2} + b_{w3} \, \chi_{w3} \right) - t_{w1} \, x_{w2} \, EA_w \, \eta_w \end{aligned}$$

The axial force inside the rope depends upon the wire axial strain only. Conversely, the torsional and bending moments may be split into two contributions: the first is due to the wire mechanical curvatures, while the second is due to the axial strain.

The coefficient that will be obtained are plotted for a specific wire rope: the 18mm 7x7 WSC stranded rope investigated in the chapter about geometry. For biaxial bending, the coefficient referred to the global axis x_2 will be considered only, since the other axis quantities are just a set of functions identical to previous ones, but phase shifted about the rope axis of 90°. The main feature that arises from these plots is the presence or not of a mean value of the functions. The importance of the mean value will be clear in the following chapter when the global response of the rope needs to be investigated. As a matter of fact, when the sum of the single wire contributions is performed on the rope cross section, only the mean value of these functions is not vanishing. Hence, it is the sole responsible of the rope response. As it will be underlined in what follows, many of the aforesaid coefficients will show a trend with zero mean value.

3.1. AXIAL FORCE WITHIN THE ROPE

Introducing the expressions (2.II.8) and (2.II.9) from the kinematics inside the first relation of (3.III.5).

$$N_R = t_{w1} \, EA_w \, \frac{dx_1}{dy_1} \left[t_{w1} \, \eta_R + (x_{w2} \, t_{w3} - x_{w3} \, t_{w2}) \, \chi_{RT} + t_{w1} (x_{w3} \, \chi_{R2} - x_{w2} \, \chi_{R3}) + (x'_{w1} - 1) \, (t_{w3} \, \varphi_{R2} - t_{w2} \, \varphi_{R3}) \right]$$

The contribution due to axial torsion of the rope and biaxial bending are split.

3.1.1. AXIAL TORSION OF THE ROPE

In this subsection it will be defined the first row of the matrix $\mathbf{K}^{AT}{}_{R}$(3.III.3a)

$$N_R^{AT} = t_{w1}\, EA_w \frac{dx_1}{dy_1} \left[t_{w1}\, \eta_R + (x_{w2}\, t_{w3} - x_{w3}\, t_{w2})\, \chi_{RT} \right]$$

The stiffness coefficients are

$$(3.III.6a) \quad \boldsymbol{EA_R = \frac{dx_1}{dy_1}\, t_{w1}^2\, EA_w}$$

$$(3.III.6b) \quad \boldsymbol{C_{AT} = \frac{dx_1}{dy_1}\, t_{w1} (x_{w2}\, t_{w3} - x_{w3}\, t_{w2})\, EA_w}$$

The axial force within the rope can be written as follows.

$$N_R^{AT} = EA_R\, \eta_R + C_{AT}\, \chi_{RT}$$

In the following, it is possible to appreciate the trend of the single wire contribution to the axial stiffness of the rope. Firstly, the function is clearly sinusoidal with the same period of the double helix. A comparison is performed between the nominal axial stiffness EA_w of the wire W4 and the coefficient (3.III.6a) in the case of real and developed (approximate) arc length dx_1/dy_1. The reason for the comparison between real and developed is the different mean value of the two sinusoidal functions. As a matter of fact, the mean value is the mechanical quantity that will provide the effective stiffness on the rope cross section. The reason of the last statement is that when a sum of the single wire contributions is performed on the cross section the oscillations about the mean value drop.

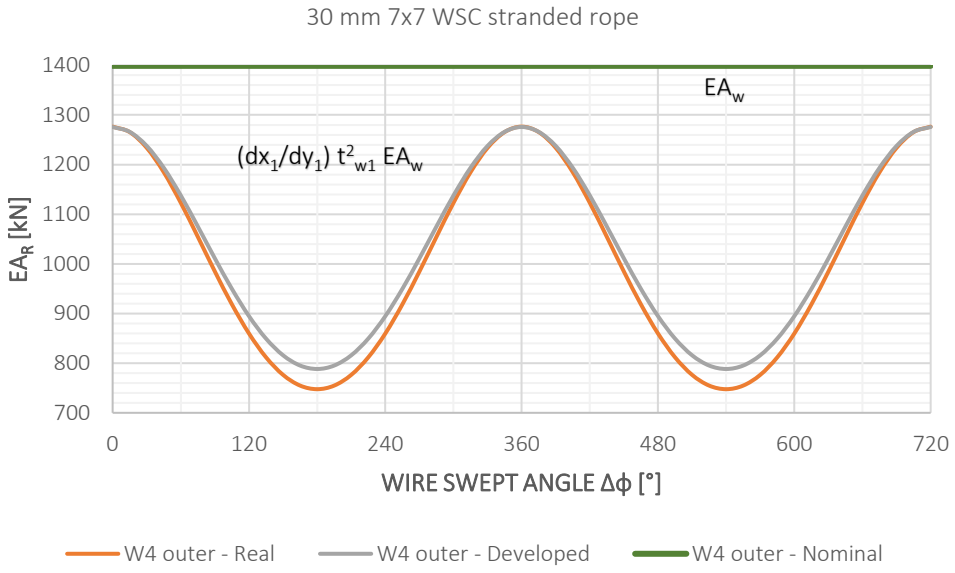

Fig 3.52 Single Wire Contribution to Wire Rope Axial Stiffness

In the following it can be appreciated the error occurring between the two formulations for maximum, minimum and mean values.

Table 3.12 Single Wire Contribution to Wire Rope Axial Stiffness

EA_R [kN]	max	min	mean
real	1276.4	747.6	1012
developed (approximate)	1275.7	788.3	1032
error	0.06%	-5.16%	-1.94%

The other coefficient that is shown is the coupling term between axial and torsional response of the rope. The same considerations aforesaid hold true for the real and developed geometry and for the mean value, which is still non-zero for that functions. This result is very interesting, and it is common in rope mechanics as well. As a matter of fact, the axial torsional problem in the rope is always coupled due to the helix geometry of its sub components.

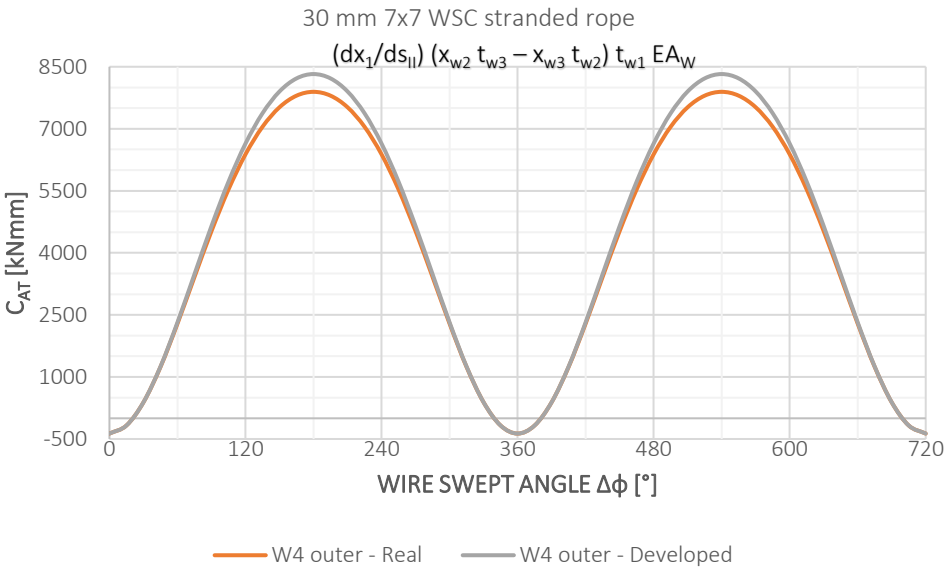

Fig 3.53 Single Wire Contribution to Wire Rope Axial Torsion Coupling Coefficient

In the following it can be appreciated the error occurring between the two formulations for maximum, minimum and mean values.

Table 3.13 Single Wire Contribution to Wire Rope Axial Torsion Coupling Coefficient

C_{AT} [kNmm]	max	min	mean
real	7894	-369	3763
developed (approximate)	8324	-368	3978
error	-5.16%	0.06%	-5.40%

3.1.2. BIAXIAL BENDING OF THE ROPE

In this subsection they will be defined the first rows of the matrices $\mathbf{K}^{B}_{R}$ (3.III.3b) and $\mathbf{A}_{R}$ (3.III.3c).

$$N_R^B = t_{w1}\, EA_w \frac{dx_1}{dy_1} \left[t_{w1}(x_{w3}\,\chi_{R2} - x_{w2}\,\chi_{R3}) + (x'_{w1} - 1)\,(t_{w3}\,\varphi_{R2} - t_{w2}\,\varphi_{R3})\right]$$

The stiffness coefficients are

$$(3.III.6c) \quad \boldsymbol{C_{AB2}} = \frac{\boldsymbol{dx_1}}{\boldsymbol{dy_1}}\, \boldsymbol{t_{w1}^2\, x_{w3}\, EA_w}$$

$$(3.III.6d) \quad \boldsymbol{C_{AB3}} = -\frac{\boldsymbol{dx_1}}{\boldsymbol{dy_1}}\, \boldsymbol{t_{w1}^2\, x_{w2}\, EA_w}$$

$$(3.III.6e) \quad \boldsymbol{C_{AR2}} = \frac{\boldsymbol{dx_1}}{\boldsymbol{dy_1}} (\boldsymbol{x'_{w1} - 1})\, \boldsymbol{t_{w1}\, t_{w3}\, EA_w}$$

$$(3.III.6f) \quad \boldsymbol{C_{AR3}} = -\frac{\boldsymbol{dx_1}}{\boldsymbol{dy_1}} (\boldsymbol{x'_{w1} - 1})\, \boldsymbol{t_{w1}\, t_{w2}\, EA_w}$$

The axial force within the rope can be written as follows.

$$N_R^B = C_{AB2}\,\chi_{R2} + C_{AB3}\,\chi_{R3} + C_{AR2}\,\varphi_{R2} + C_{AR3}\,\varphi_{R3}$$

Only the functions regarding the global axis x_2 will be plotted. The first two coefficients are the entries of the first row of $\mathbf{K}^{B}_{R}$ (3.III.3b). The function is referred to the case of real arch length only, since in both cases a zero-mean value holds true.

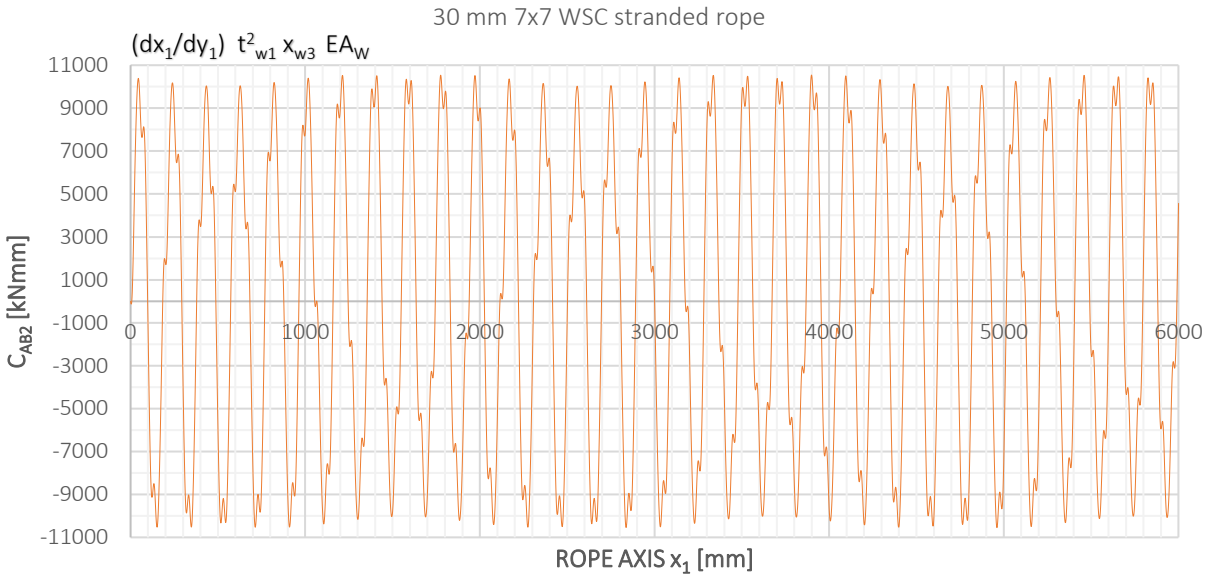

Fig 3.54 Single Wire Contribution to Wire Rope Axial Bending Coupling Coefficient

It can be clearly appreciated the periodical trend of the function. Still, the period is different from the funtions (3.III.6a) and (3.III.6b), since to appreciate the periodicity a much longer length of the rope axis needs to be considered.

The second two coefficients are the entries of the first row of $\mathbf{A}_R$ (3.III.3c). The function is referred to the case of real arch length only, since in both cases a zero-mean value holds true.

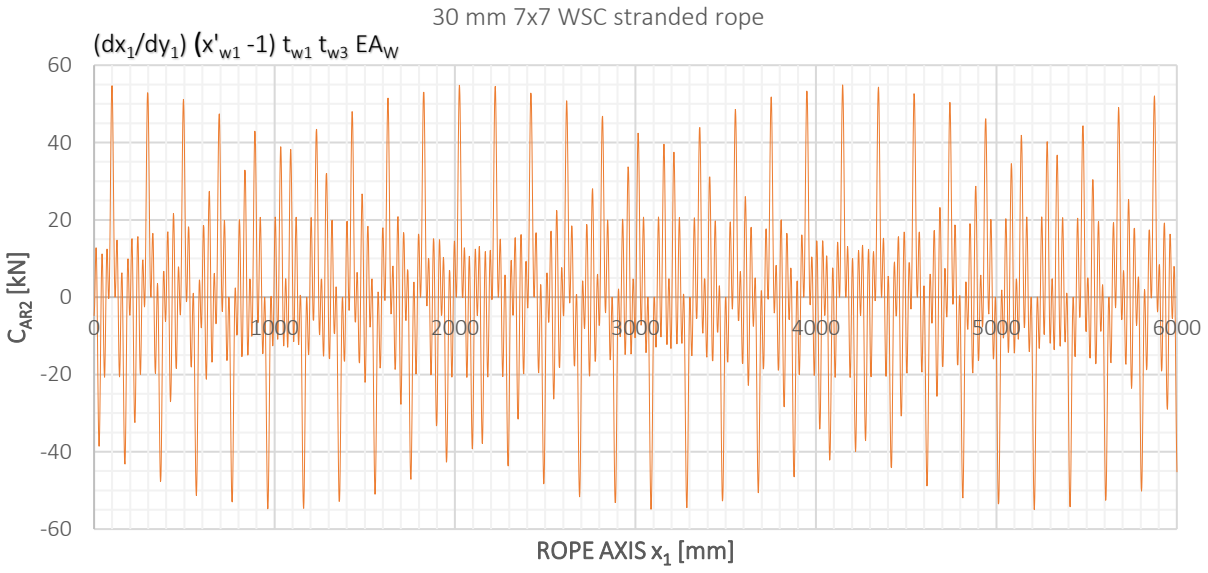

Fig 3.55 Single Wire Contribution to Wire Rope Axial Bending Rotation Coupling Coefficient

3.2. TORSIONAL MOMENT WITHIN THE ROPE

Let us introduce the expressions from the kinematics (2.II.8), (2.II.9) and (2.II.11) inside the second relation of (3.III.5). Afterwards, let us separate the contributions to the torque due to the projection of the wire moments M^{χ} and to the projection and transport of the wire axial force M^{η}.

$$M_{RT} = M_{RT}^{\chi} + M_{RT}^{\eta}$$

$$M_{RT}^{\chi} = EI_w \left(\frac{1}{1+\nu} t_{w1} \frac{dx_1}{dy_1} \sum_{i=1}^{3} \chi_{Ri}\, t_{wi} + n_{w1} \frac{dx_1}{dy_1} \sum_{i=1}^{3} \chi_{Ri}\, n_{wi} + b_{w1} \frac{dx_1}{dy_1} \sum_{i=1}^{3} \chi_{Ri}\, b_{wi} \right)$$

$$M_{RT}^{\eta} = (x_{w2}\, t_{w3} - x_{w3}\, t_{w2})\, EA_w \frac{dx_1}{dy_1} [t_{w1}\, \eta_R + (x_{w2}\, t_{w3} - x_{w3}\, t_{w2})\, \chi_{RT} + t_{w1}(x_{w3}\, \chi_{R2} - x_{w2}\, \chi_{R3}) + (x'_{w1} - 1)\, (t_{w3}\, \varphi_{R2} - t_{w2}\, \varphi_{R3})]$$

The contribution due to axial torsion of the rope and biaxial bending are split.

3.2.1. AXIAL TORSION OF THE ROPE

In this subsection it will be defined the second row of the matrix $\mathbf{K}^{AT}{}_{R}$(3.III.3a)

$$M_{RT}^{\chi AT} = EI_w \left(\frac{1}{1+\nu} t_{w1} \frac{dx_1}{dy_1} \chi_{RT}\, t_{w1} + n_{w1} \frac{dx_1}{dy_1} \chi_{RT}\, n_{w1} + b_{w1} \frac{dx_1}{dy_1} \chi_{RT}\, b_{w1} \right)$$

$$M_{RT}^{\eta AT} = (x_{w2}\, t_{w3} - x_{w3}\, t_{w2})\, EA_w \frac{dx_1}{dy_1} [t_{w1}\, \eta_R + (x_{w2}\, t_{w3} - x_{w3}\, t_{w2})\, \chi_{RT}]$$

The stiffness coefficients are

$$(3.III.7a) \quad \boldsymbol{C_{TA}} = \frac{\boldsymbol{dx_1}}{\boldsymbol{dy_1}} \boldsymbol{t_{w1}} (\boldsymbol{x_{w2}\, t_{w3} - x_{w3}\, t_{w2}})\, \boldsymbol{EA_w}$$

$$(3.III.7b) \quad \boldsymbol{GJ_R} = \frac{\boldsymbol{dx_1}}{\boldsymbol{dy_1}} \left[\left(\frac{\mathbf{1}}{\mathbf{1+\nu}} \boldsymbol{t_{w1}^2} + \boldsymbol{n_{w1}^2} + \boldsymbol{b_{w1}^2} \right) \boldsymbol{EI_w} + (\boldsymbol{x_{w2}\, t_{w3} - x_{w3}\, t_{w2}})^2\, \boldsymbol{EA_w} \right]$$

The torque within the rope can be written as follows.

$$M_{RT}^{AT} = C_{TA}\, \eta_R + GJ_R\, \chi_{RT}$$

The coupling coefficient (3.III.7a) is equal to the previously showed (3.III.6b), hence Reciprocity holds true. Let us plot the torsional stiffness coefficient (3.III.7b). This is the last case where the difference between real and developed arch length dx_1/dy_1 is reported.

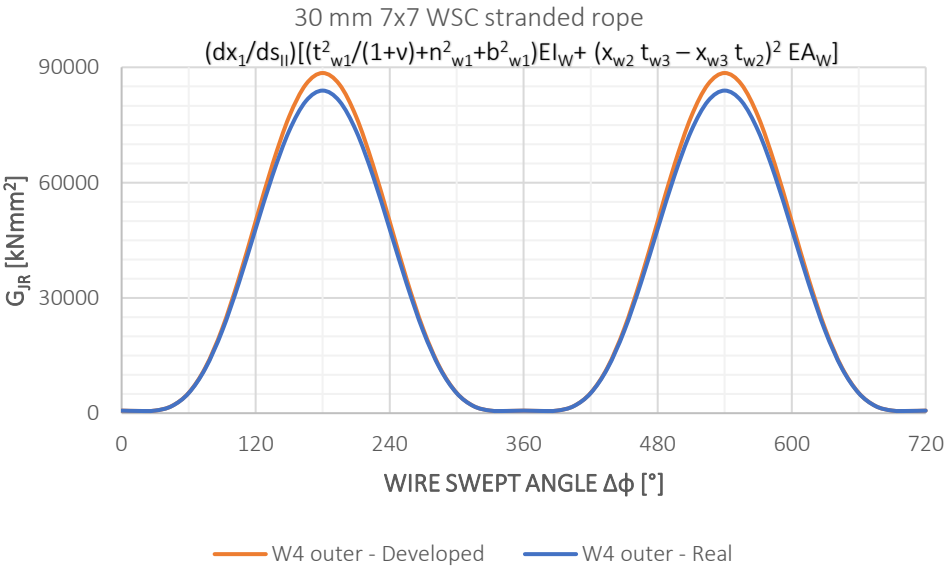

Fig 3.56 Single Wire Contribution to Wire Rope Torsional Stiffness

The presence of a non-zero mean value is an expected result, since the torsional stiffness is the direct stiffness in torsional regime. A table comparing the maximum, minimum and mean value of the two formulations is showed below.

Table 3.14 Single Wire Contribution to Wire Rope Torsional Stiffness

G_{JR}[kNmm^2]	max	min	mean
real	83941	576	42258
developed (approximate)	88510	576	44543
error	-5.16%	-0.04%	-5.13%

A further analysis is introduced for this coefficient only. Specifically, it has been shown that the contributions to the global stiffness are two: the projection of the internal moments of the wire (torque and bending) and the projection and transport of the wire axial force. This last contribution in our model is the one having the greater importance on the response. It is a direct consequence of the kinematic hypothesis of Euler Bernoulli behavior of the rope cross section. The result is trivial if we think that the moments contribution is due to the wire torsional and bending stiffness, while the axial force contribution is due to the twisting moment arising for the presence of the lever arm between the wire axis and the rope axis. In the graph "curvature" stands for moments contributions, while "axial" is the contribution of the wire axial force.

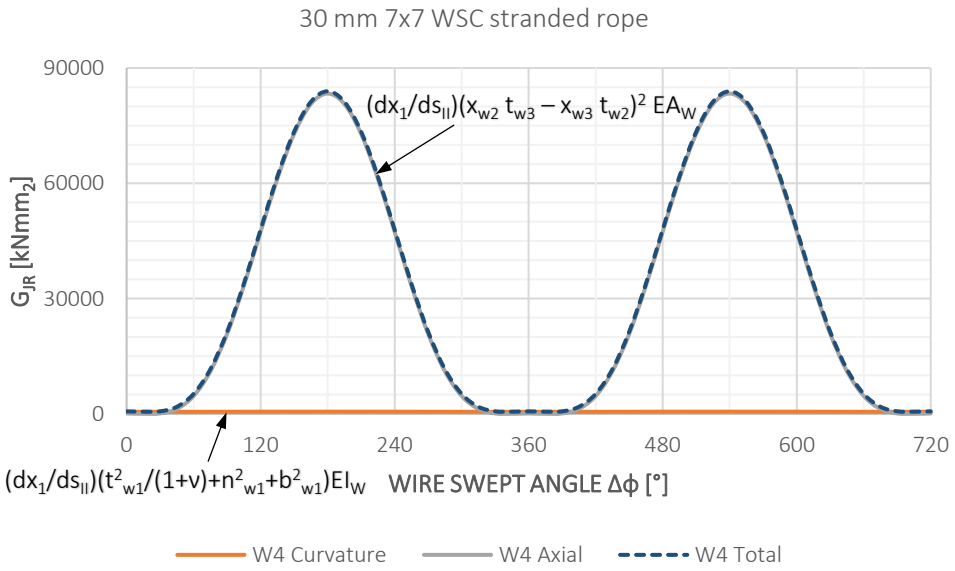

Fig 3.57 Single Wire Contribution to Wire Rope Torsional Stiffness – Wire Axial Strain and Curvatures Contributions

In the following table the numerical values of maximum, minimum and mean value are provided for the curvature, axial and total case with the weight in percentage with respect to the total.

Table 3.15 Single Wire Contribution to Wire Rope Torsional Stiffness – Wire Axial Strain and Curvatures Contributions

G_{JR} [kNmm^2]	max		min		mean	
Wire axial force	83356	99.30%	24	4.15%	41689.97	98.66%
Wire moments	585	0.70%	548	95.85%	566	1.34%
Total	83941	-	572	-	42256	-

It is clear that the fundamental internal action of the wire that weights on the rope response is the axial force, while the contribution of the internal moments of the wire is almost negligible.

3.2.2. BIAXIAL BENDING OF THE ROPE

In this subsection they will be defined the second rows of the matrices $\mathbf{K}^{B}_{R}$ (3.II.3b) and $\mathbf{A}_{R}$ (3.II.3c).

$$M^{\chi}_{RT} = EI_w \left(\frac{1}{1+\nu} t_{w1} \frac{dx_1}{dy_1} \sum_{i=2}^{3} \chi_{Ri}\, t_{wi} + n_{w1} \frac{dx_1}{dy_1} \sum_{i=2}^{3} \chi_{Ri}\, n_{wi} + b_{w1} \frac{dx_1}{dy_1} \sum_{i=2}^{3} \chi_{Ri}\, b_{wi} \right)$$

$$M^{\eta}_{RT} = (x_{w2}\, t_{w3} - x_{w3}\, t_{w2})\, EA_w \frac{dx_1}{dy_1} \left[t_{w1} (x_{w3}\, \chi_{R2} - x_{w2}\, \chi_{R3}) + (x'_{w1} - 1)\, (t_{w3}\, \varphi_{R2} - t_{w2}\, \varphi_{R3}) \right]$$

The stiffness coefficients are

$$(3.III.8a) \quad \boldsymbol{C_{TB2} = \frac{dx_1}{dy_1} \left[\left(\frac{1}{1+\nu} t_{w1} t_{w2} + n_{w1} n_{w2} + b_{w1} b_{w2} \right) EI_w + t_{w1}\, (x_{w2}\, t_{w3} - x_{w3}\, t_{w2})\, x_{w3}\, EA_w \right]}$$

$$(3.III.8b) \quad \boldsymbol{C_{TB3} = \frac{dx_1}{dy_1} \left[\left(\frac{1}{1+\nu} t_{w1} t_{w3} + n_{w1} n_{w3} + b_{w1} b_{w3} \right) EI_w - t_{w1}\, (x_{w2}\, t_{w3} - x_{w3}\, t_{w2})\, x_{w2}\, EA_w \right]}$$

$$(3.III.8c) \quad \boldsymbol{C_{TR2} = \frac{dx_1}{dy_1} (x'_{w1} - 1)\, t_{w3}\, (x_{w2}\, t_{w3} - x_{w3}\, t_{w2})\, EA_w}$$

$$(3.III.8d) \quad \boldsymbol{C_{TR3} = -\frac{dx_1}{dy_1} (x'_{w1} - 1)\, t_{w2}\, (x_{w2}\, t_{w3} - x_{w3}\, t_{w2})\, EA_w}$$

The torque within the rope can be written as follows.

$$M^{B}_{RT} = C_{TB2}\, \chi_{R2} + C_{TB3}\, \chi_{R3} + C_{TR2}\, \varphi_{R2} + C_{TR3}\, \varphi_{R3}$$

The coupling coefficients are all periodic with zero-mean value, hence they won't contribute to the rope global response.

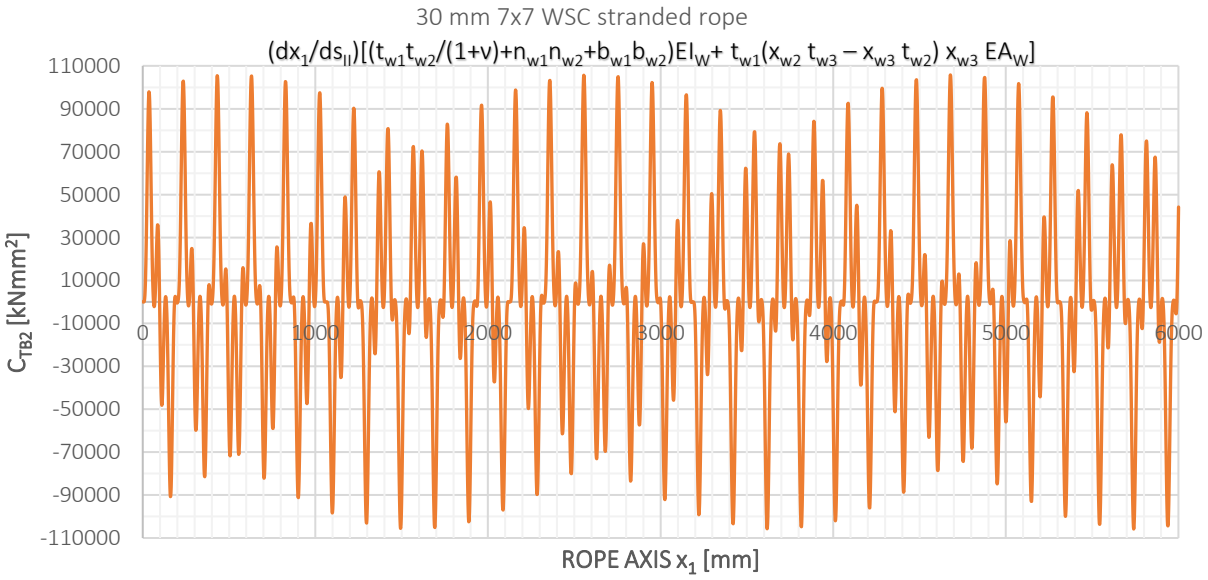

Fig 3.58 Single Wire Contribution to Wire Rope Torsion Bending Coupling Coefficient

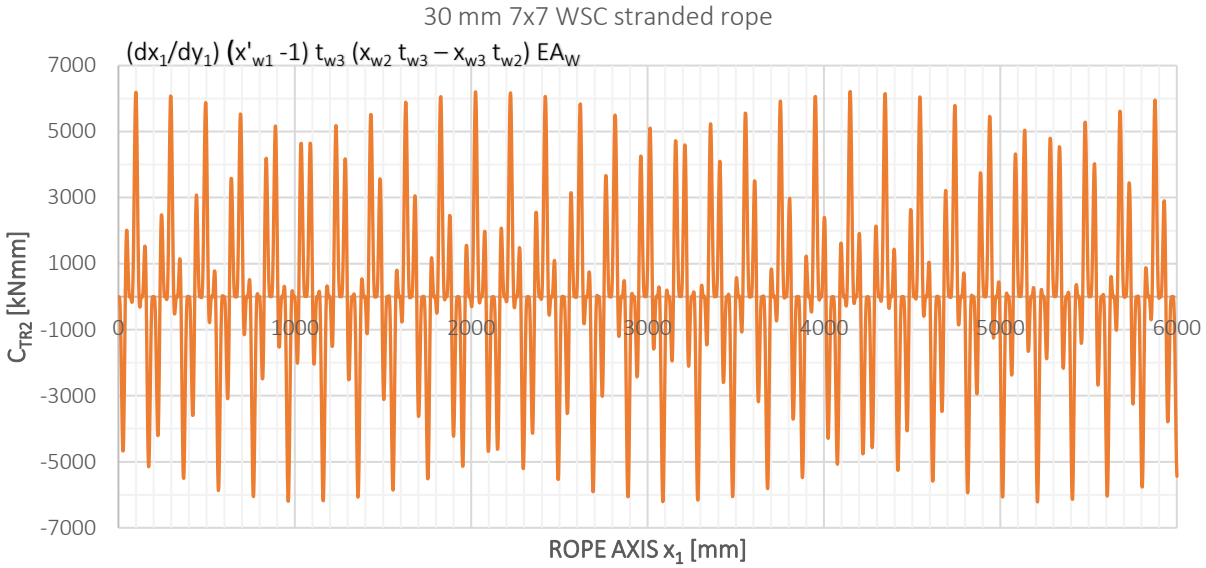

Fig 3.59 Single Wire Contribution to Wire Rope Torsion Bending Rotation Coupling Coefficient

3.3. BENDING MOMENT ABOUT AXIS 2 WITHIN THE ROPE

Let us introduce the expressions from the kinematics (2.II.8), (2.II.9) and (2.II.11) inside the third relation of (3.III.5). Afterwards, let us separate the contributions to the bending moment due to the projection of the wire moments M^{χ} and to the projection and transport of the wire axial force M^{η}.

$$M_{R2}^{\chi} = EI_w \left(\frac{1}{1+\nu} t_{w2} \frac{dx_1}{dy_1} \sum_{i=1}^{3} \chi_{Ri}\, t_{wi} + n_{w2} \frac{dx_1}{dy_1} \sum_{i=1}^{3} \chi_{Ri}\, n_{wi} + b_{w2} \frac{dx_1}{dy_1} \sum_{i=1}^{3} \chi_{Ri}\, b_{wi} \right)$$

$$M_{R2}^{\eta} = t_{w1}\, x_{w3}\, EA_w \frac{dx_1}{dy_1} \left[t_{w1}\, \eta_R + (x_{w2}\, t_{w3} - x_{w3}\, t_{w2})\, \chi_{RT} + t_{w1} (x_{w3}\, \chi_{R2} - x_{w2}\, \chi_{R3}) + (x'_{w1} - 1)\, (t_{w3}\, \varphi_{R2} - t_{w2}\, \varphi_{R3}) \right]$$

The contribution due to axial torsion of the rope and biaxial bending are split.

3.3.1. AXIAL TORSION OF THE ROPE

In this subsection it will be defined the third row of the matrix $\mathbf{K}^{AT}{}_{R}$(3.III.3a)

$$M_{R2}^{\chi} = EI_w \left(\frac{1}{1+\nu} t_{w2} \frac{dx_1}{dy_1} \chi_{R1}\, t_{w1} + n_{w2} \frac{dx_1}{dy_1} \chi_{R1}\, n_{w1} + b_{w2} \frac{dx_1}{dy_1} \chi_{R1}\, b_{w1} \right)$$

$$M_{R2}^{\eta} = t_{w1}\, x_{w3}\, EA_w \frac{dx_1}{dy_1} \left[t_{w1}\, \eta_R + (x_{w2}\, t_{w3} - x_{w3}\, t_{w2})\, \chi_{RT} \right]$$

The stiffness coefficients are

$$(3.III.9a) \quad \boldsymbol{C_{B2A}} = \frac{\boldsymbol{dx_1}}{\boldsymbol{dy_1}}\, \boldsymbol{t_{w1}^2}\, \boldsymbol{x_{w3}}\, \boldsymbol{EA_w}$$

$$(3.III.9b) \quad \boldsymbol{C_{B2T}} = \frac{\boldsymbol{dx_1}}{\boldsymbol{dy_1}} \left[\left(\frac{\mathbf{1}}{\mathbf{1+\nu}} \boldsymbol{t_{w2} t_{w1}} + \boldsymbol{n_{w2} n_{w1}} + \boldsymbol{b_{w2} b_{w1}} \right) \boldsymbol{EI_w} + \boldsymbol{t_{w1}} (\boldsymbol{x_{w2}\, t_{w3}} - \boldsymbol{x_{w3}\, t_{w2}})\, \boldsymbol{x_{w3}}\, \boldsymbol{EA_w} \right]$$

The bending moment about axis 2 within the rope can be written as follows.

$$M_{R2}^{AT} = C_{B2A}\, \eta_R + C_{B2T}\, \chi_{RT}$$

The coefficients are symmetric with respect (3.III.6c) and (3.III.8a), hence Reciprocity holds true and the plot may be seen in the previous sections.

3.3.2. BIAXIAL BENDING OF THE ROPE

In this subsection they will be defined the third rows of the matrices $\mathbf{K}^{B}_{R}$ (3.III.3b) and $\mathbf{A}_{R}$ (3.III.3c).

$$M^{\chi}_{R2} = EI_w \left(\frac{1}{1+\nu} t_{w2} \frac{dx_1}{dy_1} \sum_{i=2}^{3} \chi_{Ri}\, t_{wi} + n_{w2} \frac{dx_1}{dy_1} \sum_{i=2}^{3} \chi_{Ri}\, n_{wi} + b_{w2} \frac{dx_1}{dy_1} \sum_{i=2}^{3} \chi_{Ri}\, b_{wi} \right)$$

$$M^{\eta}_{R2} = t_{w1}\, x_{w3}\, EA_w \frac{dx_1}{dy_1} \left[t_{w1} (x_{w3}\, \chi_{R2} - x_{w2}\, \chi_{R3}) + (x'_{w1} - 1)\, (t_{w3}\, \varphi_{R2} - t_{w2}\, \varphi_{R3}) \right]$$

The stiffness coefficients are

$$(3.III.9c) \quad \boldsymbol{EI_{R2}} = \frac{\boldsymbol{dx_1}}{\boldsymbol{dy_1}} \left[\left(\frac{\mathbf{1}}{\mathbf{1+\nu}} \boldsymbol{t^2_{w2}} + \boldsymbol{n^2_{w2}} + \boldsymbol{b^2_{w2}} \right) \boldsymbol{EI_w} + \boldsymbol{t^2_{w1}}\, \boldsymbol{x^2_{w3}}\, \boldsymbol{EA_w} \right]$$

$$(3.III.9d) \quad \boldsymbol{C_{B23}} = \frac{\boldsymbol{dx_1}}{\boldsymbol{dy_1}} \left[\left(\frac{\mathbf{1}}{\mathbf{1+\nu}} \boldsymbol{t_{w2} t_{w3}} + \boldsymbol{n_{w2} n_{w3}} + \boldsymbol{b_{w2} b_{w3}} \right) \boldsymbol{EI_w} - \boldsymbol{t^2_{w1}}\, \boldsymbol{x_{w2}}\, \boldsymbol{x_{w3}}\, \boldsymbol{EA_w} \right]$$

$$(3.III.9e) \quad \boldsymbol{C_{B2R2}} = \frac{\boldsymbol{dx_1}}{\boldsymbol{dy_1}} (\boldsymbol{x'_{w1}} - \mathbf{1})\, \boldsymbol{t_{w1}}\, \boldsymbol{t_{w3}}\, \boldsymbol{x_{w3}}\, \boldsymbol{EA_w}$$

$$(3.III.9f) \quad \boldsymbol{C_{B2R3}} = -\frac{\boldsymbol{dx_1}}{\boldsymbol{dy_1}} (\boldsymbol{x'_{w1}} - \mathbf{1})\, \boldsymbol{t_{w1}}\, \boldsymbol{t_{w2}}\, \boldsymbol{x_{w2}}\, \boldsymbol{EA_w}$$

The bending moment about axis 2 within the rope can be written as follows.

$$M^{B}_{R2} = EI_{R2}\, \chi_{R2} + C_{B23}\, \chi_{R3} + C_{B2R2}\, \varphi_{R2} + C_{B2R3}\, \varphi_{R3}$$

Firstly, let us report the bending stiffness about the global axis x_2 (3.III.9c). the function shows a periodical trend with non-zero mean value; hence it will contribute to the rope global response as it was expected.

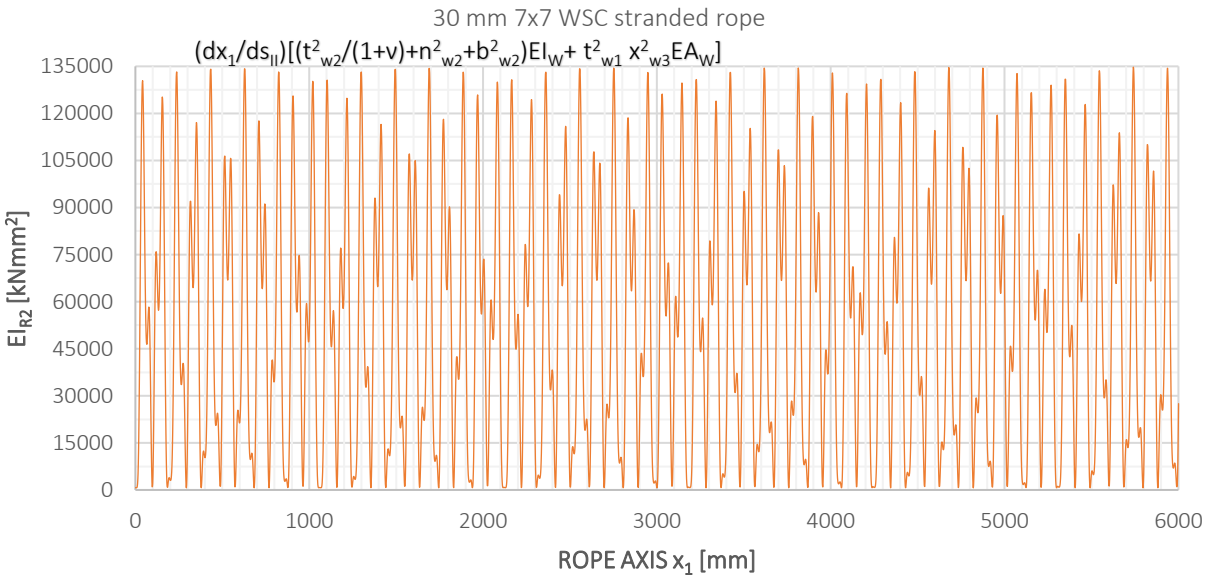

Fig 3.60 Single Wire Contribution to Wire Rope Flexural Stiffness

Table 3.16 Single Wire Contribution to Wire Rope Flexural Stiffness

EI_{R2} [kNmm^2]	max	min	mean
	134738	676	67707

In the following, it is possible to appreciate the coupling coefficient between bending the two principal directions of the rope (3.III.9d). The function is periodic with zero-mean value.

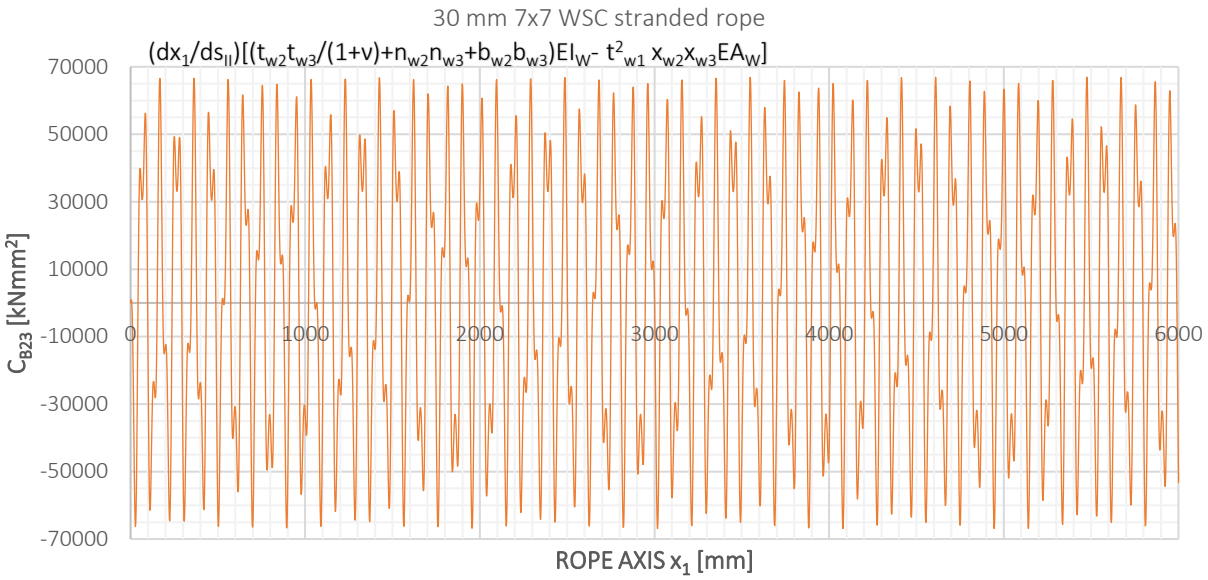

Fig 3.61 Single Wire Contribution to Wire Rope Bending Coupling Coefficient

At last, it is possible to appreciate the coupling coefficient between bending the corresponding rotation of the rope (3.III.9e). The function is periodic with zero-mean value.

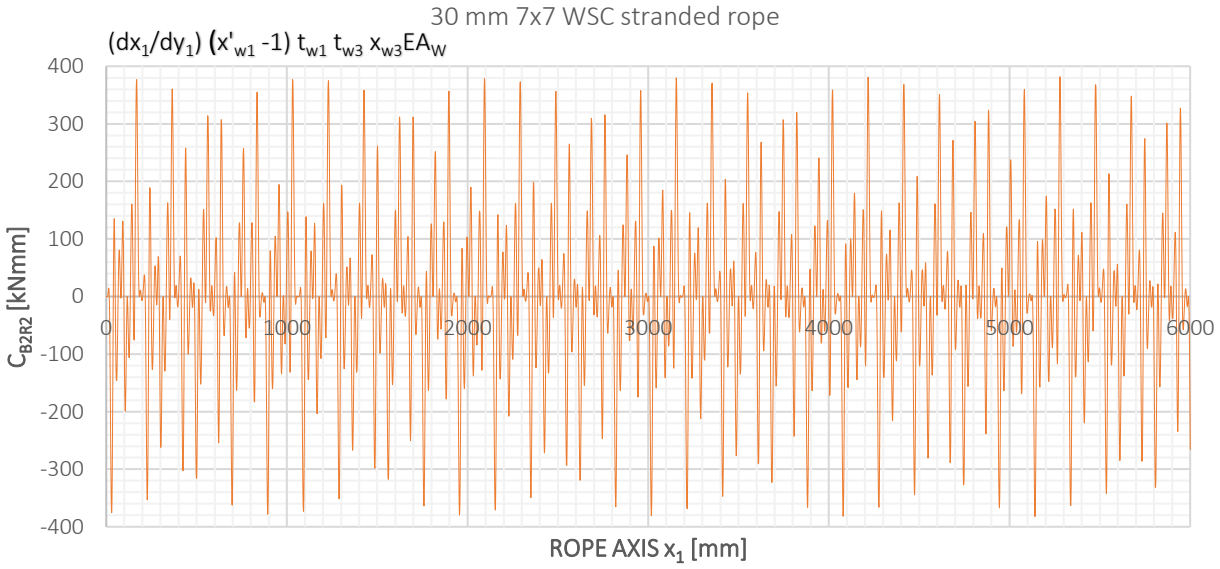

Fig 3.62 Single Wire Contribution to Wire Rope Torsion Bending and Bending Rotation Coupling Coefficient

3.4. BENDING MOMENT ABOUT AXIS 3 WITHIN THE ROPE

Let us introduce the expressions from the kinematics (2.II.8), (2.II.9) and (2.II.11) inside the fourth relation of (3.III.5). Afterwards, let us separate the contributions to the bending moment due to the projection of the wire moments M^x and to the projection and transport of the wire axial force M^η.

$$M_{R3}^{\chi} = EI_w \left(\frac{1}{1+\nu} t_{w3} \frac{dx_1}{dy_1} \sum_{i=1}^{3} \chi_{Ri}\, t_{wi} + n_{w3} \frac{dx_1}{dy_1} \sum_{i=1}^{3} \chi_{Ri}\, n_{wi} + b_{w3} \frac{dx_1}{dy_1} \sum_{i=1}^{3} \chi_{Ri}\, b_{wi} \right)$$

$$M_{R3}^{\eta} = -t_{w1}\, x_{w2}\, EA_w \frac{dx_1}{dy_1} \left[t_{w1}\, \eta_R + (x_{w2}\, t_{w3} - x_{w3}\, t_{w2})\, \chi_{RT} + t_{w1} (x_{w3}\, \chi_{R2} - x_{w2}\, \chi_{R3}) + (x'_{w1} - 1)\, (t_{w3}\, \varphi_{R2} - t_{w2}\, \varphi_{R3}) \right]$$

The contribution due to axial torsion of the rope and biaxial bending are split.

3.4.1. AXIAL TORSION OF THE ROPE

In this subsection it will be defined the fourth row of the matrix $\mathbf{K}^{AT}_{R}$(3.III.3a)

$$M_{R3}^{\chi} = EI_w \left(\frac{1}{1+\nu} t_{w3} \frac{dx_1}{dy_1} \chi_{R1}\, t_{w1} + n_{w3} \frac{dx_1}{dy_1} \chi_{R1}\, n_{w1} + b_{w3} \frac{dx_1}{dy_1} \chi_{R1}\, b_{w1} \right)$$

$$M_{R3}^{\eta} = -t_{w1}\, x_{w2}\, EA_w \frac{dx_1}{dy_1} \left[t_{w1}\, \eta_R + (x_{w2}\, t_{w3} - x_{w3}\, t_{w2})\, \chi_{RT} \right]$$

The stiffness coefficients are

$$(3.III.10a) \quad \boldsymbol{C_{B3A}} = -\frac{\boldsymbol{dx_1}}{\boldsymbol{dy_1}}\, \boldsymbol{t_{w1}^2\, x_{w2}\, EA_w}$$

$$(3.III.10b) \quad \boldsymbol{C_{B3T}} = \frac{\boldsymbol{dx_1}}{\boldsymbol{dy_1}} \left[\left(\frac{\mathbf{1}}{\mathbf{1+\nu}} \boldsymbol{t_{w3} t_{w1} + n_{w3} n_{w1} + b_{w3} b_{w1}} \right) \boldsymbol{EI_w} - \boldsymbol{t_{w1}} (\boldsymbol{x_{w2}\, t_{w3} - x_{w3}\, t_{w2}})\, \boldsymbol{x_{w2}\, EA_w} \right]$$

The bending moment about axis 3 within the rope can be written as follows.

$$M_{R3}^{AT} = C_{B3A}\, \eta_R + C_{B3T}\, \chi_{RT}$$

The coefficients are symmetric with (3.III.6d) and (3.III.8d).

3.4.2. BIAXIAL BENDING OF THE ROPE

In this subsection they will be defined the fourth rows of the matrices $\mathbf{K}^{B}_{R}$ (3.II.3b) and $\mathbf{A}_{R}$ (3.II.3c).

$$M_{R3}^{\chi} = EI_w \left(\frac{1}{1+\nu} t_{w3} \frac{dx_1}{dy_1} \sum_{i=2}^{3} \chi_{Ri}\, t_{wi} + n_{w3} \frac{dx_1}{dy_1} \sum_{i=2}^{3} \chi_{Ri}\, n_{wi} + b_{w3} \frac{dx_1}{dy_1} \sum_{i=2}^{3} \chi_{Ri}\, b_{wi} \right)$$

$$M_{R3}^{\eta} = -t_{w1}\, x_{w2}\, EA_w \frac{dx_1}{dy_1} \left[t_{w1} (x_{w3}\, \chi_{R2} - x_{w2}\, \chi_{R3}) + (x'_{w1} - 1)\, (t_{w3}\, \varphi_{R2} - t_{w2}\, \varphi_{R3}) \right]$$

The stiffness coefficients are

$$(3.III.10c) \quad \boldsymbol{C_{B32}} = \frac{\boldsymbol{dx_1}}{\boldsymbol{dy_1}} \left[\left(\frac{\mathbf{1}}{\mathbf{1+\nu}} \boldsymbol{t_{w3} t_{w2} + n_{w3} n_{w2} + b_{w3} b_{w2}} \right) \boldsymbol{EI_w} - \boldsymbol{t_{w1}^2\, x_{w2}\, x_{w3}\, EA_w} \right]$$

$$(3.III.10d) \quad \boldsymbol{EI_{R3}} = \frac{\boldsymbol{dx_1}}{\boldsymbol{dy_1}} \left[\left(\frac{\mathbf{1}}{\mathbf{1+\nu}} \boldsymbol{t_{w3}^2 + n_{w3}^2 + b_{w3}^2} \right) \boldsymbol{EI_w} + \boldsymbol{t_{w1}^2\, x_{w2}^2\, EA_w} \right]$$

$$(3.III.10e) \quad \boldsymbol{C_{B3R2}} = -\frac{\boldsymbol{dx_1}}{\boldsymbol{dy_1}} (\boldsymbol{x'_{w1} - 1})\, \boldsymbol{t_{w1}\, t_{w3}\, x_{w2}\, EA_w}$$

$$(3.III.10f) \quad \boldsymbol{C_{B3R3}} = \frac{\boldsymbol{dx_1}}{\boldsymbol{dy_1}} (\boldsymbol{x'_{w1} - 1})\, \boldsymbol{t_{w1}\, t_{w2}\, x_{w2}\, EA_w}$$

The bending moment about axis 3 within the rope can be written as follows.

$$M_{R3}^{B} = C_{B32}\, \chi_{R2} + EI_{R3}\, \chi_{R3} + C_{B3R2}\, \varphi_{R2} + C_{B3R3}\, \varphi_{R3}$$

The coupling term (3.III.10c) is symmetric with (3.III.9d). The direct bending stiffness has a trend equal to the previous one, only shifted along the rope axis.

IV. RECURSIVE MODEL

The recursive procedure to model the wire rope behavior has the aim of catching in a simplified manner how this whole system works. Specifically, the technological hierarchy wire, strand and rope is exploited. First, the strand is seen like a sum of wires, afterwards the rope is the result of different strands joined together. In this light, from the geometrical view point, the wire is not a double helix within the rope anymore, but a single helix inside the strand.

1. INTERNAL ACTIONS HIERARCHY

The relations (3.III.1) show the contributions of the single wire internal actions to the rope internal actions. The same relations are used to describe the contributions of the strand internal actions to the rope internal actions and the single wire contributions to the strand internal actions in order to exploit the hierarchical structure of this mechanical system.

1.1. SINGLE STRAND CONTRIBUTION TO THE ROPE RESPONSE

The single strand contribution to the rope response can be derived introducing inside (3.III.1) the suitable components of the Serret-Frenet frame of the single helix, i.e. of the strand, and substituting instead of the subscript "w", referred to the wire quantities, the subscript "s", referred to the strand quantities. The last formal passage has the mechanical meaning of introducing the relations between the strand and the rope internal actions with the same operations performed for the definition of (3.III.1), i.e. projection of the moments and projection and transport of the axial force within the strand. It is important to notice that the following result is exact, since it is based on the actual geometry occurring between rope and strand.

$$
\begin{aligned}
& N_R = \cos\alpha_s \; N_s \\
(3.IV.1) \quad & M_{RT} = \cos\alpha_s \; M_{sT} + \sin\alpha_s \; M_{s3} + R_s \; \sin\alpha_s \; N_s \\
& M_{R2} = -\sin\alpha_s \sin\vartheta \; M_{sT} - \cos\vartheta \; M_{s2} + \cos\alpha_s \sin\vartheta \; M_{s3} + R_s \cos\alpha_s \sin\vartheta \; N_s \\
& M_{R3} = \sin\alpha_s \cos\vartheta \; M_{sT} - \sin\vartheta \; M_{s2} - \cos\alpha_s \cos\vartheta \; M_{s3} - R_s \cos\alpha_s \cos\vartheta \; N_s
\end{aligned}
$$

Where α_s and R_s are the lay angle and the radius of the strand single helix, θ is the swept angle of the single helix strand centerline, N_s, M_{sT}, M_{s2} and M_{s3} are respectively the axial force, the torque and the bending moments about normal and binormal direction of the strand.

1.2. SINGLE STRAND CONTRIBUTION TO THE ROPE RESPONCE

The previous relations (3.IV.1) are now enforced for the strand and the wire as well. This operation is performed simply substituting the quantities related to the rope with the strand quantities and the strand quantities with the wire quantities. It is worth it to notice that the following relations would be a rigorous result if the strand was straight. Since the strand has a single helix shape, the following relations are approximated.

$$
\begin{aligned}
& N_s = \cos\alpha_w \; N_w \\
(3.IV.2) \quad & M_{sT} = \cos\alpha_w \; M_{wT} + \sin\alpha_w \; M_{w3} + R_w \; \sin\alpha_w \; N_w \\
& M_{s2} = -\sin\alpha_w \sin\varphi \; M_{wT} - \cos\varphi \; M_{w2} + \cos\alpha_w \sin\varphi \; M_{w3} + R_w \cos\alpha_w \sin\varphi \; N_w \\
& M_{s3} = \sin\alpha_w \cos\varphi \; M_{wT} - \sin\varphi \; M_{w2} - \cos\alpha_w \cos\varphi \; M_{w3} - R_w \cos\alpha_w \cos\varphi \; N_w
\end{aligned}
$$

Where α_w and R_w are the lay angle and the radius of the wire nested helix ϕ is the swept angle of the double helix wire centerline, N_w, M_{wT}, M_{w2} and M_{w3} are respectively the axial force, the torque and the bending moments about normal and binormal direction of the wire.

2. STRAND CONSTITUTIVE MODEL

The purpose of the present paragraph is to provide the constitutive model of the strand in terms of generalized stress and strain. The derivation starts with the relations (3.IV.2) that provide the strand internal actions as a function of the wire internal actions.

$$N_s = \cos\alpha_w \; N_w$$
$$M_{sT} = \cos\alpha_w \; M_{wT} + \sin\alpha_w \; M_{w3} + R_w \; \sin\alpha_w \; N_w$$
$$M_{s2} = -\sin\alpha_w \sin\varphi \; M_{wT} - \cos\varphi \; M_{w2} + \cos\alpha_w \sin\varphi \; M_{w3} + R_w \cos\alpha_w \sin\varphi \; N_w$$
$$M_{s3} = \sin\alpha_w \cos\varphi \; M_{wT} - \sin\varphi \; M_{w2} - \cos\alpha_w \cos\varphi \; M_{w3} - R_w \cos\alpha_w \cos\varphi \; N_w$$

Afterwards, the single wire constitutive model (3.II.1) in introduced in the previous relations.

$$N_w = EA_w \, \eta_w$$
$$M_{wT} = \frac{1}{1+\nu} EI_w \chi_{wT}$$
$$M_{w2} = EI_w \chi_{w2}$$
$$M_{w3} = EI_w \chi_{w3}$$

Finally, the strains within the wire are provided as functions of the strand strain field thanks to (2.III.3) and (2.III.4)

$$\eta_w^{sAT}(x_1) = \cos^2\alpha_w \; \eta_s(x_1) + R_w \; \cos\alpha_w \sin\alpha_w \; \chi_{sT}(x_1)$$
$$\chi_{wT}^{sAT}(x_1) = \cos^2\alpha_w \, \chi_{sT}(x_1)$$
$$\chi_{w2}^{sAT}(x_1) = 0$$
$$\chi_{w3}^{sAT}(x_1) = \cos\alpha_w \sin\alpha_w \, \chi_{sT}(x_1)$$

$$\eta_w^{sB}(x_1) = \cos^2\alpha_w \, R_w \sin\varphi(x_1) \; \chi_{s2}(x_1) - \cos^2\alpha_w \, R_w \cos\varphi(x_1) \; \chi_{s3}(x_1)$$
$$\chi_{wT}^{sB}(x_1) = -\cos\alpha_w \sin\alpha_w \sin\varphi(x_1) \, \chi_{s2}(x_1) + \cos\alpha_w \sin\alpha_w \cos\varphi(x_1) \, \chi_{s3}(x_1)$$
$$\chi_{w2}^{sB}(x_1) = -\cos\alpha_w \cos\varphi(x_1) \, \chi_{s2}(x_1) - \cos\alpha_w \sin\varphi(x_1) \, \chi_{s3}(x_1)$$
$$\chi_{w3}^{sB}(x_1) = \cos^2\alpha_w \sin\varphi(x_1) \, \chi_{s2}(x_1) - \cos^2\alpha_w \cos\varphi(x_1) \, \chi_{s3}(x_1)$$

From now on, the axial torsional and bending contributions of the strand will be explicitly highlighted. The purpose is the possibility of turning on and off the contributions that may be the cause of slipping among wires. To this aim, the superscripts “sAT” and “sB” will stand for strand axial torsion and strand bending respectively.

2.1. AXIAL TORSION OF THE STRAND

From the kinematics the following relations are brought.

$$\eta_w^{sAT}(x_1) = \cos^2\alpha_w \; \eta_s(x_1) + R_w \; \cos\alpha_w \sin\alpha_w \; \chi_{sT}(x_1)$$
$$\chi_{wT}^{sAT}(x_1) = \cos^2\alpha_w \, \chi_{sT}(x_1)$$
$$\chi_{w2}^{sAT}(x_1) = 0$$
$$\chi_{w3}^{sAT}(x_1) = \cos\alpha_w \sin\alpha_w \, \chi_{sT}(x_1)$$

Substituting into the constitutive model of the single wire

$$N_w^{sAT} = EA_w(\cos^2\alpha_w \; \eta_s + R_w \; \cos\alpha_w \sin\alpha_w \; \chi_{sT})$$
$$M_{wT}^{sAT} = \frac{1}{1+\nu} EI_w \cos^2\alpha_w \, \chi_{sT}$$
$$M_{w2}^{sAT} = 0$$
$$M_{w3}^{sAT} = EI_w \cos\alpha_w \sin\alpha_w \, \chi_{sT}$$

Substituting inside the internal actions within the strand cross section (3.III.2) the last expressions.

$$N_s^{sAT} = \cos\alpha_w \; [EA_w(\cos^2\alpha_w \; \eta_s + R_w \; \cos\alpha_w \sin\alpha_w \; \chi_{sT})]$$
$$M_{sT}^{sAT} = \cos\alpha_w \left[\frac{1}{1+\nu} EI_w \cos^2\alpha_w \, \chi_{sT}\right] + \sin\alpha_w \; [EI_w \cos\alpha_w \sin\alpha_w \, \chi_{sT}] + R_w \; \sin\alpha_w \; [EA_w(\cos^2\alpha_w \; \eta_s + R_w \; \cos\alpha_w \sin\alpha_w \; \chi_{sT})]$$

$$M_{s2}^{sAT} = -\sin\alpha_w \sin\varphi \left[\frac{1}{1+\nu} EI_w \cos^2\alpha_w \chi_{sT}\right] - \cos\varphi\ [0] + \cos\alpha_w \sin\varphi\ [EI_w \cos\alpha_w \sin\alpha_w \chi_{sT}]$$
$$+ R_w \cos\alpha_w \sin\varphi\ [EA_w(\cos^2\alpha_w\ \eta_s + R_w\ \cos\alpha_w \sin\alpha_w\ \chi_{sT})]$$
$$M_{s3}^{sAT} = \sin\alpha_w \cos\varphi \left[\frac{1}{1+\nu} EI_w \cos^2\alpha_w \chi_{sT}\right] - \sin\varphi\ [0] - \cos\alpha_w \cos\varphi\ [EI_w \cos\alpha_w \sin\alpha_w \chi_{sT}]$$
$$- R_w \cos\alpha_w \cos\varphi\ [EA_w(\cos^2\alpha_w\ \eta_s + R_w\ \cos\alpha_w \sin\alpha_w\ \chi_{sT})]$$

Let us collect the common terms, then the result is as follows.

$$\boldsymbol{N_s^{sAT} = \cos^3\alpha_w EA_w \eta_s + R_w\ \cos^3\alpha_w \tan\alpha_w EA_w \chi_{sT}}$$
$$(3.IV.3a)\quad \boldsymbol{M_{sT}^{sAT} = R_w \cos^3\alpha_w \tan\alpha_w EA_w \eta_s + \cos^3\alpha_w \left[\left(\frac{1}{1+\nu} + \tan^2\alpha_w\right) EI_w + R_w^2\ \tan^2\alpha_w EA_w\right] \chi_{sT}}$$
$$\boldsymbol{M_{s2}^{sAT} = R_w \cos^3\alpha_w \sin\varphi EA_w \eta_s + \cos^3\alpha_w \tan\alpha_w \sin\varphi \left[\frac{\nu}{1+\nu} EI_w + R_w^2\ EA_w\right] \chi_{sT}}$$
$$\boldsymbol{M_{s3}^{sAT} = -R_w \cos^3\alpha_w \cos\varphi EA_w \eta_s - \cos^3\alpha_w \tan\alpha_w \cos\varphi \left[\frac{\nu}{1+\nu} EI_w + R_w^2\ EA_w\right] \chi_{sT}}$$

It is important to notice that the first two terms, i.e. the strand axial force and torque, do not depend upon the position of the wire within the strand denoted by the cylindrical coordinate $R_w \sin(\phi)$, while the last two quantities do. This remark is fundamental when the global response of the strand must be investigated. As a matter of fact, the relations (3.IV.3a) represent the contribution of the single wire of position $R_w \sin(\phi)$ to the global stiffness matrix. When the entire matrix must be computed, a sum needs to be performed over the wires of the strand cross section. Hence, the terms depending on the position drop in the summation when the strand cross section is symmetric.

2.2. BIAXIAL BENDING OF THE STRAND

From the kinematics the following relations are brought.

$$\eta_w^{sB}(x_1) = \cos^2\alpha_w R_w \sin\varphi(x_1)\ \chi_{s2}(x_1) - \cos^2\alpha_w R_w \cos\varphi(x_1)\ \chi_{s3}(x_1)$$
$$\chi_{wT}^{sB}(x_1) = -\cos\alpha_w \sin\alpha_w \sin\varphi(x_1)\chi_{s2}(x_1) + \cos\alpha_w \sin\alpha_w \cos\varphi(x_1)\chi_{s3}(x_1)$$
$$\chi_{w2}^{sB}(x_1) = -\cos\alpha_w \cos\varphi(x_1)\chi_{s2}(x_1) - \cos\alpha_w \sin\varphi(x_1)\chi_{s3}(x_1)$$
$$\chi_{w3}^{sB}(x_1) = \cos^2\alpha_w \sin\varphi(x_1)\chi_{s2}(x_1) - \cos^2\alpha_w \cos\varphi(x_1)\chi_{s3}(x_1)$$

Substituting into the constitutive model of the single wire

$$N_w^{sB} = EA_w\ (\cos^2\alpha_w R_w \sin\varphi\ \chi_{s2} - \cos^2\alpha_w R_w \cos\varphi\ \chi_{s3})$$
$$M_{wT}^{sB} = \frac{1}{1+\nu} EI_w(-\cos\alpha_w \sin\alpha_w \sin\varphi\,\chi_{s2} + \cos\alpha_w \sin\alpha_w \cos\varphi\,\chi_{s3})$$
$$M_{w2}^{sB} = EI_w(-\cos\alpha_w \cos\varphi\,\chi_{s2} - \cos\alpha_w \sin\varphi\,\chi_{s3})$$
$$M_{w3}^{sB} = EI_w(\cos^2\alpha_w \sin\varphi\,\chi_{s2} - \cos^2\alpha_w \cos\varphi\,\chi_{s3})$$

Substituting inside the internal actions within the strand cross section (3.IV.2) the last expressions.

$$N_s^{sB} = \cos\alpha_w\ [EA_w\ (\cos^2\alpha_w R_w \sin\varphi\ \chi_{s2} - \cos^2\alpha_w R_w \cos\varphi\ \chi_{s3})]$$
$$M_{sT}^{sB} = \cos\alpha_w \left[\frac{1}{1+\nu} EI_w(-\cos\alpha_w \sin\alpha_w \sin\varphi\,\chi_{s2} + \cos\alpha_w \sin\alpha_w \cos\varphi\,\chi_{s3})\right] + \sin\alpha_w\ [EI_w(\cos^2\alpha_w \sin\varphi\,\chi_{s2} - \cos^2\alpha_w \cos\varphi\,\chi_{s3})]$$
$$+ R_w\ \sin\alpha_w\ [EA_w\ (\cos^2\alpha_w R_w \sin\varphi\ \chi_{s2} - \cos^2\alpha_w R_w \cos\varphi\ \chi_{s3})]$$
$$M_{s2}^{sB} = -\sin\alpha_w \sin\varphi \left[\frac{1}{1+\nu} EI_w(-\cos\alpha_w \sin\alpha_w \sin\varphi\,\chi_{s2} + \cos\alpha_w \sin\alpha_w \cos\varphi\,\chi_{s3})\right] - \cos\varphi\ [EI_w(-\cos\alpha_w \cos\varphi\,\chi_{s2} - \cos\alpha_w \sin\varphi\,\chi_{s3})]$$
$$+ \cos\alpha_w \sin\varphi\ [EI_w(\cos^2\alpha_w \sin\varphi\,\chi_{s2} - \cos^2\alpha_w \cos\varphi\,\chi_{s3})]$$
$$+ R_w \cos\alpha_w \sin\varphi\ [EA_w\ (\cos^2\alpha_w R_w \sin\varphi\ \chi_{s2} - \cos^2\alpha_w R_w \cos\varphi\ \chi_{s3})]$$
$$M_{s3}^{sB} = \sin\alpha_w \cos\varphi \left[\frac{1}{1+\nu} EI_w(-\cos\alpha_w \sin\alpha_w \sin\varphi\,\chi_{s2} + \cos\alpha_w \sin\alpha_w \cos\varphi\,\chi_{s3})\right] - \sin\varphi\ [EI_w(-\cos\alpha_w \cos\varphi\,\chi_{s2} - \cos\alpha_w \sin\varphi\,\chi_{s3})]$$
$$- \cos\alpha_w \cos\varphi\ [EI_w(\cos^2\alpha_w \sin\varphi\,\chi_{s2} - \cos^2\alpha_w \cos\varphi\,\chi_{s3})]$$
$$- R_w \cos\alpha_w \cos\varphi\ [EA_w\ (\cos^2\alpha_w R_w \sin\varphi\ \chi_{s2} - \cos^2\alpha_w R_w \cos\varphi\ \chi_{s3})]$$

Let us collect the common terms, then the result is as follows.

$$N_s^{sB} = \cos^3\alpha_w R_w \sin\varphi\, EA_w\, \chi_{s2} - \cos^3\alpha_w R_w \cos\varphi\, EA_w\, \chi_{s3}$$

$$(3.IV.3b)\quad M_{sT}^{sB} = \cos^3\alpha_w \tan\alpha_w \sin\varphi \left[\frac{\nu}{1+\nu} EI_w + R_w^2\, EA_w\right]\chi_{s2} - \cos^3\alpha_w \tan\alpha_w \cos\varphi \left[\frac{\nu}{1+\nu} EI_w + R_w^2\, EA_w\right]\chi_{s3}$$

$$M_{s2}^{sB} = \cos\alpha_w \left[\left(\frac{\sin^2\alpha_w}{1+\nu} + \cot^2\varphi + \cos^2\alpha_w\right) EI_w + \cos^2\alpha_w R_w^2\, EA_w\right]\sin^2\varphi\ \chi_{s2}$$
$$- \cos^3\alpha_w \left[-\frac{\nu}{1+\nu}\tan^2\alpha_w\, EI_w + R_w^2\, EA_w\right]\sin\varphi\cos\varphi\,\chi_{s3}$$

$$M_{s3}^{sB} = -\cos^3\alpha_w \left[-\frac{\nu}{1+\nu}\tan^2\alpha_w\, EI_w + R_w^2\, EA_w\right]\sin\varphi\cos\varphi\,\chi_{s2}$$
$$+ \cos\alpha_w \left[\left(\frac{\sin^2\alpha_w}{1+\nu} + \tan^2\varphi + \cos^2\alpha_w\right) EI_w + \cos^2\alpha_w R_w^2\, EA_w\right]\cos^2\varphi\ \chi_{s3}$$

3. SINGLE WIRE CONTRIBUTION TO THE ROPE GLOBAL RESPONSE

The purpose of the present paragraph is to provide the rope constitutive model contribution of the single wire in terms of stiffness with respect the generalized stress and strain.
The derivation starts with the relations (3.IV.1) recalled below, that provide the rope internal actions as a function of the strand internal actions.

$$N_R = \cos\alpha_s \; N_s$$
$$M_{RT} = \cos\alpha_s \; M_{sT} + \sin\alpha_s \; M_{s3} + R_s \; \sin\alpha_s \; N_s$$
$$M_{R2} = -\sin\alpha_s \sin\vartheta \; M_{sT} - \cos\vartheta \; M_{s2} + \cos\alpha_s \sin\vartheta \; M_{s3} + R_s \cos\alpha_s \sin\vartheta \; N_s$$
$$M_{R3} = \sin\alpha_s \cos\vartheta \; M_{sT} - \sin\vartheta \; M_{s2} - \cos\alpha_s \cos\vartheta \; M_{s3} - R_s \cos\alpha_s \cos\vartheta \; N_s$$

The equations (3.IV.3) reported in the following will be used to substitute in (3.IV.1) the value of the strand internal actions. They are divided according to the axial torsional and biaxial bending contribution of the strand.

$$N_s^{sAT} = \cos^3\alpha_w \, EA_w \, \eta_s + R_w \, \cos^3\alpha_w \tan\alpha_w \, EA_w \, \chi_{sT}$$
$$M_{sT}^{sAT} = R_w \cos^3\alpha_w \tan\alpha_w \, EA_w \, \eta_s + \cos^3\alpha_w \left[\left(\frac{1}{1+\nu} + \tan^2\alpha_w\right) EI_w + R_w^2 \, \tan^2\alpha_w \, EA_w\right] \chi_{sT}$$
$$M_{s2}^{sAT} = R_w \cos^3\alpha_w \sin\varphi \, EA_w \, \eta_s + \cos^3\alpha_w \tan\alpha_w \sin\varphi \left[\frac{\nu}{1+\nu} EI_w + R_w^2 \, EA_w\right] \chi_{sT}$$
$$M_{s3}^{sAT} = -R_w \cos^3\alpha_w \cos\varphi \, EA_w \, \eta_s - \cos^3\alpha_w \tan\alpha_w \cos\varphi \left[\frac{\nu}{1+\nu} EI_w + R_w^2 \, EA_w\right] \chi_{sT}$$

$$N_s^{sB} = \cos^3\alpha_w \, R_w \sin\varphi \, EA_w \, \chi_{s2} - \cos^3\alpha_w \, R_w \cos\varphi \, EA_w \, \chi_{s3}$$
$$M_{sT}^{sB} = \cos^3\alpha_w \tan\alpha_w \sin\varphi \left[\frac{\nu}{1+\nu} EI_w + R_w^2 \, EA_w\right] \chi_{s2} - \cos^3\alpha_w \tan\alpha_w \cos\varphi \left[\frac{\nu}{1+\nu} EI_w + R_w^2 \, EA_w\right] \chi_{s3}$$
$$M_{s2}^{sB} = \cos\alpha_w \left[\left(\frac{\sin^2\alpha_w}{1+\nu} + \cot^2\varphi + \cos^2\alpha_w\right) EI_w + \cos^2\alpha_w \, R_w^2 \, EA_w\right] \sin^2\varphi \; \chi_{s2} - \cos^3\alpha_w \left[-\frac{\nu}{1+\nu} \tan^2\alpha_w \, EI_w + R_w^2 \, EA_w\right] \sin\varphi \cos\varphi \, \chi_{s3}$$
$$M_{s3}^{sB} = -\cos^3\alpha_w \left[-\frac{\nu}{1+\nu} \tan^2\alpha_w \, EI_w + R_w^2 \, EA_w\right] \sin\varphi \cos\varphi \, \chi_{s2} + \cos\alpha_w \left[\left(\frac{\sin^2\alpha_w}{1+\nu} + \tan^2\varphi + \cos^2\alpha_w\right) EI_w + \cos^2\alpha_w \, R_w^2 \, EA_w\right] \cos^2\varphi \; \chi_{s3}$$

Afterwards, the relations between strand and rope strains (2.III.1) and (2.III.2) will be introduced in order to link the rope internal actions with the rope strain field. The relations are reported in the following and they are divided according to rope axial torsion and biaxial bending.

$$\eta_s^{AT}(x_1) = \cos^2\alpha_s \; \eta_R(x_1) + R_s \; \cos\alpha_s \sin\alpha_s \; \chi_{RT}(x_1)$$
$$\chi_{sT}^{AT}(x_1) = \cos^2\alpha_s \, \chi_{RT}(x_1)$$
$$\chi_{s2}^{AT}(x_1) = 0$$
$$\chi_{s3}^{AT}(x_1) = \cos\alpha_s \sin\alpha_s \, \chi_{RT}(x_1)$$

$$\eta_s^{B}(x_1) = \cos^2\alpha_s \, R_s \sin\vartheta(x_1) \; \chi_{R2}(x_1) - \cos^2\alpha_s \, R_s \cos\vartheta(x_1) \; \chi_{R3}(x_1)$$
$$\chi_{sT}^{B}(x_1) = -\cos\alpha_s \sin\alpha_s \sin\vartheta(x_1) \, \chi_{R2}(x_1) + \cos\alpha_s \sin\alpha_s \cos\vartheta(x_1) \, \chi_{R3}(x_1)$$
$$\chi_{s2}^{B}(x_1) = -\cos\alpha_s \cos\vartheta(x_1) \, \chi_{R2}(x_1) - \cos\alpha_s \sin\vartheta(x_1) \, \chi_{R3}(x_1)$$
$$\chi_{s3}^{B}(x_1) = \cos^2\alpha_s \sin\vartheta(x_1) \, \chi_{R2}(x_1) - \cos^2\alpha_s \cos\vartheta(x_1) \, \chi_{R3}(x_1)$$

The final output of the procedure will be the coefficients of the stiffness matrix, remembering that the entries are the single wire contributions to the global matrix.
The stiffness matrix is defined like in the paragraph III.2 of the present chapter. Let us recall the sub matrices forming the global matrix and superimpose them as the sum of the strand axial torsion and biaxial bending contribution, denoted with the superscripts "sAT" and "sB" respectively. Moreover, the superscripts "AT" and "B" refer to the rope axial torsional and biaxial bending.

$$(3.IV.4a) \quad \underline{\underline{K}}_R^{AT} = \begin{bmatrix} EA_R & C_{AT} \\ C_{TA} & GJ_R \\ C_{B2A} & C_{B2T} \\ C_{B3A} & C_{B3T} \end{bmatrix} = \begin{bmatrix} EA_R & C_{AT} \\ C_{TA} & GJ_R \\ C_{B2A} & C_{B2T} \\ C_{B3A} & C_{B3T} \end{bmatrix}^{sAT} + \begin{bmatrix} EA_R & C_{AT} \\ C_{TA} & GJ_R \\ C_{B2A} & C_{B2T} \\ C_{B3A} & C_{B3T} \end{bmatrix}^{sB}$$

$$(3.IV.4b) \quad \underline{\underline{K}}_R^B = \begin{bmatrix} C_{AB2} & C_{AB3} \\ C_{TB2} & C_{TB3} \\ EI_{R2} & C_{B23} \\ C_{B32} & EI_{R3} \end{bmatrix} = \begin{bmatrix} C_{AB2} & C_{AB3} \\ C_{TB2} & C_{TB3} \\ EI_{R2} & C_{B23} \\ C_{B32} & EI_{R3} \end{bmatrix}^{sAT} + \begin{bmatrix} C_{AB2} & C_{AB3} \\ C_{TB2} & C_{TB3} \\ EI_{R2} & C_{B23} \\ C_{B32} & EI_{R3} \end{bmatrix}^{sB}$$

3.1. AXIAL TORSION OF THE ROPE

Firstly, the procedure is developed for the case of axial torsional perturbation of the rope kinematic field. Hence, the strand experiences the following strain field according to (2.III.1). The superscript "AT" in the strand strains stands for "rope axial torsion contribution".

$$\eta_s^{AT}(x_1) = \cos^2\alpha_s \ \eta_R(x_1) + R_s \ \cos\alpha_s \sin\alpha_s \ \chi_{RT}(x_1)$$
$$\chi_{sT}^{AT}(x_1) = \cos^2\alpha_s \chi_{RT}(x_1)$$
$$\chi_{s2}^{AT}(x_1) = 0$$
$$\chi_{s3}^{AT}(x_1) = \cos\alpha_s \sin\alpha_s \chi_{RT}(x_1)$$

The rope response will be superimposed in the contribution of the axial torsion and the biaxial bending of the strand. This operation is performed introducing (2.III.1) respectively within (3.IV.3a) and (3.IV.3b). Afterwards, the last two set of relations are substituted inside (3.IV.1).

3.1.1. AXIAL TORSION OF THE STRAND CONTRIBUTION TO THE ROPE RESPONSE

Introducing inside the constitutive model of the single strand (3.IV.3a) the kinematic relations (2.III.1).

$$N_s^{sAT} = \cos^3\alpha_w EA_w \left[\cos^2\alpha_s \ \eta_R + R_s \ \cos\alpha_s \sin\alpha_s \ \chi_{RT}\right] + R_w \ \cos^3\alpha_w \tan\alpha_w EA_w \left[\cos^2\alpha_s \chi_{RT}\right]$$
$$= \cos^3\alpha_w \cos^2\alpha_s EA_w\eta_R + \cos^3\alpha_w \cos^2\alpha_s \left[R_s \ \tan\alpha_s + R_w \tan\alpha_w\right]EA_w \chi_{RT}$$

$$M_{sT}^{sAT} = R_w \cos^3\alpha_w \tan\alpha_w EA_w \left[\cos^2\alpha_s \ \eta_R + R_s \ \cos\alpha_s \sin\alpha_s \ \chi_{RT}\right] + \cos^3\alpha_w \left[\left(\frac{1}{1+\nu} + \tan^2\alpha_w\right) EI_w + R_w^2 \ \tan^2\alpha_w EA_w\right] \left[\cos^2\alpha_s \chi_{RT}\right]$$
$$= \cos^3\alpha_w \cos^2\alpha_s R_w \tan\alpha_w EA_w \eta_R$$
$$+ \cos^3\alpha_w \cos^2\alpha_s \left[\left(\frac{1}{1+\nu} + \tan^2\alpha_w\right) EI_w + (R_w^2 \ \tan^2\alpha_w + R_w R_s \tan\alpha_w \tan\alpha_s)EA_w\right] \chi_{RT}$$

$$M_{s2}^{sAT} = R_w \cos^3\alpha_w \sin\varphi EA_w \left[\cos^2\alpha_s \ \eta_R + R_s \ \cos\alpha_s \sin\alpha_s \ \chi_{RT}\right] + \cos^3\alpha_w \tan\alpha_w \sin\varphi \left[\frac{\nu}{1+\nu} EI_w + R_w^2 \ EA_w\right] \left[\cos^2\alpha_s \chi_{RT}\right]$$
$$= \cos^3\alpha_w \cos^2\alpha_s R_w \sin\varphi EA_w\eta_R + \cos^3\alpha_w \cos^2\alpha_s \left[\tan\alpha_w \frac{\nu}{1+\nu} EI_w + (R_w^2 \tan\alpha_w + R_w R_s \tan\alpha_s)EA_w\right] \sin\varphi \chi_{RT}$$

$$M_{s3}^{sAT} = -R_w \cos^3\alpha_w \cos\varphi EA_w \left[\cos^2\alpha_s \ \eta_R + R_s \ \cos\alpha_s \sin\alpha_s \ \chi_{RT}\right] - \cos^3\alpha_w \tan\alpha_w \cos\varphi \left[\frac{\nu}{1+\nu} EI_w + R_w^2 \ EA_w\right] \left[\cos^2\alpha_s \chi_{RT}\right]$$
$$= -\cos^3\alpha_w \cos^2\alpha_s R_w \cos\varphi EA_w \eta_R - \cos^3\alpha_w \cos^2\alpha_s \left[\tan\alpha_w \frac{\nu}{1+\nu} EI_w + (R_w^2 \tan\alpha_w + R_w R_s \tan\alpha_s)EA_w\right] \cos\varphi \chi_{RT}$$

Substituting inside the internal actions within the rope cross section (3.IV.1)

$$N_R^{sAT} = \cos\alpha_s \ \{\cos^3\alpha_w \cos^2\alpha_s EA_w\eta_R + \cos^3\alpha_w \cos^2\alpha_s \left[R_s \ \tan\alpha_s + R_w \tan\alpha_w\right]EA_w \chi_{RT}\}$$

$$M_{RT}^{sAT} = \cos\alpha_s \left\{\cos^3\alpha_w \cos^2\alpha_s R_w \tan\alpha_w EA_w \eta_R + \cos^3\alpha_w \cos^2\alpha_s \left[\left(\frac{1}{1+\nu} + \tan^2\alpha_w\right) EI_w + (R_w^2 \ \tan^2\alpha_w + R_w R_s \tan\alpha_w \tan\alpha_s)EA_w\right] \chi_{RT}\right\}$$
$$+ \sin\alpha_s \left\{-\cos^3\alpha_w \cos^2\alpha_s R_w \cos\varphi EA_w \eta_R \right.$$
$$\left. - \cos^3\alpha_w \cos^2\alpha_s \left[\tan\alpha_w \frac{\nu}{1+\nu} EI_w + (R_w^2 \tan\alpha_w + R_w R_s \tan\alpha_s)EA_w\right] \cos\varphi \chi_{RT}\right\}$$
$$+ R_s \ \sin\alpha_s \ \{\cos^3\alpha_w \cos^2\alpha_s EA_w\eta_R + \cos^3\alpha_w \cos^2\alpha_s \left[R_s \ \tan\alpha_s + R_w \tan\alpha_w\right]EA_w \chi_{RT}\}$$

$$
\begin{aligned}
M_{R2}^{sAT} = &-\sin\alpha_s \sin\vartheta \Big\{\cos^3\alpha_w \cos^2\alpha_s R_w \tan\alpha_w EA_w \eta_R \\
&+ \cos^3\alpha_w \cos^2\alpha_s \Big[\Big(\frac{1}{1+\nu} + \tan^2\alpha_w\Big) EI_w + (R_w^2 \tan^2\alpha_w + R_w R_s \tan\alpha_w \tan\alpha_s) EA_w\Big] \chi_{RT}\Big\} \\
&- \cos\vartheta \Big\{\cos^3\alpha_w \cos^2\alpha_s R_w \sin\varphi EA_w \eta_R \\
&+ \cos^3\alpha_w \cos^2\alpha_s \Big[\tan\alpha_w \frac{\nu}{1+\nu} EI_w + (R_w^2 \tan\alpha_w + R_w R_s \tan\alpha_s) EA_w\Big] \sin\varphi \chi_{RT}\Big\} \\
&+ \cos\alpha_s \sin\vartheta \Big\{-\cos^3\alpha_w \cos^2\alpha_s R_w \cos\varphi EA_w \eta_R \\
&- \cos^3\alpha_w \cos^2\alpha_s \Big[\tan\alpha_w \frac{\nu}{1+\nu} EI_w + (R_w^2 \tan\alpha_w + R_w R_s \tan\alpha_s) EA_w\Big] \cos\varphi \chi_{RT}\Big\} \\
&+ R_s \cos\alpha_s \sin\vartheta \{\cos^3\alpha_w \cos^2\alpha_s EA_w \eta_R + \cos^3\alpha_w \cos^2\alpha_s [R_s \tan\alpha_s + R_w \tan\alpha_w] EA_w \chi_{RT}\}
\end{aligned}
$$

$$
\begin{aligned}
M_{R3}^{sAT} = &\sin\alpha_s \cos\vartheta \Big\{\cos^3\alpha_w \cos^2\alpha_s R_w \tan\alpha_w EA_w \eta_R \\
&+ \cos^3\alpha_w \cos^2\alpha_s \Big[\Big(\frac{1}{1+\nu} + \tan^2\alpha_w\Big) EI_w + (R_w^2 \tan^2\alpha_w + R_w R_s \tan\alpha_w \tan\alpha_s) EA_w\Big] \chi_{RT}\Big\} \\
&- \sin\vartheta \Big\{\cos^3\alpha_w \cos^2\alpha_s R_w \sin\varphi EA_w \eta_R \\
&+ \cos^3\alpha_w \cos^2\alpha_s \Big[\tan\alpha_w \frac{\nu}{1+\nu} EI_w + (R_w^2 \tan\alpha_w + R_w R_s \tan\alpha_s) EA_w\Big] \sin\varphi \chi_{RT}\Big\} \\
&- \cos\alpha_s \cos\vartheta \Big\{-\cos^3\alpha_w \cos^2\alpha_s R_w \cos\varphi EA_w \eta_R \\
&- \cos^3\alpha_w \cos^2\alpha_s \Big[\tan\alpha_w \frac{\nu}{1+\nu} EI_w + (R_w^2 \tan\alpha_w + R_w R_s \tan\alpha_s) EA_w\Big] \cos\varphi \chi_{RT}\Big\} \\
&- R_s \cos\alpha_s \cos\vartheta \{\cos^3\alpha_w \cos^2\alpha_s EA_w \eta_R + \cos^3\alpha_w \cos^2\alpha_s [R_s \tan\alpha_s + R_w \tan\alpha_w] EA_w \chi_{RT}\}
\end{aligned}
$$

Let us collect the common terms, then the result is as follows.

$$
\begin{aligned}
\boldsymbol{N_R^{sAT}} &= \boldsymbol{\cos^3\alpha_w \cos^3\alpha_s EA_w \eta_R + \cos^3\alpha_w \cos^3\alpha_s [R_s \tan\alpha_s + R_w \tan\alpha_w] EA_w \chi_{RT}} \\
(3.IV.5a)\quad \boldsymbol{M_{RT}^{sAT}} &= \boldsymbol{\cos^3\alpha_w \cos^3\alpha_s [R_s \tan\alpha_s + R_w \tan\alpha_w - R_w \tan\alpha_s \cos\varphi] EA_w \eta_R} \\
&\quad + \boldsymbol{\cos^3\alpha_w \cos^3\alpha_s \Big[\Big(\frac{1}{1+\nu} + \tan^2\alpha_w\Big) EI_w + (R_s \tan\alpha_s + R_w \tan\alpha_w)^2 EA_w} \\
&\quad - \boldsymbol{\Big(\tan\alpha_w \tan\alpha_s \frac{\nu}{1+\nu} EI_w + (R_w^2 \tan\alpha_w \tan\alpha_s + R_w R_s \tan^2\alpha_s) EA_w\Big) \cos\varphi\Big] \chi_{RT}} \\
\boldsymbol{M_{R2}^{sAT}} &= \boldsymbol{-\cos^3\alpha_w \cos^3\alpha_s \Big[R_w \tan\alpha_w \tan\alpha_s - R_s + R_w \Big(\frac{\cot\vartheta \sin\varphi}{\cos\alpha_s} + \cos\varphi\Big)\Big] \sin\vartheta EA_w \eta_R} \\
&\quad - \boldsymbol{\cos^3\alpha_w \cos^2\alpha_s \Big\{\Big[\Big(\frac{1}{1+\nu} + \tan^2\alpha_w\Big) EI_w + (R_w^2 \tan^2\alpha_w + R_w R_s \tan\alpha_w \tan\alpha_s) EA_w\Big] \sin\alpha_s} \\
&\quad + \boldsymbol{\Big[\tan\alpha_w \frac{\nu}{1+\nu} EI_w + (R_w^2 \tan\alpha_w + R_w R_s \tan\alpha_s) EA_w\Big] (\cot\vartheta \sin\varphi + \cos\alpha_s \cos\varphi)} \\
&\quad - \boldsymbol{R_s \cos\alpha_s [R_s \tan\alpha_s + R_w \tan\alpha_w] EA_w\Big\} \sin\vartheta \chi_{RT}} \\
\boldsymbol{M_{R3}^{sAT}} &= \boldsymbol{\cos^3\alpha_w \cos^3\alpha_s \Big[R_w \tan\alpha_w \tan\alpha_s - R_s + R_w \Big(-\frac{\tan\vartheta \sin\varphi}{\cos\alpha_s} + \cos\varphi\Big)\Big] \cos\vartheta EA_w \eta_R} \\
&\quad + \boldsymbol{\cos^3\alpha_w \cos^2\alpha_s \Big\{\Big[\Big(\frac{1}{1+\nu} + \tan^2\alpha_w\Big) EI_w + (R_w^2 \tan^2\alpha_w + R_w R_s \tan\alpha_w \tan\alpha_s) EA_w\Big] \sin\alpha_s} \\
&\quad + \boldsymbol{\Big[\tan\alpha_w \frac{\nu}{1+\nu} EI_w + (R_w^2 \tan\alpha_w + R_w R_s \tan\alpha_s) EA_w\Big] (-\tan\vartheta \sin\varphi + \cos\alpha_s \cos\varphi)} \\
&\quad - \boldsymbol{R_s \cos\alpha_s [R_s \tan\alpha_s + R_w \tan\alpha_w] EA_w\Big\} \cos\vartheta \chi_{RT}}
\end{aligned}
$$

The stiffness coefficients may be written as follows.

$$
\begin{aligned}
(3.IV.5b)\quad \boldsymbol{EA_R^{sAT}} &= \boldsymbol{\cos^3\alpha_w \cos^3\alpha_s EA_w} \\
(3.IV.5c)\quad \boldsymbol{C_{AT}^{sAT}} &= \boldsymbol{\cos^3\alpha_w \cos^3\alpha_s [R_s \tan\alpha_s + R_w \tan\alpha_w] EA_w} \\
(3.IV.5d)\quad \boldsymbol{C_{TA}^{sAT}} &= \boldsymbol{\cos^3\alpha_w \cos^3\alpha_s [R_s \tan\alpha_s + R_w \tan\alpha_w - R_w \tan\alpha_s \cos\varphi] EA_w} \\
(3.IV.5e)\quad \boldsymbol{GJ_R^{sAT}} &= \boldsymbol{\cos^3\alpha_w \cos^3\alpha_s \Big[\Big(\frac{1}{1+\nu} + \tan^2\alpha_w\Big) EI_w + (R_s \tan\alpha_s + R_w \tan\alpha_w)^2 EA_w} \\
&\quad - \boldsymbol{\Big(\tan\alpha_w \tan\alpha_s \frac{\nu}{1+\nu} EI_w + (R_w^2 \tan\alpha_w \tan\alpha_s + R_w R_s \tan^2\alpha_s) EA_w\Big) \cos\varphi\Big]}
\end{aligned}
$$

$$(3.IV.5f)\quad C_{B2A}^{sAT} = -\cos^3\alpha_w \cos^3\alpha_s \left[R_w \tan\alpha_w \tan\alpha_s - R_s + R_w\left(\frac{\cot\vartheta \sin\varphi}{\cos\alpha_s} + \cos\varphi\right)\right] \sin\vartheta\, EA_w$$

$$(3.IV.5g)\quad C_{B2T}^{sAT} = -\cos^3\alpha_w \cos^3\alpha_s \left\{\left[\left(\frac{1}{1+\nu} + \tan^2\alpha_w\right) EI_w + (R_w^2 \tan^2\alpha_w + R_w R_s \tan\alpha_w \tan\alpha_s) EA_w\right] \tan\alpha_s \right.$$
$$+ \left[\tan\alpha_w \frac{\nu}{1+\nu} EI_w + (R_w^2 \tan\alpha_w + R_w R_s \tan\alpha_s) EA_w\right] (\cot\vartheta \sin\varphi + \cos\alpha_s \cos\varphi)$$
$$\left. - R_s \cos\alpha_s [R_s \tan\alpha_s + R_w \tan\alpha_w] EA_w\right\} \sin\vartheta$$

$$(3.IV.5h)\quad C_{B3A}^{sAT} = \cos^3\alpha_w \cos^3\alpha_s \left[R_w \tan\alpha_w \tan\alpha_s - R_s + R_w\left(-\frac{\tan\vartheta \sin\varphi}{\cos\alpha_s} + \cos\varphi\right)\right] \cos\vartheta\, EA_w$$

$$(3.IV.5g)\quad C_{B3T}^{sAT} = \cos^3\alpha_w \cos^2\alpha_s \left\{\left[\left(\frac{1}{1+\nu} + \tan^2\alpha_w\right) EI_w + (R_w^2 \tan^2\alpha_w + R_w R_s \tan\alpha_w \tan\alpha_s) EA_w\right] \sin\alpha_s \right.$$
$$+ \left[\tan\alpha_w \frac{\nu}{1+\nu} EI_w + (R_w^2 \tan\alpha_w + R_w R_s \tan\alpha_s) EA_w\right] (-\tan\vartheta \sin\varphi + \cos\alpha_s \cos\varphi)$$
$$\left. - R_s \cos\alpha_s [R_s \tan\alpha_s + R_w \tan\alpha_w] EA_w\right\} \cos\vartheta$$

A remark must be done on the axial torsion coupling coefficients (3.IV.5c) and (3.IV.5c). As a matter of fact, they seem to be non-symmetric from (3.IV.4a), hence violating the Reciprocity Theorem. Actually, the non-symmetry has been fictitiously introduced by the separation of the strand axial torsion and bending contributions. In fact, in the following paragraph it is possible to find the term missing inside N^{sAT}_R.
An additional remark concerns the terms containing functions like sinϕ, sinθ not at the second power. These functions hold when the single wire is investigated, still they drop when summed over the rope cross section due to symmetry.

Let us compare the axial stiffness (3.IV.5b), the coupling axial torsion coefficient (3.IV.5d) and the torsional stiffness (3.IV.5e) for the direct and recursive model. The direct model is written for the real arch length geometry only.
The first quantity inspected is the axial stiffness.

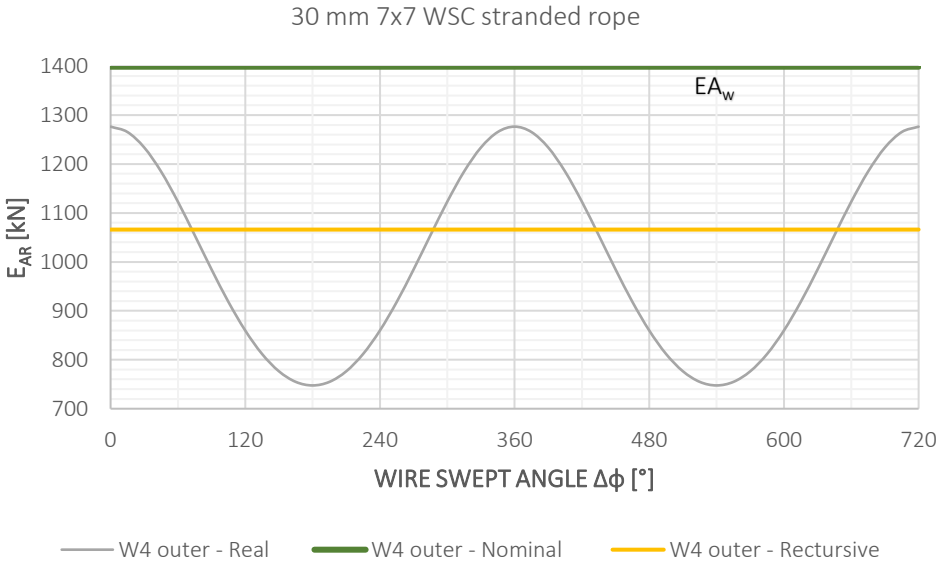

Fig 3.63 Single Wire Contribution to Wire Rope Axial Stiffness

It can be clearly appreciated the constant trend of the axial stiffness for the recursive model. A table comparing maximum, minimum and mean values is reported in the following.

Table 3.17 Single Wire Contribution to Wire Rope Axial Stiffness

E_{AR} [kN]	max	min	mean
direct	1276	748	1012
recursive	1066	1066	1066
error	-16.48%	42.60%	5.34%

The difference between the maximum value of the direct model and the value of the recursive model is of the order of 16.5%, while it is up to 42.6% between the minimum value of the direct model and the value of the recursive model. This huge difference is not relevant since this quantity does not affect neither the global response of the rope that depends on the mean value only nor the local response of the wire that depends upon the wire axial strain only, i.e. the rope kinematics. Conversely, the mean value is responsible of the global response of the rope, but it can be appreciated that the difference between the two formulations is bounded within 5%.

In the following plot, it is possible to see the differences between the coupling axial torsion coefficient with the two formulations. For the recursive model, the total value of the function is indicated with "recursive" only, while its mean value, corresponding to the quantity (3.IV.5c) is reported separately with the name "recursive sAT". The name "real" stands always for real arch length in the directs model.

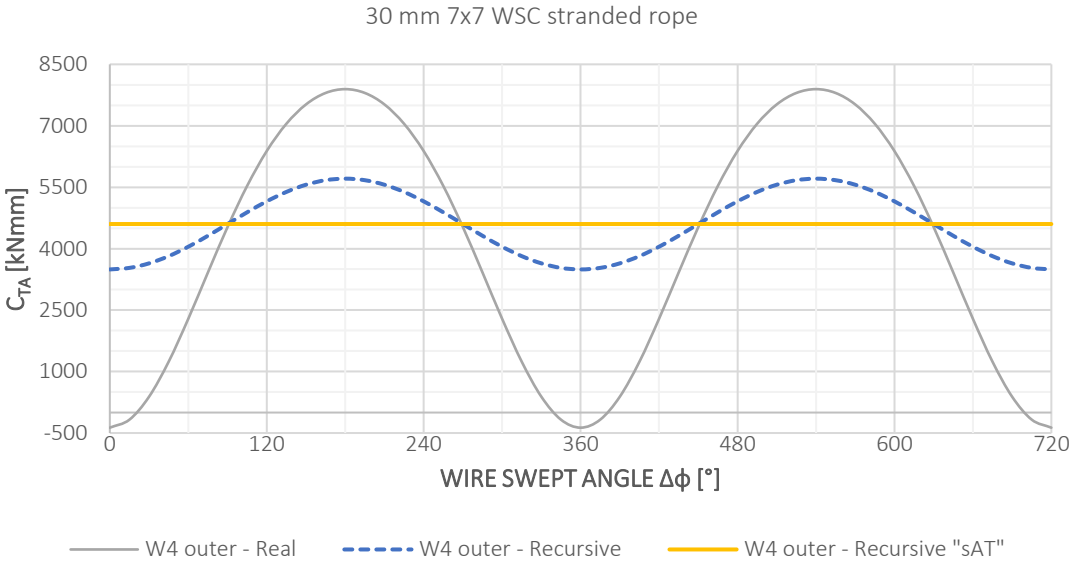

Fig 3.64 Single Wire Contribution to Wire Rope Axial Torsion Coupling Coefficient

It can be appreciated that the two functions as the same trend, still the recursive model has a higher mean value and it's smoother.

Table 3.18 Single Wire Contribution to Wire Rope Axial Torsion Coupling Coefficient

C_{TA} [kNmm]	max	min	mean
direct	7894	-369	3763
recursive	5710	3493	4602
error	-27.7%	-1048%	22.30%

Let us focus on the mean value only. It is clear, that the difference is not negligible. Hence, the global response will be significantly influenced by the choice of the model. Since, in the axial stiffness the error was not that high it can be imagined that the greater difference is in the modelling of torsion.

Finally, let us analyze the torsional stiffness. It must be underline that this is the contribution due to axial torsion of the strand only. In the following paragraph, it will be completed with the missing contribution due to biaxial bending of the strand. In the expression

(3.IV.5e) it is possible to identify a constant contribution that will be the mean value of the plotted function and an oscillatory contribution due to the function cos(ϕ). The first is indicated as "Rec.sAT.Mean", while the sum of the two contribution is "Rec.sAT.tot" in the following plot.

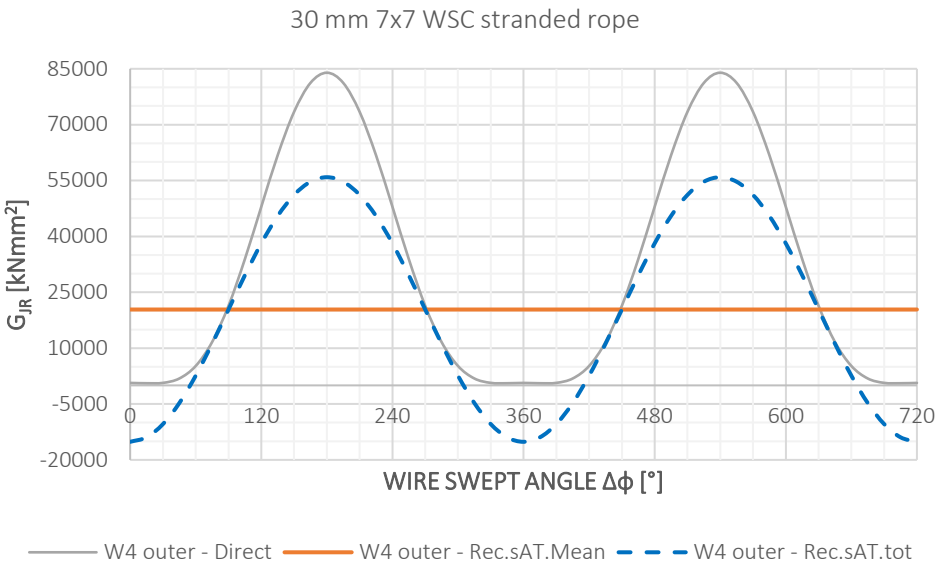

Fig 3.65 Single Wire Contribution to Wire Rope Torsional Stiffness – Strand Axial Torsion Contribution

In the table below, it is possible to see the difference between maximum, minimum and mean value of the two formulations.

Table 3.19 Single Wire Contribution to Wire Rope Torsional Stiffness– Strand Axial Torsion Contribution

GJ_R [kNmm²]	max	min	mean
direct	83941	576	42258
recursive	55890	-15151	20370
error	50%	-104%	107%

The mean value of the recursive formulation is almost half of the one from the direct model, hence the torsional response is significantly affected by the choice between the two.
A very important remark needs to be done so far. It can be clearly appreciated by the previous plot how the two models differ in terms of sign. As a matter of fact, the direct model has a torsional stiffness that is positive in every point of the wire centerline, while the recursive model shows also a negative trend. From the thermodynamic view point this last statement would appear inconsistent. Actually, two considerations have to be introduced: firstly, the torsional stiffness under investigation is the single wire contribution only to the global response of the rope, thus from a mechanical vantage point this quantity does not represent the global torsional stiffness; furthermore, the mean value of this function is strictly positive, hence when the global response is investigated through an integration over the cross section the torsional stiffness will be strictly positive.

3.1.2. BIAXIAL BENDING OF THE STRAND CONTRIBUTION TO THE ROPE RESPONSE

Introducing inside the constitutive model of the single strand (3.IV.3b) the kinematic relations (2.III.1).

$$N_s^{sB} = \cos^3\alpha_w\, R_w \sin\varphi\, EA_w\, [0] - \cos^3\alpha_w\, R_w \cos\varphi\, EA_w\, [\cos\alpha_s \sin\alpha_s\, \chi_{RT}] = -\cos^3\alpha_w \cos^2\alpha_s\, R_w \tan\alpha_s \cos\varphi\, EA_w\, \chi_{RT}$$

$$M_{sT}^{sB} = \cos^3\alpha_w \tan\alpha_w \sin\varphi \left[\frac{\nu}{1+\nu} EI_w + R_w^2\, EA_w\right][0] - \cos^3\alpha_w \tan\alpha_w \cos\varphi \left[\frac{\nu}{1+\nu} EI_w + R_w^2\, EA_w\right][\cos\alpha_s \sin\alpha_s\, \chi_{RT}]$$

$$= -\cos^3\alpha_w \cos^2\alpha_s \tan\alpha_w \tan\alpha_s \left[\frac{\nu}{1+\nu} EI_w + R_w^2\, EA_w\right] \cos\varphi\, \chi_{RT}$$

$$M_{s2}^{sB} = \cos\alpha_w \left[\left(\frac{\sin^2\alpha_w}{1+\nu} + \cot^2\varphi + \cos^2\alpha_w\right) EI_w + \cos^2\alpha_w\, R_w^2\, EA_w\right] \sin^2\varphi \;\; [0]$$

$$- \cos^3\alpha_w \left[-\frac{\nu}{1+\nu}\tan^2\alpha_w\, EI_w + R_w^2\, EA_w\right] \sin\varphi\cos\varphi \;\; [\cos\alpha_s \sin\alpha_s\, \chi_{RT}]$$

$$= -\cos^3\alpha_w \cos^2\alpha_s \tan\alpha_s \left[-\frac{\nu}{1+\nu}\tan^2\alpha_w\, EI_w + R_w^2\, EA_w\right] \sin\varphi\cos\varphi\, \chi_{RT}$$

$$M_{s3}^{sB} = -\cos^3\alpha_w \left[-\frac{\nu}{1+\nu}\tan^2\alpha_w\, EI_w + R_w^2\, EA_w\right] \sin\varphi\cos\varphi \;\; [0]$$

$$+ \cos\alpha_w \left[\left(\frac{\sin^2\alpha_w}{1+\nu} + \tan^2\varphi + \cos^2\alpha_w\right) EI_w + \cos^2\alpha_w\, R_w^2\, EA_w\right] \cos^2\varphi \;\; [\cos\alpha_s \sin\alpha_s\, \chi_{RT}]$$

$$= \cos^3\alpha_w \cos^2\alpha_s \tan\alpha_s \left[\left(\frac{\tan^2\alpha_w}{1+\nu} + \frac{\tan^2\varphi}{\cos^2\alpha_w} + 1\right) EI_w + R_w^2\, EA_w\right] \cos^2\varphi\, \chi_{RT}$$

Substituting inside the internal actions within the rope cross section (3.IV.1)

$$N_R^{sB} = \cos\alpha_s \; \{-\cos^3\alpha_w \cos^2\alpha_s\, R_w \tan\alpha_s \cos\varphi\, EA_w\, \chi_{RT}\}$$

$$M_{RT}^{sB} = \cos\alpha_s \left\{-\cos^3\alpha_w \cos^2\alpha_s \tan\alpha_w \tan\alpha_s \left[\frac{\nu}{1+\nu} EI_w + R_w^2\, EA_w\right] \cos\varphi\, \chi_{RT}\right\}$$

$$+ \sin\alpha_s \left\{\cos^3\alpha_w \cos^2\alpha_s \tan\alpha_s \left[\left(\frac{\tan^2\alpha_w}{1+\nu} + \frac{\tan^2\varphi}{\cos^2\alpha_w} + 1\right) EI_w + R_w^2\, EA_w\right] \cos^2\varphi\, \chi_{RT}\right\}$$

$$+ R_s \; \sin\alpha_s \; \{-\cos^3\alpha_w \cos^2\alpha_s\, R_w \tan\alpha_s \cos\varphi\, EA_w\, \chi_{RT}\}$$

$$M_{R2}^{sB} = -\sin\alpha_s \sin\vartheta \left\{-\cos^3\alpha_w \cos^2\alpha_s \tan\alpha_w \tan\alpha_s \left[\frac{\nu}{1+\nu} EI_w + R_w^2\, EA_w\right] \cos\varphi\, \chi_{RT}\right\}$$

$$- \cos\vartheta \left\{-\cos^3\alpha_w \cos^2\alpha_s \tan\alpha_s \left[-\frac{\nu}{1+\nu}\tan^2\alpha_w\, EI_w + R_w^2\, EA_w\right] \sin\varphi\cos\varphi\, \chi_{RT}\right\}$$

$$+ \cos\alpha_s \sin\vartheta \left\{\cos^3\alpha_w \cos^2\alpha_s \tan\alpha_s \left[\left(\frac{\tan^2\alpha_w}{1+\nu} + \frac{\tan^2\varphi}{\cos^2\alpha_w} + 1\right) EI_w + R_w^2\, EA_w\right] \cos^2\varphi\, \chi_{RT}\right\}$$

$$+ R_s \cos\alpha_s \sin\vartheta \; \{-\cos^3\alpha_w \cos^2\alpha_s\, R_w \tan\alpha_s \cos\varphi\, EA_w\, \chi_{RT}\}$$

$$M_{R3}^{sB} = \sin\alpha_s \cos\vartheta \left\{-\cos^3\alpha_w \cos^2\alpha_s \tan\alpha_w \tan\alpha_s \left[\frac{\nu}{1+\nu} EI_w + R_w^2\, EA_w\right] \cos\varphi\, \chi_{RT}\right\}$$

$$- \sin\vartheta \left\{-\cos^3\alpha_w \cos^2\alpha_s \tan\alpha_s \left[-\frac{\nu}{1+\nu}\tan^2\alpha_w\, EI_w + R_w^2\, EA_w\right] \sin\varphi\cos\varphi\, \chi_{RT}\right\}$$

$$- \cos\alpha_s \cos\vartheta \left\{\cos^3\alpha_w \cos^2\alpha_s \tan\alpha_s \left[\left(\frac{\tan^2\alpha_w}{1+\nu} + \frac{\tan^2\varphi}{\cos^2\alpha_w} + 1\right) EI_w + R_w^2\, EA_w\right] \cos^2\varphi\, \chi_{RT}\right\}$$

$$- R_s \cos\alpha_s \cos\vartheta \; \{-\cos^3\alpha_w \cos^2\alpha_s\, R_w \tan\alpha_s \cos\varphi\, EA_w\, \chi_{RT}\}$$

Let us collect the common terms, then the result is as follows.

$$\boldsymbol{N_R^{sB} = -\cos^3\alpha_w \cos^3\alpha_s\, R_w \tan\alpha_s \cos\varphi\, EA_w\, \chi_{RT}}$$

$$(3.IV.6a) \quad \boldsymbol{M_{RT}^{sB} = \cos^3\alpha_w \cos^3\alpha_s \left\{-\tan\alpha_w \tan\alpha_s \left[\frac{\nu}{1+\nu} EI_w + R_w^2\, EA_w\right] \cos\varphi\right.}$$

$$\boldsymbol{\left. + \tan^2\alpha_s \left[\left(\frac{\tan^2\alpha_w}{1+\nu} + \frac{\tan^2\varphi}{\cos^2\alpha_w} + 1\right) EI_w + R_w^2\, EA_w\right] \cos^2\varphi - R_w R_s \tan^2\alpha_s \cos\varphi\, EA_w\right\} \chi_{RT}}$$

$$\boldsymbol{M_{R2}^{sB} = \cos^3\alpha_w \cos^3\alpha_s \left\{-\tan\alpha_w \tan^2\alpha_s \left[\frac{\nu}{1+\nu} EI_w + R_w^2\, EA_w\right] \sin\vartheta\cos\varphi\right.}$$

$$\boldsymbol{+ \frac{\tan\alpha_s}{\cos\alpha_s}\left[-\frac{\nu}{1+\nu}\tan^2\alpha_w\, EI_w + R_w^2\, EA_w\right] \cos\vartheta \sin\varphi\cos\varphi}$$

$$\boldsymbol{\left. + \tan\alpha_s \left[\left(\frac{\tan^2\alpha_w}{1+\nu} + \frac{\tan^2\varphi}{\cos^2\alpha_w} + 1\right) EI_w + R_w^2\, EA_w\right] \sin\vartheta\cos^2\varphi - R_s R_w \tan\alpha_s \sin\vartheta\cos\varphi\, EA_w\right\} \chi_{RT}}$$

$$\boldsymbol{M_{R3}^{sB} = \cos^3\alpha_w \cos^3\alpha_s \left\{-\tan\alpha_w \tan^2\alpha_s \left[\frac{\nu}{1+\nu} EI_w + R_w^2\, EA_w\right] \cos\vartheta\cos\varphi\right.}$$

$$\boldsymbol{+ \frac{\tan\alpha_s}{\cos\alpha_s}\left[-\frac{\nu}{1+\nu}\tan^2\alpha_w\, EI_w + R_w^2\, EA_w\right] \sin\vartheta \sin\varphi\cos\varphi}$$

$$\boldsymbol{\left. - \tan\alpha_s \left[\left(\frac{\tan^2\alpha_w}{1+\nu} + \frac{\tan^2\varphi}{\cos^2\alpha_w} + 1\right) EI_w + R_w^2\, EA_w\right] \cos\vartheta\cos^2\varphi + R_s R_w \tan\alpha_s \cos\vartheta\cos\varphi\, EA_w\right\} \chi_{RT}}$$

The stiffness coefficients may be written as follows.

$$(3.IV.6b)\quad EA_R^{sB} = 0$$

$$(3.IV.6c)\quad C_{AT}^{sB} = -\cos^3\alpha_w \cos^3\alpha_s R_w \tan\alpha_s \cos\varphi\, EA_w$$

$$(3.IV.6d)\quad C_{TA}^{sB} = 0$$

$$(3.IV.6e)\quad GJ_R^{sB} = \cos^3\alpha_w \cos^3\alpha_s \left\{-\left[\tan\alpha_w \tan\alpha_s \frac{\nu}{1+\nu} EI_w + (R_w^2 \tan\alpha_w \tan\alpha_s + R_w R_s \tan^2\alpha_s) EA_w\right]\cos\varphi \right.$$
$$\left. + \tan^2\alpha_s \left[\left(\frac{\tan^2\alpha_w}{1+\nu} + \frac{\tan^2\varphi}{\cos^2\alpha_w} + 1\right) EI_w + R_w^2\, EA_w\right]\cos^2\varphi\right\}$$

$$(3.IV.6f)\quad C_{B2A}^{sB} = 0$$

$$(3.IV.6g)\quad C_{B2T}^{sB} = \cos^3\alpha_w \cos^3\alpha_s \left\{-\tan\alpha_w \tan^2\alpha_s \left[\frac{\nu}{1+\nu} EI_w + R_w^2\, EA_w\right]\sin\vartheta\cos\varphi \right.$$
$$+ \frac{\tan\alpha_s}{\cos\alpha_s}\left[-\frac{\nu}{1+\nu}\tan^2\alpha_w\, EI_w + R_w^2\, EA_w\right]\cos\vartheta\sin\varphi\cos\varphi$$
$$\left. + \tan\alpha_s \left[\left(\frac{\tan^2\alpha_w}{1+\nu} + \frac{\tan^2\varphi}{\cos^2\alpha_w} + 1\right) EI_w + R_w^2\, EA_w\right]\sin\vartheta\cos^2\varphi - R_s R_w \tan\alpha_s \sin\vartheta\cos\varphi\, EA_w\right\}$$

$$(3.IV.6h)\quad C_{B3A}^{sB} = 0$$

$$(3.IV.6g)\quad C_{B3T}^{sB} = \cos^3\alpha_w \cos^3\alpha_s \left\{-\tan\alpha_w \tan^2\alpha_s \left[\frac{\nu}{1+\nu} EI_w + R_w^2\, EA_w\right]\cos\vartheta\cos\varphi \right.$$
$$+ \frac{\tan\alpha_s}{\cos\alpha_s}\left[-\frac{\nu}{1+\nu}\tan^2\alpha_w\, EI_w + R_w^2\, EA_w\right]\sin\vartheta\sin\varphi\cos\varphi$$
$$\left. - \tan\alpha_s \left[\left(\frac{\tan^2\alpha_w}{1+\nu} + \frac{\tan^2\varphi}{\cos^2\alpha_w} + 1\right) EI_w + R_w^2\, EA_w\right]\cos\vartheta\cos^2\varphi + R_s R_w \tan\alpha_s \cos\vartheta\cos\varphi\, EA_w\right\}$$

It is possible to notice that the contribution $N^{sB}{}_R$ restores the symmetry to the stiffness matrix when it is summed to $N^{sAT}{}_R$ as it was explained in the previous paragraph.

Let us show the trend of the torsional stiffness (3.IV.6e). Two contributions are distinguished: the oscillatory term that is equal to the term arised in (3.IV.5e), and the term depending on $\cos^2(\phi)$ that is still oscillatory, but always strictly positive. The two contribution are denoted respectively as "Rec.sB.Osc" and "Rec.sB.Pos", while their sum is "Rec.sB".

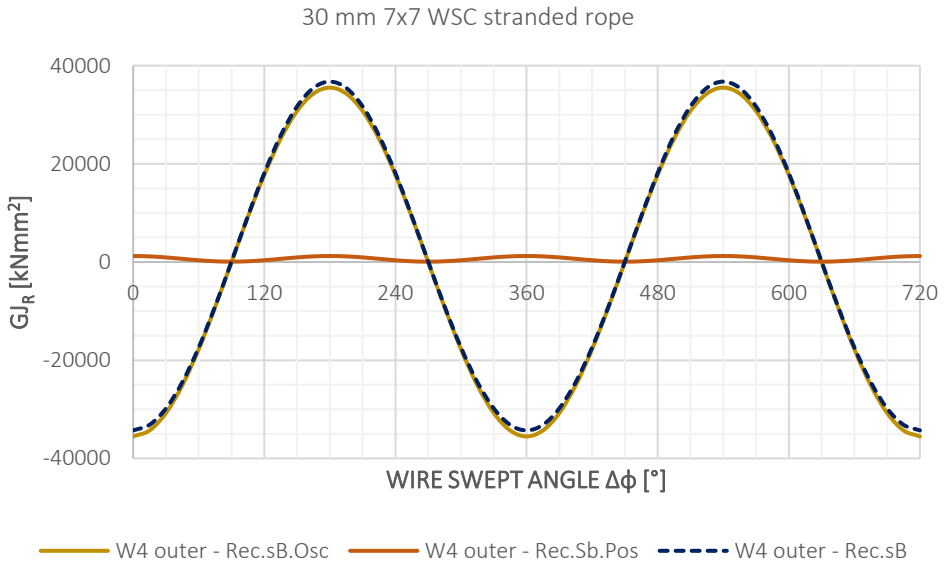

Fig 3.66 Single Wire Contribution to Wire Rope Torsional Stiffness – Strand Bending Contribution and Total Value

From the table below, it can be appreciated the significant numerical difference between the two contributions. Since, the positive contribution is very low with respect to the other.

Table 3.20 Single Wire Contribution to Wire Rope Torsional Stiffness – Strand Bending Contribution

GJ_R [kNmm^2]	max	min	mean
sB.Osc	35520	-35520	0
sB.Pos	1223	75	649

In the last plot, it will be showed the comparison between the direct model and the recursive one, including all the contributions, i.e. the axial torsion and bending of the strand. Furthermore, in order to underline which part of the recursive torsional stiffness will weight in the global response, an ulterior function has been introduced: the recursive coefficient without the oscillatory contributions. The three functions are indicated respectively as "Direct", "Recursive" and "Rec.No.Oscil".

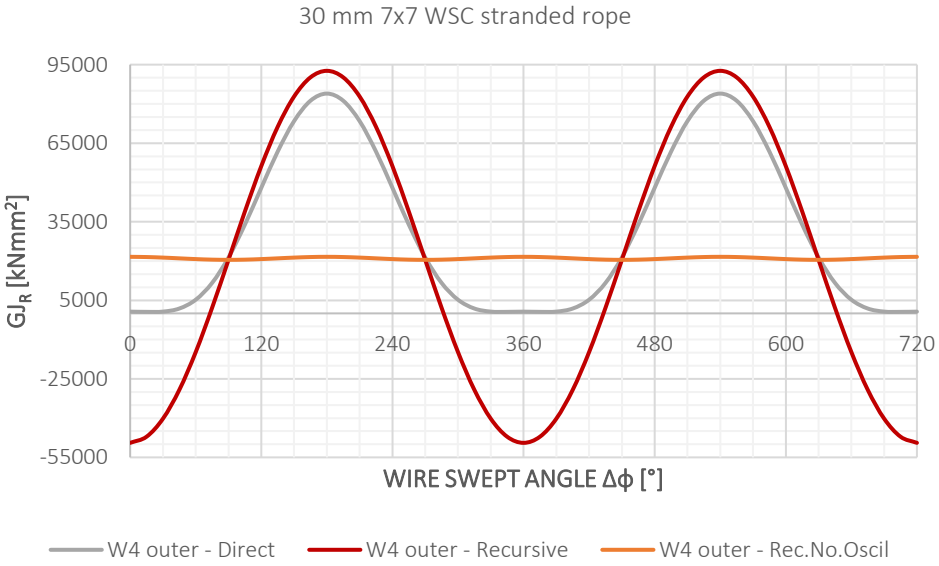

Fig 3.67 Single Wire Contribution to Wire Rope Torsional Stiffness –Total Value

The mean value of the recursive torsional stiffness is only slightly different with respect to the one showed for (3.IV.5e).

3.2. BIAXIAL BENDNG OF THE ROPE

The procedure is developed for the case of biaxial bending perturbation of the rope kinematic field. Hence, the strand experiences the following strain field according to (2.III.2). The superscript "B" in the strand strains stands for "rope bending contribution".

$$\eta_s^B(x_1) = \cos^2\alpha_s\, R_s \sin\vartheta(x_1)\ \chi_{R2}(x_1) - \cos^2\alpha_s\, R_s \cos\vartheta(x_1)\ \chi_{R3}(x_1)$$
$$\chi_{sT}^B(x_1) = -\cos\alpha_s \sin\alpha_s \sin\vartheta(x_1)\,\chi_{R2}(x_1) + \cos\alpha_s \sin\alpha_s \cos\vartheta(x_1)\,\chi_{R3}(x_1)$$
$$\chi_{s2}^B(x_1) = -\cos\alpha_s \cos\vartheta(x_1)\,\chi_{R2}(x_1) - \cos\alpha_s \sin\vartheta(x_1)\,\chi_{R3}(x_1)$$
$$\chi_{s3}^B(x_1) = \cos^2\alpha_s \sin\vartheta(x_1)\,\chi_{R2}(x_1) - \cos^2\alpha_s \cos\vartheta(x_1)\,\chi_{R3}(x_1)$$

The rope response will be superimposed in the contribution of the axial torsion and the biaxial bending of the strand. This operation is performed introducing (2.III.2) respectively within (3.IV.3a) and (3.IV.3b). Afterwards, the last two set of relations are substituted inside (3.IV.1).

3.2.1. AXIAL TORSION OF THE STRAND CONTRIBUTION TO THE ROPE RESPONSE

Introducing inside the constitutive model of the single strand (3.IV.3a) the kinematic relations (2.III.2).

$$N_s^{sAT} = \cos^3\alpha_w\, EA_w\, [\cos^2\alpha_s\, R_s \sin\vartheta\ \chi_{R2} - \cos^2\alpha_s\, R_s \cos\vartheta\ \chi_{R3}] + R_w\ \cos^3\alpha_w \tan\alpha_w\, EA_w\, [-\cos\alpha_s \sin\alpha_s \sin\vartheta\, \chi_{R2} + \cos\alpha_s \sin\alpha_s \cos\vartheta\, \chi_{R3}]$$
$$= \cos^3\alpha_w \cos^2\alpha_s\, (R_s - R_w \tan\alpha_w \tan\alpha_s) \sin\vartheta\, EA_w\, \chi_{R2} - \cos^3\alpha_w \cos^2\alpha_s\, (R_s - R_w \tan\alpha_w \tan\alpha_s) \cos\vartheta\, EA_w\, \chi_{R3}$$

$$M_{sT}^{sAT} = R_w \cos^3\alpha_w \tan\alpha_w\, EA_w [\cos^2\alpha_s\, R_s \sin\vartheta\ \chi_{R2} - \cos^2\alpha_s\, R_s \cos\vartheta\ \chi_{R3}]$$
$$+ \cos^3\alpha_w \left[\left(\frac{1}{1+\nu} + \tan^2\alpha_w\right) EI_w + R_w^2\ \tan^2\alpha_w\, EA_w\right] [-\cos\alpha_s \sin\alpha_s \sin\vartheta\, \chi_{R2} + \cos\alpha_s \sin\alpha_s \cos\vartheta\, \chi_{R3}]$$
$$= \cos^3\alpha_w \cos^2\alpha_s \left\{R_s R_w \tan\alpha_w\, EA_w - \tan\alpha_s \left[\left(\frac{1}{1+\nu} + \tan^2\alpha_w\right) EI_w + R_w^2\ \tan^2\alpha_w\, EA_w\right]\right\} \sin\vartheta\, \chi_{R2}$$
$$- \cos^3\alpha_w \cos^2\alpha_s \left\{R_s R_w \tan\alpha_w\, EA_w - \tan\alpha_s \left[\left(\frac{1}{1+\nu} + \tan^2\alpha_w\right) EI_w + R_w^2\ \tan^2\alpha_w\, EA_w\right]\right\} \cos\vartheta\, \chi_{R3}$$

$$M_{s2}^{sAT} = R_w \cos^3\alpha_w \sin\varphi\, EA_w\, [\cos^2\alpha_s\, R_s \sin\vartheta\ \chi_{R2} - \cos^2\alpha_s\, R_s \cos\vartheta\ \chi_{R3}]$$
$$+ \cos^3\alpha_w \tan\alpha_w \sin\varphi \left[\frac{\nu}{1+\nu} EI_w + R_w^2\ EA_w\right] [-\cos\alpha_s \sin\alpha_s \sin\vartheta\, \chi_{R2} + \cos\alpha_s \sin\alpha_s \cos\vartheta\, \chi_{R3}]$$
$$= \cos^3\alpha_w \cos^2\alpha_s \left\{R_s R_w EA_w - \tan\alpha_w \tan\alpha_s \left[\frac{\nu}{1+\nu} EI_w + R_w^2\ EA_w\right]\right\} \sin\varphi \sin\vartheta\ \chi_{R2}$$
$$- \cos^3\alpha_w \cos^2\alpha_s \left\{R_s R_w EA_w - \tan\alpha_w \tan\alpha_s \left[\frac{\nu}{1+\nu} EI_w + R_w^2\ EA_w\right]\right\} \sin\varphi \cos\vartheta\ \chi_{R3}$$

$$M_{s3}^{sAT} = -R_w \cos^3\alpha_w \cos\varphi\, EA_w\, [\cos^2\alpha_s\, R_s \sin\vartheta\ \chi_{R2} - \cos^2\alpha_s\, R_s \cos\vartheta\ \chi_{R3}]$$
$$- \cos^3\alpha_w \tan\alpha_w \cos\varphi \left[\frac{\nu}{1+\nu} EI_w + R_w^2\ EA_w\right] [-\cos\alpha_s \sin\alpha_s \sin\vartheta\, \chi_{R2} + \cos\alpha_s \sin\alpha_s \cos\vartheta\, \chi_{R3}]$$
$$= \cos^3\alpha_w \cos^2\alpha_s \left\{R_s R_w EA_w - \tan\alpha_w \tan\alpha_s \left[\frac{\nu}{1+\nu} EI_w + R_w^2\ EA_w\right]\right\} \cos\varphi \sin\vartheta\ \chi_{R2}$$
$$- \cos^3\alpha_w \cos^2\alpha_s \left\{R_s R_w EA_w - \tan\alpha_w \tan\alpha_s \left[\frac{\nu}{1+\nu} EI_w + R_w^2\ EA_w\right]\right\} \cos\varphi \cos\vartheta\ \chi_{R3}$$

Substituting inside the internal actions within the rope cross section (3.IV.1)

$$N_R^{sAT} = \cos\alpha_s\ \{\cos^3\alpha_w \cos^2\alpha_s\, (R_s - R_w \tan\alpha_w \tan\alpha_s) \sin\vartheta\, EA_w\, \chi_{R2} - \cos^3\alpha_w \cos^2\alpha_s\, (R_s - R_w \tan\alpha_w \tan\alpha_s) \cos\vartheta\, EA_w\, \chi_{R3}\}$$

$$M_{RT}^{sAT} = \cos\alpha_s \left\{\cos^3\alpha_w \cos^2\alpha_s \left\{R_s R_w \tan\alpha_w\, EA_w - \tan\alpha_s \left[\left(\frac{1}{1+\nu} + \tan^2\alpha_w\right) EI_w + R_w^2\ \tan^2\alpha_w\, EA_w\right]\right\} \sin\vartheta\, \chi_{R2}\right.$$
$$\left. - \cos^3\alpha_w \cos^2\alpha_s \left\{R_s R_w \tan\alpha_w\, EA_w - \tan\alpha_s \left[\left(\frac{1}{1+\nu} + \tan^2\alpha_w\right) EI_w + R_w^2\ \tan^2\alpha_w\, EA_w\right]\right\} \cos\vartheta\, \chi_{R3}\right\}$$
$$+ \sin\alpha_s \left\{\cos^3\alpha_w \cos^2\alpha_s \left\{R_s R_w EA_w - \tan\alpha_w \tan\alpha_s \left[\frac{\nu}{1+\nu} EI_w + R_w^2\ EA_w\right]\right\} \cos\varphi \sin\vartheta\ \chi_{R2}\right.$$
$$\left. - \cos^3\alpha_w \cos^2\alpha_s \left\{R_s R_w EA_w - \tan\alpha_w \tan\alpha_s \left[\frac{\nu}{1+\nu} EI_w + R_w^2\ EA_w\right]\right\} \cos\varphi \cos\vartheta\ \chi_{R3}\right\}$$
$$+ R_s\ \sin\alpha_s\ \{\cos^3\alpha_w \cos^2\alpha_s\, (R_s - R_w \tan\alpha_w \tan\alpha_s) \sin\vartheta\, EA_w\, \chi_{R2}$$
$$- \cos^3\alpha_w \cos^2\alpha_s\, (R_s - R_w \tan\alpha_w \tan\alpha_s) \cos\vartheta\, EA_w\, \chi_{R3}\}$$

$$M_{R2}^{sAT} = -\sin\alpha_s \sin\vartheta \left\{\cos^3\alpha_w \cos^2\alpha_s \left\{R_s R_w \tan\alpha_w\, EA_w - \tan\alpha_s \left[\left(\frac{1}{1+\nu} + \tan^2\alpha_w\right) EI_w + R_w^2\ \tan^2\alpha_w\, EA_w\right]\right\} \sin\vartheta\, \chi_{R2}\right.$$
$$\left. - \cos^3\alpha_w \cos^2\alpha_s \left\{R_s R_w \tan\alpha_w\, EA_w - \tan\alpha_s \left[\left(\frac{1}{1+\nu} + \tan^2\alpha_w\right) EI_w + R_w^2\ \tan^2\alpha_w\, EA_w\right]\right\} \cos\vartheta\, \chi_{R3}\right\}$$
$$- \cos\vartheta \left\{\cos^3\alpha_w \cos^2\alpha_s \left\{R_s R_w EA_w - \tan\alpha_w \tan\alpha_s \left[\frac{\nu}{1+\nu} EI_w + R_w^2\ EA_w\right]\right\} \sin\varphi \sin\vartheta\ \chi_{R2}\right.$$
$$\left. - \cos^3\alpha_w \cos^2\alpha_s \left\{R_s R_w EA_w - \tan\alpha_w \tan\alpha_s \left[\frac{\nu}{1+\nu} EI_w + R_w^2\ EA_w\right]\right\} \sin\varphi \cos\vartheta\ \chi_{R3}\right\}$$
$$+ \cos\alpha_s \sin\vartheta \left\{\cos^3\alpha_w \cos^2\alpha_s \left\{R_s R_w EA_w - \tan\alpha_w \tan\alpha_s \left[\frac{\nu}{1+\nu} EI_w + R_w^2\ EA_w\right]\right\} \cos\varphi \sin\vartheta\ \chi_{R2}\right.$$
$$\left. - \cos^3\alpha_w \cos^2\alpha_s \left\{R_s R_w EA_w - \tan\alpha_w \tan\alpha_s \left[\frac{\nu}{1+\nu} EI_w + R_w^2\ EA_w\right]\right\} \cos\varphi \cos\vartheta\ \chi_{R3}\right\}$$
$$+ R_s \cos\alpha_s \sin\vartheta\ \{\cos^3\alpha_w \cos^2\alpha_s\, (R_s - R_w \tan\alpha_w \tan\alpha_s) \sin\vartheta\, EA_w\, \chi_{R2}$$
$$- \cos^3\alpha_w \cos^2\alpha_s\, (R_s - R_w \tan\alpha_w \tan\alpha_s) \cos\vartheta\, EA_w\, \chi_{R3}\}$$

$$
\begin{aligned}
M_{R3}^{sAT} = \sin\alpha_s \cos\vartheta \; & \Big\{\cos^3\alpha_w \cos^2\alpha_s \Big\{R_s R_w \tan\alpha_w \, EA_w - \tan\alpha_s \Big[\Big(\frac{1}{1+\nu} + \tan^2\alpha_w\Big) \, EI_w + R_w^2 \, \tan^2\alpha_w \, EA_w\Big]\Big\} \sin\vartheta \, \chi_{R2} \\
& - \cos^3\alpha_w \cos^2\alpha_s \Big\{R_s R_w \tan\alpha_w \, EA_w - \tan\alpha_s \Big[\Big(\frac{1}{1+\nu} + \tan^2\alpha_w\Big) \, EI_w + R_w^2 \, \tan^2\alpha_w \, EA_w\Big]\Big\} \cos\vartheta \, \chi_{R3}\Big\} \\
& - \sin\vartheta \; \Big\{\cos^3\alpha_w \cos^2\alpha_s \Big\{R_s R_w EA_w - \tan\alpha_w \tan\alpha_s \Big[\frac{\nu}{1+\nu} EI_w + R_w^2 \, EA_w\Big]\Big\} \sin\varphi \sin\vartheta \; \chi_{R2} \\
& - \cos^3\alpha_w \cos^2\alpha_s \Big\{R_s R_w EA_w - \tan\alpha_w \tan\alpha_s \Big[\frac{\nu}{1+\nu} EI_w + R_w^2 \, EA_w\Big]\Big\} \sin\varphi \cos\vartheta \; \chi_{R3}\Big\} \\
& - \cos\alpha_s \cos\vartheta \; \Big\{\cos^3\alpha_w \cos^2\alpha_s \Big\{R_s R_w EA_w - \tan\alpha_w \tan\alpha_s \Big[\frac{\nu}{1+\nu} EI_w + R_w^2 \, EA_w\Big]\Big\} \cos\varphi \sin\vartheta \; \chi_{R2} \\
& - \cos^3\alpha_w \cos^2\alpha_s \Big\{R_s R_w EA_w - \tan\alpha_w \tan\alpha_s \Big[\frac{\nu}{1+\nu} EI_w + R_w^2 \, EA_w\Big]\Big\} \cos\varphi \cos\vartheta \; \chi_{R3}\Big\} \\
& - R_s \cos\alpha_s \cos\vartheta \; \{\cos^3\alpha_w \cos^2\alpha_s \, (R_s - R_w \tan\alpha_w \tan\alpha_s) \sin\vartheta \, EA_w \, \chi_{R2} \\
& - \cos^3\alpha_w \cos^2\alpha_s \, (R_s - R_w \tan\alpha_w \tan\alpha_s) \cos\vartheta \, EA_w \, \chi_{R3}\}
\end{aligned}
$$

Let us collect the common terms, then the result is as follows.

$$
\boldsymbol{N_R^{sAT} = \cos^3\alpha_w \cos^3\alpha_s \, (R_s - R_w \tan\alpha_w \tan\alpha_s) \sin\vartheta \, EA_w \, \chi_{R2} - \cos^3\alpha_w \cos^3\alpha_s \, (R_s - R_w \tan\alpha_w \tan\alpha_s) \cos\vartheta \, EA_w \, \chi_{R3}}
$$

$$
\begin{aligned}
(3.IV.5a) \quad \boldsymbol{M_{RT}^{sAT}} = & \boldsymbol{\cos^3\alpha_w \cos^3\alpha_s \Big\{R_s R_w \tan\alpha_w \, EA_w - \tan\alpha_s \Big[\Big(\frac{1}{1+\nu} + \tan^2\alpha_w\Big) \, EI_w + R_w^2 \, \tan^2\alpha_w \, EA_w\Big]} \\
& \boldsymbol{+ \tan\alpha_s \Big[R_s R_w EA_w - \tan\alpha_w \tan\alpha_s \Big(\frac{\nu}{1+\nu} EI_w + R_w^2 \, EA_w\Big)\Big] \cos\varphi + (R_s^2 \tan\alpha_s - R_s R_w \tan\alpha_w \tan^2\alpha_s) EA_w\Big\} \sin\vartheta \, \chi_{R2}} \\
& \boldsymbol{- \cos^3\alpha_w \cos^3\alpha_s \Big\{R_s R_w \tan\alpha_w \, EA_w - \tan\alpha_s \Big[\Big(\frac{1}{1+\nu} + \tan^2\alpha_w\Big) \, EI_w + R_w^2 \, \tan^2\alpha_w \, EA_w\Big]} \\
& \boldsymbol{+ \tan\alpha_s \Big[R_s R_w EA_w - \tan\alpha_w \tan\alpha_s \Big(\frac{\nu}{1+\nu} EI_w + R_w^2 \, EA_w\Big)\Big] \cos\varphi} \\
& \boldsymbol{+ (R_s^2 \tan\alpha_s - R_s R_w \tan\alpha_w \tan^2\alpha_s) EA_w\Big\} \cos\vartheta \, \chi_{R3}}
\end{aligned}
$$

$$
\begin{aligned}
\boldsymbol{M_{R2}^{sAT}} = & \boldsymbol{\cos^3\alpha_w \cos^3\alpha_s \Big\{-R_s R_w \tan\alpha_s \tan\alpha_w \, EA_w + \tan^2\alpha_s \Big[\Big(\frac{1}{1+\nu} + \tan^2\alpha_w\Big) \, EI_w + R_w^2 \, \tan^2\alpha_w \, EA_w\Big]} \\
& \boldsymbol{+ \Big(\cos\varphi - \frac{\cot\vartheta \sin\varphi}{\cos\alpha_s}\Big) \Big[R_s R_w EA_w - \tan\alpha_w \tan\alpha_s \Big(\frac{\nu}{1+\nu} EI_w + R_w^2 \, EA_w\Big)\Big]} \\
& \boldsymbol{+ (R_s^2 - R_s R_w \tan\alpha_w \tan\alpha_s) EA\Big\} \sin^2\vartheta \, \chi_{R2}} \\
& \boldsymbol{- \cos^3\alpha_w \cos^3\alpha_s \Big\{-R_s R_w \tan\alpha_s \tan\alpha_w \, EA_w + \tan^2\alpha_s \Big[\Big(\frac{1}{1+\nu} + \tan^2\alpha_w\Big) \, EI_w + R_w^2 \, \tan^2\alpha_w \, EA_w\Big]} \\
& \boldsymbol{+ \Big(\cos\varphi - \frac{\cot\vartheta \sin\varphi}{\cos\alpha_s}\Big) \Big[R_s R_w EA_w - \tan\alpha_w \tan\alpha_s \Big(\frac{\nu}{1+\nu} EI_w + R_w^2 \, EA_w\Big)\Big]} \\
& \boldsymbol{+ (R_s^2 - R_s R_w \tan\alpha_w \tan\alpha_s) EA\Big\} \sin\vartheta \cos\vartheta \, \chi_{R3}}
\end{aligned}
$$

$$
\begin{aligned}
\boldsymbol{M_{R3}^{sAT}} = & \boldsymbol{\cos^3\alpha_w \cos^3\alpha_s \Big\{R_s R_w \tan\alpha_s \tan\alpha_w \, EA_w - \tan^2\alpha_s \Big[\Big(\frac{1}{1+\nu} + \tan^2\alpha_w\Big) \, EI_w + R_w^2 \, \tan^2\alpha_w \, EA_w\Big]} \\
& \boldsymbol{- \Big(\cos\varphi + \frac{\tan\vartheta \sin\varphi}{\cos\alpha_s}\Big) \Big[R_s R_w EA_w - \tan\alpha_w \tan\alpha_s \Big(\frac{\nu}{1+\nu} EI_w + R_w^2 \, EA_w\Big)\Big]} \\
& \boldsymbol{+ (R_s^2 - R_s R_w \tan\alpha_w \tan\alpha_s) EA\Big\} \sin\vartheta \cos\vartheta \, \chi_{R2}} \\
& \boldsymbol{- \cos^3\alpha_w \cos^3\alpha_s \Big\{R_s R_w \tan\alpha_s \tan\alpha_w \, EA_w - \tan^2\alpha_s \Big[\Big(\frac{1}{1+\nu} + \tan^2\alpha_w\Big) \, EI_w + R_w^2 \, \tan^2\alpha_w \, EA_w\Big]} \\
& \boldsymbol{- \Big(\cos\varphi + \frac{\cot\vartheta \sin\varphi}{\cos\alpha_s}\Big) \Big[R_s R_w EA_w - \tan\alpha_w \tan\alpha_s \Big(\frac{\nu}{1+\nu} EI_w + R_w^2 \, EA_w\Big)\Big]} \\
& \boldsymbol{- (R_s^2 - R_s R_w \tan\alpha_w \tan\alpha_s) EA\Big\} \cos^2\vartheta \, \chi_{R3}}
\end{aligned}
$$

3.2.2. BIAXIAL BENDING OF THE STRAND CONTRIBUTION TO THE ROPE RESPONSE

Introducing inside the constitutive model of the single strand (3.IV.3b) the kinematic relations (2.III.2).

$$N_s^{sB} = \cos^3\alpha_w R_w \sin\varphi\, EA_w \left[-\cos\alpha_s \cos\vartheta\, \chi_{R2} - \cos\alpha_s \sin\vartheta\, \chi_{R3}\right] - \cos^3\alpha_w R_w \cos\varphi\, EA_w \left[\cos^2\alpha_s \sin\vartheta\, \chi_{R2} - \cos^2\alpha_s \cos\vartheta\, \chi_{R3}\right]$$

$$= -\cos^3\alpha_w \cos^2\alpha_s \left(\cos\varphi + \frac{\cot\vartheta \sin\varphi}{\cos\alpha_s}\right) R_w \sin\vartheta\, EA_w \chi_{R2} + \cos^3\alpha_w \cos^2\alpha_s \left(\cos\varphi - \frac{\tan\vartheta \sin\varphi}{\cos\alpha_s}\right) R_w \cos\vartheta\, EA_w \chi_{R3}$$

$$M_{sT}^{sB} = \cos^3\alpha_w \tan\alpha_w \sin\varphi \left[\frac{\nu}{1+\nu} EI_w + R_w^2\, EA_w\right] \left[-\cos\alpha_s \cos\vartheta\, \chi_{R2} - \cos\alpha_s \sin\vartheta\, \chi_{R3}\right]$$

$$- \cos^3\alpha_w \tan\alpha_w \cos\varphi \left[\frac{\nu}{1+\nu} EI_w + R_w^2\, EA_w\right] \left[\cos^2\alpha_s \sin\vartheta\, \chi_{R2} - \cos^2\alpha_s \cos\vartheta\, \chi_{R3}\right]$$

$$= -\cos^3\alpha_w \cos^2\alpha_s \tan\alpha_w \left[\frac{\nu}{1+\nu} EI_w + R_w^2\, EA_w\right] \left(\cos\varphi + \frac{\cot\vartheta \sin\varphi}{\cos\alpha_s}\right) \sin\vartheta\, \chi_{R2}$$

$$+ \cos^3\alpha_w \cos^2\alpha_s \tan\alpha_w \left[\frac{\nu}{1+\nu} EI_w + R_w^2\, EA_w\right] \left(\cos\varphi - \frac{\tan\vartheta \sin\varphi}{\cos\alpha_s}\right) \cos\vartheta\, \chi_{R3}$$

$$M_{s2}^{sB} = \cos\alpha_w \left[\left(\frac{\sin^2\alpha_w}{1+\nu} + \cot^2\varphi + \cos^2\alpha_w\right) EI_w + \cos^2\alpha_w R_w^2\, EA_w\right] \sin^2\varphi \; \left[-\cos\alpha_s \cos\vartheta\, \chi_{R2} - \cos\alpha_s \sin\vartheta\, \chi_{R3}\right]$$

$$- \cos^3\alpha_w \left[-\frac{\nu}{1+\nu} \tan^2\alpha_w\, EI_w + R_w^2\, EA_w\right] \sin\varphi \cos\varphi \left[\cos^2\alpha_s \sin\vartheta\, \chi_{R2} - \cos^2\alpha_s \cos\vartheta\, \chi_{R3}\right]$$

$$= -\cos^3\alpha_w \cos^2\alpha_s \left\{\left[\left(\frac{\tan^2\alpha_w}{1+\nu} + \frac{\cot^2\varphi}{\cos^2\alpha_w} + 1\right) EI_w + R_w^2\, EA_w\right] \frac{\sin^2\varphi \cos\vartheta}{\cos\alpha_s}\right.$$

$$\left. + \left[-\frac{\nu}{1+\nu} \tan^2\alpha_w\, EI_w + R_w^2\, EA_w\right] \sin\varphi \cos\varphi \sin\vartheta\right\} \chi_{R2}$$

$$+ \cos^3\alpha_w \cos^2\alpha_s \left\{-\left[\left(\frac{\tan^2\alpha_w}{1+\nu} + \frac{\cot^2\varphi}{\cos^2\alpha_w} + 1\right) EI_w + R_w^2\, EA_w\right] \frac{\sin^2\varphi \sin\vartheta}{\cos\alpha_s}\right.$$

$$\left. + \left[-\frac{\nu}{1+\nu} \tan^2\alpha_w\, EI_w + R_w^2\, EA_w\right] \sin\varphi \cos\varphi \cos\vartheta\right\} \chi_{R3}$$

$$M_{s3}^{sB} = -\cos^3\alpha_w \left[-\frac{\nu}{1+\nu} \tan^2\alpha_w\, EI_w + R_w^2\, EA_w\right] \sin\varphi \cos\varphi \left[-\cos\alpha_s \cos\vartheta\, \chi_{R2} - \cos\alpha_s \sin\vartheta\, \chi_{R3}\right]$$

$$+ \cos\alpha_w \left[\left(\frac{\sin^2\alpha_w}{1+\nu} + \tan^2\varphi + \cos^2\alpha_w\right) EI_w + \cos^2\alpha_w R_w^2\, EA_w\right] \cos^2\varphi \; \left[\cos^2\alpha_s \sin\vartheta\, \chi_{R2} - \cos^2\alpha_s \cos\vartheta\, \chi_{R3}\right]$$

$$= \cos^3\alpha_w \cos^2\alpha_s \left\{\left[\left(\frac{\tan^2\alpha_w}{1+\nu} + \frac{\cot^2\varphi}{\cos^2\alpha_w} + 1\right) EI_w + R_w^2\, EA_w\right] \cos^2\varphi \sin\vartheta\right.$$

$$\left. + \left[-\frac{\nu}{1+\nu} \tan^2\alpha_w\, EI_w + R_w^2\, EA_w\right] \frac{\sin\varphi \cos\varphi \cos\vartheta}{\cos\alpha_s}\right\} \chi_{R2}$$

$$- \cos^3\alpha_w \cos^2\alpha_s \left\{\left[\left(\frac{\tan^2\alpha_w}{1+\nu} + \frac{\cot^2\varphi}{\cos^2\alpha_w} + 1\right) EI_w + R_w^2\, EA_w\right] \cos^2\varphi \cos\vartheta\right.$$

$$\left. + \left[-\frac{\nu}{1+\nu} \tan^2\alpha_w\, EI_w + R_w^2\, EA_w\right] \frac{\sin\varphi \cos\varphi \sin\vartheta}{\cos\alpha_s}\right\} \chi_{R3}$$

Substituting inside the internal actions within the rope cross section (3.IV.1)

$$N_R^{sB} = \cos\alpha_s \left\{-\cos^3\alpha_w \cos^2\alpha_s \left(\cos\varphi + \frac{\cot\vartheta \sin\varphi}{\cos\alpha_s}\right) R_w \sin\vartheta\, EA_w \chi_{R2} + \cos^3\alpha_w \cos^2\alpha_s \left(\cos\varphi - \frac{\tan\vartheta \sin\varphi}{\cos\alpha_s}\right) R_w \cos\vartheta\, EA_w \chi_{R3}\right\}$$

$$
\begin{aligned}
M_{RT}^{sB} = \cos\alpha_s \Big\{ & -\cos^3\alpha_w \cos^2\alpha_s \tan\alpha_w \left[\frac{\nu}{1+\nu} EI_w + R_w^2\, EA_w\right]\left(\cos\varphi + \frac{\cot\vartheta \sin\varphi}{\cos\alpha_s}\right)\sin\vartheta\, \chi_{R2} \\
& + \cos^3\alpha_w \cos^2\alpha_s \tan\alpha_w \left[\frac{\nu}{1+\nu} EI_w + R_w^2\, EA_w\right]\left(\cos\varphi - \frac{\tan\vartheta \sin\varphi}{\cos\alpha_s}\right)\cos\vartheta\, \chi_{R3}\Big\} \\
& + \sin\alpha_s \Big\{\cos^3\alpha_w \cos^2\alpha_s \Big\{\left[\left(\frac{\tan^2\alpha_w}{1+\nu} + \frac{\cot^2\varphi}{\cos^2\alpha_w} + 1\right) EI_w + R_w^2\, EA_w\right]\cos^2\varphi \sin\vartheta \\
& + \left[-\frac{\nu}{1+\nu}\tan^2\alpha_w\, EI_w + R_w^2\, EA_w\right]\frac{\sin\varphi\cos\varphi\cos\vartheta}{\cos\alpha_s}\Big\}\chi_{R2} \\
& - \cos^3\alpha_w \cos^2\alpha_s \Big\{\left[\left(\frac{\tan^2\alpha_w}{1+\nu} + \frac{\cot^2\varphi}{\cos^2\alpha_w} + 1\right) EI_w + R_w^2\, EA_w\right]\cos^2\varphi \cos\vartheta \\
& + \left[-\frac{\nu}{1+\nu}\tan^2\alpha_w\, EI_w + R_w^2\, EA_w\right]\frac{\sin\varphi\cos\varphi\sin\vartheta}{\cos\alpha_s}\Big\}\chi_{R3}\Big\} \\
& + R_s\ \sin\alpha_s\ \Big\{-\cos^3\alpha_w \cos^2\alpha_s \left(\cos\varphi + \frac{\cot\vartheta \sin\varphi}{\cos\alpha_s}\right) R_w \sin\vartheta\, EA_w \chi_{R2} \\
& + \cos^3\alpha_w \cos^2\alpha_s \left(\cos\varphi - \frac{\tan\vartheta \sin\varphi}{\cos\alpha_s}\right) R_w \cos\vartheta\, EA_w \chi_{R3}\Big\}
\end{aligned}
$$

$$
\begin{aligned}
M_{R2}^{sB} = & -\sin\alpha_s \sin\vartheta \Big\{-\cos^3\alpha_w \cos^2\alpha_s \tan\alpha_w \left[\frac{\nu}{1+\nu} EI_w + R_w^2\, EA_w\right]\left(\cos\varphi + \frac{\cot\vartheta \sin\varphi}{\cos\alpha_s}\right)\sin\vartheta\, \chi_{R2} \\
& + \cos^3\alpha_w \cos^2\alpha_s \tan\alpha_w \left[\frac{\nu}{1+\nu} EI_w + R_w^2\, EA_w\right]\left(\cos\varphi - \frac{\tan\vartheta \sin\varphi}{\cos\alpha_s}\right)\cos\vartheta\, \chi_{R3}\Big\} \\
& - \cos\vartheta\ \Big\{-\cos^3\alpha_w \cos^2\alpha_s \Big\{\left[\left(\frac{\tan^2\alpha_w}{1+\nu} + \frac{\cot^2\varphi}{\cos^2\alpha_w} + 1\right) EI_w + R_w^2\, EA_w\right]\frac{\sin^2\varphi\cos\vartheta}{\cos\alpha_s} \\
& + \left[-\frac{\nu}{1+\nu}\tan^2\alpha_w\, EI_w + R_w^2\, EA_w\right]\sin\varphi\cos\varphi\sin\vartheta\Big\}\chi_{R2} \\
& + \cos^3\alpha_w \cos^2\alpha_s \Big\{-\left[\left(\frac{\tan^2\alpha_w}{1+\nu} + \frac{\cot^2\varphi}{\cos^2\alpha_w} + 1\right) EI_w + R_w^2\, EA_w\right]\frac{\sin^2\varphi\sin\vartheta}{\cos\alpha_s} \\
& + \left[-\frac{\nu}{1+\nu}\tan^2\alpha_w\, EI_w + R_w^2\, EA_w\right]\sin\varphi\cos\varphi\cos\vartheta\Big\}\chi_{R3}\Big\} \\
& + \cos\alpha_s \sin\vartheta\ \Big\{\cos^3\alpha_w \cos^2\alpha_s \Big\{\left[\left(\frac{\tan^2\alpha_w}{1+\nu} + \frac{\cot^2\varphi}{\cos^2\alpha_w} + 1\right) EI_w + R_w^2\, EA_w\right]\cos^2\varphi \sin\vartheta \\
& + \left[-\frac{\nu}{1+\nu}\tan^2\alpha_w\, EI_w + R_w^2\, EA_w\right]\frac{\sin\varphi\cos\varphi\cos\vartheta}{\cos\alpha_s}\Big\}\chi_{R2} \\
& - \cos^3\alpha_w \cos^2\alpha_s \Big\{\left[\left(\frac{\tan^2\alpha_w}{1+\nu} + \frac{\cot^2\varphi}{\cos^2\alpha_w} + 1\right) EI_w + R_w^2\, EA_w\right]\cos^2\varphi \cos\vartheta \\
& + \left[-\frac{\nu}{1+\nu}\tan^2\alpha_w\, EI_w + R_w^2\, EA_w\right]\frac{\sin\varphi\cos\varphi\sin\vartheta}{\cos\alpha_s}\Big\}\chi_{R3}\Big\} \\
& + R_s \cos\alpha_s \sin\vartheta\ \Big\{-\cos^3\alpha_w \cos^2\alpha_s \left(\cos\varphi + \frac{\cot\vartheta \sin\varphi}{\cos\alpha_s}\right) R_w \sin\vartheta\, EA_w \chi_{R2} \\
& + \cos^3\alpha_w \cos^2\alpha_s \left(\cos\varphi - \frac{\tan\vartheta \sin\varphi}{\cos\alpha_s}\right) R_w \cos\vartheta\, EA_w \chi_{R3}\Big\}
\end{aligned}
$$

$$
\begin{aligned}
M_{R3}^{sB} = \sin\alpha_s \cos\vartheta \Big\{ & -\cos^3\alpha_w \cos^2\alpha_s \tan\alpha_w \Big[\frac{\nu}{1+\nu} EI_w + R_w^2\, EA_w\Big]\Big(\cos\varphi + \frac{\cot\vartheta \sin\varphi}{\cos\alpha_s}\Big)\sin\vartheta\, \chi_{R2} \\
& + \cos^3\alpha_w \cos^2\alpha_s \tan\alpha_w \Big[\frac{\nu}{1+\nu} EI_w + R_w^2\, EA_w\Big]\Big(\cos\varphi - \frac{\tan\vartheta \sin\varphi}{\cos\alpha_s}\Big)\cos\vartheta\, \chi_{R3}\Big\} \\
& - \sin\vartheta \Big\{ -\cos^3\alpha_w \cos^2\alpha_s \Big\{\Big[\Big(\frac{\tan^2\alpha_w}{1+\nu} + \frac{\cot^2\varphi}{\cos^2\alpha_w} + 1\Big) EI_w + R_w^2\, EA_w\Big]\frac{\sin^2\varphi\cos\vartheta}{\cos\alpha_s} \\
& + \Big[-\frac{\nu}{1+\nu}\tan^2\alpha_w\, EI_w + R_w^2\, EA_w\Big]\sin\varphi\cos\varphi\sin\vartheta\Big\}\chi_{R2} \\
& + \cos^3\alpha_w \cos^2\alpha_s \Big\{-\Big[\Big(\frac{\tan^2\alpha_w}{1+\nu} + \frac{\cot^2\varphi}{\cos^2\alpha_w} + 1\Big) EI_w + R_w^2\, EA_w\Big]\frac{\sin^2\varphi\sin\vartheta}{\cos\alpha_s} \\
& + \Big[-\frac{\nu}{1+\nu}\tan^2\alpha_w\, EI_w + R_w^2\, EA_w\Big]\sin\varphi\cos\varphi\cos\vartheta\Big\}\chi_{R3}\Big\} \\
& - \cos\alpha_s\cos\vartheta \Big\{\cos^3\alpha_w\cos^2\alpha_s\Big\{\Big[\Big(\frac{\tan^2\alpha_w}{1+\nu} + \frac{\cot^2\varphi}{\cos^2\alpha_w} + 1\Big) EI_w + R_w^2\, EA_w\Big]\cos^2\varphi\sin\vartheta \\
& + \Big[-\frac{\nu}{1+\nu}\tan^2\alpha_w\, EI_w + R_w^2\, EA_w\Big]\frac{\sin\varphi\cos\varphi\cos\vartheta}{\cos\alpha_s}\Big\}\chi_{R2} \\
& - \cos^3\alpha_w\cos^2\alpha_s\Big\{\Big[\Big(\frac{\tan^2\alpha_w}{1+\nu} + \frac{\cot^2\varphi}{\cos^2\alpha_w} + 1\Big) EI_w + R_w^2\, EA_w\Big]\cos^2\varphi\cos\vartheta \\
& + \Big[-\frac{\nu}{1+\nu}\tan^2\alpha_w\, EI_w + R_w^2\, EA_w\Big]\frac{\sin\varphi\cos\varphi\sin\vartheta}{\cos\alpha_s}\Big\}\chi_{R3}\Big\} \\
& - R_s\cos\alpha_s\cos\vartheta\Big\{-\cos^3\alpha_w\cos^2\alpha_s\Big(\cos\varphi + \frac{\cot\vartheta\sin\varphi}{\cos\alpha_s}\Big)R_w\sin\vartheta\, EA_w\chi_{R2} \\
& + \cos^3\alpha_w\cos^2\alpha_s\Big(\cos\varphi - \frac{\tan\vartheta\sin\varphi}{\cos\alpha_s}\Big)R_w\cos\vartheta\, EA_w\chi_{R3}\Big\}
\end{aligned}
$$

Let us collect the common terms, then the result is as follows.

$$
\boldsymbol{N_R^{sB} = -\cos^3\alpha_w\cos^3\alpha_s\Big(\cos\varphi + \frac{\cot\vartheta\sin\varphi}{\cos\alpha_s}\Big)R_w\sin\vartheta\, EA_w\chi_{R2} + \cos^3\alpha_w\cos^3\alpha_s\Big(\cos\varphi - \frac{\tan\vartheta\sin\varphi}{\cos\alpha_s}\Big)R_w\cos\vartheta\, EA_w\chi_{R3}}
$$

$$
\begin{aligned}
(3.IV.5b)\quad \boldsymbol{M_{RT}^{sB}} = & \boldsymbol{\cos^3\alpha_w\cos^3\alpha_s\tan\alpha_s\Big\{-\frac{\tan\alpha_w}{\tan\alpha_s}\Big(\frac{\nu}{1+\nu}EI_w + R_w^2\, EA_w\Big)\Big(\cos\varphi + \frac{\cot\vartheta\sin\varphi}{\cos\alpha_s}\Big)\sin\vartheta} \\
& \boldsymbol{+\Big[\Big(\frac{\tan^2\alpha_w}{1+\nu} + \frac{\cot^2\varphi}{\cos^2\alpha_w} + 1\Big)EI_w + R_w^2\, EA_w\Big]\cos^2\varphi\sin\vartheta + \Big[-\frac{\nu}{1+\nu}\tan^2\alpha_w\, EI_w + R_w^2\, EA_w\Big]\frac{\sin\varphi\cos\varphi\cos\vartheta}{\cos\alpha_s}} \\
& \boldsymbol{-\Big(\cos\varphi + \frac{\cot\vartheta\sin\varphi}{\cos\alpha_s}\Big)R_s\, R_w\sin\vartheta\, EA_w\Big\}\chi_{R2}} \\
& \boldsymbol{+\cos^3\alpha_w\cos^3\alpha_s\tan\alpha_s\Big\{\frac{\tan\alpha_w}{\tan\alpha_s}\Big(\frac{\nu}{1+\nu}EI_w + R_w^2\, EA_w\Big)\Big(\cos\varphi - \frac{\tan\vartheta\sin\varphi}{\cos\alpha_s}\Big)\cos\vartheta} \\
& \boldsymbol{-\Big[\Big(\frac{\tan^2\alpha_w}{1+\nu} + \frac{\cot^2\varphi}{\cos^2\alpha_w} + 1\Big)EI_w + R_w^2\, EA_w\Big]\cos^2\varphi\cos\vartheta + \Big[-\frac{\nu}{1+\nu}\tan^2\alpha_w\, EI_w + R_w^2\, EA_w\Big]\frac{\sin\varphi\cos\varphi\sin\vartheta}{\cos\alpha_s}} \\
& \boldsymbol{+\Big(\cos\varphi - \frac{\tan\vartheta\sin\varphi}{\cos\alpha_s}\Big)R_s\, R_w\cos\vartheta\, EA_w\Big\}\chi_{R3}}
\end{aligned}
$$

The last two expressions are not reported because they are cumbersome. The derivation is like all the other expressions seen so far.

V. CONCLUSIONS

The present chapter provides the single wire contribution to the rope internal actions when the wire itself is experiencing the fundamental modes of the rope. The reason why this peculiar response is investigated lies in the mechanical model that is framed within the small displacements and strains hypothesis and the material behaves linearly elastic. These assumptions allow to see the global response of the wire rope as the algebraic sum of the single wires contributions. The result is pursued for either the direct model and the recursive model. The idea is always the same: the relation between the rope internal actions and the sub component (both strand and wire) internal actions is investigated. Afterwards, the internal actions of the sub component are substituted with the suitable generalized constitutive model, or sectional response, so that the internal actions of the wire rope are related with the sub component kinematics. The final passage consists in introducing the kinematic relations that link the wire rope kinematics with the sub component kinematics. The outcome is a set of equations describing how the internal actions of the rope depend upon the kinematics of the sub component. The coefficients (3.III.3) fully describe the pursued model.

The first concept to introduce is about the trend of the aforesaid coefficients along the rope axis, or equivalently along the wire centerline. Specifically, all the functions are periodical and oscillate about a mean value. The oscillations do not provide a contribute to the global response of the rope when the contributions of all the wires are summed. The reason lies in the symmetry of the cross section. As a matter of fact, for every entry of the stiffness matrix due to a single wire, there exists another wire that provides a contribution opposite in sign. The consequence of this concept is that the mean value affects the global response of the wire rope. Hence, the functions with a zero-mean value will vanish, while non-zero mean value functions won't. From the analysis performed for the two models it appeared that the non-zero entries are the axial stiffness, the axial torsion coupling coefficient, the torsional and bending stiffness; while all other quantities have zero-mean value. The main consequence of the previous statement is that axial and torsional internal actions of the wire rope are always coupled, while bending is always uncoupled. The existing coupling is the direct consequence of the twisted geometry of the sub components of the rope.

The direct model has been studied for either real arc length and developed arc length that is the approximation of the first, since the difference between the two formulations have been introduced in the chapter concerning the geometry of wires. The difference among the two arises in correspondence of the maximum or minimum values with an error around 5% like it is shown in Tables 3.1, 3.2 and 3.3 respectively for axial stiffness, coupling coefficient and torsional stiffness. This difference won't affect the response for what have been said before, while the error on the mean value will. It is around 2% for axial stiffness, while it is around 5% for coupling coefficient and torsional stiffness.

The recursive model has been compared to the previous one. Focusing on the mean value of the respective functions the following results have been found according to Tables 3.6, 3.7 and 3.8: the axial stiffness differs of 5%, the axial torsion coefficient of 22% and the torsional stiffness of the recursive model is half of the direct one.

These numbers that have been computed for a 30 mm 7x7 WSC stranded rope have a precise mechanical consequence. As a matter of fact, wire ropes are very elongated elements, such that they can be considered curves in space. In this light, a 5% error in the evaluation of the stiffness causes a similar error on the evaluation of the strains. Still, when the displacements need to be computed, the error increases much more. For instance, if a uniform torsional curvature is the result of an analysis, the rotation along the wire rope will have a linear trend as function of the rope axis coordinate. Assuming one end clamped, the section at distance 1000 m from the constraint will experience a rotation that is the torsional curvature times 1000, thus 50 radiant (2865°) more from passing from one model to the other. This simple example wants to give a clue about the importance of investigating the different formulations.

REFERENCES

(Love, 1944) Love A.E.H., 1944. *A treatise on the Mathematical Theory of Elasticity*. Dover Publications, New York.

(Huang, 1973) Huang N.C., 1973. *Theories of Elastic Slender Curved Rods.* Journal of Applied Mathematics and Physics Vol.24 (1973).

(Velinsky et al., 1984) Velinsky S.A., Anderson G.L., Costello G.A., 1984. *Wire rope with complex cross sections.* Eng. Mech. Div., ASCE 110 (3), 380-391.

(Ramsey, 1988) Ramsey, H., 1988. *A theory of thin rods with application to helical constituent wires in cables*. Int. J. Mech. Sci., 30(8), 559–570.

(Raoof & Kraincanic, 1995) Raoof M., Kraincanic I., 1995. *Analysis of large diameter steel ropes.* Journal of Engineering Mechanics / June 1995 / 667-675.

(Leech, 2002) Leech C.M., 2002. *The modelling of friction in polymer in fiber ropes*. International Journal of Mechanical Sciences 44 (2002) 621–643.

(Elata et al., 2004) Elata D., Eshkenazy R., Weiss M.P., 2004. *The mechanical behaviour of a wire rope with an independent wire rope core.* International Journal of Solids and Structures 41 (2004) 1157-1172.

(Feyrer, 2007) Feyrer K., 2007. *Wire Ropes. Tension, Endurance, Reliability*. Springer.

(Usabiaga & Pagalday, 2008) Usabiaga H., Pagalday J.M., 2008. *Analytical procedure for modelling recursively and wire by wire stranded ropes subjected to traction and torsion loads.* International Journal of Solids and Structures 45 (2008) 5503-5520.

(Foti, 2013) Foti. F., 2013. *A corotational beam element and a refined mechanical model for the nonlinear dynamic analysis of cables*. Doctoral dissertation. Doctoral Programme in Structural, Seismic and Geotechnical Engineering XXV Cycle. Politecnico di Milano.

(Xiang et al., 2015) Xiang L., Wang H.Y., Chen Y., Guan Y.J., Wang Y.L., Dai L.H., 2015. *Modelling of multi-stranded wire ropes subjected to axial tension and torsion loads*. International Journal of Solids and Structures 58 (2015) 233-246.

(Foti & Martinelli, 2016) Foti F., Martinelli L., 2016. *Mechanical modelling of metallic strands subjected to tension, torsion and bending*. International Journal of Solids and Structures 91 (2016) 1-17.

(Meleddu et al., 2017) Meleddu M., Foti F., Martinelli L., 2017. *Temperature in active heave compensation ropes*. OIPEEC Conference – Le Rochelle – April 2017.

CHAPTER 4

GLOBAL AND LOCAL MECHANICAL RESPONSE

I. INTRODUCTION

The present chapter pursues the objective of providing the response of the wire rope at two different levels. The global level of the response concerns the internal actions of the rope. Specifically, providing such kind of response means to provide the axial force, the torque and the two bending moments arising within the rope when it experiences a certain kinematic perturbation. The internal actions are the one corresponding to the Euler Bernoulli formulation of the rope kinematics. For the global information on the response many theoretical predictions may be found in literature like in (Usabiaga & Pagalday, 2008) and (Xiang et al., 2015), while for experimental results only few papers are available like (Kraincanic & Hobbs, 1999) and (Elata et al., 2004). Furthermore, the latter articles investigate the axial torsional response of the rope only.
Conversely, the local response of the wire rope concerns the stresses experienced by the single wire when it undergoes the kinematic perturbation that acts on the rope. This topic is much more complex of the previous one, since for instance no experimental data are available in literature, but only theoretical models like in (Usabiaga & Pagalday, 2008) and (Xiang et al., 2015).

The previous chapter studied the response of the single wire in terms of contribution to the global internal actions of the rope when the wire itself experiences the kinematic field acting on the rope. The reason of this analysis is the choice of the mechanical model. As a matter of fact, the present work concerns a linear elastic model, thus the global response of the rope may be seen like the sum of the responses of the single wires. Hence, in the present chapter the first part will deal with the integration of the single wires contributions to compute the internal actions of the rope.
The results coming from the direct and recursive model will be compared with either the theoretical and experimental results available in literature and considered more significative. The comparison will be on the axial torsional response of the rope only. The numerical evaluation is dealt for the two ropes introduced in the first chapter about geometry: the 30 mm 7x7 WSC stranded rope and the 76 mm 6x41 IWRC wire rope. The first case is analyzed only theoretically through comparison with the model proposed by (Usabiaga & Pagalday, 2008) and (Xiang et al., 2015). The second rope is compared with (Kraincanic & Hobbs, 1999), where either theoretical and experimental results are provided.
The computation of the local response will be easier instead. In fact, the second chapter deals with the kinematic model of the present thesis. There it was established for either direct and recursive model the connection between the wire and the rope strain fields. Hence, the local stresses can be computed easily using the generalized constitutive model of the wire, or sectional response (3.II.1). The comparison is done for the 30 mm 7x7 WSC stranded rope only, since theoretical results are available in (Usabiaga & Pagalday, 2008) and (Xiang et al., 2015).

II. GLOBAL RESPONSE OF THE ROPE

The present part of the thesis aims to provide the global response of the rope. The term "global" hints to the generalized stress and strain arising within the rope according to the Euler Bernoulli kinematic hypothesis, thus to the quantities concerning the sectional response of the rope. If we set as global reference frame of the rope (x_1, x_2, x_3), where x_1 is directed as the rope axis and the vector (x_2, x_3) lays within the rope cross section, the kinematic assumption involves as DOFs of the section the longitudinal displacement of the center of gravity u_R, the torsional rotation ϕ_{RT} and the bending rotations ϕ_{R2}, ϕ_{R3} according to (2.II.1). Hence, the internal actions or generalized displacements are the axial force N_R, the torque M_{RT}, and the bending moments M_{R2}, M_{R3}. Conversely, the generalized strains are the axial strain η_R, the torsional curvature χ_{RT}, and the bending curvatures χ_{R2}, χ_{R3}. The vectors of generalized stresses and strains are mutually connected with the stiffness matrix. This matrix has been already computed in chapter 3 as the contribution of a single wire to the matrix entries.
The path pursuit in the present paragraph is the following: the definition of the integration over the rope cross section of the single wire contributions, then the global stiffness matrix is computed through that, finally the model will be compared with the theoretical and experimental results available in literature for the case of axial torsional perturbation experienced by the rope like in (Usabiaga & Pagalday, 2008); (Xiang et al., 2015) and (Kraincanic & Hobbs, 1999).

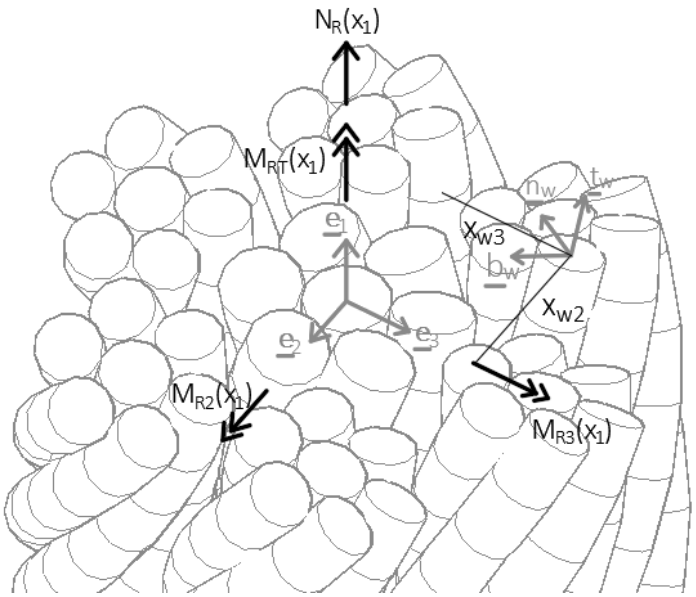

Fig 4.68 Global Response of the Wire Rope

1. SECTIONAL RESPONSE OF THE WIRE ROPE

In the present thesis work it was stated many times that the operation of integration of the periodical quantities concerning the wire over the rope's length corresponding to one period of the functions is the same of summing the same quantities over the cross section of the rope.
The relation between the rope axis and the rope cross section is clear if we think about the geometry. As a matter of fact, the description of either single and double helix is performed with a single free coordinate, usually the global coordinate x_1 corresponding to the rope axis. The relations (1.IV.3.1) and (1.IV.3.2) show the constraints holding true between the different coordinates. The relations have a shape as follows.

$$\vartheta(x_1) - \vartheta_0 = A\, x_1$$

Where A is a constant quantity, θ is the in plane polar angle to the rope current cross section and θ_0 is the value of the polar angle at the coordinate x_1 equal to zero.

The summation of a periodical quantity over the rope cross section involves that we are considering all the wires. They are usually symmetric with respect of the rope axis; hence they are equally spaced in terms of angles. More precisely they are uniformly shifted in terms of phase angle θ_0. Thus, when we are talking about the summation over the cross section, what makes vary the investigated function is the phase angle and not the global coordinate anymore.
Let us call P the period of the function, n the number of wires (even since we assume a symmetric cross section) and i the index spanning from zero to n which detect the i-th wire in terms of phase angle. The period in term of polar angle is $\theta - \theta_0$ equal to 2π. Thus, the period along the rope axis correspond to the following quantity.

$$P = \frac{2\pi}{A}$$

Let us establish the connection between the variation of phase angle θ_{0i} and the correspondent variation along the rope axis. If we fix a certain cross section of coordinate x_1, let us increment the phase angle as follows.

$$\vartheta(\overline{x}_1) - \vartheta_0 + i\,\frac{2\pi}{n} = A\,\overline{x}_1$$

$$\vartheta\left(\overline{x}_1 - i\frac{P}{n}\right) - \vartheta_0 = A\left(\overline{x}_1 - i\frac{P}{n}\right)$$

The last two relations show how sampling the function at different phase angles is like sampling the functions at different position of the rope axis for the initial wire θ_0. Sampling a periodical function at constant intervals P/n from zero to P and summing all the contributions correspond to extract the mean value of the periodical function itself, hence it is the same of integrating over the rope length the function.

$$\int_0^P f(x_1)\,dx_1 = \sum_{i=1}^{n} f(\vartheta(\overline{x}_1) - \vartheta_{0i}) = \sum_{i=0}^{n} f\left(\overline{x}_1 - i\frac{P}{n}\right)$$

2. GLOBAL STIFFNESS MATRIX OF THE WIRE ROPE

In the present paragraph the objective is the definition of the mechanical quantities that identify the response of wire rope. Let us define the vectors of the generalized stresses $\underline{\sigma}$, generalized strains $\underline{\varepsilon}$ and rotations $\underline{\omega}$ as follows.

$$\underline{\sigma} = (N_R, M_{RT}, M_{R2}, M_{R3})^T$$
$$\underline{\varepsilon} = (\eta_R, \chi_{RT}, \chi_{R2}, \chi_{R3})^T$$
$$\underline{\omega} = (\varphi_{R2}, \varphi_{R3})^T$$

The stiffness matrix of the structural system is conventionally defined through the generalized stresses and strains of the model.

$$\underline{\underline{K}}_R = \frac{\partial \underline{\sigma}}{\partial \underline{\varepsilon}} = \sum_{i=1}^{All\ wires} \begin{bmatrix} EA_R & C_{AT} & C_{AB2} & C_{AB3} \\ C_{TA} & GJ_R & C_{TB2} & C_{TB3} \\ C_{B2A} & C_{B2T} & EI_{R2} & C_{B23} \\ C_{B3A} & C_{B3T} & C_{B32} & EI_{R3} \end{bmatrix}_i$$

Let us recall that in the direct model the generalized stresses do not depend upon the corresponding work conjugated strains only, yet on the bending rotations as well. This result is a consequence of the kinematic model of the wire rope. Specifically, these contributions arise from the variation of position of the single wire between two subsequent cross sections of the rope.

$$\begin{pmatrix} N_R \\ M_{RT} \\ M_{R2} \\ M_{R3} \end{pmatrix} = \sum_{i=1}^{All\ wires} \begin{bmatrix} EA_R & C_{AT} & C_{AB2} & C_{AB3} \\ C_{TA} & GJ_R & C_{TB2} & C_{TB3} \\ C_{B2A} & C_{B2T} & EI_{R2} & C_{B23} \\ C_{B3A} & C_{B3T} & C_{B32} & EI_{R3} \end{bmatrix}_i \begin{pmatrix} \eta_R \\ \chi_{RT} \\ \chi_{R2} \\ \chi_{R3} \end{pmatrix} + \sum_{i=1}^{All\ wires} \begin{bmatrix} C_{AR2} & C_{AR3} \\ C_{TR2} & C_{TR3} \\ C_{B2R2} & C_{B2R3} \\ C_{B3R2} & C_{B3R3} \end{bmatrix}_i \begin{pmatrix} \varphi_{R2} \\ \varphi_{R3} \end{pmatrix}$$

The chapter three provides explicitly the coefficient of the two matrices. In many occasions, it was underlined that many coefficients were vanishing when summed over the cross section. The reason is that the integration over the length of the rope corresponding to a period of the function is the same of integrating the same function over the rope cross section. Specifically, checking the results of the previous chapter it easy to find the following result.

$$\sum_{i=1}^{All\ wires} \begin{bmatrix} C_{AR2} & C_{AR3} \\ C_{TR2} & C_{TR3} \\ C_{B2R2} & C_{B2R3} \\ C_{B3R2} & C_{B3R3} \end{bmatrix}_i = \begin{bmatrix} 0 & 0 \\ 0 & 0 \\ 0 & 0 \\ 0 & 0 \end{bmatrix}$$

$$\sum_{i=1}^{All\ wires} \begin{bmatrix} EA_R & C_{AT} & C_{AB2} & C_{AB3} \\ C_{TA} & GJ_R & C_{TB2} & C_{TB3} \\ C_{B2A} & C_{B2T} & EI_{R2} & C_{B23} \\ C_{B3A} & C_{B3T} & C_{B32} & EI_{R3} \end{bmatrix}_i = \begin{bmatrix} EA_R & C_{AT} & 0 & 0 \\ C_{TA} & GJ_R & 0 & 0 \\ 0 & 0 & EI_{R2} & 0 \\ 0 & 0 & 0 & EI_{R3} \end{bmatrix}$$

The global stiffness matrix and the generalized constitutive model of the rope, or sectional response of the rope, may be written as follows.

$$(4.II.1) \quad \begin{pmatrix} N_R \\ M_{RT} \\ M_{R2} \\ M_{R3} \end{pmatrix} = \begin{bmatrix} EA_R & C_{AT} & 0 & 0 \\ C_{TA} & GJ_R & 0 & 0 \\ 0 & 0 & EI_{R2} & 0 \\ 0 & 0 & 0 & EI_{R3} \end{bmatrix} \begin{pmatrix} \eta_R \\ \chi_{RT} \\ \chi_{R2} \\ \chi_{R3} \end{pmatrix}$$

It is worth to notice that (4.II.1) holds true for either the direct and the recursive model, since the stiffness coefficients have similar trend in term of mean value and the coupling coefficients of the rotations vanish.
Furthermore, the axial torsional problem is fully coupled, while the axial torsional and biaxial bending behavior is completely uncoupled. Hence, it is possible to superimpose the two problems as follows.

$$(4.II.2a) \quad \begin{pmatrix} N_R \\ M_{RT} \end{pmatrix} = \begin{bmatrix} EA_R & C_{AT} \\ C_{TA} & GJ_R \end{bmatrix} \begin{pmatrix} \eta_R \\ \chi_{RT} \end{pmatrix}$$

$$(4.II.2b) \quad \begin{pmatrix} M_{R2} \\ M_{R3} \end{pmatrix} = \begin{bmatrix} EI_{R2} & 0 \\ 0 & EI_{R3} \end{bmatrix} \begin{pmatrix} \chi_{R2} \\ \chi_{R3} \end{pmatrix}$$

The presence of coupling between axial and torsional internal actions is a trivial consequence of the internal geometry of the wire. For instance, let us pull the rope, the wire will experience an axial strain that will cause stretching and thus axial force within the wire itself. This axial force is directed as the wire centerline, hence a component will be along the wire axis, while another will be in plane with the rope cross section. The first is responsible of the axial force and bending moment within the rope, while the second provide a torque. Since all wires are coiled with the same coiling angle, the in-plane contribution will sum, while the components directed as the rope axis will sum to generate a resultant axial force, still the won't provide bending because of the symmetry of the cross section. As a matter of fact, two wires at opposite sides of the rope section will produces bending moments that have same magnitude, but opposite sign.

3. CASE STUDY FOR AXIAL TORSION RESPONSE OF THE WIRE ROPE

The current section has the aim of comparing the theoretical results of the present thesis work with the available references in literature. The comparison is performed for axial torsional perturbation of the rope only. Hence, the quantities being investigated are the coefficient of the stiffness matrix (4.II.2a) that is reported in the following.

$$\begin{pmatrix} N_R \\ M_{RT} \end{pmatrix} = \begin{bmatrix} EA_R & C_{AT} \\ C_{TA} & GJ_R \end{bmatrix} \begin{pmatrix} \eta_R \\ \chi_{RT} \end{pmatrix}$$

The first case study concerns the 30 mm 7x7 WSC stranded rope that has been investigated in the first chapter. It has been considered in the papers of Usabiaga & Pagalday (2008) and Xiang et. al (2015) from a theoretical view point. Conversely, the second case study analyzes the 76 mm 6x41 IWRC wire rope in the article of Kraincanic & Hobbs (1999). In the last paper either experimental and theoretical results are provided. Specifically, the analytical predictions of the rope response in this reference come from other two works by Velinsky et al (1984) and Raoof & Kraincanic (1995).

3.1. STRANDED ROPE 30 mm 7x7 WSC

The present section aims to provide a validation of the present mechanical model comparing the results obtained with other two formulations due to Usabiaga & Pagalday (2008) and Xiang et al (2015). The articles deal with a wire by wire approach both. This means that no homogenization is performed over the strand and the wire is fully accounted with its double helix geometry. The main difference with the present thesis work is in the kinematics.

Usabiaga & Pagalday assume kinematics in between the full stick and full slip condition, i.e. the hypothesis of material point of the wire rigidly attached to the rope axis is partially removed. As a matter of fact, the wire material point is considered constrained to the strand axis, while the strand material point is not attached to rope axis. Hence, slipping is allowed among strands, still it is not among wires within the same strand. On the other hand, Xiang et al assume a complete frictionless condition. Furthermore, the generalized axial strain of the wire is defined according to the Love thin curved rod theory (Huang, 1973):

$$(4.II.3) \quad \eta_w = u_{w,1} - \kappa_w \, v_{w2} = \frac{ds_w}{ds_{w0}} - 1$$

Where η_w is the wire strain of the centerline, u_{w1} is the centerline displacement of the wire along the tangent direction, κ_w is the geometrical curvature in the undeformed configuration, v_{w2} is the transverse displacement of the wire centerline along the normal direction of the Serret-Frenet frame, ds_w is the arch length in the current configuration and ds_{w0} is the arch length in the undeformed configurations. The last relation (4.II.3) has been assumed in the present work as it can be seen in (2.II.2a).
The difference between the present thesis work and the two articles lies in the degree of freedom associated to slipping only, since the computation of (4.II.3) is the same of the other authors.

3.1.1. GEOMETRY

The rope is a stranded 7x7. This means that it is made by seven strands that are composed by seven wires each. Both strands and wires are divided in one core and six outers like the following picture is showing. Moreover, the main geometrical features are provided in the table below.

Table 4.21 Stranded Rope 30 mm 7x7 WSC Geometry

Rope layer	wire layer	wire radius r_w [mm]	wire lay angle α_w [°]	number of wires per strand layer	wire helix radius R_w [mm]	wire lay lenght p_w [mm]	strand lay angle α_s [°]	number of strands per rope layer	strand helix radius R_s [mm]	strand lay lenght p_s [mm]
	0	1.970	-	1	-	-				
0	1	1.865	18.99	6	3.835	70	-	1	-	-
	0	1.600	-	1	-	-				
1	1	1.500	15.55	6	3.100	70	18.54	6	10.3	193

Where r_w is the wire cross section radius, p_w is the wire centerline pith, R_s is the radius of the strand helix and R_w is the radius of the wire helix.

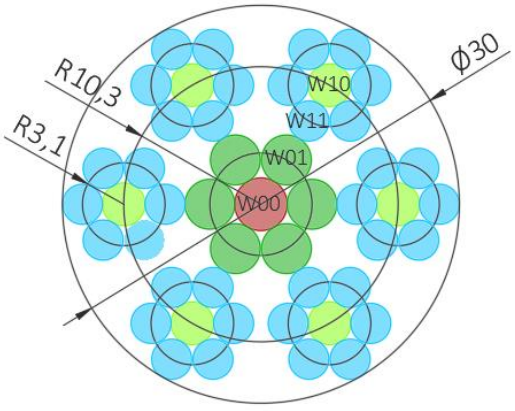

Fig 4.69 Stranded Rope 30 mm 7x7 WSC Geometry

3.1.2. STIFFNESS MATRIX COEFFICIENTS

The result of the analysis is provided in the following table, where It can be clearly appreciated the non-symmetry of the stiffness matrix for the formulation proposed by Usabiaga & Pagalday (2008) and Xiang et al (2015) since C_{AT} and C_{TA} slightly differ. In the right column of each model an error is provided. It is measured as variation from the corresponding value of the direct model.

$$error = \frac{current\ model - direct\ model}{direct\ model}$$

It must be remembered that the model "Recursive sAT" is the recursive model where the bending contribution of the strand is turned off and only the axial torsional one is considered.

Table 4.22 Stiffness Matrix Coefficients

	Direct		Recursive		Recursive sAT		Usabiaga 2008		Xiang 2015	
EA_R [kN]	5.68E+04	-	5.92E+04	4.30%	5.92E+04	4.30%	5.73E+04	0.85%	5.88E+04	3.53%
C_{AT} [kNmm]	1.91E+05	-	2.08E+05	8.61%	2.08E+05	8.61%	1.97E+05	3.26%	2.07E+05	8.23%
C_{TA} [kNmm]	1.91E+05	-	2.08E+05	8.61%	2.08E+05	8.61%	1.96E+05	2.44%	2.01E+05	5.04%
GJ_R [kNmm^2]	1.28E+06	-	8.86E+05	-30.51%	8.63E+05	-32.34%	1.06E+06	-16.70%	8.97E+05	-29.68%

The results show that the axial stiffness EA_R is very similar among the various model, while the torsional stiffness GJ_R is varies considerably. A more thorough analysis of the coefficient is performed in the following. In general, it can be appreciated that the direct model is the stiffer one, while the recursive model is very close to Xiang et al, beside the kinematic hypothesis are deeply different (full stick for the recursive model and full slip condition for Xiang). Finally, the formulation proposed by Usabiaga & Pagalday is in between, like it was expected according to the kinematic assumptions.

3.1.2.1. AXIAL STIFFNESS

The axial stiffness doesn't vary significantly from a model to the other. The reason is that the axial stiffness is closely related to the nominal axial stiffness that can be computed roughly as EA_0 where A_0 is the area of steel that is crossed by a cutting plane orthogonal to the rope axis.

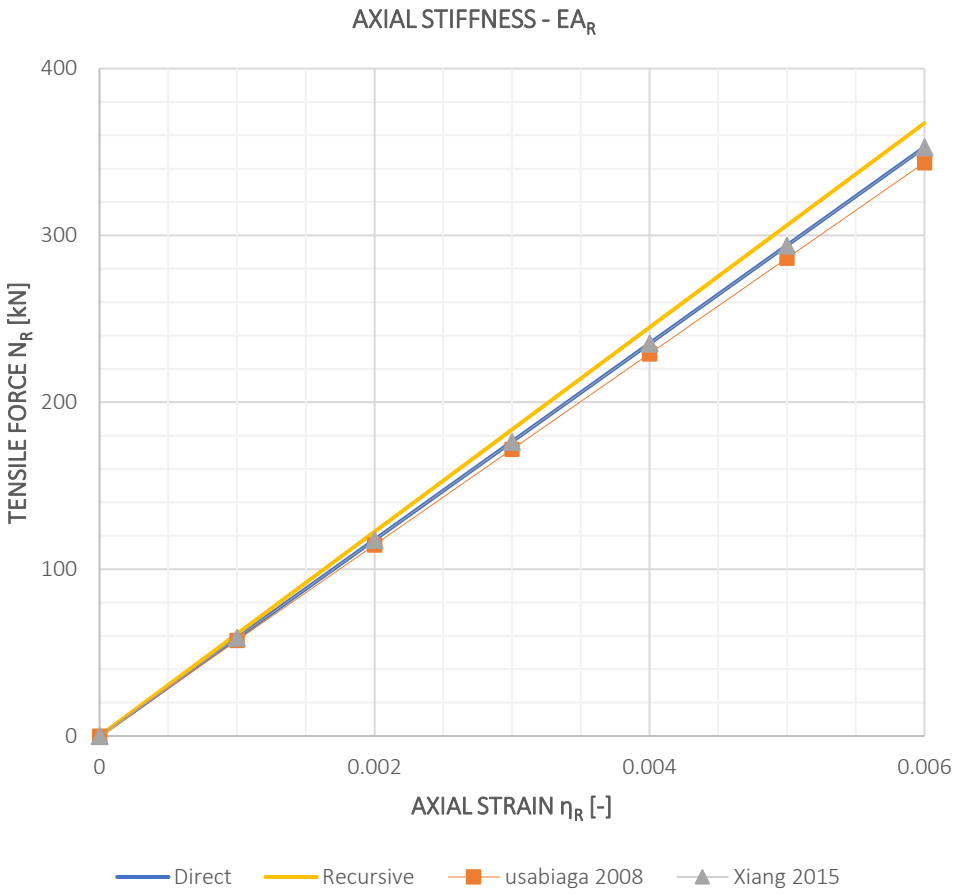

Fig 4.70 Wire Rope Global Axial Stiffness

3.1.2.2. COUPLING COEFFICIENT

The coupling coefficients are not very different from a numerical view point, like it can be seen in the following plot of the quantity C_{AT}. Conversely, they are deeply different form a conceptual view point. As a matter of fact, for the models proposed by Usabiaga & Pagalday (2008) and Xiang et al (2015) the Reciprocity theorem is violated, hence the formulations show a certain degree of inconsistency from the thermodynamic vantage point.

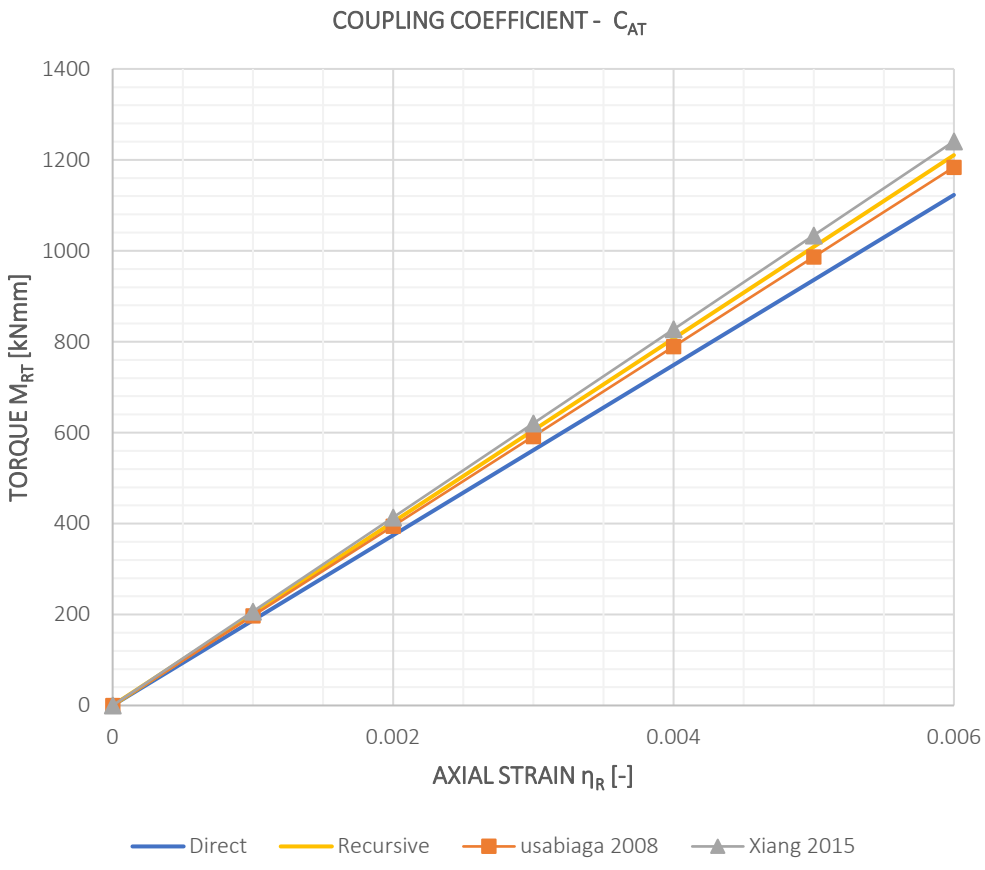

Fig 4.71 Wire Rope Global Axial Torsional Coupling Coefficient

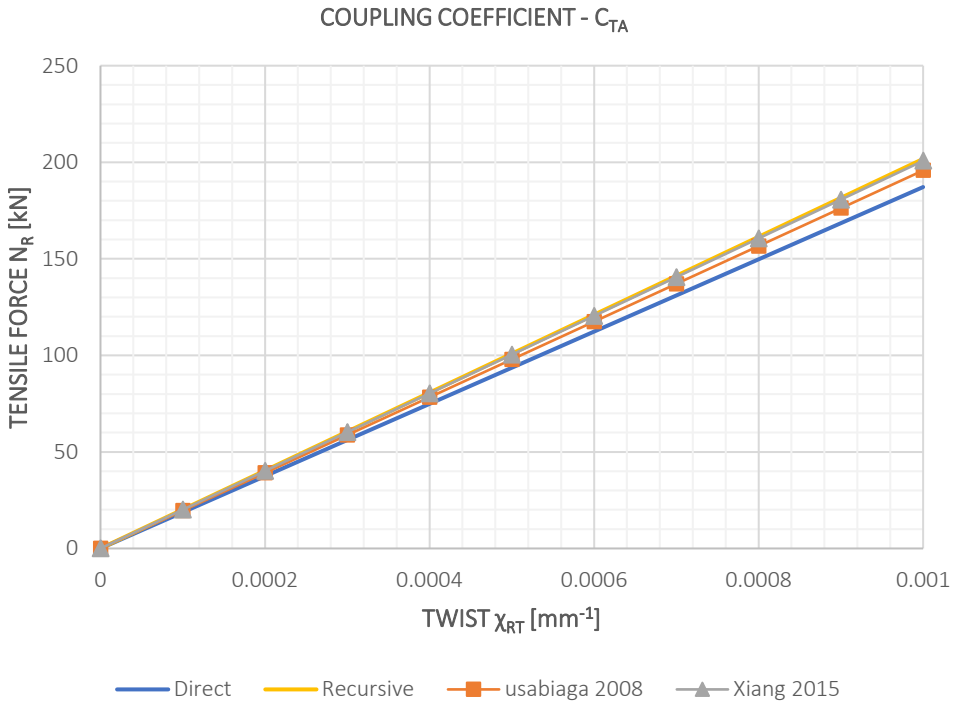

Fig 4.72 Wire Rope Global Axial Torsional Coupling Coefficient

3.1.2.3. TORSIONAL STIFFNESS

The torsional stiffness is the global mechanical quantity that shows the greater difference among the various model. The reason is double: first, the axial strain of the wire centerline (4.II.3) affects the global response since it represent the mean value of the stress field experienced by the wire cross section; on the other hand, the three formulations have different degrees of freedom. As a matter of fact, the direct formulation is the stiffer model since it represents a full stick condition. The model of Xiang et al assuming a frictionless condition more compliant with a -29.7% error from the direct one, while the Usabiaga & Pagalday (2008) formulation is in between the direct and the Xiang (2015) ones with an error of -16.7%. Conversely, despite the kinematic model is the same of the direct model, the recursive one has the lower stiffness with an error ranging between -32% and -30% if the strand bending contribution is neglected or not respectively. This last result is mainly caused by the approximation introduced with the hierarchical approach.

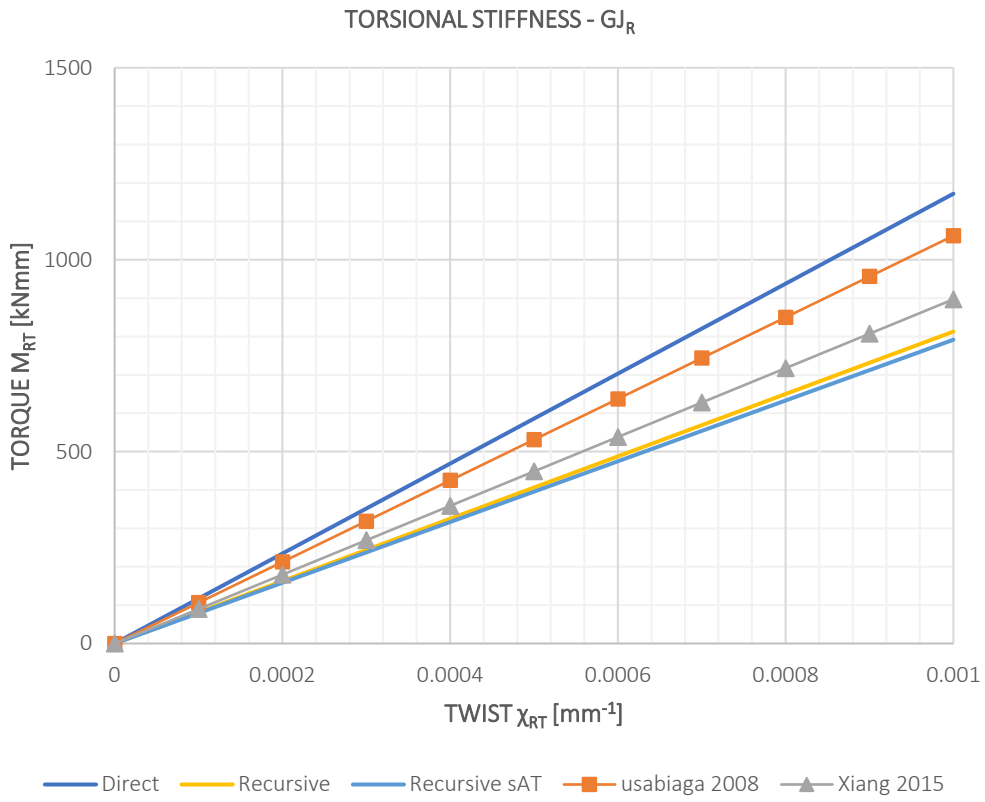

Fig 4.73 Wire Rope Global Torsional Stiffness

3.2. WIRE ROPE 76 mm 6x41 IWRC

The present paragraph aims to describe the global response of a 76 mm wire rope. The main reference is the paper of Hobbs & Kraincanic (1999). The two authors perform some experimental tests on a 7 m specimen of a IWRC wire rope with elastic modulus equal to 200 GPa. The results obtained are the axial stiffness, the torsional stiffness and the coupling coefficient between axial and torsion. In the article an interesting phenomenon is recorded. In the present thesis work like in several other models, for instance Usabiaga & Pagalday (2008) and Xiang et al (2015), the axial stiffness of the wire rope is a constant quantity, since it assumes a constant stretching of the rope cross section. Truly, this quantity isn't constant, still it is affected by slipping among the wires. This empirical evidence will be the main cause of difference among the various formulations.
The stiffness matrix in the aforesaid paper is defined as follows.

$$(4.II.3)\quad \begin{pmatrix} N_R \\ M_{RT} \end{pmatrix} = \begin{bmatrix} EA_R & C_{AT} \\ C_{TA} & GJ_R \end{bmatrix} \begin{pmatrix} \eta_R \\ \chi_{RT} \end{pmatrix} = E \begin{bmatrix} a_1 & a_2 \\ a_3 & a_4 \end{bmatrix} \begin{pmatrix} \eta_R \\ \chi_{RT} \end{pmatrix}$$

The axial force and the consequent generated torque are measured in the same test. The reason is that if we apply an axial strain to the rope and the torsional rotation is constrained the relation (4.II.3) becomes as follows.

$$(4.II.4)\quad \begin{pmatrix} N_R \\ M_{RT} \end{pmatrix} = \begin{pmatrix} EA_R \\ C_{TA} \end{pmatrix} \eta_R$$

On the other hand, the measurement of the torsional stiffness can't be done directly. As a matter of fact, if the torsional rotation is enforced and no axial force is applied, the rope experiences a shortening due to coupling of axial and torsion.

$$\begin{pmatrix} 0 \\ M_{RT} \end{pmatrix} = \begin{bmatrix} EA_R & C_{AT} \\ C_{TA} & GJ_R \end{bmatrix} \begin{pmatrix} \eta_R \\ \chi_{RT} \end{pmatrix}$$

From the first equation the following relation is derived.

$$EA_R\,\eta_R + C_{AT}\,\chi_{RT} = 0 \quad \Rightarrow \quad \eta_R = -\frac{C_{AT}}{EA_R}\,\chi_{RT}$$

If we substitute the derived relation into the second equation the effective torsional stiffness that is measured in the experimental test is as follows.

$$M_{RT} = \left(GJ_R - \frac{C_{TA}\,C_{AT}}{EA_R}\right)\chi_{RT} = E\left(a_4 - \frac{a_2\,a_3}{a_1}\right)\chi_{RT}$$

Hence the effective torsional stiffness that will be computed to compare results properly is the following quantity.

$$(4.II.5)\quad GJ_R^{Eff} = \left(GJ_R - \frac{C_{TA}\,C_{AT}}{EA_R}\right) = E\left(a_4 - \frac{a_2\,a_3}{a_1}\right)$$

It is clear from (4.II.5) how the axial stiffness influences the torsional stiffness as well. As a matter of fact, a decreasing in the axial stiffness of the rope caused by interwire slipping produces a decreasing of the torsional stiffness as well. This effect is not catch by neither most of the theoretical models nor the formulations of the present thesis.

3.2.1. GEOMETRY

The wire rope is a 76 mm global diameter IWRC, which stands for "independent wire rope core", because it is made by a central 7x7 stranded rope which correspond to the independent core and by an additional layer of strands. The core stranded rope has the same internal structure of the one described in the previous paragraph 3.1. Only the diameters of the wires change according to the following table.

Table 4.23 Wire rope 76 mm 6x41 IWRC Geometry

Rope layer	wire layer	wire diameter d_w [mm]	wire lay angle α_w [°]	number of wires per strand layer	wire helix radius R_w [mm]	wire lay lenght p_w [mm]	strand lay angle α_s [°]	number of strands per rope layer	strand helix radius R_s [mm]	strand lay lenght p_s [mm]
	0	3.962	-	1	-	-				
0	1	3.607	20.76	6	3.797	62.74	-	1	-	-
	0	3.607	-	1	-	-				
1	1	3.150	18.70	6	3.283	62.74	17.09	6	10.06	206
	0	6.350	-	1	-	-				
	1	3.658	-8.21	8	4.822	210				
	2a	3.302	-12.69	8	7.533	210				
	2b	2.438	-12.69	8	7.533	210				
2	3	3.785	-16.97	16	10.123	210	16.08	6	24.77	540

Where r_w is the wire cross section radius, p_w is the wire centerline pith, R_s is the radius of the strand helix and R_w is the radius of the wire helix. The strands 0 and 1 are the component of the independent core, while the strand 2 is used within the outer layer. The correspondence between the previous table and the physical position of the wires is shown in the picture below. Specifically, the wire Wij is in the i-th strand layer and in the j-th wire layer.

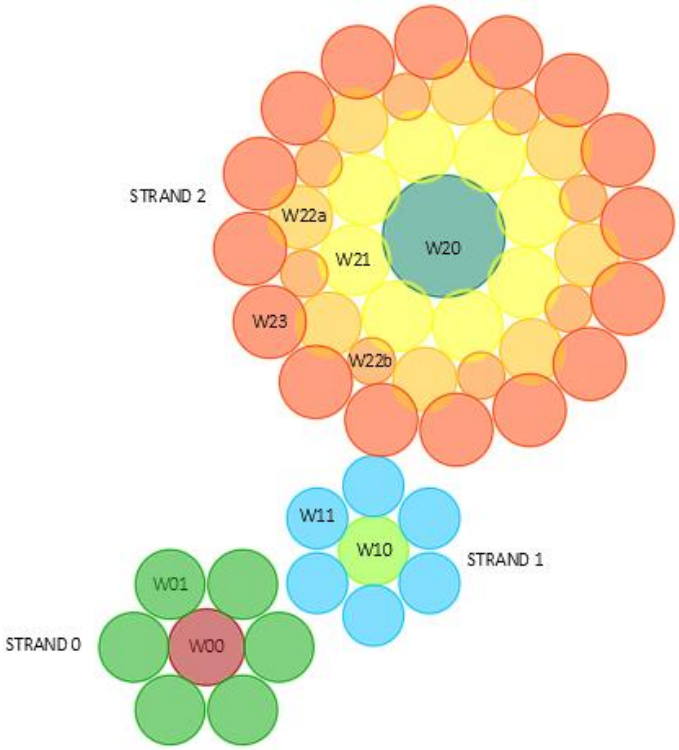

Fig 4.74 Wire Rope 76 mm 6x41 IWRC Wires and Strands Nomenclature

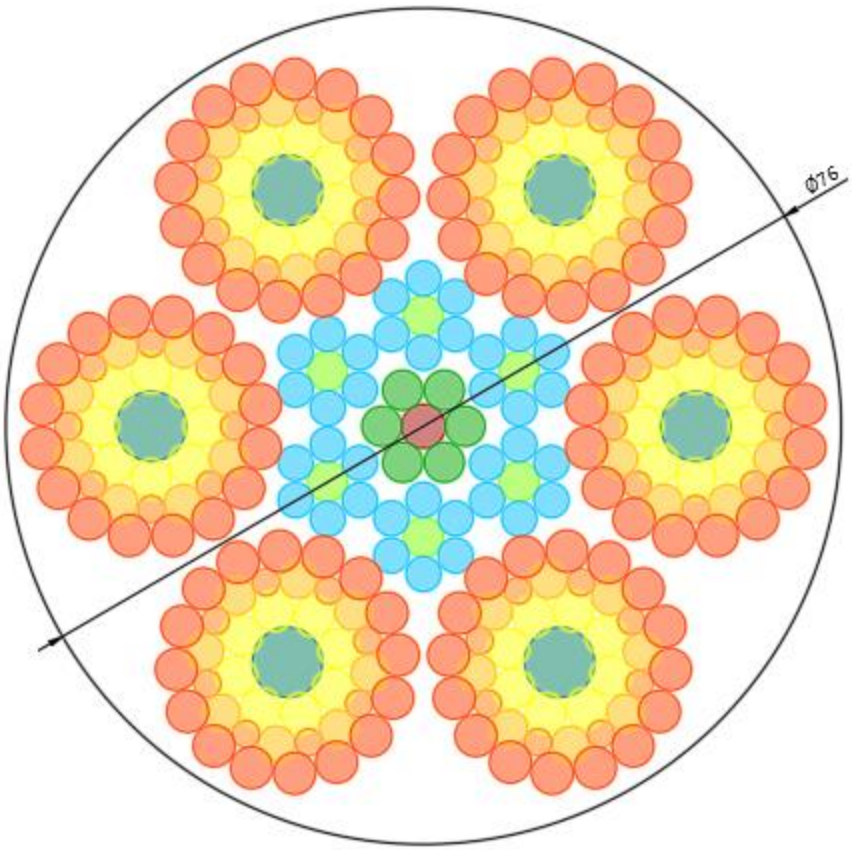

Fig 4.75 Wire Rope 76 mm 6x41 IWRC General View

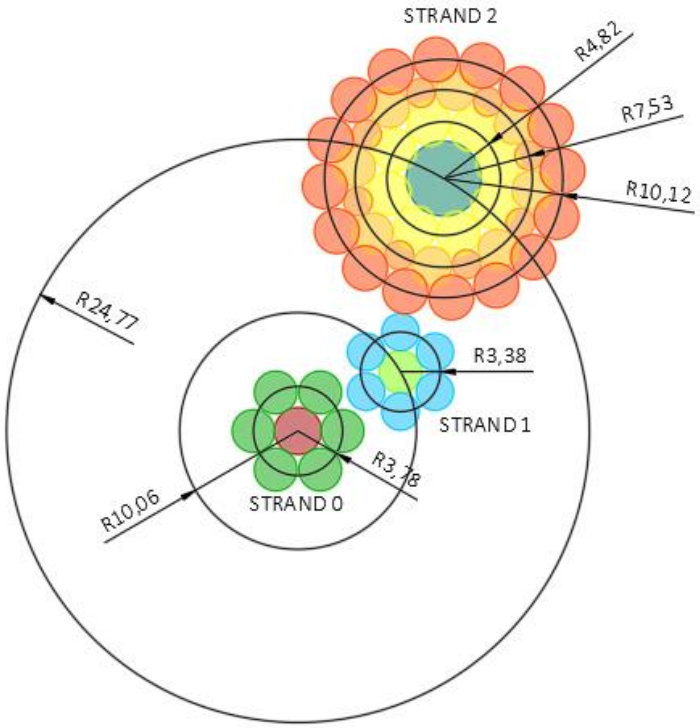

Fig 4.76 *Wire Rope 76 mm 6x41 IWRC Wire and Strand Helix Radii*

3.2.2. STIFFNESS MATRIX COEFFICIENTS

In the following table, it is possible to see the different entries of the stiffness matrix corresponding to the various formulations. It must be noticed that in the recursive model the contribution to the rope response of the strand have been slit in axial torsion of the strand and bending of the strand. The reason is the possibility of turning off the contribution due to bending when the rope experiences torsion in order to simulate slipping. The recursive model without the bending contribution of the strand is called "Rec.sAT", since the axial torsional contribution is active only.
The other formulation that are involved in the comparison are the modes proposed by Velinsky (1984) and Raoof & Kraincanic (1995). The latter is able to catch either the full slip and full stick condition, while the previous can predict the frictionless condition only.

Table 4.24 Stiffness Matrix Coefficients

	a_1 [mm^2]	a_2 [mm^3]	a_3 [mm^3]	a_4 [mm^4]	Effective GJ [Nm^2]
Direct	2369	13288	13288	86136	2322
Recursive	2288	11454	11454	68115	2155
Rec.sAT	2288	11454	11454	62702	1072
R & K stick	2148	14467	11887	128912	9770
R & K slip	1960	12351	9894	89499	5430
Velinsky	2221	13791	13241	87842	1125

It can be noticed that the Raoof & Kraincanic model is able to predict the difference full stick and full slip when the rope experiences axial excitation only. In the following table the values aforesaid are reported in terms of stiffnesses. Moreover, the direct model is used as reference value to evaluate the error in percentage in the right column.

Table 4.25 Stiffness Matrix Coefficients

	EA_R [kN]		C_{AT} [kNmm]		C_{TA} [kNmm]		GJ_R [kNmm^2]	
Direct	4.74E+05	-	2.66E+06	-	2.66E+06	-	1.72E+07	-
Recursive	4.58E+05	-3%	2.29E+06	-14%	2.29E+06	-14%	1.36E+07	-21%
Rec.sAT	4.58E+05	-3%	2.29E+06	-14%	2.29E+06	-14%	1.25E+07	-27%
R & K stick	4.30E+05	-9%	2.89E+06	9%	2.38E+06	-11%	2.58E+07	50%
R & K slip	3.92E+05	-17%	2.47E+06	-7%	1.98E+06	-26%	1.79E+07	4%
Velinsky	4.44E+05	-6%	2.76E+06	4%	2.65E+06	0%	1.76E+07	2%

The direct model shows the higher axial stiffness among all formulations. This result was expected since the kinematic assumption on the rope cross section is the stiffer that is possible. The difference with the others is very low except for the full slip case of Raoof & Kraincanic (1995). This observation is trivial if we think that the axial stiffness in the roughest approximation is EA_0, where A_0 is the area of the cross section of the rope with the usual definition.
An interesting comment concerns the torsional stiffness. As a matter of fact, the order of magnitude is similar for the direct model, Velinsky (1984) and Raoof & Kraincanic (1995) in full slip conditions. Both the last formulations assume a frictionless kinematics.

3.2.2.1. AXIAL STIFFNESS

The axial stiffness has been computed through four tensile tests and the average has been evaluated in either full stick and full slip conditions. In the table below, it possible to appreciate the results and the comparison with the theoretical models. They have been split in full stick and full slip where it is possible. Furthermore, the error between the measurement and the theoretical value is reported in the column on the right of the theoretical result.

$$error = \frac{model - measurement}{measurement}$$

Table 4.26 Axial Stiffness of the Rope

		Axial Stiffness EA_R [kN]							
Mode	Test number	Measured	Raoof & Kraincanic		Velinsky		Direct		Recursive	
full slip	1	3.96E+05		-1.1%		12.1%		19.6%		15.5%
	2	4.11E+05		-4.7%		8.0%		15.2%		11.2%
	3	3.95E+05		-0.8%		12.4%		19.9%		15.8%
	4	4.02E+05		-2.6%		10.4%		17.8%		13.7%
	average	4.01E+05	3.92E+05	-2.3%	4.44E+05	10.7%	-	18.1%	-	14.0%
full stick	1	4.16E+05		3.4%		6.9%		14.0%		10.1%
	2	4.38E+05		-1.9%		1.4%		8.2%		4.5%
	3	4.39E+05		-2.1%		1.2%		8.0%		4.3%
	4	4.97E+05		-13.5%		-10.6%		-4.6%		-7.9%
	average	4.47E+05	4.30E+05	-4.0%	-	-0.7%	4.74E+05	5.9%	4.58E+05	2.3%

It can be clearly appreciated that direct and recursive formulation have a behavior much closer to the full stick condition, for instance the error between the two models and the average measured stiffness in full stick is respectively 5.9% and 2.3%. Consequently, the error increase significantly when slipping occurs within the rope. Let us recall that the other two models Raoof & Kraincanic (1995) and Velinsky (1984) can predict respectively either full stick and full slip conditions and full slip only.
In the following graph, it is possible to see the plot (η_R, N_R) corresponding to the stiffnesses afore mentioned in full slip condition. Specifically, the maximum, minimum and average values are reported.

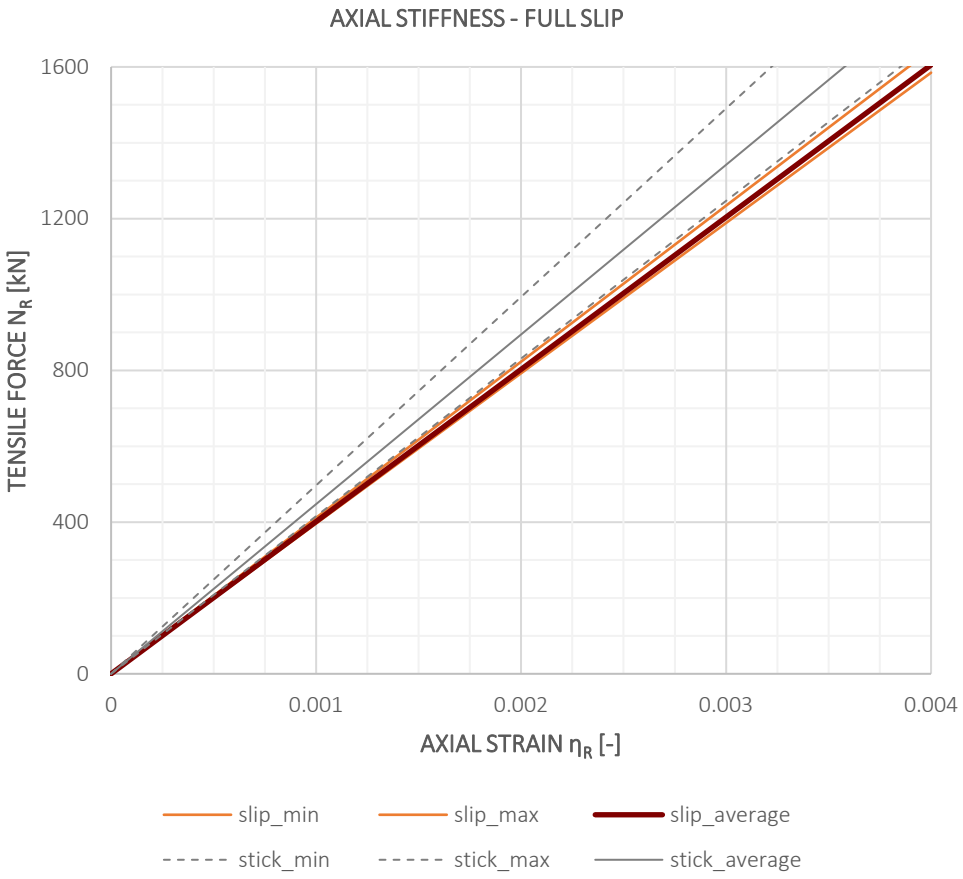

Fig 4.77 Wire Rope Global Axial Stiffness – Experimental Results

Conversely, the graph below shows the plot (η_R, N_R) corresponding to the stiffnesses afore mentioned in full stick condition. Specifically, the maximum, minimum and average values are reported.

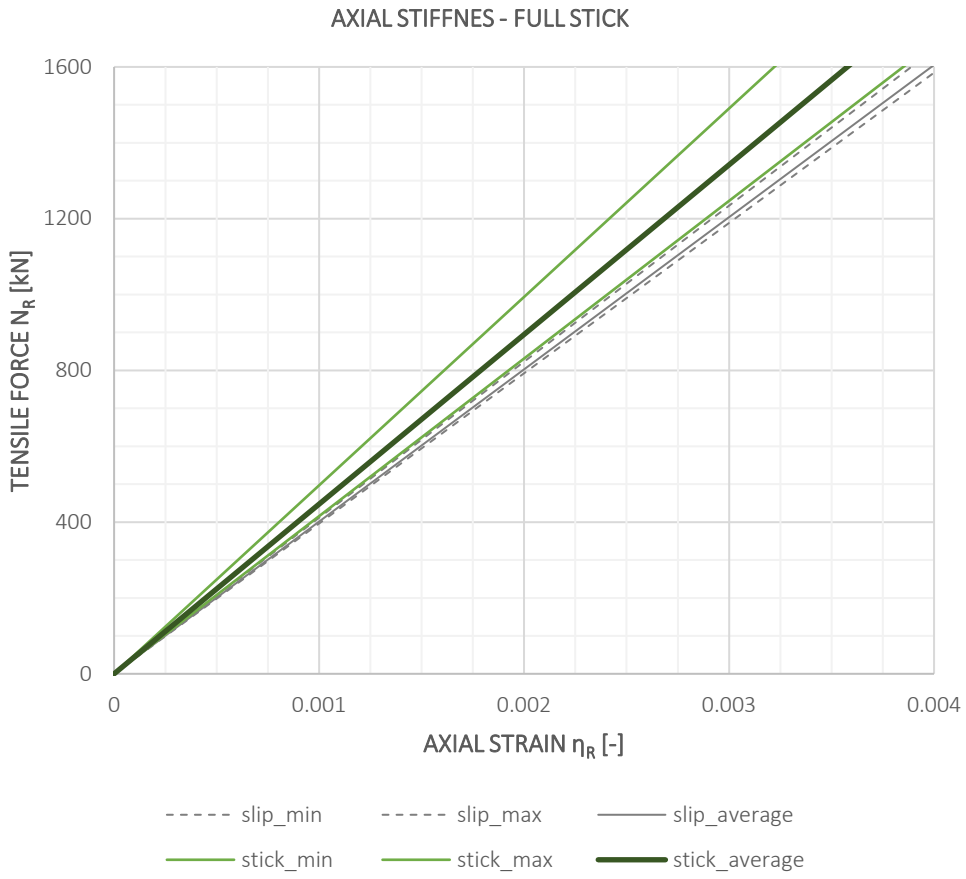

Fig 4.78 Wire Rope Global Axial Stiffness – Experimental Results

A comparison between the different models is provided in the last plot. In the graph, the maximum and minimum measured axial stiffness curves are plotted to relate the theoretical formulations with the experimental tests for either full stick and full slip conditions. It must be remembered that the present thesis work deals with a full stick model and it is not able to account slipping under axial excitation only, while Velinsky (1984) involves a full slip condition and Raoof & Kraincanic (1995) can catch either scenarios.

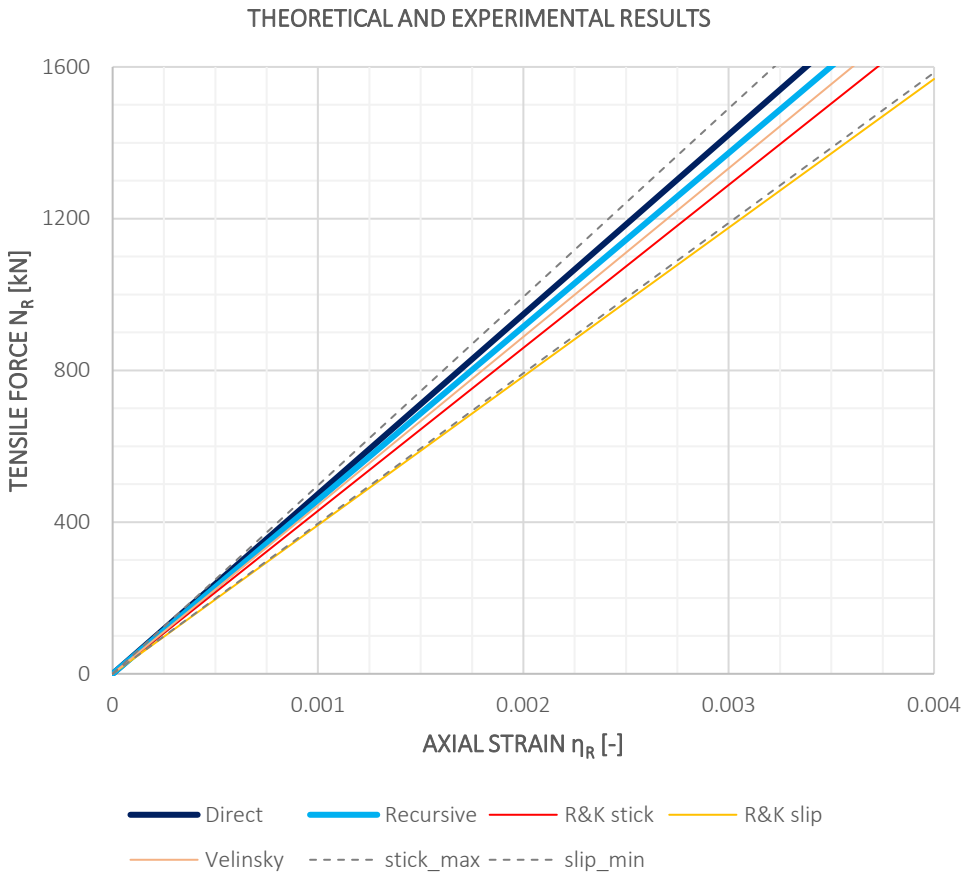

Fig 4.79 Wire Rope Global Axial Stiffness – Results Comparison

It can be appreciated that the current work provides a response closer to the full stick condition like it was expected because of the Euler Bernoulli kinematic hypothesis on the wire rope cross section. The other theoretical models show an axial stiffness always lower compared to either direct and recursive formulation.

3.2.2.2. COUPLING COEFFICIENT

The present section aims to provide information about coupling between axial and torsional internal actions within the wire rope. This point is very important for the comparison of the different formulations. As a matter of fact, in order to be thermodynamically consistent, the stiffness matrix (4.II.3) must be symmetric to fulfill the Reciprocity theorem. All models fail on that aspect, while the direct and recursive formulations don't.
In the following graph, the all the models are compared to the experimental result that is represented in grey.

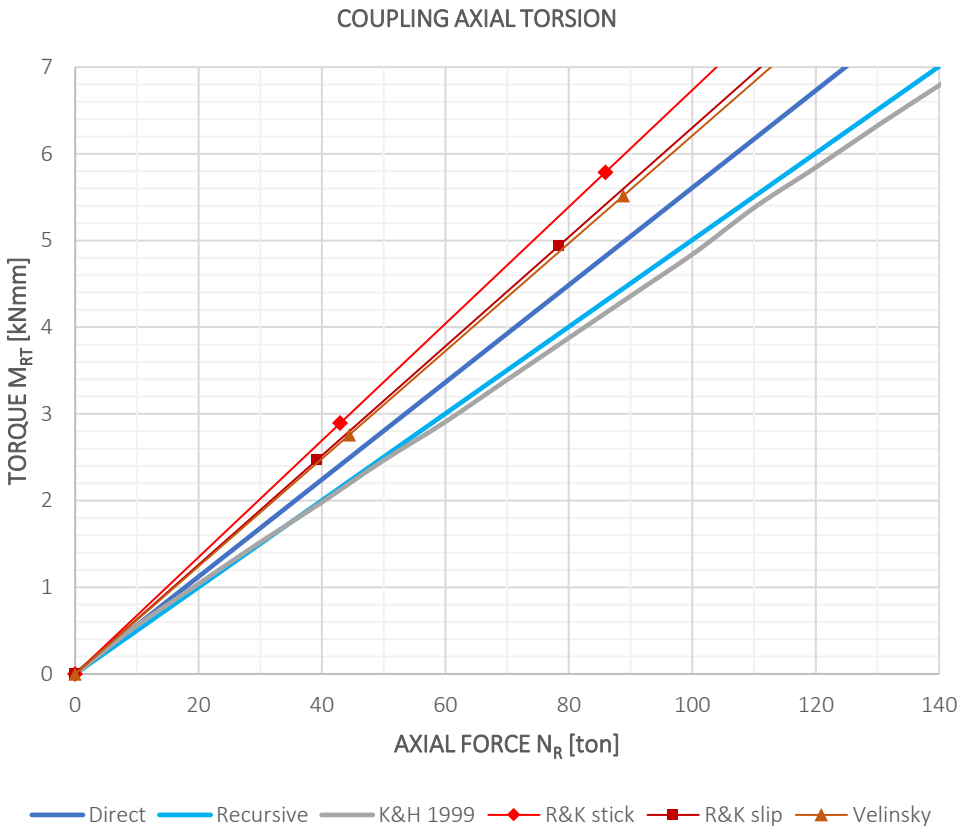

Fig 4.80 Wire Rope Global Axial Torsional Coupling – Results Comparison

3.2.2.3. TORSIONAL STIFFNESS

The experimental results that are reported below are for small strains where the behavior is almost linear. The same doesn't hold if the magnitude of the kinematic field is enlarged. The results provided in (Kraincanic & Hobbs, 1999) are derived from an experimental set up as follows: since the rope needs a tensile force to show a significant torsional stiffness it is pre-loaded with an axial force N, the torque is applied. For that reason, the results are provided for different axial forces and the stiffness increases according to that internal action. The analytical models of the present thesis and of the other papers are not able to account this effect.

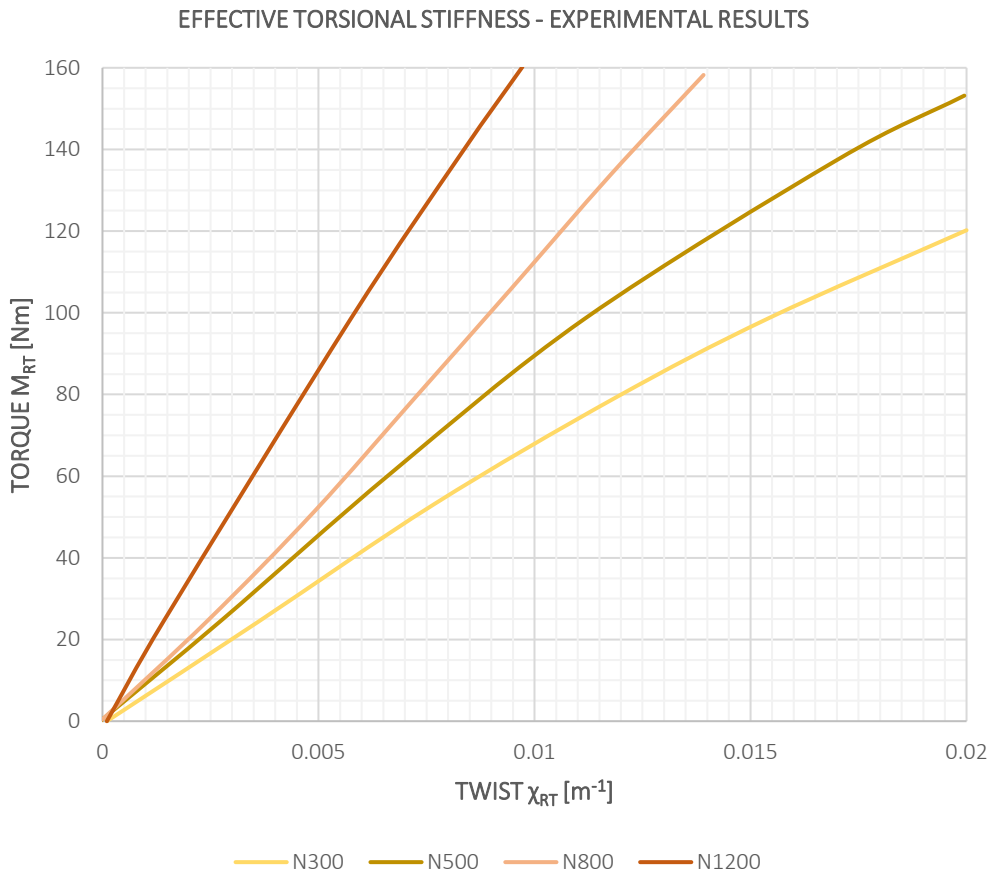

Fig 4.81 Wire Rope Global Torsional Stiffness – Experimental Results for Different Initial Tensile Force

In the following graph, the comparison between experimental and theoretical results is performed. The experimental results are reported with grey dashed lines, the current work models are represented in blue and light blue, while the other models are in scale of reds.

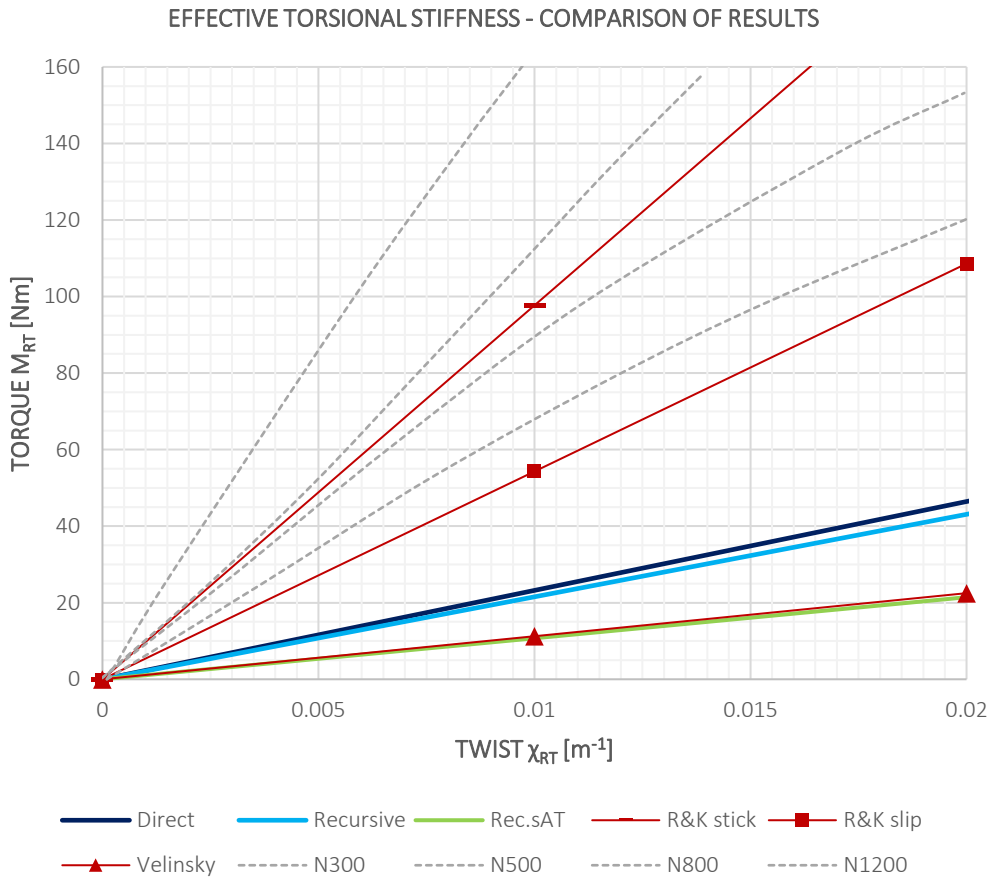

Fig 4.82 Wire Rope Global Torsional Stiffness – Results Comparison

From the previous plot is possible to extract the initial stiffness of the different tests with the tangent in the origin of the cartesian system. The results are reported into the following table. The stiffness evaluated through the direct model in full stick condition is taken as reference value for the comparison of the other models.

Table 4.27 Effective Torsional Stiffness

	Effective GJ [Nm²]	
Direct	2322	0%
Recursive	2155	-7%
Rec.sAT	1072	-54%
R&K stick	9770	321%
R&K slip	5430	134%
Velinsky	1125	-52%
H&K N300	6752	191%
H&K N500	8968	286%
H&K N800	10115	336%
H&K N1200	17298	645%

It is possible to notice that the results are very different from each other. The direct and recursive model have the lower value of effective stiffness. The reason is the relation (4.II.5) where the dependence is upon the axial stiffness and the coupling coefficients as well. Furthermore, the experimental tests show a dependence upon the pre-axial load of the effective torsional stiffness. This effect is neither predicted in the models available in literature nor mentioned in the various papers. Probably, the reason of that dependence stems from the second order effect of the axial force on the stiffness of the wire rope. Unfortunately, this statement can't be checked because of the lack of further experimental results, since they are very rare in literature. Hence, additional tests shall be performed to better understand this phenomenon that has some degree of uncertainty so far.

III. LOCAL RESPONSE OF THE WIRE

The present section of the thesis aims to provide an estimation of the local response of the wire. This mechanical information about the response of the rope is particularly important. Firstly, the stresses are difficult to measure, thus in literature there is no presence of experimental results about these quantities. Moreover, a simple tool to evaluate the local internal action of the structural systems has obvious interesting implications like fatigue analysis and elasto-plastic analysis of the wire rope.
In literature the investigation of that mechanical quantity is almost recent, since earlier articles like Velinsky (1984) and Raoof & Kraincanic (1995) used to study the system only from a global view point. As a matter of fact, the present paragraph will deal with the references of Usabiaga & Pagalday (2008) and Xiang et al (2015) that provide theoretical results for the normal and tangential stress experienced by the 30 mm 7x7 WSC stranded rope already investigated in section 3.1.

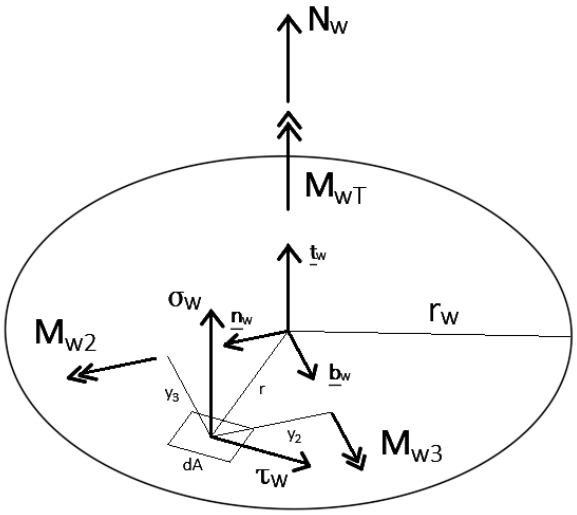

Fig 4.83 Local Stress and Internal Actions of the Wire

1. NORMAL AND TANGENTIAL STRESS

The stress filed experienced by the wire can be evaluated simply combining the kinematic relations of the wire strain field derived in chapter 2 with the generalized constitutive model of the wire introduced in chapter 3. The normal and tangential stresses acting upon the wire cross section are computed according to the Love thin curved rod theory (Huang, 1973) and they have the same structure of the Euler Bernoulli beam circular cross section. Let us recall the local reference frame of the wire: the coordinates are (y_1, y_2, y_3) and they correspond to the tangent, normal and binormal direction of the Serret-Frenet frame.

$$\sigma_w(y_1, y_2, y_3) = E\left[\frac{N_w(y_1)}{EA_w} + \frac{M_{w2}(y_1)}{EI_w}y_3 - \frac{M_{w3}(y_1)}{EI_w}y_2\right]$$

$$\tau_w(y_1, y_2, y_3) = E\left[\frac{M_{wT}(y_1)}{2\,EI_w}\,r(y_2, y_3)\right]$$

Where σ_w and τ_w are the normal and tangential stress respectively, E is the elastic modulus of the wire and I_w is the second order moment of the wire cross section. Moreover, it must be remembered that $y_1 = y_1(x_1)$ where x_1 is the global coordinate directed as the rope axis, while the geometrical quantity r is the polar coordinate of the wire cross section with maximum value equal to the wire radius r_w and it defined as follows:

$$r(y_2, y_3) = \sqrt{y_2^2 + y_3^2}$$

Introducing the expressions of chapter 3 (3.II.1) providing the generalized constitutive model of the wire cross section the previous quantity can be written as follows.

$$(4.III.6a) \quad \sigma_w(x_1, y_2, y_3) = E[\eta_w(x_1) + \chi_{w2}(x_1)\, y_3 - \chi_{w3}(x_1) y_2]$$

$$(4.III.6b) \quad \tau_w(x_1, y_2, y_3) = G\ \chi_{wT}(x_1)\, r(y_2, y_3)$$

Where G is the tangential modulus of the of the wire. It is worth it to notice that according to our model the normal stresses are caused by the wire stretching and bending, while the tangential stresses are induced by torsion of the wire only. The remark is done since in the other authors formulations, stretching only produces either normal and tangential stresses.

1.1. CENTROID AND MAXIMUM NORMAL STRESS

The normal stresses can be split into two contributions: the centroid normal stress, that represent the average value of the stress profile over the wire cross section, and the bending normal stresses. The last quantity varies linearly with the position according to (4.III.6a), thus the maximum value of the normal stress is reached in correspondence of the wire cross section perimeter and is provided by the sum of centroid and maximum bending value. The average value is provided by the following relation.

$$(4.III.7a) \quad \boldsymbol{\sigma_{w0}(x_1) = E\, \eta_w(x_1)}$$

Conversely, the maximum bending stress and the correspondent maximum value can be written as follows.

$$(4.III.7b) \quad \boldsymbol{\sigma_{wB}(x_1) = E\, r_w[\, |\chi_{w2}(x_1)| + |\chi_{w3}(x_1)|\,]}$$

$$(4.III.7c) \quad \boldsymbol{\sigma_{wMAX}(x_1) = \sigma_{w0}(x_1) + \sigma_{wB}(x_1)}$$

The function that will be involved for the comparison with other authors are (4.III.7a) and (4.III.7c). In the case study, the explicit dependence upon the rope kinematics is provided for either direct and recursive model under axial torsion.

1.2. MAXIMUM TANGENTIAL STRESS

This quantity varies linearly with the distance from the centroid of the wire cross section, thus the maximum value is reached in correspondence of the perimeter. Introducing r = r_w in (4.III.6b) the maximum shear stress has the following shape.

$$(4.III.8) \quad \boldsymbol{\tau_{wMAX}(x_1) = G\, r_w\ \chi_{wT}(x_1)}$$

In the case study, the explicit dependence upon the rope kinematics is provided for either direct and recursive model under axial torsion.

2. CASE STUDY: 30 mm 7x7 WSC STRANDED ROPE UNDER AXIAL TORSIONAL LOAD

In the present section let us analysis the local response of the 30 mm 7x7 WSC stranded rope already mentioned in the papers of Usabiaga & Pagalday (2008) and Xiang et al (2015). The main difference between the current thesis and the formulation proposed into the two articles lays in the kinematic assumptions on the slipping condition of the rope. The direct and recursive model assume that the wire material point, i.e. the point obtained by the intersection of the wire centerline with the cutting plane orthogonal to the rope axis, is rigidly connected to the rope axis corresponding to the relevant cross section. On the other hand, Usabiaga & Pagalday (2008) states that this hypothesis isn't enough realistic, thus the suggest that the material point of the wire is rigidly attached to the strand

centerline, while the strand material point is not linked with the rope axis. Finally, Xiang et al assume a frictionless condition, thus full slip condition.
Hence, from the present thesis through Usabiaga & Pagalday (2008) to Xiang et al (2015) the system is modelled progressively more compliant. For that reason, the local response will decrease in magnitude accordingly.
Firstly, let us derive the normal and tangential stresses expressions for the rope undergoing axial torsional load. The aim of this step is to get an explicit relation providing the local stress of the wire as a function of the rope generalized strains. The result is achieved introducing inside the (4.III.7) and (4.III.8) the kinematic relations introduced in the second chapter of the present thesis.
The numerical comparison of the results is introduced at the end of each section.

2.1. CENTROID AND MAXIMUM NORMAL STRESS

In the present paragraph let us introduce inside (4.III.7) the kinematic relations of the wire axial strain and curvatures. From the direct model the axial strain is (2.II.3) and curvature is (2.II.6), while in the recursive model they are split for the strand axial torsion (2.III.6a) and (2.III.6b).

2.1.1. DIRECT MODEL

Let us introduce inside (4.III.7a) the relation (2.II.3). Hence, the centroid normal stress is as follows.

$$(4.III.9a) \quad \boldsymbol{\sigma_{w0}(x_1) = E \frac{dx_1}{dy_1}(x_1) \left[t_{w1}(x_1)\, \eta_R(x_1) + \left(x_{w2}(x_1)\, t_{w3}(x_1) - x_{w3}(x_1)\, t_{w2}(x_1) \right) \chi_{RT}(x_1) \right]}$$

Then substituting inside (4.III.7b) the last two relations of (2.II.6). Hence, the maximum bending normal stress is as follows.

$$(4.III.9b) \quad \boldsymbol{\sigma_{wB}(x_1) = E\, r_w \frac{dx_1}{dy_1}(x_1) [\, |n_{w1}(x_1)| + |b_{w1}(x_1)| \,] \, |\chi_{RT}(x_1)|}$$

The maximum normal stress is given by the sum of (4.III.9a) and (4.III.9b) as follows.

$$(4.III.9c) \quad \boldsymbol{\sigma_{wMAX}(x_1) = \sigma_{w0}(x_1) + \sigma_{wB}(x_1)}$$

2.1.2. RECURSIVE MODEL

The first contribution is provided by the strand axial torsion field. Let us introduce inside (4.III.7a) the first relation of (2.III.6a). Hence, the centroid normal stress is as follows.

$$(4.III.10a) \quad \boldsymbol{\sigma_{w0}^{sAT}(x_1) = E\, \cos^2 \alpha_w \cos^2 \alpha_s\, \eta_R(x_1) + E[R_s\, \cos \alpha_s \sin \alpha_s \cos^2 \alpha_w + R_w\, \cos \alpha_w \sin \alpha_w \cos^2 \alpha_s\,] \, \chi_{RT}(x_1)}$$

Then substituting inside (4.III.7b) the last two relations of (2.III.6a). Hence, the maximum bending normal stress is as follows.

$$(4.III.10b) \quad \boldsymbol{\sigma_{wB}^{sAT}(x_1) = E\, r_w |\cos \alpha_w \sin \alpha_w| \cos^2 \alpha_s \, |\chi_{RT}(x_1)|}$$

Finally, the maximum normal stress is given by the sum of (4.III.10a) and (4.III.10b).

$$(4.III.10c) \quad \boldsymbol{\sigma_{wMAX}^{sAT}(x_1) = \sigma_{w0}^{sAT}(x_1) + \sigma_{wB}^{sAT}(x_1)}$$

The second contribution is provided by the strand biaxial bending field. Let us introduce inside (4.III.7a) the first relation of (2.III.6b). Hence, the centroid normal stress is as follows.

$$(4.III.11a) \quad \boldsymbol{\sigma_{w0}^{sB}(x_1) = -\cos^2 \alpha_w\, \cos \alpha_s \sin \alpha_s\, R_w \cos \varphi(x_1)\, \chi_{RT}(x_1)}$$

Then substituting inside (4.III.7b) the last two relations of (2.III.6b). Hence, the maximum bending normal stress is as follows.

$$(4.III.11b) \quad \boldsymbol{\sigma_{wB}^{sB}(x_1) = E\, r_w |\cos \alpha_w \cos \alpha_s \sin \alpha_s| [\, |\sin \varphi(x_1)| + |\cos \alpha_w \cos \varphi(x_1)| \,] \, \left| \chi_{RT}(x_1) \right|}$$

Finally, the maximum normal stress is given by the sum of (4.III.11a) and (4.III.11b).

$$(4.III.11c) \quad \boldsymbol{\sigma_{wMAX}^{sB}(x_1) = \sigma_{w0}^{sB}(x_1) + \sigma_{wB}^{sB}(x_1)}$$

2.1.3. NUMERICAL COMPARISON WITH USABIAGA & PAGALDAY (2008)

The comparison is performed for the following kinematic field experienced by the rope.

$\eta_R(x_1) = 0.001$

$\chi_{RT}(x_1) = 0.001$

The results are periodic over the same period of the geometrical curvature and torsion of the wire double helix. For that reason, in the following plots the wire rope axis length is limited on one period.
The wire analyzed is the outer wire of the outer strand and the comparison is performed for the real and developed arch length of the direct model, the recursive model and the formulation of Usabiaga & Pagalday (2008) indicated respectively "Real", "Devel", "Rec" and "Usabiaga 2008".
The first comparison is introduced upon the centroid normal stress as follows.

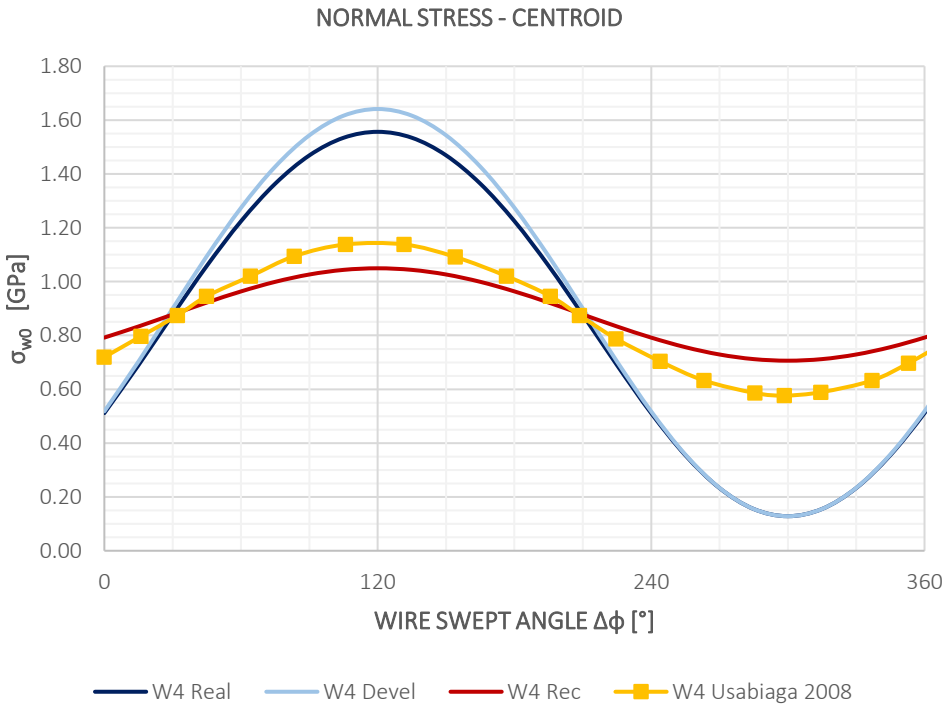

Fig 4.84 Normal Stress of the Wire Cross Section Centroid – Results Comparison

The maximum, minimum and mean value of the previous functions. The error from the real direct model is computed below each row. For Usabiaga & Pagalday (2008) only, the error is provided from either real and recursive model.

Table 4.28 Centroid Normal Stress

σ_{w0} [GPa]	max	min	mean
real	1.556	0.129	0.843
	0%	*0%*	*0%*
developed	1.641	0.128	0.885
	5.44%	*-0.06%*	*5.02%*
recursive	1.049	0.706	0.878
	-32.58%	*449.45%*	*4.19%*
U&P 2008	1.138	0.577	0.857
real	*-26.89%*	*349%*	*1.76%*
recursive	*8.44%*	*-18.33%*	*-2.33%*

It is interesting to observe the great error occurring between direct and recursive model, and the difference occurring between the direct model and the article model. While the last result is expected due to the more compliant assumptions on kinematics, the first result is affected by the approximation introduced with the hierarchical procedure.
In the following, let us show the comparison of the maximum value of normal stress.

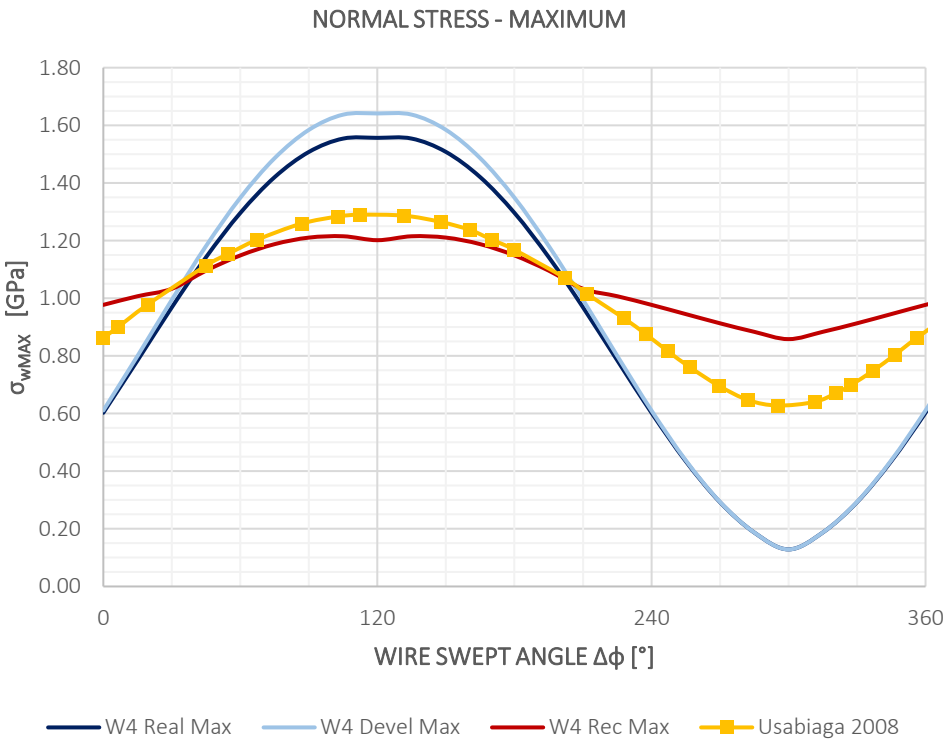

Fig 4.85 Maximum Normal Stress of the Wire Cross Section – Results Comparison

The response in the direct models is mainly provided by the centroid value of the normal stress, while in the recursive and Usabiaga & Pagalday (2008) models the influence of the bending contributions of the wire is not negligible. Furthermore, the functions are periodical but not sinusoidal, the reason of the peculiar trends is the absolute value of (4.II.7b).
The maximum, minimum and mean value of the previous functions. The error from the real direct model is computed below each row. For Usabiaga & Pagalday (2008) only, the error is provided from either real and recursive model.

Table 4.29 Maximum Normal Stress

σ_{w0} [GPa]	max	min	mean
real	1.556	0.129	0.843
	0%	*0%*	*0%*
developed	1.641	0.128	0.885
	5.44%	*-0.06%*	*5.02%*
recursive	1.215	0.858	1.037
	-21.94%	*567.68%*	*23.04%*
U&P 2008	1.290	0.628	0.959
real	*-17.14%*	*388%*	*13.80%*
recursive	*6.14%*	*-26.84%*	*-7.51%*

2.1.4. NUMERICAL COMPARISON WITH XIANG ET AL (2015)

The comparison is performed for the following kinematic field experienced by the rope.

$$\eta_R(x_1) = 0.001$$

$$\chi_{RT}(x_1) = 0.000$$

The results are periodic over the same period of the geometrical curvature and torsion of the wire double helix. For that reason, in the following plots the wire rope axis length is limited on one period.
The wire analyzed is the outer wire of the outer strand and the comparison is performed for the real and developed arch length of the direct model, the recursive model and the formulation of Xiang et al (2015) indicated respectively “Real”, “Devel”, “Rec” and “Usabiaga 2008”.
The comparison is introduced upon the centroid normal stress only, since the torsional contribution is null. For that reason, according to (4.III.9b), (4.III.10b) and (4.III.11b) the bending stresses are not acting on the wire cross section.

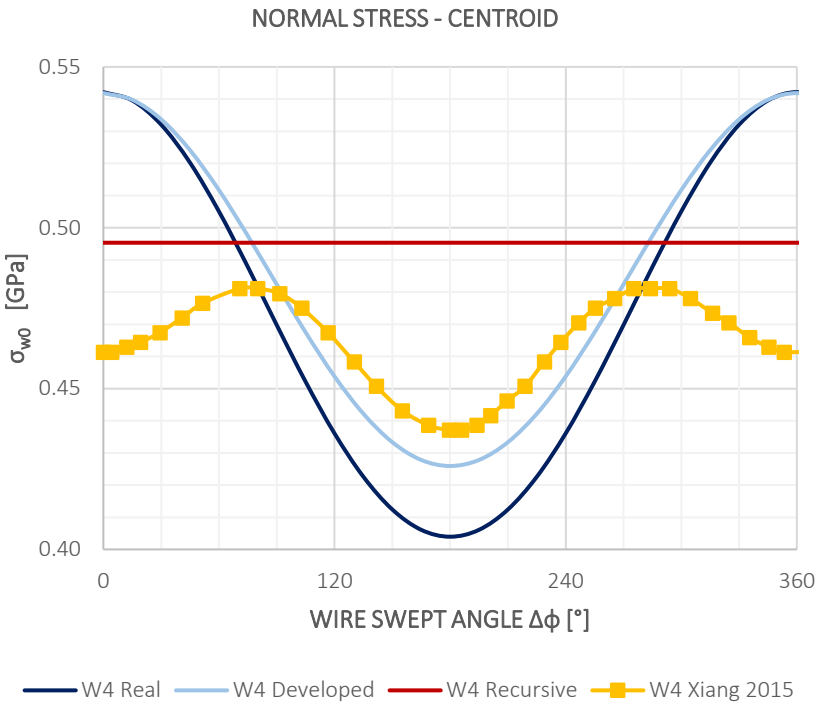

Fig 4.86 Normal Stress of the Wire Cross Section Centroid – Results Comparison

The maximum, minimum and mean value of the previous functions. The error from the real direct model is computed below each row. For Xiang et al (2015) only, the error is provided from either real and recursive model.

Table 4.30 Centroid Normal Stress

σ_{w0} [GPa]	max	min	mean
real	0.542	0.404	0.473
	0%	*0%*	*0%*
developed	0.542	0.426	0.484
	-0.06%	*5.44%*	*2.29%*
recursive	0.495	0.495	0.495
	-8.64%	*22.62%*	*4.71%*
X 2015	0.481	0.437	0.459
real	*-11.27%*	*8%*	*-2.95%*
recursive	*-2.88%*	*-11.76%*	*-7.32%*

2.2. MAXIMUM TANGENTIAL STRESS

In the present paragraph let us introduce inside (4.III.8) the kinematic relations of the wire torsional curvature. From the direct model the curvature is the first of (2.II.6), while in the recursive model they are split for the strand axial torsion (2.III.6a) and (2.III.6b).

2.2.1. DIRECT MODEL

Let us introduce inside (4.III.8) the third relation of (2.II.6). Hence, the maximum tangential stress is as follows.

$$(4.III.12) \quad \boldsymbol{\tau_{wMAX}(x_1) = \left[G\, r_w\, \frac{dx_1}{dy_1}(x_1)\, t_{w1}(x_1)\right]\, \chi_{RT}(x_1)}$$

2.2.2. RECURSIVE MODEL

The first contribution is provided by the strand axial torsion field. Let us introduce inside (4.III.8) the second relation of (2.III.6a). Hence, the maximum tangential stress due to the strand axial torsion is as follows.

$$(4.III.13a) \quad \boldsymbol{\tau_{wMAX}^{sAT}(x_1) = [G\, r_w \cos^2 \alpha_w \cos^2 \alpha_s]\, \chi_{RT}(x_1)}$$

The second contribution is provided by the strand biaxial bending field. Let us introduce inside (4.III.8) the second relation of (2.III.6b). Hence, the maximum tangential stress due to the strand bending is as follows.

$$(4.III.13b) \quad \boldsymbol{\tau_{wMAX}^{sB}(x_1) = [G\, r_w \cos \alpha_w \sin \alpha_w \cos \alpha_s \sin \alpha_s \cos \varphi(x_1)]\, \chi_{RT}(x_1)}$$

Finally, the maximum tangential stress is given by the sum of (4.III.13a) and (4.III.13b).

$$(4.III.13c) \quad \boldsymbol{\tau_{wMAX}(x_1) = \tau_{wMAX}^{sAT}(x_1) + \tau_{wMAX}^{sB}(x_1)}$$

2.2.3. NUMERICAL COMPARISON WITH USABIAGA & PAGALDAY (2008)

The comparison is performed for the following kinematic field experienced by the rope.

$\eta_R(x_1) = 0.001$

$\chi_{RT}(x_1) = 0.001$

The article of Usabiaga & Pagalday provides the formula used for the computation of the shear stresses caused by torsion of the rope, i.e. the shear flow of a solid circular cross section under twisting moment, still they do not plot the function. For that reason, in the following the comparison is made between the direct and recursive model only. The wire analyzed is the outer wire of the outer strand and the comparison is performed for the real and developed arch length of the direct model and the recursive model indicated respectively “Real”, “Devel” and “Rec”.

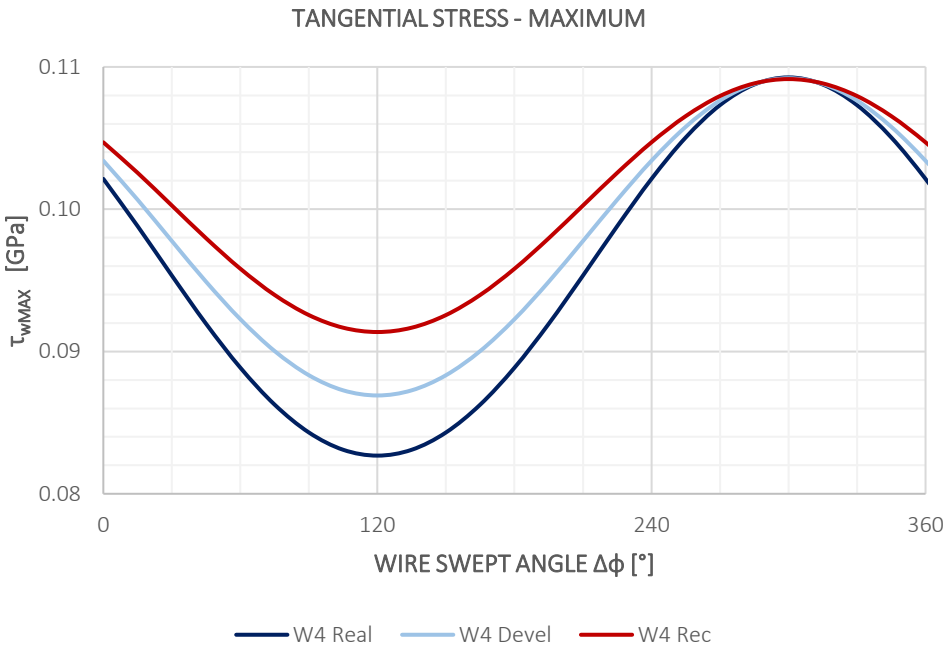

Fig 4.87 Maximum Tangential Stress of the Wire Cross Section

.

The maximum, minimum and mean value of the previous functions. The error from the real direct model is computed below each row.

Table 4.31 Maximum Tangential Stress

τ_{wMAX} [GPa]	max	min	mean
real	0.104	0.078	0.091
	0%	*0%*	*0%*
developed	0.104	0.082	0.093
	-0.06%	*5.44%*	*2.29%*
recursive	0.104	0.086	0.095
	-0.11%	*11.18%*	*4.71%*

It is interesting to notice that the tangential stresses due to torsion are one order of magnitude lower then the correspondent normal stresses.

2.2.4. NUMERICAL COMPARISON WITH XIANG ET AL (2015)

The comparison is performed for the following kinematic field experienced by the rope.

$\eta_R(x_1) = 0.001$

$\chi_{RT}(x_1) = 0.000$

Since the torsional curvature is null, in the present formulations no torsional moment is arising inside the wire. Hence, the tangential stresses are identically zero. Conversely, the model proposed by Xiang et al shows non-zero stress. The wire analyzed is the outer wire of the outer strand and the comparison is performed for the real and developed arch length of the direct model, the recursive model and the formulation of Xiang et al (2015) indicated respectively “Real”, “Devel”, “Rec” and “Usabiaga 2008”.

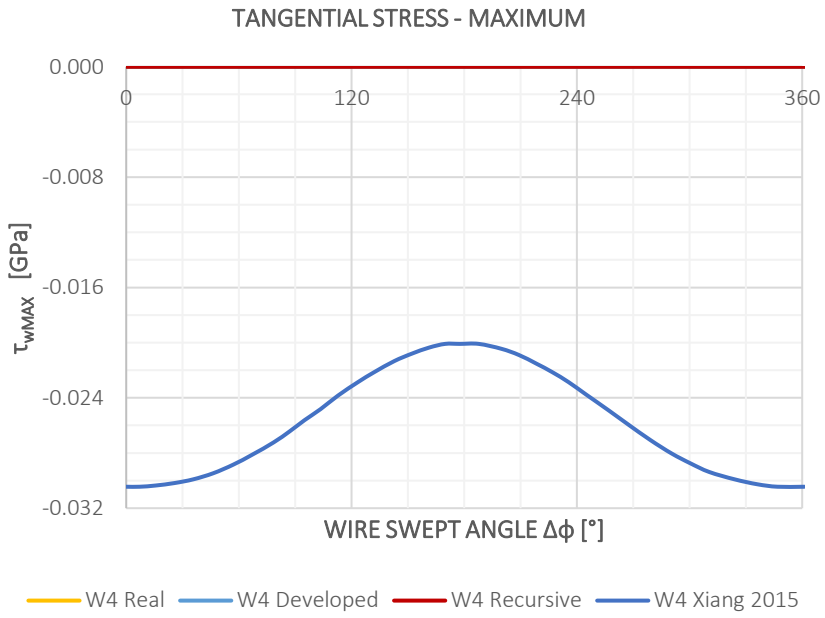

Fig 4.88 Maximum Tangential Stress of the Wire Cross Section

The maximum, minimum and mean value of the previous functions.

τ_{wMAX} [GPa]	max	min	mean
Xiang 2015	-0.020	-0.030	-0.025

It can be noticed that the magnitude of the shear stresses is always one order lower than the one of the correspondent normal stresses.

IV. CONCLUSIONS

The present chapter aims to provide a validation of the mechanical model proposed for the prediction of the global and local response of wire ropes. Basically, the difference among the various models lies in the kinematic hypothesis. The direct and recursive formulation introduced in this thesis assume that slipping among adjacent wires is utterly prevented, hence a perfect friction condition is introduced (the so called “full stick” state). This strong constraint has some degree of arbitrariness, since complex slipping phenomena occur inside the wire rope. Still the present work aims to provide the simplest model that can provide a reasonable prediction of the mechanical response. Moreover, it will be the starting point for more refined analysis where inter wire contact is fully accounted.

Firstly, let us focus on the global response of the rope. The axial stiffnesses reported in Table 4.2 and 4.3 are not very different among the different models. This result was expected since beside the choice of the formulation the response in term of axial stiffness is not very far from the rough approximation given by the axial load over the axial strain. Still, differences occur because of slipping. It may introduce a non-uniform stress state among the wires, thus slightly changing the response. The present thesis is not able to catch this behavior and Table 4.6 clearly show it. An interesting point in the comparison of the models is the coupling between axial and torsion. As a matter of fact, neither of the articles provide a stiffness matrix fulfilling symmetry, thus clearly violating the Reciprocity theorem and being thermodynamically inconsistent like it can be seen in Tables 4.2 and 4.5. Hence, despite the results are not very different from the numerical view point, they are from the mechanical point of view indeed. Finally, the comparison of the torsional stiffness shows the greatest differences among the various formulations. As a matter of fact, the direct model is the stiffer formulation if compared with the recursive model, Usabiaga & Pagalday (2008) and Xiang et al (2015) - (Table 4.2) where the error may reach up to 30%. Unexpectedly, the same result doesn’t occur with the theoretical models of Raaof & Kraincanic (1995) and Velinsky (1984) - (Table 4.5) where in full stick condition the formulation of Raoof & Kraincanic is 50% stiffer then the direct counterpart, while in full split and in (Velinsky et al, 1984) the results are almost the same. Conversely, the results differ considerably in term of effective stiffness because this kind of response is the outcoming combination of axal stiffness, coupling between axial and torsion and torsional stiffness (Table 4.7). As a matter of fact, the direct and recursive model lay in between the full slip Raoof & Kraincanic (1995) model and the Velinsky (1984) one (that assumes frictionless condition).

The last aspect to analyze is the local response of the wire. The available articles provide only theoretical predictions and not experimental evidences. In axial torsion the stiffer response and thus the higher stresses are provided by the direct model, while the recursive one is the more compliant with an error up to 30% from the previous one (Fig 4.17 and 4.18). The results provided by Usabiaga & Pagalday (2008) are in between the aforesaid formulations with a difference of 27% from the direct model like it is shown in Table 4.8. Conversely, in pure axial regime Xiang et al shows a different trend from the current work like it can be appreciated in Fig 4.19.

REFERENCES

(Love, 1994) Love A.E.H., 1944. *A treatise on the Mathematical Theory of Elasticity*. Dover Publications, New York.

(Huang, 1973) Huang N.C., 1973. *Theories of Elastic Slender Curved Rods.* Journal of Applied Mathematics and Physics Vol.24 (1973).

(Velinsky et al., 1984) Velinsky S.A., Anderson G.L., Costello G.A., 1984. *Wire rope with complex cross sections.* Eng. Mech. Div., ASCE 110 (3), 380-391.

(Ramsey, 1988) Ramsey, H., 1988. *A theory of thin rods with application to helical constituent wires in cables*. Int. J. Mech. Sci., 30(8), 559–570.

(Raoof & Kraincanic, 1995) Raoof M., Kraincanic I., 1995. *Analysis of large diameter steel ropes.* Journal of Engineering Mechanics / June 1995 / 667-675.

(Kraincanic & Hobbs, 1999) Hobbs R.E., Kraincanic I., 1999. *Axial stiffness and torsional effects in a 76 mm wire rope: experimental data and theoretical predictions.* Journal of Strain Analysis Vol 34 No 1.

(Leech, 2002) Leech C.M., 2002. *The modelling of friction in polymer in fiber ropes*. International Journal of Mechanical Sciences 44 (2002) 621–643.

(Elata et al., 2004) Elata D., Eshkenazy R., Weiss M.P., 2004. *The mechanical behaviour of a wire rope with an independent wire rope core.* International Journal of Solids and Structures 41 (2004) 1157-1172.

(Feyrer, 2007) Feyrer K., 2007. *Wire Ropes. Tension, Endurance, Reliability*. Springer.

(Usabiaga & Pagalday, 2008) Usabiaga H., Pagalday J.M., 2008. *Analytical procedure for modelling recursively and wire by wire stranded ropes subjected to traction and torsion loads.* International Journal of Solids and Structures 45 (2008) 5503-5520.

(Foti, 2013) Foti. F., 2013. *A corotational beam element and a refined mechanical model for the nonlinear dynamic analysis of cables*. Doctoral dissertation. Doctoral Programme in Structural, Seismic and Geotechnical Engineering XXV Cycle. Politecnico di Milano.

(Xiang et al., 2015) Xiang L., Wang H.Y., Chen Y., Guan Y.J., Wang Y.L., Dai L.H., 2015. *Modelling of multi-stranded wire ropes subjected to axial tension and torsion loads*. International Journal of Solids and Structures 58 (2015) 233-246.

(Foti & Martinelli, 2016) Foti F., Martinelli L., 2016. *Mechanical modelling of metallic strands subjected to tension, torsion and bending*. International Journal of Solids and Structures 91 (2016) 1-17.

CONCLUSIONS

The present thesis work aims to provide a simple tool to predict the mechanical response of wire ropes. The wire ropes are complex structural systems that need a suitable analysis to be modelled properly. The main features influencing the mechanics of wire ropes are the internal geometry of the sub components and the kinematic condition assumed. The geometry of wire wires has been studied in the first chapter. This section of the thesis pursued the objective of providing on one side the mathematical equations that describe the position of helixes in space and on the other hand the attached reference frame unit vectors, i.e. the Serret-Frenet frame. The reason to analyse that type of curves is due to the shape assumed by the wire and strand when assembled in the wire rope. As a matter of fact, the wire centreline may be either a single helix or a double helix, i.e. a single helix with a revolution axis being a simple helix itself, while the strand is coiled in single helix shapes about the rope axis. To catch the actual behaviour of the structural system the nested helix geometry needs to be utterly accounted. This manner of studying wire ropes is almost recent like in (Elata et al., 2004), (Usabiaga & Pagalday, 2008) and (Xiang et al., 2015), while previous formulations like (Velinsky et al., 1984) used to homogenize the properties of wires within the strand to treat it like an equivalent wire with single helix shape. The geometrical quantities of helixes that contain all the information about the Serret-Frenet frame are the curvature and the torsion. Their expressions have been compared with other references available in literature like (Wang et al., 1998) and (Xiang et al., 2015) where the results were basically identical. Hence, the geometry of wires has been considered as a safe starting point for the analysis of wire ropes. Furthermore, the simplicity in generating the geometry of the wire centreline and local frame is very useful for more refined analysis like FEA. As a matter of fact, an excel spread sheet is enough to have all the information needed to implement the geometry in a CAD software that can be subsequently imported in FEA software. All figures of the current thesis were obtained in this manner.

The second aspect a fundamental relevance for the determination of the mechanical response is the kinematic model assumed for the formulation. Like it was underlined several times during the current thesis, two main kinematic condition are usually introduced for this type of structures, i.e. “full stick” and “full slip” state (Raoof & Kraincanic, 1995). When adjacent wires experience a gradient in the axial force, only tangential stresses along the so called “contact surfaces” (Foti & Martinelli, 2016) guarantee equilibrium and ensure compatibility because of friction. If the magnitude of the tangential stress overpasses a certain threshold a slipping mechanism is activated. The kinematic state before slipping is called full stick, while it is called full slip when all wires are enabled to move among each other. The present thesis is framed within the first kinematic condition since a Euler Bernoulli behaviour, i.e. rigid behaviour, is assumed for the rope cross section. This is the stiffest model that can be thought indeed. Hence, the current work is not able to catch neither the opposite full slip state nor the evolution between the first state to the other one. As a matter of fact, the first improvement of this formulation would be the possibility to account either inter strands or inter wire contact like it has been already introduced in (Foti & Martinelli, 2016) for straight strands. The interest of this type of mechanism lies in the possibility of studying in a very refined way all kind of problems that involve bending of the rope (main cause of gradient of axial force among wires). For instance, like it was done by (Meleddu et al., 2017) where the focus is in the temperature increase within the rope due to friction phenomena. The current thesis proposes two different formulations for the same kinematics: the direct or wire by wire model that explicitly exploits the nested helix geometry of the single wire; and the recursive or hierarchical model that uses the manufacturing hierarchy of the wire rope, i.e. the response of the single strand is studied in its straight configuration and then it is enforced in the single helix configuration.

The kinematics is developed in the small displacements and strain framework, while the material behaviour is always assumed within the linear elastic filed. For that reason, the mechanical response of the wire rope to its fundamental modes can be split in the sum of the single wires contribution to the global response when the sole wire itself experiences the same fundamental modes. This is the reason why the entire chapter three were dedicated to this topic. As a matter of fact, in this section all the entries of the wire rope stiffness matrix were studied, still only the contribution of the single wire was accounted. Basically, the helix centreline of the wire was subjected to the fundamental modes of the rope axis, i.e. axial strain, torsional and bending curvatures of the wire rope. For instance, an axial strain applied to the rope axis induces a uniform strain field over the rope cross section that in this chapter is constituted by a single wire only. This strain will induce an axial strain in the wire as well, thus causing an axial force. This internal action of the wire, when projected in the global reference frame of the rope provides an axial force that induces torsion and bending in the rope when it is transported into the rope axis.

The last chapter investigates the response of the wire rope comparing the results obtained through the current work with the theoretical prediction of some authors (Usabiaga & Pagalday, 2008) and (Xiang et al., 2015) for either global and local response and the experimental results obtained in (Kraincanic & Hobbs, 1999) for the global response only. All the references study the structural system subjected to axial torsional loads only. The outcome of that analysis shows that the axial stiffness is modelled in a reasonable way since for the same kinematic condition, i.e. full stick, the response is comparable between the different formulations and the experimental evidences. An interesting feature concerns the coupling coefficients of the axial torsional stiffness matrix. As a matter of fact, despite similar results from a numerical view point, all the theoretical predictions of other authors lack in symmetry, thus violating the Reciprocity theorem and being very different from a conceptual vantage point. Conversely, the current thesis has a perfectly symmetric stiffness matrix that highlights the consistency of the choice of the kinematic generalized variables. Finally, the torsional stiffness shows very diverse results for either theoretical predictions and experimental tests. This last diversity is due to another important fact: the effective stiffness of the wire rope of the specimens have been measured when a pre-axial load was applied, thus providing geometrical effects to the stiffness that the present work is not able to catch. The reason is inside the kinematic hypothesis of the model that seems to be very unlike to occur, thus they can be considered an approximation of the actual behaviour of the wire rope.

These considerations demonstrate the possibility of further development in the present model of the wire rope. Firstly, the inter wire contact would be introduced following the way already traced by (Foti & Martinelli, 2016). Then the bending behaviour shall be investigated, since the direct and recursive model have been derived to predict this type of response as well, still it has not been

studied. Another interesting aspect would be the introduction of geometrical effects to deal with the stiffness increase due to the axial force value. Finally, the computation of the local response needs to be studied to obtain affordable results. This would introduce non-linear analysis that account yielding of the material.

The reason of a more refined model for wire ropes seems necessary for a very important feature of this structural system: the high slenderness. As a matter of fact, the response of the wire rope is studied with a sectional approach, still the cross section has dimensions that are much lower with respect the longitudinal one. To understand the importance of this consideration let us focus on a uniform strain field of the rope. This means that generalized displacements increase linearly along the rope length, thus an error in the evaluation of the stiffness, and consequently of the strain, may propagate in terms of displacements. Hence, a thorough model is to be pursued to minimize this error. For instance, in the lifting wire rope of an elevator an error in the torsional rotation caused by the axial force may cause undesirable results in terms of kinematics.

REFERENCES

(Love, 1944) Love A.E.H., 1944. *A treatise on the Mathematical Theory of Elasticity*. Dover Publications, New York.

(Huang, 1973) Huang N.C., 1973. *Theories of Elastic Slender Curved Rods.* Journal of Applied Mathematics and Physics Vol.24 (1973).

(Velinsky et al., 1984) Velinsky S.A., Anderson G.L., Costello G.A., 1984. *Wire rope with complex cross sections.* Eng. Mech. Div., ASCE 110 (3), 380-391.

(Ramsey, 1988) Ramsey, H., 1988. *A theory of thin rods with application to helical constituent wires in cables*. Int. J. Mech. Sci., 30(8), 559–570.

(Raoof & Kraincanic, 1995) Raoof M., Kraincanic I., 1995. *Analysis of large diameter steel ropes.* Journal of Engineering Mechanics / June 1995 / 667-675.

(Kraincanic & Hobbs, 1999) Hobbs R.E., Kraincanic I., 1999. *Axial stiffness and torsional effects in a 76 mm wire rope: experimental data and theoretical predictions.* Journal of Strain Analysis Vol 34 No 1.

(Leech, 2002) Leech C.M., 2002. *The modelling of friction in polymer in fiber ropes*. International Journal of Mechanical Sciences 44 (2002) 621–643.

(Elata et al., 2004) Elata D., Eshkenazy R., Weiss M.P., 2004. *The mechanical behaviour of a wire rope with an independent wire rope core.* International Journal of Solids and Structures 41 (2004) 1157-1172.

(Feyrer, 2007) Feyrer K., 2007. *Wire Ropes. Tension, Endurance, Reliability*. Springer.

(Usabiaga & Pagalday, 2008) Usabiaga H., Pagalday J.M., 2008. *Analytical procedure for modelling recursively and wire by wire stranded ropes subjected to traction and torsion loads.* International Journal of Solids and Structures 45 (2008) 5503-5520.

(Foti, 2013) Foti. F., 2013. *A corotational beam element and a refined mechanical model for the nonlinear dynamic analysis of cables*. Doctoral dissertation. Doctoral Programme in Structural, Seismic and Geotechnical Engineering XXV Cycle. Politecnico di Milano.

(Xiang et al., 2015) Xiang L., Wang H.Y., Chen Y., Guan Y.J., Wang Y.L., Dai L.H., 2015. *Modelling of multi-stranded wire ropes subjected to axial tension and torsion loads*. International Journal of Solids and Structures 58 (2015) 233-246.

(Foti & Martinelli, 2016) Foti F., Martinelli L., 2016. *Mechanical modelling of metallic strands subjected to tension, torsion and bending*. International Journal of Solids and Structures 91 (2016) 1-17.

(Meleddu, 2017) Meleddu M., Foti F., Martinelli L., 2017. *Temperature in active heave compensation ropes*. OIPEEC Conference – Le Rochelle – April 2017.